THE UNIVERSITY
of EDINBURGH

The role of chondrolectin in motor axon development in zebrafish

Hannah L Smith

Doctor of Philosophy
The University of Edinburgh

2019

Statement of original contribution

Unless otherwise stated in the text, the work in this thesis was performed by the candidate, Hannah L Smith.

Neither the thesis or the research work discussed within have been submitted for academic merit at any other institution.

The work in this thesis is currently being prepared for publication, with a working title as the following:

Smith HL[1], Oprişoreanu AM[1], Arya S[1], Wehner D, Cardozo MR, Talbot K[2], Becker T[2], Becker CG[2] (2019). “Interaction of the SMA downstream gene Chondrolectin with Collagen XIXaI stabilises the neuromuscular junction”.
1 – Equally contributing first authors. 2 – Equally contributing last authors.

Signed,

Hannah L Smith, 26/09/18

Abstract

Spinal Muscular Atrophy (SMA) is a childhood form of motor neuron disease (MND). It is monogenic, caused by loss of Smn1. Although Smn is ubiquitously expressed in all cells, and acts in a housekeeping function to correctly assemble the spliceosome, motor neurons are specifically vulnerable to loss of Smn. This leads to degeneration of the motor neurons. Mounting evidence shows that this degeneration starts at the neuromuscular junction and then proceeds to the motor axon. Studies have identified chondrolectin as a downstream gene adversely affected by the Smn deficiency. Chondrolectin is mis-spliced pre-symptomatically in mouse models of SMA. The protein is required for motor axon outgrowth in zebrafish, and over-expression of chondrolectin partially rescues smn knockdown.

In this project, I generated a CRISPR/Cas9 knockout of chondrolectin in the zebrafish. The mutant is homozygous viable and has no gross morphological defects, but the primary motor axons phenocopy previously published morpholino knockdown. The axons are stalled at a choice point called the horizontal myoseptum, which is known to be rich in ECM proteins such as collagens. Using both acute manipulation and a stable transgenic line, I demonstrate that only full-length chondrolectin is able to rescue the axon length, and loss of any of its protein domains leaves the protein non-functional. From this, we hypothesise a mechanism of action for this protein where it binds an ECM molecule on the axon surface and transduces a signal via phosphorylation of its intracellular domain. We suggest the binding partner for chondrolectin to be collagenXIXa1.

SMA has been linked to synaptic defects, therefore, I analysed the synaptic compartments of the axons in the chondrolectin mutant at embryonic and larval stages. At embryonic stages, the pre-synaptic compartment is enlarged around the horizontal myoseptum in the mutant compared to wild-types, and fully rescued in a stable chondrolectin-FLAG line. When the secondary motor neurons have also extended axons to innervate the myotome, there are fewer synaptic puncta in the mutant compared to wild-type. This synapse phenotype is partially rescued in the stable transgenic chondrolectin-FLAG line.

Due to the stereotypical phenotype of the chondrolectin mutant, and its relationship with SMA, we developed a drug screening protocol to discover molecules that improve axon growth. We identified two hits after screening a 40-compound library. Developing this protocol allows refinement of potentially useful compounds from larger libraries to use in other models of SMA.

Overall, this project offers new insight into the mechanism and function of chondrolectin, a gene linked to SMA. Novel findings include the domain analysis demonstrating that all protein domains are required for its function in zebrafish. We also found that loss of chondrolectin leads to synaptic defects, with embryonic synapse puncta enlarged in the mutant, and a loss of synaptic puncta in the larval stage. Finally, we have demonstrated potential translational uses for this mutant by designing a protocol to identify axon growth-enhancing compounds.

Lay summary

Motor neuron disease is an umbrella term for multiple diseases related by their effect on the motor neurons (the nerve cells which carry movement signals from the brain and spinal cord to the muscle). When these cells are damaged in the course of the disease, it leads to an inability to move, swallow, or talk, as the movement signals can no longer travel to the muscle. Spinal Muscular Atrophy (SMA) is a form of motor neuron disease which mostly affects children, and its most severe form is fatal by the age of 2. As well as studying the disease directly, it is also vital to understand how these motor neuron cells function normally, and how they develop. During my PhD project I studied the development of motor neurons, and specifically the axon portion of these cells. An axon is the long 'cable' part of the neuron which extends out of the spinal cord and forms connections onto the muscle. However, due to the difficulty in observing these cells directly in humans, I used embryonic zebrafish as my experimental subjects instead. These small zebrafish develop motor neurons and axons very rapidly and are transparent, so their spinal cords and nerve growth can be imaged under a microscope. It is also possible to test drugs on them easily, as they can be dissolved into the water that the embryos develop in.

My PhD project focused specifically on a gene called chondrolectin. Very little is known about how this gene affects the cell's function, but it has previously been shown that it is required for the motor neurons to extend from the spinal cord properly. It has also been linked to the disease Spinal Muscular Atrophy and is disrupted in mice that have SMA. I created a zebrafish mutant that did not have a functional chondrolectin gene, and further investigated the effect this had on the motor neurons. As well as affecting the growth of the axons, the mutant also failed to develop proper synapses (the junction points between the nerve and the muscle). These changes affect the behaviour of the zebrafish, and the mutant cannot turn away from touch to escape as well as a normal zebrafish would.

As previously mentioned, the zebrafish is an excellent animal to use in biological studies as it can be easily treated with drugs and the effects observed. As part of my project, I designed a screening tool to test with 40 drugs, looking for an improvement in the nerve growth. I found one drug which improved the growth of the motor axons in the chondrolectin mutant zebrafish. We hope to take this drug forward into other

models of SMA such as human cells or mice to discover if they can alleviate the disease in other animals aside from zebrafish.

Acknowledgments

Firstly, my deepest thanks to Catherina and Thomas Becker, who took a chance to offer me a PhD place in their group. I am incredibly grateful for their guidance, help, and encouragement both scientifically and emotionally throughout the journey of this project. I would also like to thank the other professors that have helped me to become a scientist – Jonathan Flint who allowed me to spend my summer holidays in his lab, and Mary Board who tutored me as an undergraduate biochemist and always supported my ambition to work in science.

To the other members of the Becker group, you have made this PhD a joy to do. For all of the help, support, teaching, and entertainment during the last four years, thank you all. The other cohort of PhD students – Themis, Tess and Lindsey, we've made it! Through the ups, downs, tears, anger, despair, excitement, and exhaustion. Thanks for all the moral support to keep going as a group. To the absolutely inspiring women in the lab, past and present. Penelope, Helena, Cristina, the most amazing post-docs. Special thanks also to Ana-Maria as the other member of Team Chondrolectin. To Leo, Marcus, Marcos, and Daniel – thank you so much for all the training and preparation you gave me for my PhD. I know I've become a much more resilient and knowledgeable scientist thanks to you – even when you were laughing at my mistakes (especially the Wnt King Daniel).

To my wonderful friends in Edinburgh and beyond, I'm sure I can't name all of you and the wildly different levels of support I've received. Thanks for reminding me of life outside of the PhD! Jemma, Chris, Emily, Russell, Jess, Tam. Especially Andrew, who always helped and encouraged me to do a PhD. Special shout-out to the members of BFS, who helped me unleash my creativity to make something unique, breath-taking, scary, and wonderful.

From the bottom of my heart, thanks to my family, who always told me I was capable of pursuing a PhD. Even at my lowest points you have always pushed me to achieve my dreams and I couldn't have asked for more loving and lovely members of a family. I dedicate all of this work to you.

Finally, thank you so much to Nico. You managed to keep me sane throughout the last three years of this project. Your support has meant so much that I can't put it into words.

List of Abbreviations

aa	amino acid
Ala	Alanine
ALS	Amyotrophic lateral sclerosis
bp	base pairs
CaP	Caudal primary axon
Chodl	Chondrolectin
CDS	Coding sequence
CRISPR	Clustered regularly interspaced short palindromic repeats
CTLD	C-type lectin domain
dpf	days post-fertilisation
DSBs	Double strand breaks
ECM	Extracellular matrix
HB9	Homeobox gene 9
HEK	Human embryonic kidney
HM	Horizontal myoseptum
hpf	hours post-fertilisation
ID	Intracellular domain
ISH	*in situ* hybridisation
MCS	Multiple cloning site
MiP	Middle primary axon
MNs	Motor neurons
MND	Motor neuron disease
Mnx1	Motor neuron and pancreas homeobox 1
MuSK	Muscle-specific kinase
PAM	Protospacer adjacent motif
PBS	Phosphate-buffered saline
PCR	Polymerase chain reaction
RoP	Rostral primary axon
RNP	Ribonucleoprotein
SDCM	Spinning disk confocal microscope
Ser	Serine
SMA	Spinal muscular atrophy
Smn	Survival of motor neuron
Thr	Threonine
VAST	Vertebrate Automated Screening Tool

Table of Contents

Chapter One - General introduction

1.1 – Zebrafish as a model organism

1.1.1 – Zebrafish in biological and biomedical research

Zebrafish (*Danio rerio*) have been used as a model organism in biomedical studies for approximately 30 years. Although mammalian systems such as mice and rats have traditionally been the most widely used in research, zebrafish are increasingly important. Their large clutch sizes and *ex utero* development of embryos give them a sampling advantage over rodents. The have modest husbandry requirements, and the adults become sexually mature at 3 months of age (Kimmel, 1989; Lawrence, 2007). The zebrafish has been classically used as a developmental model due to the advantages its embryonic and larval form offers, toxicological studies due to its aqueous environment, and large genetic screens (Lele and Krone, 1996; Lawson and Wolfe, 2011).

Zebrafish are excellent models for neuronal development. The developmental stages of the zebrafish have been well characterised, and zebrafish rapidly develop, with motor neuron differentiation starting just 9 hours post-fertilisation (hpf) (Myers, Eisen and Westerfield, 1986; Kimmel *et al.*, 1995). The motor system is extremely well characterised, with individually identified axons with stereotyped pathfinding (Westerfield and Eisen, 1988; Pike, Melancon and Eisen, 1992; Lewis and Eisen, 2003). The embryos are optically transparent during their development, meaning that zebrafish larvae are incredibly easy to image in wholemount preparations. Furthermore, fluorescent cell-reporter transgenic lines are widely available for a variety of cell types, allowing live time-lapse imaging.

Their genetic tractability make zebrafish an excellent biomedical model. Multiple models of motor neuron diseases (MNDs) are available (Babin, Goizet and Raldúa, 2014; Patten *et al.*, 2014). This includes Amyotrophic Lateral Sclerosis (ALS), with mutant SOD1 over-expression (Lemmens *et al.*, 2007; Ramesh *et al.*, 2010), C9ORF72 knockdown (Ciura *et al.*, 2013), and Spinal Muscular Atrophy (McWhorter *et al.*, 2003; Boon *et al.*, 2009; Hao, Burghes and Beattie, 2011; Hao *et al.*, 2013).

1.1.2 – Mutagenesis, transgenesis, and gene expression manipulations in zebrafish

Zebrafish are teleosts (bony fish, and thus vertebrates) and have an almost fully annotated genome, with 70% of human genes having a direct orthologue in the zebrafish (Howe *et al.*, 2013). Their genetic tractability and the wide range of mutants generated is one of the key features of the zebrafish system. The earliest papers published using the zebrafish focus on generating mutants, using γ-radiation to mutagenise fertilised eggs (Walker and Streisinger, 1983), and breeding strategies to generate homozygous mutants (Streisinger *et al.*, 1981). Large-scale forward genetics screens, such as the Tübingen ENU screen from 1993-1996, identified mutants for multiple genes involved in development (Mullins *et al.*, 1994; Driever *et al.*, 1996; Furutani-Seiki *et al.*, 1996). Overall, zebrafish are extremely amenable to genetic manipulation, and many tools are available. (Lawson and Wolfe, 2011; Auer and Del Bene, 2014)

A wealth of techniques are available in zebrafish to generate both stable transgenic lines as well as acute manipulations. Complete knockout, over-expression, and knockdown are achievable. Tissue-specific expression, or temporal induction via chemical or heat treatment may also be performed (Akerberg, Stewart and Stankunas, 2014).Traditional transgenesis, used to generate cell reporter lines, is straightforward in zebrafish as microinjection of linear DNA into single-cell eggs can randomly integrate into the genome. For example, generation of the Tg:mnx1:GFP line (HB9:GFP) was achieved by injecting DNA fragments containing the mnx1 promoter fused to the GFP sequence (Flanagan-Steet *et al.*, 2005). However, integration rates are random and may be very low.

1.1.2.1 – Acute genetic manipulations in embryonic and larval stages - Injection of mRNA allows gene over-expression, while morpholino allows gene knockdown

Injection of mRNA into single-cell eggs is a widely used technique to induce acute gene over-expression in zebrafish. Given the ease of capped mRNA production using

commercial kits, this has been used extensively to investigate proteins of interest. For example, over-expression of Delta in zebrafish embryos caused a reduction in Islet-1 positive cells (i.e. neurons), showing that Delta is involved in neuron differentiation (Dornseifer, Takke and Campos-Ortega, 1997). As well as investigating the effect of gene over-expression, this technique can also be used to confirm that knockdown or knockout of the putative gene are specific, as the mRNA should rescue the phenotype. However, this technique contains some caveats. For example, the mRNA is not tissue-specific, and so aberrant expression in non-specific tissue may have its own phenotype. Furthermore, given that mRNA must be injected at the single-cell stage, the protein may be translated and thus present during developmental stages when it is not normally expressed. For certain proteins, this may induce a phenotype or be toxic because of this aberrant expression (Beis and Stainier, 2006).

Morpholinos (MOs) have been extensively used to acutely knock down gene expression in the embryo and larval stages. Morpholinos are RNA analogues, around 25 bp in length, and achieve knockdown in a similar mechanism to siRNA, where the MO binds to mRNA and sterically prevent access by the cellular machinery during translation or RNA processing. The morpholino backbone, an uncharged morpholine ring, is resistant to degradation in the cell, allowing the morpholino and thus knockdown effect to persist until approximately 3 days post fertilisation (dpf) (Bill *et al.*, 2009). Design of morpholinos for use in zebrafish embryos are quite straightforward as long as the sequence of the gene of interest is known. Morpholinos can be designed to bind to the start site, blocking translation via steric inhibition of the ribosome. Splice-site morpholinos can also be designed to bind an intron-exon boundary, preventing the correct splicing and leading to intron inclusion or exon skipping (Eisen and Smith, 2008; Bill *et al.*, 2009).

Like with all techniques, several flaws to morpholino use have been documented, and experiments using them must be tightly controlled to ensure that the phenotype is specific. Firstly, the effective window for morpholino knockdown is from 0-3 dpf, and so phenotypes expected at later stages may not be possible to observe. A control of specificity might be to compare the knockdown to a known mutant and look for phenocopy. However, morpholinos may bind to maternally deposited mRNA present in the eggs, leading to a phenotype that may be different to a mutant produced from heterozygote incrosses. This was observed in *smn* mutants compared to the *smn* MO, an extremely well-established morpholino phenotype (Boon *et al.*, 2009). Off-target

effects may also lead to misleading phenotypes. It has been shown that some morpholino effects attributed to the gene knockdown, most notably developmental delays and excessive cell death, may be due to activation of p53 (Robu *et al.*, 2007). Controls have been suggested, such as use of multiple morpholinos which phenocopy each other and can act synergistically, as well as knockdown confirmation using Western blot or RT-PCR. Rescue of the phenotype by mRNA injection (i.e. a combined knockdown and over-expression of the same gene) is also recommended to confirm a specific phenotype (Eisen and Smith, 2008; Stainier *et al.*, 2017). With the advent of CRISPR/Cas9 to generate targeted mutants, there have been reported discrepancies between MO knockdown and mutant phenotypes, which do not phenocopy each other, suggesting a mechanism of compensation in mutants (Place and Smith, 2017). For example, (Rossi *et al.*, 2015) demonstrates that *egfl7* mutants do not recapitulate vascular defects observed in the morphants, due to upregulation of *vegfab*.

1.1.2.2 – The Tol2 system allows integration of large cassettes into the zebrafish genome to generate stable transgenic lines

The Tol2 system allows transgenesis of almost any cassette into the zebrafish genome with a higher integration rate than injection of linear DNA only. The Tol2 mechanism acts via transposable elements, and was first identified in medaka (Koga *et al.*, 1996). Cassettes containing a promoter region and protein of interest, flanked on each side by Tol2 motifs. By co-injecting mRNA of the transposase enzyme, these cassettes are cleaved and integrated at high efficiency into the genome using these transposable element motifs (Kawakami, 2005). The Tol2 system has been further refined, allowing integration of cassettes over 10 kb, and the minimal sequence required for efficient integration found (MiniTol2), (Balciunas *et al.*, 2006). A gateway-based Tol2Kit to increase the ease of cloning such constructs has also been developed (Kwan *et al.*, 2007). As well as generating reporter lines, the Tol2 system has been used to generate GAL4-UAS lines with higher efficiency than was previously achievable (Fisher *et al.*, 2006; Asakawa and Kawakami, 2008; Asakawa *et al.*, 2008).

1.1.2.3 Genome editing – The CRISPR/Cas9 system offers better efficiency than previous methods such as TALENs and zinc finger nucleases

To perform targeted genome editing, several methods have been developed in zebrafish. Protein-based targeting and nuclease techniques include transcription activator-like effect nucleases (TALENs) and zinc finger nucleases (ZFNs). With each tool, the mechanism by which mutations are induced is via double-strand breaks (DSBs) in the DNA, which is improperly repaired by non-homologous end joining (NHEJ) (Rodgers and Mcvey, 2016). This error-prone repair may lead to small insertions or deletions (indels) which can cause frame-shift mutations and premature stop codons, leading to nonsense-mediated decay of the mRNA and a lack of protein translation (Pelley, 2007; Popp and Maquat, 2016).

Zinc finger nucleases (ZFNs) act as chimeric proteins to target and cleave DNA. The DNA recognition and binding domains are zinc finger transcription factors, combined with a FokI nuclease which causes the DNA lesion (Urnov *et al.*, 2010). Adaptations to ZFNs for use in zebrafish genome editing represents the first time that targeted mutations were performed (Meng *et al.*, 2008). However, ZFNs are difficult to generate and screen for efficient cleavage. As each zinc finger motif recognises only 3 bp, multiple motifs must be assembled together to generate a targeting sequence that is unique in the genome. This can be difficult to achieve due to the complexity of the zinc finger assembly (Ramirez *et al.*, 2008). Commercial companies which assemble and screen ZFNs means that the price point to achieve genome editing is very high (Huang *et al.*, 2012; Sertori *et al.*, 2016; Simone *et al.*, 2018). TALENs function in a similar way to ZFNs, except instead of zinc fingers as the DNA recognition motif, transcription activator like effector (TALE) sequences are used (Y. Liu *et al.*, 2014). TALE sequences are protein-based, with 35aa sequences recognising a single DNA base. TALENs were demonstrated to generate germline transmission of indel mutations in zebrafish (Huang *et al.*, 2011; Sander *et al.*, 2011). TALEN targeting sequences are easier to design than ZFNs, with PCR-based gateway cloning systems available (Y. Liu *et al.*, 2014). However, similarly to ZFNs their efficiency is variable, and so to generate the chondrolectin mutant we chose to use CRISPR/Cas9. As CRISPR/Cas9 targeting is RNA-based rather than protein-based, it is less complex to design targets than ZFNs or TALENs and cheaper than ZFNs (Pattanayak, Guilinger and Liu, 2014).

The CRISPR/Cas9 system has rapidly expanded in the last few years as a method for targeted gene knockout and knock-in with high efficiency. Clustered Regularly Interspaced Short Palindromic Repeats (CRISPR) / CRISPR associated system (Cas) (CRISPR/Cas9) naturally occurs in prokaryotes and archaea as an immune response against viral infection. When foreign DNA integrates into the genome, it disrupts the CRISPR locus and RNA transcribed from this locus becomes processed into short RNAs. The Cas protein binds these short RNAs and recognise the disrupted CRISPR locus, cleaving the foreign DNA to destroy it (Wiedenheft, Sternberg and Doudna, 2012).

CRISPR/Cas9 was adapted for eukaryotic systems to generate mutants, as by artificially designing the guidance RNAs and injecting Cas9, theoretically any gene could be targeted for cleavage by the RNA-Cas9 complex.

Like ZFNs and TALENs, CRISPR/Cas9 mediates gene knockout by generating DSBs which are improperly repaired by non-homologous end-joining. As well as gene knockout using these indels, gene knock-in can also be performed by introducing homologous sequences for use as an artificial template during homology-directed repair (Auer and Del Bene, 2014). This allows integration of mutagenised sequences during the knock-in, to generate inactive or constituently active forms of the protein, or to knock-in tags to generate fusion proteins directly in the genome (Auer and Del Bene, 2014; Gonzales and Joanna Yeh, 2014).

By modifying the Cas9 and guidance RNAs (gRNAs) for the zebrafish, highly efficient gene disruption can be achieved. For example, cloning a Cas9 optimised for zebrafish codon usage, and containing a nuclear-localisation sequence to improve the efficiency of the Cas9 cleavage enzyme is presented in Jao, Wente and Chen, 2013. Online-based tools for gRNA design based on the sequence of interest have also been produced (Hsu *et al.*, 2013; Hwang *et al.*, 2013). This allows simultaneous searches for the PAM motif and thus putative gRNA targets, with genomic cross-reference for off-target binding. The tool thereby generates a score and ranks all potential gRNAs according to sequence similarity to other genomic regions, allowing selection of the most suitable gRNA.

1.2 – Motor axon development and synaptogenesis in zebrafish and other organisms

1.2.1 – The zebrafish primary motor neuron system

In zebrafish, the motor neurons develop as two subtypes, differentiating at different stages and with different morphology. The primary motor system is simple and excellently characterised, allowing easy phenotypic characterisation after genetic manipulation (discussed in next section) (Lewis and Eisen, 2003; Goldsmith and Jobin, 2012).

The primary motor neurons begin to differentiate at ~9 hpf, and each somite contains three cell bodies which begin to extend axons from ~16 hpf, the caudal primary (CaP), middle primary (MiP) and rostral primary (RoP) (Myers, Eisen and Westerfield, 1986; Seredick *et al.*, 2012). Motor neuron differentiation and axon growth develops rostral to caudal, and so exact developmental timings vary. Motor neurons at the anterior sections of the trunk will have already begun to extend axons when the posterior motor neurons differentiate. Each axon from the primary motor neurons follows a shared pathway until a pathfinding choice point at the horizontal myoseptum (HM). The HM region is rich in ECM proteins, including Tenascin-C and collagens (Schweitzer *et al.*, 2005; Bader *et al.*, 2009). After pausing at the horizontal myoseptum, the axons then diverge in their paths. The CaP axon continues on a ventral path along the vertical myoseptum, the MiP extends dorsally, and the RoP axon extends along the lateral line of the trunk (Shown below, Figure 1.1, adapted from Seredick et al., 2012).

.

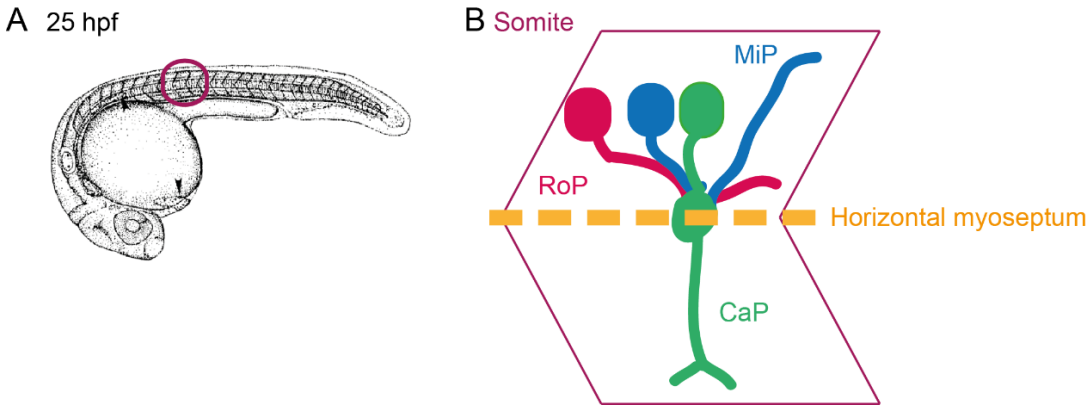

Figure 1.1: The primary motor system in zebrafish embryos at 25 hpf.
A: Illustration of a zebrafish embryo at 25 hpf, in lateral orientation. The red circle indicates the chevron-shaped somites which each contains three primary motor neurons. **B**: A single somite is shown. The RoP (red), MiP (blue) and CaP (green) extend axons along a common path as they exit the spinal cord, until the horizontal myoseptum choice point (dashed yellow line). The primary axons then take divergent paths in the somite. Adapted from Seredick *et al*., 2012.

1.2.2 – The primary motor axon morphology is a classic readout for identifying crucial proteins for axonal growth

The CaP axon of the primary motor neurons have a stereotypical appearance, as well as well-characterised development over time (Myers, Eisen and Westerfield, 1986; Grunwald *et al.*, 1988; Lewis and Eisen, 2003). Because of this, the morphology of the CaP axons has been used as a readout for aberrant gene expression linked to motor neuron development or maintenance, as well as disease models.

Pathfinding by the primary motor axons requires interaction between muscle-derived proteins and axon-expressed proteins. For example, the muscle specific kinase (MuSK) mutant zebrafish *unplugged* exhibit pathfinding errors in the primary axons, demonstrating its necessity for axonal growth (Zhang *et al.*, 2004). Knockdown of

collagen15 leads to branched CaP axons, and the collagen19a1 mutant *stumpy* exhibits axon stalling at the HM choice point (Pagnon-Minot *et al.*, 2008; Hilario, Wang and Beattie, 2010) (Figure 1.2 F, G). Knockdown of *notum*2, a hydroxylase that can cleave GPI-anchored cell signalling proteins and is expressed in the horizontal myoseptum, by morpholino also causes CaP axons to stall at the HM, preventing the axons from exiting the choice point (Cantu, Flowers and Topczewski, 2013). These observations suggest the key contribution of ECM molecules during axon growth, especially at the horizontal myoseptum. Knockdown of axon-expressed proteins also causes morphological changes to the CaP axon, such as morpholino-mediated knockdown of agrin, which causes truncated axons (Kim *et al.*, 2007). Axonal RNA transport and local translation in the growth cone is also vital for correct axon growth, and RNA transport is impaired in SMA (discussed in Section 1.3.2). Knockout mutants of the splicing factor SFPQ have widespread axonal defects, with axons unable to exit the spinal cord, which is rescued when human SFPQ is re-expressed without its nuclear localisation signal (Thomas-Jinu *et al.*, 2017). This paper demonstrates not only the cell-autonomous function of the splicing factor, but also the importance of subcellular localisation.

Changes to the CaP axon morphology have been used as phenotypes for motor neurons diseases including Amyotrophic Lateral Sclerosis (ALS) and Spinal Muscular Atrophy (SMA). Over-expression of mutant SOD1, modelling familial ALS, causes branching and shortening of the primary motor axons (Lemmens *et al.*, 2007) (Figure 1.2 A, B). Knockdown of C9ORF72, associated with ALS, also causes branching of the CaP axons (Ciura *et al.*, 2013). Knockdown of *smn* expression, the causative gene of SMA, also leads to truncated, branching, or missing axons (McWhorter *et al.*, 2003) (Figure 1.2 C, D, E).

Overall, changes to the CaP axon morphology have been used as a readout for disease models, developmental processes, and to find novel pathways.

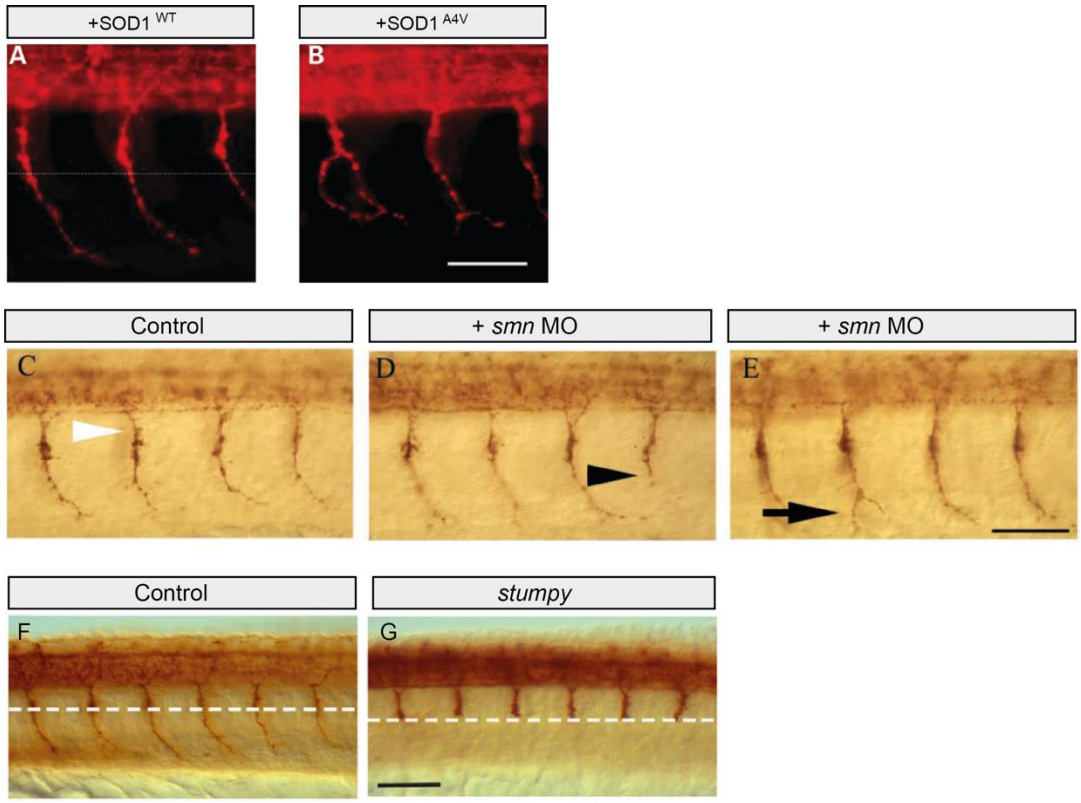

Figure 1.2: Examples of morphological changes to the CaP axon after genetic manipulation. Lateral trunk views of embryos between 24-30 hpf are shown. Axons are labelled with HB9:RFP (A, B) or znp-1 (C-G).
A: Injection of wild-type SOD1 mRNA does not affect the CaP axon. **B**: Injection of mutant SOD1A4V causes bifurcation and branching of the CaP axon. (From Lemmens *et al.,* 2007). **C**: Wild-type embryos show normal CaP axon morphology (White arrowhead). **D, E**: Injection of smn morpholino causes shortened (black arrowhead) or branched (black arrow) CaP axons (From McWhorter *et al*., 2003). **F**: Wild-type embryos show normal CaP axon morphology. **G**: In the collagen 19a1 mutant, stumpy, the CaP axons stall at the horizontal myoseptum (white dashed line). Scale bars = 50 µm

1.2.3 – The secondary motor system in zebrafish

A secondary set of motor neurons differentiate starting at 14 hpf (Kimmel, Warga and Kane, 1994) and begin to extend axons from ~ 33 hpf. The secondary motor neurons have smaller cell bodies and are more numerous than the primary system, which only comprise 3 cells per somite (Babin, Goizet and Raldúa, 2014).

The secondary motor axons follow the path of the primary motor neurons as pioneers, but this is not necessary for axonal growth. Ablation studies demonstrate that although the secondary axons are delayed in the absence of the pioneers, they eventually do extend correctly (Pike, Melancon and Eisen, 1992). After following the vertical myoseptum along the CaP axon trajectory, the secondary motor axons then branch excessively to infiltrate axons onto the myotome and innervate the musculature. The primary axons also branch after reaching their targets, but this is less extensive than secondary axon branching (Babin, Goizet and Raldúa, 2014). Similarly to the primary motor axons, changes to the secondary axons can be quantified after mutations or exposure to toxic stimuli. For example, secondary motor axon outgrowth is impaired after nicotine exposure (Menelaou and Svoboda, 2009). An miRNA model of SMA shows a reduction in axonal branching and aberrant pathfinding by the secondary motor axons (Laird *et al.*, 2016).

The zebrafish larvae hatch from their chorions between 2 and 3 dpf. At this stage, the zebrafish do not freely swim, but exhibit spontaneous burst movement. They can also perform escape behaviour in response to vibratory or touch stimuli (Budick and O'Malley, 2000; Bhandiwad *et al.*, 2013). This escape response has been widely used to quantify functional changes to the zebrafish motor and sensory circuit. For example, after spinal lesion, the ability to escape from a tail stimulus is lost, but upon recovery of the axons across the lesion site, functional behaviour and swimming is restored (Wehner *et al.*, 2017; Tsarouchas *et al.*, 2018). Zebrafish with mutations to their neuromuscular junctions, such as AChR and rapsyn mutants, are also either completely paralysed or unable to maintain swimming when touched (Ono *et al.*, 2001, 2002; Fetcho, Higashijima and McLean, 2008).

As well as the distance covered during an escape flight, larval zebrafish turn from a startle stimulus using a highly stereotypical C-bend, where the trunk contracts to allow the head to touch the tail to induce a turn of ~180° (Bhandiwad *et al.*, 2013). The contraction is induced by the Mauthner cells, two large reticulospinal cells which

induce all motor neurons on the contralateral side of the trunk to contract (Kohashi and Oda, 2008). *space cadet*, a zebrafish hindbrain mutant, cannot induce this turning motion correctly, instead performing several C-bend turns in succession, leading to a spiralling swimming pattern (Lorent *et al.*, 2001). The SMA model zebrafish described in Hao *et al.*, 2013 also demonstrates motor deficits, with a reduction in the swim distance at 5 dpf compared to wild-types, and a reduction in body curvature during swimming.

1.2.4 – Synaptogenesis in zebrafish and mammals

1.2.4.1 – Synapse formation in zebrafish

Synaptogenesis in zebrafish and mammals share many similarities in terms of signalling pathways and pre-and post-synaptic proteins. These include muscle-expressed factors such a muscle-specific kinase (MuSK), acetylcholine receptors (AChRs) and rapsyn, and axon-expressed proteins such as agrin.

Pre-patterns of acetylcholine receptors, which will form the post-synaptic puncta, form clusters in the muscle before the axons exit the spinal cord. The pre-patterns form from around 16 hpf onwards (Flanagan-Steet *et al.*, 2005), while primary axons extend from 19 hpf (Westerfield and Eisen, 1988). The pre-patterns form along the vertical myoseptum, the same path that the CaP axon will extend along, (Panzer, Song and Balice-Gordon, 2006) (Schematic shown in Figure 1.3 A).

The pre-patterning of AChRs in zebrafish is dependent on the muscle-specific kinase (MuSK). In the MuSK mutant zebrafish *unplugged*, the pre-patterns remain scattered on the muscle fibres, and do not form into a clustered pre-pattern along the middle of the myotome as is seen in wild-types (Jing *et al.*, 2009). As the motor axon extends from the spinal cord, the growth cone filopodia are preferentially stabilised upon contact with AChRs on the muscle. This means that axonal pathfinding tends to follow these pre-patterns as pioneers (Panzer, Song and Balice-Gordon, 2006). As well as the axon becoming stabilised by the presence of AChRs, the AChRs are also stabilised by the motor axons. Aneural AChRs not contacted by axons are eventually dispersed, but the clusters contacted by axons become stabilised and do not (Figure 1.3 B,C) (Flanagan-Steet *et al.*, 2005). These are known as *en passant* synapses, as

they continue to remodel as the axons pass over them, and the co-localisation of pre- and post-synapse improves over time. Although initially elongated, the AChRs become more punctate and condensed over time (Panzer *et al.*, 2005) (Compare Figure 1.3 B and C).

The further stabilisation of the post-synapse after axonal contact, to form mature synapses, requires both muscle-derived and neuron-derived signal proteins, such as agrin in the axon (Wu, Xiong and Mei, 2010). In morpholino-mediated knockdown of agrin, zebrafish embryos form AChR pre-patterns, but they are not stabilised, and the AChR clusters disperse after axonal growth (Kim *et al.*, 2007). However, zebrafish *unplugged* mutants still develop synapses, although the larvae have reduced numbers of, and smaller sized, post-synaptic puncta, showing that it is dispensable in zebrafish (Zhang *et al.*, 2004). As well as stabilising the pre-patterned AChR clusters, zebrafish can spontaneously induce synaptic sites, (Flanagan-Steet *et al.*, 2005; Panzer *et al.*, 2005) which explains why the *unplugged* mutants are able to form a few synapses.

There is a close relationship between axonal pathfinding and synaptogenesis in zebrafish. The mutant *unplugged* exhibits axonal pathfinding defects, including stalling of the CaP axon at the HM with excessive branching, and aberrant pathfinding of the RoP axon (Zhang *et al.*, 2004). MuSK signalling induces expression of ECM molecules in axonal pathfinding choice points including the horizontal myoseptum, for example u*nplugged* mutants do not express Tenascin-C, an ECM molecule important for the correct axonal pathfinding (Schweitzer *et al.*, 2005). The Collagen19a1 mutant *stumpy*, whose primary axons stall at the horizontal myoseptum (Hilario, Wang and Beattie, 2010), exhibit reduced number of synapses in larval stages (Panzer *et al.*, 2005).

In larval zebrafish, when the secondary axons have differentiated and extended motor axons, the axons begin to branch and innervate the myotome outside of the ventral axon bundle (Figure 1.3 D, E). Pathfinding of these branches does not require pre-patterning of AChR clusters (Panzer, Song and Balice-Gordon, 2006). Further zebrafish mutants have indicated proteins required for correct synapse stabilisation. For example, the rapsyn mutant *twitch once* is unable to correctly initiate an escape swim when startled, due to diffuse AChR clusters which leads to reduced motility (Ono *et al.*, 2002). Rapsyn is a scaffolding protein which stabilises the post-synaptic density on the muscle fibres. Defects in rapsyn have been linked to myasthenic syndrome in

humans (Ohno *et al.*, 2002). Rapsyn requires acetylcholine receptors for the protein to be transported from the Golgi apparatus to the synapse (Ono *et al.*, 2001; Park *et al.*, 2012).

As well as the link between pathfinding and synaptogenesis, we hypothesise that there is a link between motor axon branching and synaptogenesis. In *Xenopus* motor axons, pre-synaptic puncta are required to stabilise nascent motor branches, and branches tend to extend from synaptic sites (Javaherian and Cline, 2005). Retinal ganglion cells (RGCs) in both zebrafish and *Xenopus* also exhibit a similar requirement for synapses to stabilise extending dendrites. In RGCs, pre-synaptic puncta are required in order to stabilise nascent dendritic arbours, which retract without the presence of these pre-synaptic proteins. Branches also emerge from pre-synaptic sites on the trunk of the axon (Meyer and Smith, 2006; Ruthazer, Li and Cline, 2006).

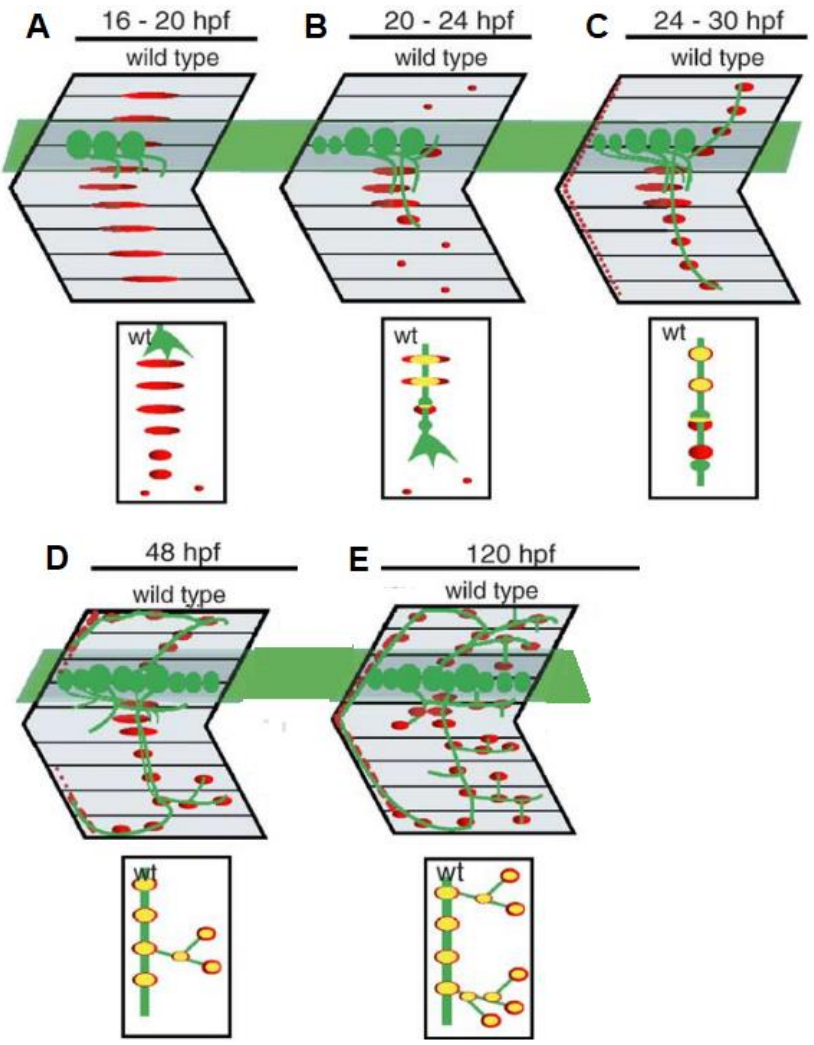
A
16 - 20 hpf
wild type
wt
B
20 - 24 hpf
wild type
wt
C
24 - 30 hpf
wild type
wt
D
48 hpf
wild type
wt
E
120 hpf
wild type
wt

Figure 1.3*:* Synaptogenesis in the wild-type zebrafish motor system.
At each time-point, a single somite of the trunk is shown from a lateral view, with a higher magnification view in the bottom box. Motor neurons are green, AChRs in the post-synapse are red, and co-localisation is yellow. **A**: Between 16-20 hpf, before motor axons exit the spinal cord, the AChRs form aneural pre-patterns on the muscle. **B**: Between 20-24 hpf, the AChRs contacted by axons are stabilised but remain larger than the pre-synapse on the axon, while the aneural clusters begin to disperse. **C**: From 24-30 hpf, the axons have grown to the edges of the myotome. Pre- and post-synapse proteins are being remodelled into co-localised synaptic puncta. **D**: At 48 hpf, the axons are slightly branched into the muscle and the synaptic compartments are tightly co-localised. **E**: At 120 hpf, the motor axons are highly branched into the myotome and have co-localised puncta of the pre- and post-synaptic compartment. Adapted from Panzer *et al.,* 2005.

1.2.4.2 – Similarities and differences in mammalian synaptogenesis

Mammalian motor synaptogenesis share several key features with the process in zebrafish, but there are some key differences. Similarly to zebrafish, the muscle forms AChR pre-patterns on the muscle fibres before the motor axon contacts the muscle (Figure 1.4 A) (Wu, Xiong and Mei, 2010). These pre-patterns assemble without any axonal signalling, although their stabilisation requires axonal factors including agrin, and will dissipate if not innervated (Darabid, Perez-Gonzalez and Robitaille, 2014) (Figure 1.4 B).

MuSK is necessary for post-synaptic differentiation in mammals, where it recruits rapsyn and AChR to the post-synaptic density after agrin signalling from the axon MuSK-null mice do not form neuromuscular junctions and die at birth due to an inability to breathe (Burden, 2002). This is dispensable in zebrafish, where MuSK mutants do eventually form synapses, albeit smaller and fewer in number (Zhang *et al.*, 2004). Agrin-null mice do not develop NMJs and die at birth (Gautam *et al.*, 1996). There is a reciprocal relationship between agrin and the neurotransmitter acetylcholine, as double-mutant mice for agrin and ACh develop synapses (Misgeld *et al.*, 2005). Ectopic expression of MuSK in mice promotes synapse formation and can rescue the lack of synapses normally observed in agrin-null mice. Increased levels of MuSK also promote axonal growth, causing excessive axonal branching across the muscle (Kim and Burden, 2008).

Comparing Figure 1.3 and Figure 1.4 shows that there are clear similarities between zebrafish and mammal synapse formation, including shared pathways. The faster genetic manipulation and increased ability to image zebrafish larvae over mouse muscle makes studies of zebrafish synapses a useful tool.

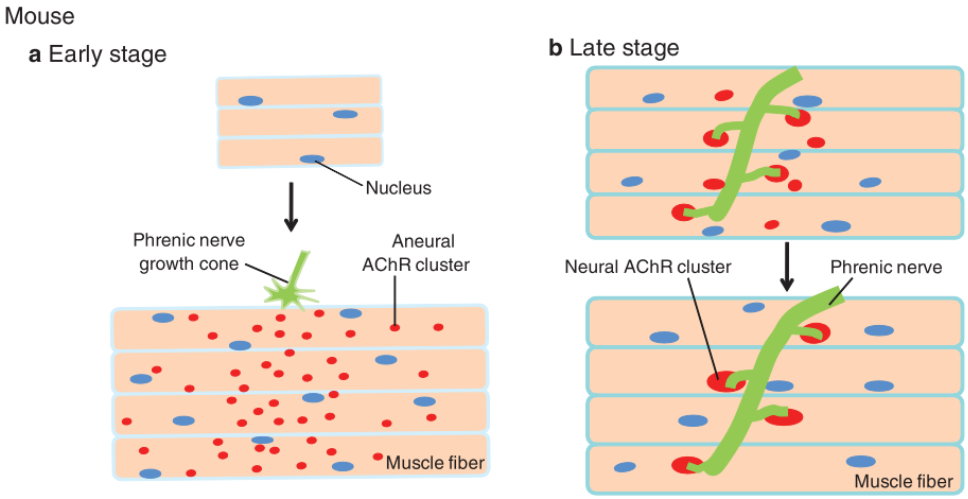

Figure 1.4: Mouse synaptogenesis and stabilisation.
A: At early stages, the muscle fibres for small, scattered pre-patterns of AChRs before the arrival of the nerve growth cone. **B**: At later stages, after the muscle fibres become innervated, the AChR clusters contacted by the axon are stabilised and grow in size, while the aneural clusters disappear. (From Wu *et al*., 2010).

1.3 – Spinal Muscular Atrophy is an inherited, childhood form of motor neuron disease

1.3.1 – The genetics of Spinal Muscular Atrophy

Spinal Muscular Atrophy (SMA) is an inherited form of motor neuron disease and is the leading cause of inherited child mortality. SMA is monogenic, in that it is caused by loss of function mutations in SMN1, but it exhibits a spectrum of severity due to the presence of a compensatory gene in humans, SMN2 (Lefebvre *et al.*, 1995). The SMN2 is a duplication of SMN1 but contains a single base substitution in exon 7 (C to T) which causes exon 7 skipping during translation (Cartegni *et al.*, 2006). This leads to 50-90% of SMN2 transcripts to be non-functional and thus quickly degraded in all humans, so in normal conditions the optimal cellular dosage of Smn protein is expressed from SMN1. Thus, in the event of SMN1 loss of function, SMN2 is unable to compensate with the right expression level of Smn. The reduced level of Smn protein leads to SMA. The severity of SMA is determined by the number of copies of SMN2 and thus the spectrum of SMN protein level which is able to be translated from the SMN2 (Lunn and Wang, 2008). Other primates including chimpanzees do not have SMN1/SMN2, but rather multiple copies of the same SMN gene, demonstrating that the divergence and C to T mutation came very late in human evolution (Rochette, Gilbert and Simard, 2001). Mice, zebrafish, fruit flies and yeast also have only one copy of SMN.

Complete loss of function of SMN1 and SMN2 in humans is embryonically lethal, and complete knockout in animal models also causes embryonic lethality. For example, mice homozygous for SMN knockout do not develop much beyond the implantation stage and exhibit massive cell death within 4 days of the mouse mating (Schrank *et al.*, 1997). Zebrafish homozygote knockouts have an average survival of just 12 days post fertilisation (Hao *et al.*, 2013). Therefore, in animal models of SMA, either gene knockdown or knockout combined with low-level expression of the human form of SMN2 is used (McWhorter *et al.*, 2003; Hao, Burghes and Beattie, 2011; Sleigh *et al.*, 2014).

1.3.2 – The functional role of SMN

SMN is ubiquitously expressed in all model systems and is necessary for cell survival in all tissue types. SMN is involved in splicing, forming part of a complex known as the spliceosome (Kolb, Battle and Dreyfuss, 2007). There is also increasing evidence that SMN is vital for bioenergetic and protein homeostasis in the cell (Chaytow *et al.*, 2018). In an SMA mouse model, an increased oxidative stress and fragmented mitochondria were observed before the onset of motor symptoms (Miller *et al.*, 2016), and changes to mitochondria and energy requirement were observed in zebrafish with *smn* knockdown (Boyd *et al.*, 2017). SMN also has vital roles in the ubiquitin pathway, interacting with UBA1 (Wishart *et al.*, 2014).

SMN is named for *survival of motor neuron*, as despite its ubiquitous expression and function as a housekeeping protein, motor neuron cells are selectively vulnerable to the reduced level of SMN (Burghes and Beattie, 2009; Ling *et al.*, 2012; Boyd and Gillingwater, 2016). Motor neurons may be vulnerable due to the role of SMN in RNA transport and local translation in the growth cones of motor neurons (Dombert *et al.*, 2014; Fallini *et al.*, 2016). A tissue-specific model of SMA in zebrafish demonstrates that reduction in motor neuron Smn levels causes axonopathy, but reducing muscle expression does not (Laird *et al.*, 2016). Widespread splicing defects have been reported in SMA model mice, especially in the spinal cord (Zhang *et al.*, 2008), although some evidence suggests that this may be a consequence of late-stage disease pathology rather than a causative of the degeneration (Bäumer *et al.*, 2009). However, at early stages in severe SMA mouse models, before the onset of motor symptoms, several genes are already dysregulated, including chondrolectin. Chondrolectin is down-regulated by a fold change of 1.7 at p7, and shows a shift in the ratio of its isoforms in SMA mice compared to wild-type (Bäumer *et al.*, 2009). Given that this down-regulation is observed prior to motor symptoms, it suggests that chondrolectin could be a key gene affected by SMN dysfunction and thus contributes to the motor pathology (discussed in detail in this chapter, Section 1.4.3).

1.3.3 – SMA pathology is linked to neuromuscular junction dysfunction

As previously discussed, although SMN protein is ubiquitously expressed and required for splicing in all cell types, the motor neurons are specifically vulnerable to loss of SMN. Several mechanisms have been proposed for this vulnerability, including defects in spliceosome and snRNP assembly (Burghes and Beattie, 2009). Other suggested mechanisms include failures in axonal transport of RNA (Fallini *et al.*, 2016), or the higher energetic requirement of motor neurons to generate neuromuscular signals (Lefebvre *et al.*, 2004; Miller *et al.*, 2016; Boyd *et al.*, 2017). SMN protein has also been observed localised to the motor terminal of the axon, suggesting a local role in the neuromuscular junction (NMJ) (Dombert *et al.*, 2014). In particular, deficits to the NMJ are a key feature of SMA pathology, both in symptomatic stages with degeneration to the NMJ, as well as pre-symptomatically (Kariya *et al*., 2008). These pre-symptomatic defects to the NMJ are of particular interest, as they suggest that rather than a purely degenerative disease, SMA patients exhibit developmental changes to their motor neurons and so early intervention by therapeutics is key. As well as a putative target for further investigations into the disease mechanism, this also suggests potential therapeutic targets.

In human Type I SMA patients, motor symptom onset occurs before 6 months of age, with the average lifespan less than two years (Lunn and Wang, 2008). In foetal tissue of Type I SMA patients, neurofilament accumulation is observed in the neuromuscular junctions, and there is a failure of the pre-synapse to fully occupy the post-synaptic compartment (Martínez-Hernández *et al.*, 2013). This demonstrates that aberrant changes to the NMJ are quantifiable during development. This aggregation of neurofilament was confirmed in diaphragm muscle samples donated from human SMA Type I patients, as well as poor arborisation of the motor terminals (Kariya *et al.*, 2008). In both papers, there is also a weakening of the post-synaptic signal, suggestive of an instability of the post-synaptic density as it is not maintained. Immaturity of the post-synapse is also present in SMA patients, quantified by an increase in foetal forms of AChR and smaller post-synaptic density (Harding *et al.*, 2015). These defects suggest that in human SMA patients, there is arrest of delay in the maturation of the NMJ. SMN is required for the maturation of the NMJ, as an inducible mouse model of SMA showed that inactivation of SMN before the full

maturation of NMJs (p17) caused defects in the pre- and post-synapse (Kariya *et al.*, 2014). This study also demonstrated that inactivation of SMN after NMJ maturation did not cause degeneration directly but made those NMJs more vulnerable to damage by crush injury, as well as impaired recovery. Similarly to the foetal human tissue, which exhibited neurofilament accumulation (Martínez-Hernández *et al.*, 2013), the same NF accumulation is observed in mouse pre-synapses (Kariya *et al.*, 2008), along with bulb-like axon terminal which cannot correctly occupy the post-synaptic density. However, axonal growth and pathfinding does not appear to be impaired, as normal axon extension is observed in severe SMA mouse models (Mcgovern *et al.*, 2008). However, the NMJ occupancy by the axon is impaired, even though the axon reaches its muscle target.

It is established that in the mid- and late-symptomatic stages of disease in mice models of SMA, there is NMJ pathology including withdrawal of the pre-synaptic terminal and shrinkage of the post-synapse, and this is also observed in early symptomatic stages of the most vulnerable muscle groups (Murray *et al.*, 2008). Electrophysiology data in mouse models of SMA also demonstrates functional defects in diseased NMJs. The NMJ excitability is affected in SMA, as mouse neuronal culture of healthy and SMA mice demonstrate reduced Ca^{2+} channel clustering and reduced calcium transients (Jablonka *et al.*, 2007). Impaired synaptic vesicle release is observed in mouse electrophysiology data (Kong *et al.*, 2009). SMN is required for organisation of the active zone of the motor synapse. This includes microtubule and synaptic vesicle maturation, and synaptic vesicle recycling (Torres-Benito *et al.*, 2011).

A zebrafish SMA model also exhibits pre-synaptic deficits, labelled with SV2 (Boon *et al.*, 2009). The SV2 staining in 11 dpf larvae is reduced compared to controls, but the post-synaptic labelling remains intact, leading to a decrease in co-localisation of the two labels. This reduction is SV2-specific, with synaptotagmin labelling unchanged between controls and mutants. Introduction of the human *SMN2* gene in these mutant zebrafish extended their lifespan by several days, and rescued the synaptic defects for these days, although the loss of SV2 staining re-emerged by the time these mutants died (Hao, Burghes and Beattie, 2011). This demonstrates that zebrafish models of the disease recapitulate certain synaptic defects associated with SMA.

1.3.4 – Current therapies available or in development to treat SMA

SMA is considered a rare disease, with incidence of 1 in 10000 live births (Lunn and Wang, 2008), and similarly to other MNDs such as ALS has limited treatment options. Currently, only one therapy has been approved for use in SMA, nusinersen, which is an antisense oligonucleotide (ASO).

Nusinersen, as an antisense oligonucleotide, functions by binding to the SMN2 mRNA, preventing the skipping of exon 7 (Rigo *et al.*, 2012). This decreases the proportion of *SMNΔ7* and the proportion of normal SMN protein increases. After undergoing multiple clinical trials, nusinersen was approved for use in Type I SMA (Swoboda *et al.*, 2016; Finkel *et al.*, 2017). However, ASOs have a high production cost, due to the frequency of treatment and lifelong treatment requirements. Nusinersen must be administered 4 times in the first 2 months of treatment, followed by doses every 4 months, potentially for life, and long-term studies have not yet been performed. In its appraisal, NICE estimated a cost of approximately £450,000 per patient for the first year of treatment, and £225,000 for subsequent years, as the baseline level of nusinersen must be maintained in the spinal cord to modify the splicing of all transcribed SMN mRNAs. It is for these reasons NICE rejected nusinersen for use by the NHS in England and Wales (NICE, 2018). There is thus an unmet need for further compounds to treat SMA or supplement the treatment by nusinersen.

Before the development of nusinersen, there were attempts to repurpose existing drugs for use in SMA (Calder, Androphy and Hodgetts, 2016). The splicing error in *SMN2* leads to a high proportion of its transcript being degraded, as exon 7 is skipped. However, some transcripts are successfully spliced and thus produce full-length SMN protein (Cartegni *et al.*, 2006). The repurposed drugs included epigenetic modulators such as trichostatin A or valproic acid, which are HDAC inhibitors. The rationale was to increase levels of SMN by increasing the expression of *SMN2* despite its large proportion of defective transcripts. This approach is known as SMN-dependent. Although *SMN2* transcription levels increased after HDAC inhibition in patient cell cultures and mice (Tsai *et al.*, 2008; H. Liu *et al.*, 2014), HDAC is involved in multiple processes and its inhibition could affect other key genes. It thus would affect *SMN2* in an indirect way. Riluzole, a neuroprotective compound approved for ALS, was also

trialled in SMA patients. Riluzole prolongs survival of ALS patients by two or three months (Miller, Mitchell and Moore, 2012), but in a phase I trial with SMA patients, mean survival increased but the sample size was too small for statistical testing (Russman, Iannaccone and Samaha, 2003).

Potential treatments have been developed to specifically target SMN2; either to increase its transcription rate, to increase the proportion of transcripts which include the exon 7, or to stabilise the SMN protein to increase its lifespan in the cells (Calder, Androphy and Hodgetts, 2016). One example was discovered through a large-scale screen performed in mouse motor neuron cell culture, to determine compounds which increase the SMN expression (Jarecki *et al.*, 2005). A class of hits were identified, 2,4-Diaminoquinazolines, and derivatives of the structural family were further trialled (Thurmond *et al.*, 2008). Although the best compound, RG3039, showed increased survival of SMA mouse models (Gogliotti *et al.*, 2013), it has not been passed into clinical trials due to the acquisition of the rights by Pfizer Inc., who terminated further work into the compound.

Several other potential treatments are undergoing clinical trials at different phases, mostly focused on SMA Type I as this is the most severe form (Shorrock, Gillingwater and Groen, 2018). A viral vector delivering an enhanced *SMN1* through the blood-brain barrier to neurons, AVXS-101, is currently entering a Phase 2 trial after success in Phase 1 (Shell *et al.*, 2018). After a high-throughput screen to find compounds which caused specific increases in the SMN2 transcript, Roche identified a compound called RG7800 which showed promising results pre-clinically but failed in human trials. After extensive structure refinement, risdiplam (RG7916) has been designed with improved pharmacokinetics. This compound is now entering part 2 of its first clinical trials (Ratni *et al.*, 2018). A neuroprotective compound, olesoxime, which increases the stability of the mitochondria to resist stress, has recently shown to be safe and shows efficacy in Type 2 and 3 SMA patients in Phase 1 trials (Bertini *et al.*, 2017).

1.4 – Chondrolectin

1.4.1 – Chondrolectin is a transmembrane protein containing a C-type lectin domain

Structural domains determined from the chondrolectin sequence predicts a single-pass type I transmembrane domain and a carbohydrate recognition domain, known as a C-type lectin domain (CTLDs). C-type lectin domains require Ca^{2+} to bind carbohydrates, and are often found in proteins which interact with glycoproteins (Zelensky and Gready, 2005; Cummings and McEver, 2017). CTLDs also have an important role in immunity, as leukocytes express a class of adhesion molecules called selectins which aid their movement around tissues during infection surveillance (Rini and Leffler, 2010; Mayer, Raulf and Lepenies, 2017). Dectins recognise fungal proteins during infection and signal to induce cytokine release (Yan, Ohno and Tsuji, 2013; Dambuza and Brown, 2015).

Further structural domains for chondrolectin have been predicted from their sequence motifs (UniProt: Q568T5, https://www.uniprot.org/). This includes an N-terminal signal peptide (1-20aa) followed by the C-type lectin (38-187aa). The transmembrane domain spans aa position 239-266, and the C-terminus contains a short, 30aa intracellular domain (267-296 aa). A schematic of zebrafish chondrolectin is shown below, Figure 1.5.

Figure 1.5: Schematic of the protein domains of zebrafish chondrolectin. Chondrolectin is a 296 aa sized protein, comprising of a signal peptide (SP), C-type lectin domain (CTLD), transmembrane domain (TMD) and intracellular domain (ID). Adapted from Zhong et al., 2012 and www.uniprot.org, Q568T5

Publications examining the protein interactions, or the function of each structural domain, are scarce for chondrolectin. Chondrolectin's closest homologue, layilin (45% homology), also contains a lectin domain and functions as a cytoskeleton protein. Layilin was identified as a hyaluronan receptor via its lectin domain (Bono *et al.*, 2001), but researchers were unable to detect any interaction between chondrolectin and hyaluronan (Weng *et al.*, 2002). There is no known binding partner of the C-type lectin domain in chondrolectin published. A zebrafish mutant for collagen XIXaI, *stumpy*, phenocopies the morphant and mutant to chondrolectin, suggesting a functional link between the proteins (Hilario, Wang and Beattie, 2010).

The transmembrane domain is a single pass, type I transmembrane domain. Although the transmembrane domain and C-type lectin domain are most commonly associated with ECM interactions at the cell surface, previous published papers show perinuclear signal of chondrolectin. In Weng *et al*., 2002, transfected cells with HA-tagged chondrolectin show a strong perinuclear signal using a monoclonal HA antibody, with further punctate signal in the cytoplasm and plasma membrane of the transfected cells. An anti-chondrolectin antibody was generated for Western blotting in that paper, and later used in Enjin *et al*, 2010. Chondrolectin immunohistochemistry in mouse motor neurons showed wide immunofluorescence in the cytoplasm and it was excluded from the motor neuron nuclei. However, there is no published antibody to chondrolectin that is validated in zebrafish, and custom antibodies to chondrolectin did not give any specific signal. The subcellular localisation of chondrolectin, and its mechanism in the cell, is thus a key unanswered question which we investigated during this thesis.

The intracellular domain of chondrolectin is a short helical chain with no structural motifs, 30 amino acids in length. The only published study of this domain is the one by Claessens, Weyn and Merregaert, 2008, in which an Sos recruitment screen of this domain was used to pull down binding proteins. The protein isolated was Rab geranylgeranyl transferase β (Rabggtb), a protein that associates with Rab GTPase to prenylate it for its association with the plasma membrane. The paper does not hypothesis if the Rab geranylgeranyl transferase binds as part of the function of chondrolectin but posits that chondrolectin could stabilise the Ranggtb during its catalytic prenylation of the Rab GTPase. 12/30 (40%) of the residues are serine or threonine, which means a high proportion of this domain can be phosphorylated. This suggests that chondrolectin acts as a signalling molecule, where its C-type lectin

domain binds a target ligand in the ECM and a phosphorylation-dependent change occurs via the C-terminal intracellular domain.

1.4.1.1 – The human and mouse chondrolectin has several isoforms, caused by alternative splicing, while zebrafish have only one isoform

Zebrafish chondrolectin has only a single isoform and has a high homology with the human and mouse chondrolectin, with 92% sequence identity to the canonical sequences of both mouse and human chondrolectin (Zhong *et al*., 2012). There are multiple human and mouse splice isoforms of chondrolectin, however, and their localisation and the amount of information about their function is varied. An alignment across species and isoforms is shown below (generated using UniProt's alignment tool, Figure 1.6). For example, Figure 1.6 A shows all 4 isoforms of human chondrolectin and the 3 mouse isoforms aligned with the single zebrafish protein sequence. However, two of the human isoforms of chondrolectin are not expressed in the spinal cord and so do not contribute to the function of chondrolectin in the motor neurons. These isoforms, known as chodl_F and chodl_FΔE, are instead expressed by lymphocytes and involved in the maturation of T-cells (Weng *et al*., 2003, Claessens *et al.,* 2007), and neither isoform contains the signal peptide sequence. Human chodl_FΔE also lacks most of the transmembrane domain seen in other isoforms, demonstrating it is soluble (Claessens *et al*., 2007). The C-type lectin domain is frequently observed as a recognition domain in proteins in the immune system (Zelensky and Gready, 2005.), which supports the potential role of these isoforms in T-cells. The mouse splice isoform known as Chodl-003 is also not detected in the spinal cord, and its function and localisation is unknown (Sleigh *et al*., 2014).

Focusing on the isoforms which have been detected in cells in the spinal cord, the alignment of these protein sequences is duplicated in Figure 1.6 B for clarity. These isoforms share the common protein domains of a signal peptide, C-type lectin domain, and transmembrane domain. Of the two mouse isoforms, Chodl-001 shows the most homology with both the human and zebrafish orthologues of chondrolectin (Sleigh et al., 2014). The two isoforms also show a differential rate of expression in the spinal cord, and in severe SMA model mice, RT-PCR shows downregulation of Chodl-001 but not Chodl-002 at p7 and p13 (Bäumer et al., 2009). The link between chondrolectin and SMA is discussed in more detail in Section 1.4.3. Chodl-001 and Chodl-002 differ in their intracellular, C-terminal sequence, where Chodl-002 has 19

more amino acids in the intracellular domain than either the human or other mouse isoform. However, there is no published data on the potential differences in mechanism that these extra residues may have, or other differences between these two isoforms. From these alignments, there is a high degree of homology between the zebrafish and mammal orthologues of chondrolectin, especially in the negative- or positive-charged properties of the residues, or their hydrophobicity. However, the zebrafish protein sequence contains an extra 9 amino acids in the C-type lectin domain compared to all mammal isoforms, and also contains an extra 14 amino acids in the extracellular region between the C-type lectin domain and the transmembrane domain. It is not known what effects, if any, these extra residues have on the function of the protein, or if they are an artefact of the difference between teleosts and mammals.

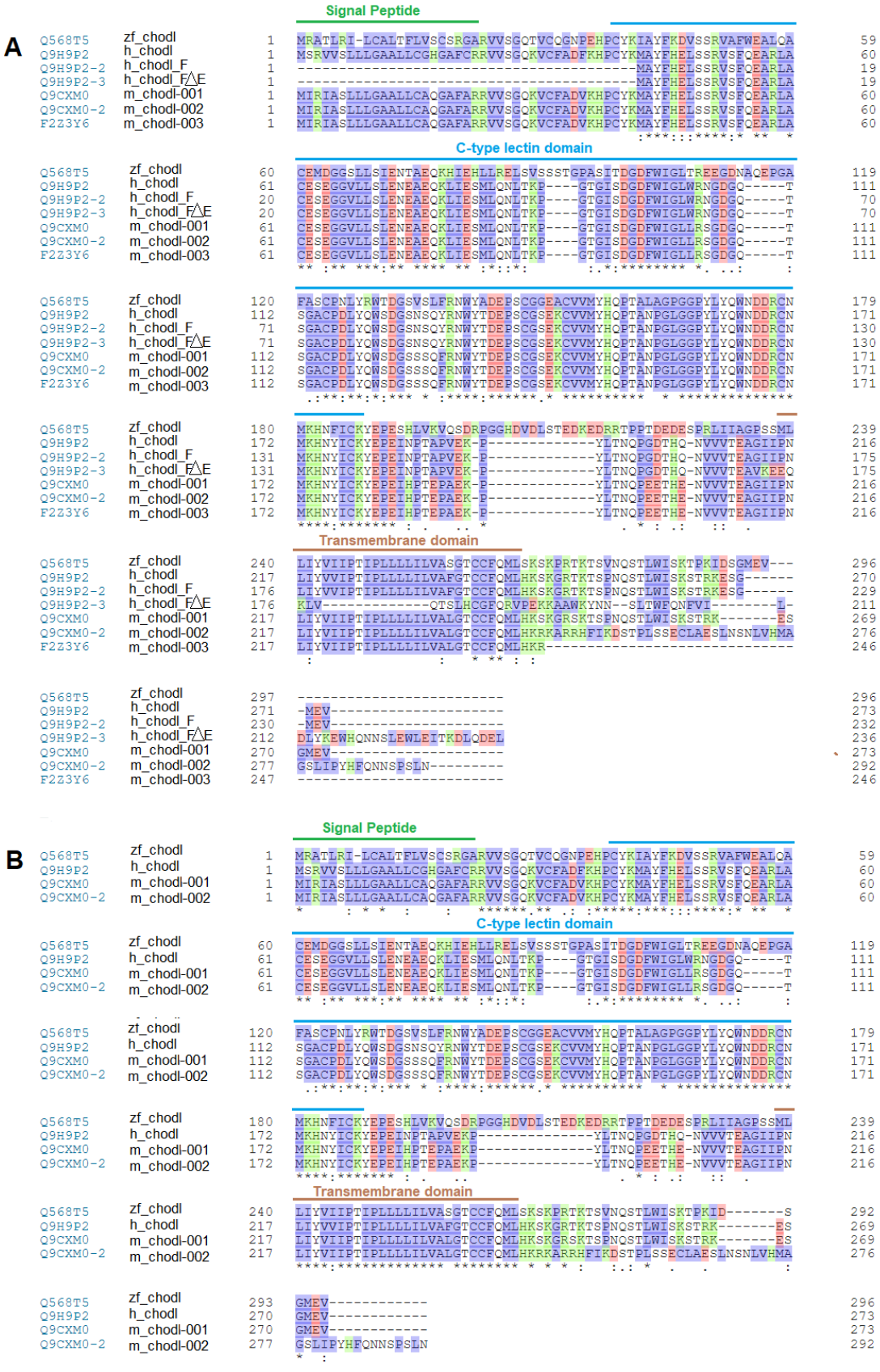
A
Signal Peptide
C-type lectin domain
Transmembrane domain
B
Signal Peptide
C-type lectin domain
Transmembrane domain

Figure 1.6: Protein sequence alignments for the multiple isoforms of chondrolectin across zebrafish, human, and mouse.
For all alignments, the UniProt code and then the species/isoform title is shown. The starting and ending amino acid number for each line is shown, and the proteins domains are labelled above the amino acid sequence. The residues are coloured according to their properties (blue= hydrophobic, red= negatively charged, green= positively charged). The symbol under the alignment identifies similarity between residues across isoforms, where * indicates an identical, conserved residue. A : (colon) indicates a strongly similar properties but not complete conservation of residues, and . (period) indicates
A: Alignment of all isoforms of chondrolectin. zf_chodl = zebrafish, h_chodl = human canonical chondrolectin, h_chodl_F = human isoform of chodl known as chodl_F, h_chodl_FΔE = human isoform known as chodl_FΔE, m_chodl-001= mouse chondrolectin isoform-001, m_chodl-002= mouse isoform chodl-002, m_chodl-003= mouse isoform chodl-003. **B**: Alignment of the protein sequences of chondrolectin isoforms known to be located in the motor neurons and spinal cord. zf_chodl = zebrafish, h_chodl = human canonical chondrolectin, m_chodl-001= mouse isoform Chodl-001, m_chodl-002= mouse isoform Chodl-002.

1.4.2 – The expression pattern of chondrolectin shows it is highly enriched in motor neurons

Chondrolectin (*chodl*) was first identified during a PCR-based screening for novel genes expressed in neonatal mice during endochondral ossification (bone formation), and thus was named chondrolectin due to this link with bone (*chondro*-) (Weng *et al.*, 2002). Comparison to human expressed sequence tags (ESTs) found homologues in human transcripts, and Chodl was isolated from human testis muscle RNA and then found to be highly expressed in human skeletal muscle, heart, and spleen tissue using Southern and Western blotting (Weng *et al.*, 2002; Weng, Hübner, *et al.*, 2003). Further studies probed motor neuron expression arrays using *in situ hybridisation* in foetal mouse tissue. This analysis found that chondrolectin is highly expressed in motor neurons, and this was verified with immunostaining using a CHODL antibody,

where staining was clustered around the perinuclear region in motor neuron cell bodies. Furthermore, electrophysiology of these CHODL-positive motor neurons suggested that these were the fast-twitch subtype of α motor neurons (Enjin *et al.*, 2010).

In zebrafish, chondrolectin was identified as being highly expressed in motor neurons during axon outgrowth (Zhong *et al.*, 2012). Preventing axon exit from the spinal cord using a dominant-negative cofactor to the LIM homeodomain construct (transcription factors that regulate motor neuron development, DN-CLIM) abolishes the expression of genes which are necessary for axon growth. By comparing the gene expression between control motor neurons and those injected with the DN-CLIM, several genes were identified that were likely to be involved in axon growth. These included *chodl*, *tac1*, and *calca*. *In situ hybridisation* analysis of chondrolectin expression showed detectable expression exclusively in HB9:GFP-positive motor neurons. This ISH expression was detectable from ~12 hpf and was strongly detectable in the spinal cord until at least 60 hpf, which correlates with motor neuron development stages (Figure 1.7). There is also detectable signal in several regions of the brain, including the diencephalon, tectum, and hindbrain.

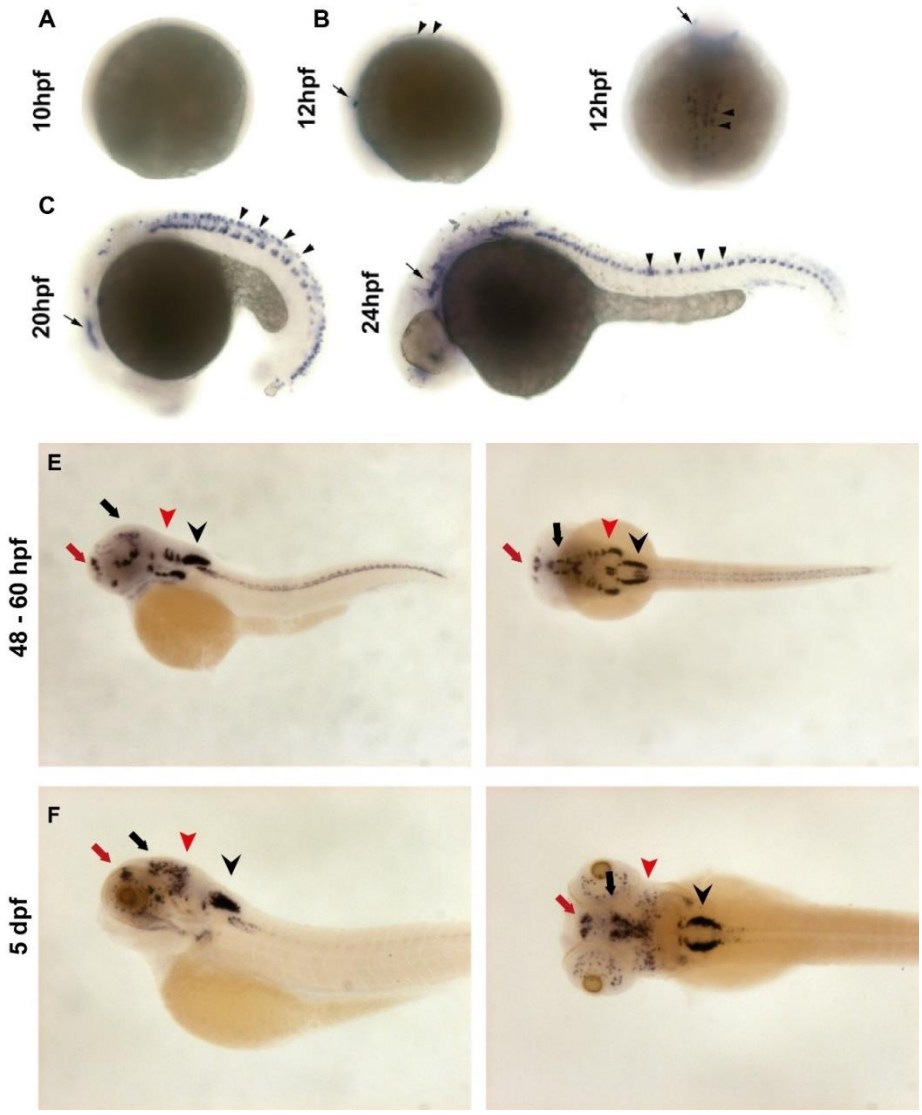

Figure 1.7: *in situ hybridisation* shows the expression pattern of chondrolectin. **A**: At 10hpf, there is no detectable expression of chondrolectin. **B-D**: Arrows show that the trigeminal ganglion contains detectable *chodl* signal. **B**: At 12 hpf, arrowheads show cells in the trunk which are putative motor neurons. **C**: At 20 hpf, the chodl signal is strongly detectable in the trunk, both in motor neurons and dorsal of the MNs (arrowheads). **D**: At 24 hpf, the ISH signal is strongly enriched in motor neurons (arrowheads). (Adapted from Zhong et al., 2012). **E**: Representative images of chodl ISH are shown between 48-60hpf, as a lateral view and a dorsal view. Between 48-60 hpf, there is detectable expression of chodl mRNA in the olfactory bulb (red arrow), diencephalon (black arrow) tectal neurons (red arrowhead), and hindbrain (black arrowhead), as well as in the trunk**. F**: Lateral and dorsal views of a 5 dpf larvae after *chodl* ISH. Detectable signal is observed in the olfactory bulb (red arrow), diencephalon (black arrow) tectal neurons (red arrowhead), and hindbrain (black arrowhead). E & F are taken from Thisse *et al*., 2004.

Morpholino (MO) knockdown of chondrolectin caused stalled motor axons at 24 hpf, confirming its importance during axon growth. In particular, the axons stalled at the horizontal myoseptum (HM), an important choice point during the primary axon growth in zebrafish (Zhong *et al.*, 2012). During normal motor axon growth, all three primary axons extend to the HM, before diverging paths. In wild-type embryos, the CaP axons pause at the HM for around 1 hour, between 21.5 and 22.5 hpf, before extending further (Myers, Eisen and Westerfield, 1986; Westerfield and Eisen, 1988). In the published MO knockdown of *chodl* (Zhong et al., 2012), the CaP axons stall around the horizontal myoseptum (HM) for several hours, and although their growth rate is unchanged from controls, this delay means that many axons are still shorter than controls up to 33 hpf (Figure 1.8).

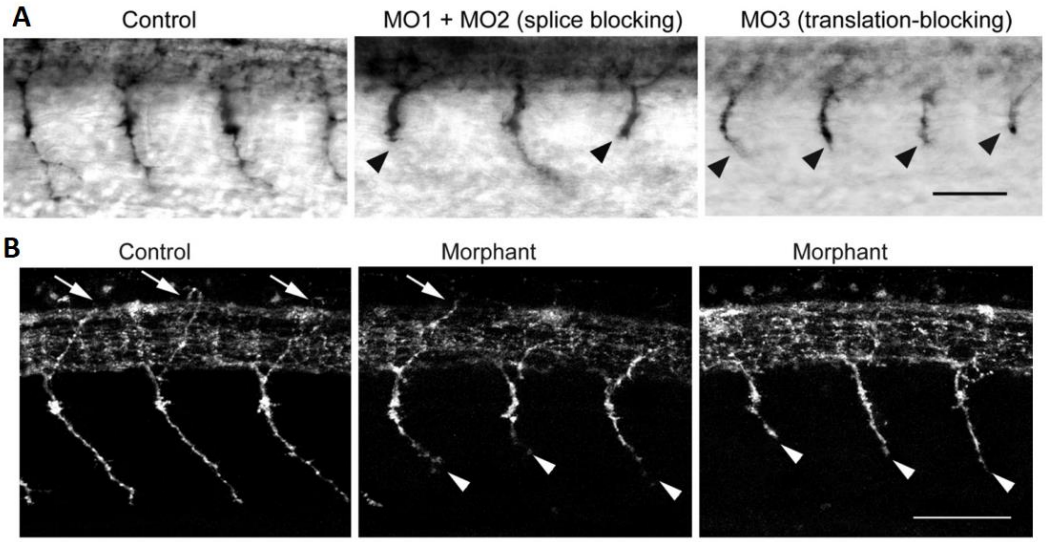

Figure 1.8: Morpholino knockdown of chondrolectin causes stalled CaP axons. **A:** At 24 hpf, the CaP axons have extended past the HM, while chondrolectin morphants show CaP axons stalled at the HM (arrowheads). **B:** At 33 hpf, the CaP axons are shorter than in controls (arrowheads), and some MiP axons have failed to extend (MiPs shown with arrows). Axons were labelled with znp-1 antibody. Scale bars = 50 µm. Adapted from Zhong *et al.,* 2012.

Over-expression of chondrolectin using mRNA injection rescued the morpholino-mediated knockdown, although over-expression alone also resulted in a shorter axon phenotype (Figure 1.9). This suggests that the gene dosage of chondrolectin is tightly

regulated to maintain its correct function in zebrafish motor axons. This technique contains the caveat that mRNA injection is not tissue-specific, and so ectopic expression of chondrolectin in muscle or other tissues could cause the aberrant morphology.

Overall, although Zhong *et al.,* 2012 demonstrated that chondrolectin has a key role in axonal growth, localises mostly to motor neurons, and its expression level in the embryo must be tightly controlled, there are still unanswered questions. The study does not offer any functional data and only speculates on the potential mechanism by which chondrolectin regulates axonal growth, namely that as a transmembrane protein it likely traffics to the cell surface, and its C-type lectin domain may be used in ligand interactions. Functional assays form a key aspect of this thesis, to attempt to address this gap in knowledge. Due to the temporal limit of morpholino of around 3 dpf, there is no behavioural test performed to investigate if the motor axon deficit affects the larval swimming activity. There was also no way to speculate on phenotypes in the adult stage. Another unanswered question that this thesis addresses is any potential effect of chondrolectin knockdown in synapse formation. This is related to the relationship between NMJ defects and Spinal Muscular Atrophy. There are also links between chondrolectin and Spinal Muscular Atrophy, discussed in the next section.

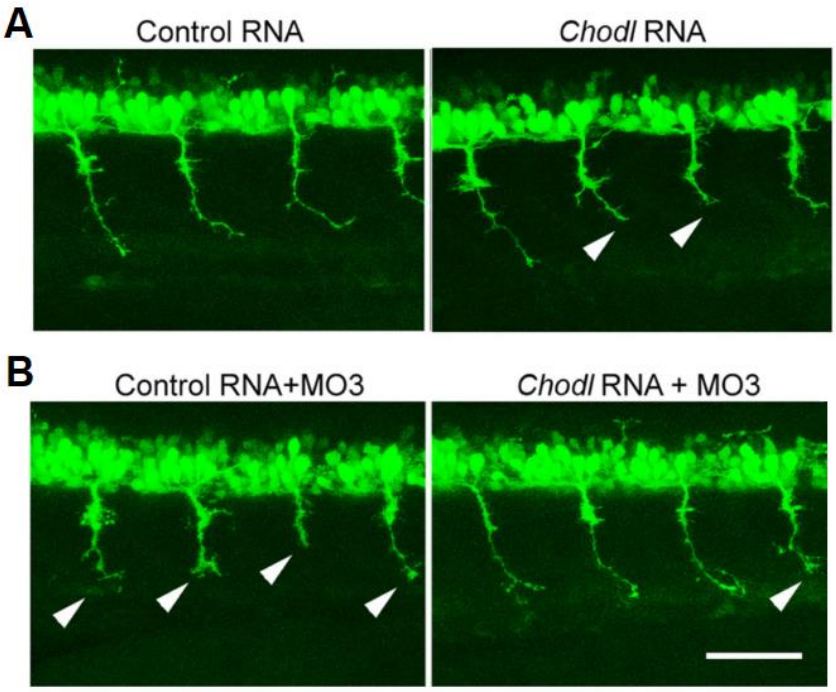

Figure 1.9: Injection of chodl mRNA causes aberrant axons in wild-type embryos and rescues the morpholino knockdown phenotype.
A: In wild-type embryos at 26 hpf, injection of scrambled control mRNA does not change the axon phenotype, but over-expression of chodl mRNA causes shortened axons (arrowheads). **B**: Co-injection of control mRNA and morpholino leads to the morphant phenotype of stalled axons, which co-injection of mRNA and morpholino leads to axons which are closer in appearance to the wild-type (shorter axons indicated with arrowheads). Scale bar = 50 µm. Adapted from Zhong et al., 2012.

1.4.3 – Chondrolectin is a key downstream target of Smn dysfunction seen in SMA models

Due to the complexing of SMN in the spliceosome, and its role in mRNA processing, SMA was hypothesised to lead to splicing defects, and the potentially toxic mis-spliced proteins could contribute to the pathology (Kolb, Battle and Dreyfuss, 2007). Splicing defects are widespread particularly in the brain and spinal cord of SMN-deficient mice, at both the onset of motor symptoms (p6) and at the end-stage of the disease (p11) (Zhang *et al.*, 2008). One of the down-regulated genes in the spinal cord is chondrolectin, suggesting a link between SMN dysfunction and changes to chondrolectin expression. Another study investigated splicing defects before the onset of motor symptoms in the SMA model mice, to investigate if the splicing defects may be causative and contributing to the SMA pathology, or are a consequence of already-degenerating cells (Bäumer *et al.*, 2009). This study demonstrated that most mis-spliced products were late onset, although several transcripts were mis-spliced before the onset of motor symptoms, including confirming chondrolectin mis-splicing and downregulation at p7. Overall, this indicates a potential link between chondrolectin and Spinal Muscular Atrophy.

The link between SMA and dysregulation of chondrolectin has also been observed in a study of miRNAs and their contribution to SMA disease pathology (Wertz *et al.*, 2016). miRNAs are involved in post-transcriptional modification of mRNAs. Profiling mRNA and miRNA expression profiles in SMN knockdown, including human SMA

iPSC-derived motor neurons, identified several miRNAs which are significantly upregulated in neurons. These neurons exhibit shorter neurite lengths, and one miRNA which is upregulated is miRNA-431. Inhibition of miRNA-431 rescues the neurite length, showing its link to axonal growth, and the targets of miRNA-431 include chondrolectin.

Further evidence of a relationship between chondrolectin and Smn comes from the zebrafish. Knockdown of Smn by morpholino leads to aberrations in the primary motor axon, including truncations, branching, and missing axons (McWhorter *et al.*, 2003). This morpholino data is phenocopied in several mutant lines, including one which is *smn* -/- but has human SMN2 expressed as a transgene (Hao, Burghes and Beattie, 2011), and an *smn* -/- mutant which expresses a low level of Smn due to a leaky hsp70:*smn*-RFP transgene (Hao *et al.*, 2013). Crucially, over-expression of chondrolectin by injection of *chodl* mRNA in *smn* knockdown embryos partially rescues the axonal phenotype observed in *smn* knockdown alone (Figure 1.10, below) (Sleigh *et al.*, 2014). This suggests that in *smn* knockdown, at least part of the axonal phenotype may be due to reduction in, or mis-splicing of, the chondrolectin protein. This paper also demonstrates that *in vitro* culture of mouse neuronal cells with SMN knockdown exhibited shorter neurites, and transfection with *chodl* rescues the neurite length. Overall, this validates chondrolectin as a potentially important target for further study, both from its role in development and its link to disease.

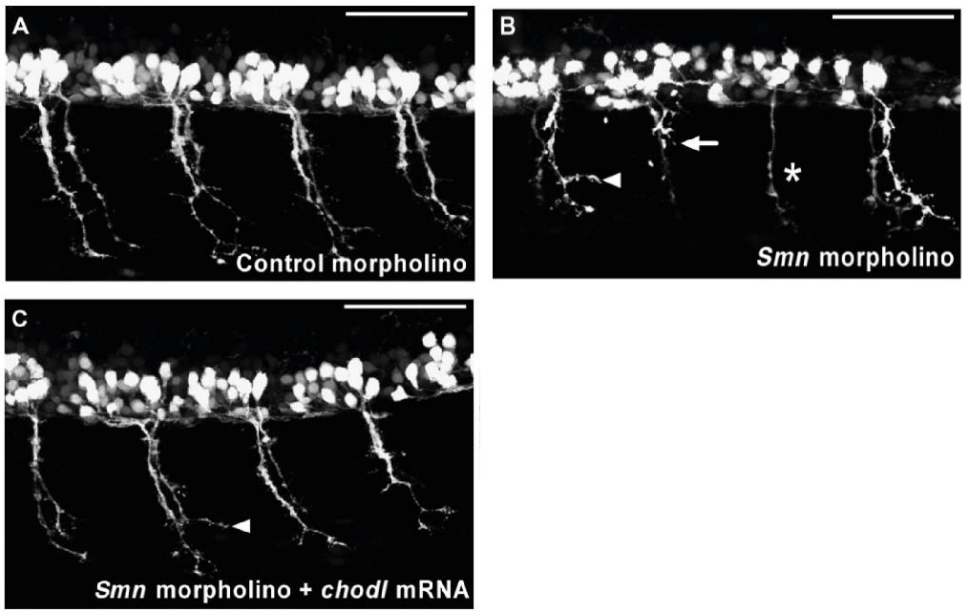

Figure 1.10: Over-expression of chondrolectin in *Smn* morpholino embryos partially rescues the axonal phenotype in zebrafish.
A: Embryos injected with control morpholino do not exhibit morphological changes to the CaP axons. **B:** Injection of *smn* morpholino leads to excessive branching (arrowheads), shortened (arrows) or missing axons (asterisk). **C:** Co-injection of *smn* morpholino and *chodl* mRNA partially rescues the axonal phenotype, although some branching is still observed (arrowhead). Scale bar= 50 µm. (Figure adapted from Sleigh *et al.,* 2014).

1.5 – Zebrafish are highly amenable for use in drug screens

Zebrafish are an increasingly popular model system for modelling motor neuron diseases (MNDs). With approximately 70% gene orthology between human and zebrafish (Howe *et al.*, 2013), multiple disease models have been generated in zebrafish, including for SMA and other MNDs (reviewed in Patten *et al.*, 2014), and so utilisation of the zebrafish for translational approaches is also increasing. Due to the large clutch sizes, ease of drug incubation in the aqueous medium, and physiological relevance of analysing the whole organism, zebrafish are an excellent model for medium- to high-throughput drug screening (Langheinrich, 2003; Tamplin *et al.*, 2012; Phillips and Westerfield, 2014).

Zebrafish have been traditionally used in phenotypic screens to identify biologically active compounds (MacRae and Peterson, 2015). This is because of their biological accessibility during embryonic and larval stages, and their optical transparency for imaging studies. There are a wide array of both forward-genetics mutants (extensively generated for example in the Tübingen/Harvard ENU mutagenesis screen and published in Development in 1996, (e.g. Driever *et al.*, 1996; Furutani-Seiki *et al.*, 1996)) and targeted genomic editing tools such as CRISPR/Cas9. Comparison between the drug phenotype and phenocopied mutants helps to rapidly identify the protein target of the compound.

There are two general strategies for phenotypic screens in zebrafish. Wild-type larvae may be treated with drugs, and any aberrant phenotype identified to find similarity with an expected mutant or tissue target. For example, drugs which altered the gross morphology were identified as phenocopying hedgehog-null mutants. Further study into the compound target showed that it bound to other proteins than the canonical Hedgehog / Patched / Smoothened pathway (Williams *et al.*, 2015). An increased motor response to light was used to find compounds which activate sensory neurons in the embryo (Kokel *et al.*, 2013).

The other strategy used in zebrafish screens is to identify compounds which rescue a mutant or injury model. For example, cessation of a seizure response in mutant zebrafish were used to screen compounds that could treat Dravet syndrome

(Baraban, Dinday and Hortopan, 2013). Ephrin4A was identified as a disease-modifying protein in ALS using a morpholino-based screen. A SOD1 overexpression model was screened for axonal rescue after injection by a library of morpholino. Knockdown of Ephrin4A rescued the axons, demonstrating that inhibition of its expression could be a therapeutic target (Van Hoecke *et al.*, 2012). A screen to identify regenerative pathways used a fin amputation model and looked for compounds which abolished regeneration. From this, glucocorticoids were identified as necessary for the regeneration, offering insight into the regenerative mechanisms (Mathew *et al.*, 2007).

1.6 – Statement of Aims

Overall, in this thesis I developed our understanding of the role and mechanism of chondrolectin during motor axon development. It has already been established that chondrolectin is required for motor axon growth in zebrafish, and that there is a link between chondrolectin and SMA, observed in zebrafish, mouse, and rat models of the disease. However, little was known about the mechanism by which chondrolectin acts in the motor axon to induce axon growth. There was also very limited information about how loss of chondrolectin function could impact later developmental stages in the larvae or adult, including behaviour.

My overarching hypothesis is that there is a link between chondrolectin, SMA, synapse deficits, and motor axon growth. Therefore, I speculate that chondrolectin is required for motor axon growth due to facilitating synapse stabilisation, and synaptogenesis is required for correct axonal growth. Thus, chondrolectin dysfunction is involved in SMA pathology by contributing to synaptic defects.

The main aims of this thesis are as such:

1. Generate and characterise a knockout zebrafish mutant for chondrolectin, detailed in Chapter Three.
2. Investigate the mechanism of the chondrolectin protein to perform its function in zebrafish, described in Chapter Three.
3. Analyse any changes to the motor synapses in the chondrolectin knockout, both at embryonic and larval stages. This is analysed in Chapter Four.

4. Design a drug screening protocol using the chondrolectin mutant to find axon-stabilising compounds, presented in Chapter Five.

Chapter Two – Materials and Methods

Methods

2.1 – Zebrafish husbandry and techniques

2.1.1 - Zebrafish husbandry

All fish were kept and bred in our laboratory fish facility according to standard procedures (Westerfield, 2000). The adults were kept on a 14-hour light/10hour dark cycle at 26.5 °c. The embryos were raised at 27.5°c in E3 medium with 0.00001% methylene blue. All embryonic and larval experiments were performed under the 5 dpf developmental stage (the time-point that the animals become regulated under the Animals in Scientific Procedures Act (1986)). Generation and maintenance of genetically-modified animals as adults were approved by the British Home Office (project license no.: 70/8805).

Fish lines used were the WIK wild-type strain of zebrafish and the HB9:GFP transgenic line (Tg:mnx1:GFP) (Flanagan-Steet *et al.*, 2005). Further transgenic lines and mutants were generated using CRISPR/Cas9 and Tol2 transgenesis as described below. These lines are *chodl* -/-, and *chodl*-/-;HB9:Chodl-FLAG.

Line name	**Background strain**	**Method**	**Specific mutation**	**Phenotype**
chodl -/-	HB9:GFP (GFP+ motor neurons) WIK, wild-type	CRISPR/Cas9	ΔACACT or ΔCTCA in Exon 1. Premature stop within 9 aa of the start site	Short CaP motor axons at 24-30 hpf
HB9:Chodl-FLAG	HB9:GFP, *chodl* -/-	Tol2	Insertion of the HB9 promoter	Axonal rescue of the chodl -/-

			and Chodl fused to the FLAG tag	phenotype, FLAG immunoreactivity in motor neurons

2.1.2 - Microinjection of eggs

Thin-walled glass capillaries containing an internal filament (World Precision Instruments) were prepared as microinjection needles. The glass capillary tubes were pulled using a P-97 Sutter needle puller and stored in petri dishes containing blu-tack to prop the tips up until use. The needle-pulling settings are tabled below:

Ramp – 598	Pull – 100	Velocity – 150
Heat – 410	Time – 200	

Prepared injection solutions were backfilled into the glass needles using long-tailed pipette tips (Eppendorf). The needles were loaded into a micromanipulator attached to a microinjector (Narishige IM-300) and the tips broken using tweezers. The injection volume was calibrated by injecting a bolus into mineral oil on a slide marked with a µm scale bar. Adjusting the pressure and injection duration manually, we calibrated the bolus to total 1 nl.

Freshly-laid eggs at the single cell stage were arrayed in a line against a microscope slide in a petri dish and the majority of liquid removed. Using a fine pipette tip, the eggs were each oriented with the cell in view and injected into the single cell. Approximately every 8 eggs the needle was rinsed in the medium and checked for volume injection, to ensure no blockages of the needle-tip. Injected eggs were rinsed from the dish and raised separately, with their uninjected siblings raised as survival controls.

2.1.3 - Zebrafish DNA extraction & genotyping

Embryos were digested whole using a solution containing 2.5µl Proteinase K (Invitrogen), 10µl Taq polymerase buffer (New England Biolabs) and 90µl dH_2O and heating to 65° for 20 minutes, vortexing, and then heating to 95' for 15mins. The solution was then vortexed again, spun down and 40ul of supernatant removed for storage at -20° for use as a PCR template.

Adult zebrafish fins were cut by first anaesthetising the fish in 1:500 MS-222 (Sigma) and cutting off a small portion of fin (approximately 2 mm from the fin edge) using a clean scalpel blade. The fish were then returned immediately to water in single tanks and monitored for recovery. The fin piece was digested in the same buffer as the embryos above and heated in the same sequence as the embryo DNA extraction.

The DNA was amplified using genotyping primers which span a ~300bp region around the gRNA target sequence. The amplicons were digested with the restriction enzyme for each target and run on a 2% agarose gel with the undigested amplicon for comparison. An undigested band demonstrates destruction of the restriction site via indel mutations by the Cas9. For gRNA1, which generated the chodl mutant line, the primers are (forward 5'GAC TGG AGC AAG TCT GTG 3' and reverse 5' CTG CAC GAG ACC AGA AAA 3', with BspCNI as the restriction site). gRNA2 genotyping primers are (forward 5' GTT CTG GGA GGC TCT GC 3' and reverse 5' AAA CGC AGA GCC TCC CAG AAC G 3', with PstI as the restriction enzyme). gRNA3 genotyping primers are (forward 5' TAG GTC CTG TCC CAA TCT GTA C 3' and reverse 5' AAA CGT ACA GAT TGG GAC AGG A 3', with BsrGI as the restriction enzyme site). The full list of primers arranged in a table are available in Section 2.3.

2.1.4 - Generation of a *chodl* -/- mutant zebrafish using CRISPR/Cas9

Three gRNAs targeting Exon 1 of the chondrolectin gene were designed using http://crispr.mit.edu/. (Hsu *et al.*, 2013). The top guides were selected for estimated cutting efficiency and fewest off-target sites, and for a restriction site to use in genotyping. Oligos for these gRNA sequences were generated using http://ZiFit.partners.org/ to insert into the pT7-gRNA expression vector. Oligos were

annealed and ligated into the pT7 vector as described (Jao, Wente and Chen, 2013). The pT7-gRNA plasmid maps are shown in Figure 2.1, Figure 2.2, and Figure 2.3.

The gRNAs and Cas9 mRNA were transcribed and purified before being stored at -80°c (described in the next section, 2.1.6). Each gRNA was co-injected with Cas9 mRNA into single-cell HB9:GFP embryos, with an injection volume of 1nl. The injected gRNA concentration was 15ng/ul and the Cas9 concentration was 150ng/ul.

At 24hpf, the embryos were checked for normal gross morphology and motor axon appearance. 5 embryos in each injection clutch were pooled for DNA extraction and genotyping to determine cutting efficiency of the gRNA target sequence.

G0 injected fish for gRNA1 were raised and outcrossed into the HB9:GFP fish line. F1 adults were fin-clipped and genotyped for heterozygous mutation in the target sequence. Founders had deletions of ΔCTCA and ΔACACT in Exon1 of chondrolectin, leading to frameshift mutations and premature stops in Exon 2. The ΔCTCA founder was then crossed into both the HB9:GFP and WIK lines to generate mutant lines with and without GFP in the motor neurons. These adults were then incrossed. In the HB9:GFP line, 25% of the clutch showed a shortened axon phenotype. These phenotypic embryos were selected and raised to generate homozygous mutant stocks, and some were used to sequence the DNA and confirm homozygosity of the indel. For the WIK mutant line, homozygous adults were selected by genotyping through fin-clipping. The shortened axon phenotype in these fish were later confirmed by SV2 staining in their offspring.

2.1.5 - Generation of a *chodl* -/-;HB9:*chodl*-FLAG zebrafish line using Tol2 transgenesis

chodl -/- embryos were injected at the single-cell stage with 1nl of a mixture of transposase mRNA (50ng/µl) and tol2-HB9:*chodl*-FLAG (25ng/µl) dissolved in RNAse-free water. At 24hpf, embryos were selected which showed a mosaic rescue of axon length. These fish were raised and backcrossed into the *chodl* -/- line, with F1 embryos selected which showed rescue of all motor axons at 24hpf. Transmission of the HB9:*chodl*-FLAG expression was also confirmed using FLAG immunohistochemistry in the fish at 24hpf.

2.1.6 - Zebrafish larval behaviour

To analyse swimming differences between wild-type and mutant larvae, 3dpf larvae were touched with a fire-pulled pipette on the median fin fold. The swim path of their escape response was recorded and analysed using a Noldus behaviour analysis set-up and EthoVision software (v. 7). Behavioural data is shown as distance travelled within 15 s after touch, averaged for triplicate measures per larvae.

To measure turning defects in the chodl mutants, we recorded larvae using a Casio EX-ZR1300 camera with high-speed recording set to 1000 frames/second. Larvae were recorded before, during, and after an escape response from a head tap using a fire-pulled glass pipette. The videos were manually viewed, and the angle of the initial escape after the C-bend recorded. The escape response was recorded in triplicate per larva.

2.1.7 - Drug treatment of embryos

24-well plates were prepared by filling each well with 699 µl of E3 medium. 1 µl of each drug solution (10 mM stock concentration) was added and the plate gently swirled to dissolve the compound in each well. A pipette tip was widened by trimming the tip off. At 6 hpf, once embryos had reached the shield stage and gastrulated, they were carefully dechorionated using insect pins. After dechorionation, 6 embryos in a group were carefully drawn up into the widened pipette tip in a volume of 300 µl, and carefully dispensed into each well, to a total volume of 1000 µl. The embryos were then returned to the incubator to develop in the compound solution until imaging.

2.2 – Molecular biology

2.2.1 – Primer design

Primer oligos for PCR were designed manually, by planning the binding sequences and calculating the GC content to be between 40-60%. The melting temperature (Tm) of the primers was calculated using the OligoCalc online tool (http://biotools.nubic.northwestern.edu/OligoCalc.html). The addition of any further restriction sites or tags was then added onto these oligos, without adjusting the Tm as these do not bind the target sequence. The oligos were ordered from and produced by Integrated DNA Technologies (IDT).

2.2.2 – Polymerase Chain Reaction (PCR)

PCRs were carried out using the Expand High Fidelity PCR System (Roche). This kit includes a proof-reading polymerase, allowing higher efficiency when amplifying larger fragments or inducing mutations via primers during the PCR. The reaction mixture per PCR was made as a master mix according to manufacturers' instructions.

The PCR cycler was set to the following reaction protocol, with the extension time adjusted according to the expected amplicon size.

2.2.3 – Gel electrophoresis and extraction of DNA

Initial denaturation:		3 min	94°
Denaturation: Annealing: Elongation:	35 cycles	20s 30s 30s per 1kb amplicon	94 ° Primer Tm 68°
Final elongation		5 min	68°
Cooled / Idle		0-indefinite	4°

2.5% Agarose gels with 0.0001% Gel Red (Biotium) in TAE buffer were used to separate PCR amplicons and digested plasmid fragments using electrophoresis. Appropriately sized DNA ladders (NEB) were also run in adjacent columns and used to determine the correctly sized band. The bands were illuminated under UV light and excised using a clean scalpel. The DNA was extracted from the gel using the QIAquick Gel Extraction Kit (Qiagen).

2.2.4 – Ligation of PCR fragments

TA cloning was performed using either a TOPO TA Cloning Kit (Invitrogen), or Strataclone PCR Cloning Kit (Agilent) according to manufacturers' instructions. This ligates a PCR fragment containing A base overhangs (left by the Taq polymerase during PCR) into a linear vector with T base overhangs. The ligated vector is then transformed into competent cells. TA cloning was used to amplify PCR fragments in plasmids for mini-prepping and sequencing.

T4 ligation of DNA fragments into linearised vectors was performed to generate the final plasmids for injection into zebrafish. T4 ligase and ligase buffer (NEB) were used to ligate DNA fragments according to protocols available from the manufacturer.

2.2.5 – Transformation of competent bacterial cells and growth on agar plates

5-alpha competent cells (NEB) were stored at -80°c until use, then thawed on ice. To maintain an aseptic environment, bacterial work was performed adjacent to a Bunsen burner to generate an air stream. The cells were gently mixed with 2µl of plasmid solution after ligation or TA cloning mix and incubated on ice for 15 minutes. Heat-shocking was performed at 42° for 45 seconds before returning the tubes to ice for 2

mins. 200 µl of LB medium was added to the cells and incubated on a 37 ° shaking incubator for at least one hour before being spread onto antibiotic-treated agar plates and incubated overnight at 37°.

2.2.6 – Picking bacterial colonies and growing bacteria in LB media

After overnight incubation following bacterial transformation, agar plates were wrapped in parafilm to prevent drying out and stored in a 4° cold room until needed. To maintain an aseptic environment, bacterial work was performed adjacent to a Bunsen burner to generate an air stream. Bacterial colonies were prepped for mini- or midi- kits by first preparing antibiotic-containing LB medium in either 5ml or 50ml falcon tubes, depending on downstream application. The antibiotic chosen depended on the antibiotic resistance included in the plasmid, either ampicillin at 100 µg/ml or kanamycin at 50 µg/ml. A single colony at a time was carefully picked using a pipette tip, streaked on a fresh agar plate to generate a master plate, and then dropped into the falcon tube. After overnight incubation on a shaking incubator at 37°, the broth was then used to isolate plasmid DNA for sequencing or further applications.

2.2.7 – Isolation of plasmid DNA from bacterial culture

Plasmid DNA was isolated using commercial Mini- or Midi- Kits (Qiagen) according to manufacturers' instructions. Glycerol stocks of the bacterial culture were generated for long term storage at -80° by mixing 175 µl of glycerol with 325 µl of bacterial broth. Determination of the DNA concentration was performed using a Nanodrop (Thermo Scientific) calibrated against the elution medium. DNA solutions were stored at -20° until needed.

2.2.8 – Sanger sequencing of DNA

Sequencing of plasmid DNA was performed using the commercial service from Source Bioscience (www.sourcebioscience.com). Sequencing primers were provided by the company. Potential sequencing primers were selected in one or both directions

flanking the region of interest to be checked, and the specific primers were selected according to the expected sequence or the vector backbone.

The sequences were sent from Source Bioscience as SEQ or AB1 files via email and viewed using ContigExpress. Sequences were compared on ContigExpress with reference sequences from NCBI (https://www.ncbi.nlm.nih.gov/) to determine if the correct sequence had been generated (e.g. when generating mutated constructs) or if the cassettes had been ligated correctly into the plasmids.

2.2.9 – Restriction digest of DNA by restriction enzymes

Restriction digest of DNA was performed using restriction enzymes (NEB) and a suitable buffer (NEB) according to standard protocols. Double digestion using two enzymes simultaneously was first checked for the most suitable buffer using the NEB Double Digest online tool (https://nebcloner.neb.com/#!/redigest). The following enzymes were used:

Restriction enzyme	**Buffer used for single digests**	**Optimal temperature**
BamHI (High-Fidelity)	CutSmart	37°
BglII	Buffer 3.1	37°
BspCNI	CutSmart (+SAM)	25°
BsmBI	Buffer 3.1	55°
BsrGI	Buffer 2.1	37°
ClaI	CutSmart	37°
EcoRI	Buffer 2.1 / EcoRI Buffer	37°
EcoRV	Buffer 3.1	37°
HindIII	Buffer 2.1	37°
NotI	Buffer 3.1	37°
PstI (High Fidelity)	CutSmart	37°
SalI (High Fidelity)	CutSmart	37°
XbaI	CutSmart	37°
XhoI	CutSmart	37°

2.2.10 - Production of capped mRNA for microinjection

gRNA was transcribed using the mMessage mMachine T7 Transcription kit (Invitrogen) after the plasmids were linearised with BamHI. Because of the small size of the gRNAs, the RNA was cleaned up using the mirVana miRNA Kit (Ambion).

The Cas9 mRNA was prepared from the pT3TS-nCas9n plasmid, linearised with XbaI and transcribed using the mMessage mMachine T3 Transcription Kit (Invitrogen). The mRNA was cleaned up using the RNeasy Mini Kit (Qiagen) and stored as aliquots at -80°c.

The pT3TS-Tol2 plasmid was linearised by digestion with XbaI, and capped mRNA produced using the mMessage mMachine T3 Transcription kit (Invitrogen). RNA cleanup was performed using the RNeasy Mini Kit (Qiagen) and aliquots stored at -80°c.

2.2.11 – Cloning and generated plasmids

To generate the plasmids used in various experimental procedures the following vectors were used: The gRNA scaffold vector pT7-gRNA was a gift from Wenbiao Chen (Addgene plasmid # 46759), the Cas9 expression vector pCS2-nCas9n was a gift from Wenbiao Chen (Addgene plasmid # 47929). Tol2 transgenesis plasmids of transposase mRNA sequence pT3TS-Tol2 was a gift from Stephen Ekker (Addgene plasmid # 31831) and pminiTol2 vector (gift from Stephen Ekker, Addgene #31829). pCS2P+ was a gift from Marc Kirschner (Addgene # 17095). pCMV-chodl-myc was used in Zhong et al., 2012, generated in our group. All restriction enzymes and buffers used were from New England Biolabs.

The full list of primers arrayed in a table are available in Section 2.8, as are schematics of the plasmids generated in Section 2.9.

The chodl gRNA1 was generated by ordering two overlapping oligos, generated using http://ZiFit.partners.org/ using the target sequence. The oligos were annealed together using a PCR cycler and ligated into the pT7 vector as described (Jao, Wente and Chen, 2013). (Forward 5’ TAG GAG GAT GCG CGC GAC ACT C 3’, reverse 5’ AAA CGA GTG TCG CGC GCA TCC T 3’.) The chodl gRNA2 was generated in the

same manner as gRNA1. (Forward 5' TAG GCG TTC TGG GAG GCT CTG C 3', reverse 5' AAA CGC AGA GCC TCC CAG AAC G 3'). The chodl gRNA3 was generated in the same manner as gRNA1 above. (Forward 5' TAG GTC CTG TCC CAA TCT GTA C 3', reverse 5' AAA CGT ACA GAT TGG GAC AGG A 3').

pCS2P-chodl-FLAG was generated by amplifying the chondrolectin coding sequence from pCMV-chodl-myc, adding an artificial Kozak sequence (AAC) 5' of the start site and adding a Gly-Pro-Gly linker and a synthetic FLAG tag to the 3'end. (Forward EcoRI 5' GCG GAA TTC AAC ATG CGC GCG ACA CTC AGG 3', Reverse XhoI 5' GCG CTC GAG TCA TTT ATC ATC ATC ATC TTT ATA ATC TGG TCC TGG GAC CTC CAT GCC ACT 3'). The amplified chodl-FLAG was digested and ligated into pCS2P+ to generate pCS2P-chodl-FLAG. The map for this plasmid is included as Figure 2.4.

The pMiniTol2-HB9 plasmid was generated by Dr Ana-Maria Oprişoreanu. The 3kb promoter fragment of HB9 was amplified from genomic DNA using the forward primer (NotI) 5'- GCG GCG GCC GCC CAT TTA AAT TAG CCT GGC ATC TGG AC-3' and reverse primer (EcoRI) 5'-GCG GAA TTC TCT GGC CCA CCT CAC AAA CAG-3'), and the fragment was cloned into the NotI-EcoRI pminiTol2 digested vector.

The pMiniTol2-HB9:chodl-FLAG plasmid was cloned by amplifying the chodl-FLAG cassette and SV40 from the pCS2P-chodl-FLAG, and subcloning into the pMiniTol2-HB9 plasmid. (Forward EcoRI 5' GAT TCG AAT TCA ACA TGC GCG 3', Reverse EcoRV 5' CGA TGA TAT CAA AAA ACC TCC CAC ACC TCC C 3'). The map is linked as Figure 2.5.

To generate the construct pMiniTol2-HB9:Chodl-FLAG (w/o ID)(1-263aa), the chondrolectin coding sequence until the TM domain was amplified and a linker with FLAG tag added, using the pCS2P-chodl-FLAG as template. (Forward EcoRI 5' ATG CGA ATT CAA ACA TGC GCG CGA CAC TCA GG 3', Reverse XhoI 5' GCA TCT CGA GTT ACT TGT CGT CAT CGT CTT TGT AGT CAG GGC CAG GGA AAC AGC ACG TCC CTG AAG 3'). This fragment was subcloned into the pCS2P+ vector and used as a PCR template to add the SV40 sequence for ligation into the pMiniTol2-HB9 plasmid (Forward EcoRI 5' GAT TCG AAT TCA AAC ATG CGC G 3', Reverse EcoRV 5' CGA TGA TAT CAA AAA ACC TCC CAC ACC TCC C 3'). The map is included as Figure 2.6.

To generate pMiniTol2-HB9:Chodl-FLAG (w/o CTLD) (1-29Δ188-296aa), two intermediate chodl fragments were generated 5' and 3' of the C-type Lectin domain sequence (Cassette 1 Forward EcoRI 5' ATG CGA ATT CAA ACA TGC GCG CGA CAC TCA GG 3, Reverse XhoI 5' GCA TCT CGA GCA CTG TCT GAC CGC TCA CAA 3', Cassette 2 Forward XhoI 5' ATG CCT CGA GTA TGA ACC AGA AAG TCA TCT GG 3', Reverse XbaI 5' GCA TTC TAG ATT ACT TGT CGT CAT CGT CTT TGT AGT CAG GGC CAG GGA CCT CCA TGC CAC 3'). These were ligated together into the pCS2P+ vector, and then the whole chondrolectin cassette and SV40 amplified to ligate into pMiniTol2-HB9. The primers for this amplification are the same as previously used to generate the final cassette of the chodl w/o ID. The map is available at Figure 2.7.

To generate pMiniTol2-HB9:Chodl-FLAG (w/ ID S/T->A) (1-263aa, S/T-A 264-296aa), the intracellular sequence 3' of the transmembrane domain was mutagenised using PCR primers. A sequence of 4 primers were used, which first bound to the TM domain and added 30bp of mutagenised sequence, then bound to the last 20bp of each successive mutagenised sequence and added another 30bp. The final primer also contained the Gly-Pro-Gly linker and FLAG tag. In each case, the forward primer was the same. (Forward EcoRI 5' ATG CGA ATT CAA ACA TGC GCG CGA CAC TCA GG 3', Reverse 1 5' AGC TTT AGC CCG TGG TTT AGC CTT AGC CAA CAT CTG GAA ACA GCA CGT CCC TGA AG 3', Reverse 2 5' CGT CTT AGC GAT CCA GAG AGC AGC TTG GTT GAC AGC AGC TTT AGC CCG TGG TTT AGC 3', Reverse 3 5' GAC CTC CAT GCC AGC GTC TAT CTT AGC CGT CTT AGC GAT CCA GAG AG 3', Reverse 4 5' GCA TCT CGA GTT ACT TGT CGT CAT CGT CTT TGT AGT CAG GGC CAG GGA CCT CCA TGC CAG CGT C 3'). As described for the other truncated constructs, the cassette was ligated into the pCS2P+ vector and re-amplified with the SV40 sequence, and ligated into the pMiniTol2-HB9 plasmid. The map is available as Figure 2.8.

2.3 – Histology, staining, imaging, and analysis

2.3.1 - Zebrafish wholemount immunohistochemistry

2.3.1.1 – Immunohistochemistry at 28 and 31 hpf

Between 24 and 30hpf, the zebrafish embryos were dechorionated and fixed for 45 minutes at RT in 4%PFA/1%DMSO. This under-fixation is necessary for the low signal in the synapse preparations and the injected FLAG constructs. The embryos are then rinsed 3x5mins with PBS+0.1%Triton-X100 and blocked using blocking buffer containing 1% normal donkey serum (1%DMSO, 1%BSA, 0.7%Triton-X100 in PBS pH7.4) for 60-90minutes at RT with gentle shaking. The embryos are then incubated O/N at 4' with the primary antibodies in blocking buffer with 1% NDS. Primary antibodies were: anti-GFP (1:400, AbCam, AB13970), anti-FLAG (1:100, Sigma, F1804), anti-SV2 (1:200, DSHB), and anti-AChR (1:200, DSHB, mAb35). The primary antibodies were washed off using PBS-Tx 6x10mins and the secondary antibody incubated for 4h at RT. Secondary antibodies used were: AlexaFluor488 donkey anti-chicken (1:400, Jackson ImmunoResearch), AlexaFluor 594 donkey anti-mouse (1:400 Jackson ImmunoResearch), AlexaFluor 594 donkey anti-mouse with pre-adsorbtion against rat protein (1:400, Jackson ImmunoResearch), and AlexaFluor 488 donkey anti-rat with pre-adsorbtion against mouse protein (1:400, Jackson ImmunoResearch). After fully rinsing off the secondary antibody, the embryos were settled in 70% glycerol/30% PBS and stored wrapped in foil at 4' until imaging.

2.3.1.2 – Immunohistochemistry at 3 dpf

At 3dpf, the larvae were fixed in 4% PFA/1%DMSO for 4h at 4'. After 3x10 mins rinsing in PBS+0.1% Triton-X100, the larvae were skinned to permeabilise the muscle to the synaptic antibodies. The larvae were insect-pinned to a sylgard-coated petri dish and most of the liquid sucked away from the larvae. Sharpened tungsten wire was used to gently pull the skin away from the head area, and fine forceps were then used to fully pull the skin off the trunk and tail. After skinning, the larvae were blocked for 60-90 minutes in blocking buffer as described above at RT. Primary and secondary

antibodies were used at the same concentrations and incubation time as described for the embryos.

2.3.1.3 – Phalloidin staining at 30 hpf

Carrying out all steps on a gentle shaker, embryos were fixed overnight at 4° in 4% PFA in PBS, OR 2 hours at RT. After washing 2 x 5 minutes in PBSTw (PBS+0.1% Tween-20) OR in PBSTx (PBS+ 0.2% Triton-X-100), embryos were inncubated for 2h in PBS + 2% Triton X-100 to permeabilise the tissue. Further washes were performed, 2 x 5 mins in PBSTw or PBSTx, before 1.5h incubation in phalloidin-AlexaFluor564 solution (dilute the stock 1:20 in PBSTw). Final washes of 6x 10 minutes in PBSTw or PBSTx were performed before mounting in glycerol and imaging.

To quantify differences in myotube architecture, the average number of myotubes per somite were counted, and the average thickness of a myotube measured. Measurements were taken along the midline of the somite, and the values from 3 somites were averaged for each embryo.

2.3.2 – Microscopes and imaging

All zebrafish were mounted onto glass slides using 70% glycerol, deyolked with insect pins, and covered with coverslips anchored with silicone gel. Several microscopes were used during this study.

To sort reporter lines by their fluorescence, and to initially sort phenotypic embryos during establishment of transgenic lines, a fluorescent stereomicroscope (Leica) was used. To image axons for the initial phenotypic analysis of the *chodl* -/- phenotype, a Zeiss Apotome.2/ImagerZ1 upright microscope was used. To image the zebrafish after immunohistochemistry, a Zeiss LSM880 with Airyscan was used.

To image the embryos during the drug screening, the VAST BioImager was linked to a custom spinning disk confocal microscope. Information on the set-up is available from Early et al., 2018. An Axio Examiner D1 (Carl Zeiss) microscope was fitted with a high- speed CSU-X1 spinning disk confocal scanner (Yokogawa, Tokyo, Japan), with a high-speed piezo drive to generate rapid Z-stacks. (PIFOC P-725.4CD piezo objective scanner (Physik Instrumente, Karlsruhe, Germany)).

2.3.3 – Loading and imaging by the VAST BioImager

After drug treatment, 25 hpf embryos were carefully pipetted 3 at a time in 300 µl of medium and transferred into 96 well plates. The vehicle-treated control groups were randomly arrayed in the wells to control for the development of the embryos over time during imaging. The 96 well plate was then fitted into the plate loading bay of the VAST BioImager platform.

The VAST BioImager (Union Biometrica) was combined with a spinning disk confocal microscope (SDCM, Zeiss) (further described in Early et al., 2018). Following an adapted protocol from this publication, optimised for 26-30 hpf embryos (described in detail during Chapter Five), the embryos from each well were automatically loaded, rotated in the imaging chamber to the lateral view, and imaged with both brightfield and GFP channels. During imaging, a CSV format file was generated giving each image set a number and well location. After imaging, this CSV and the images were loaded into a Zen macro (Early et al., 2018) which generated maximal intensity projections of each stack. The MIPs were then stitched together using an ImageJ macro (Early et al., 2018) and these stitched images were scored. After scoring, the experiments were unblinded using the image number and well location from the CSV file to determine the treatment.

2.3.4 – Body length and eye diameter measurements

For both body length and eye measurement, ImageJ and its straight line tool was used to measure the diameter of the eyes and the body length from nose to tail tip, from HB9:GFP and *chodl*-/- embryos at 30hpf. When using the VAST BioImager to sort and image embryos, the VAST platform generates a brightfield image of the capillary chamber containing the embryo. These images are BMP files without scaling, so the diameter of the capillary, 600 µm, was used to calculate the pixel-to-µm scale.

2.3.5 – Analysis of axon score and axon length

Axons scoring was performed by loading maximum intensity projections (MIPs) into Image J. The axons were scored if they were at the position of the horizontal myoseptum (HM) or if they had grown past that point (HM+). The horizontal myoseptum location is visible due to the slight morphological thickening of the axon at this choice point. For the axonal scoring, 8 axons from somite 7-15 per embryo were scored and the mean percentage of HM+ axons calculated.

Axon length measurements were performed using ImageJ. The images were loaded containing the metadata for pixel-µm scale. Using the segmented line feature, axons were traced from the border between the axon and cell body, to the tip of the axon. If the axon was branched at the tip, the longest branch was followed. Upon completing the axon trace, the length of the segmented line was measured. For all experiments which recorded CaP axon length, unless otherwise stated, 8 axons per embryo were measured.

To quantify branching of the axons at 48 hpf and 72 hpf, maximum intensity projections of the trunk were generated, with both wild-type and chodl -/- larvae expressing the HB9:GFP transgene. Branching from 8 axons (from somite 7-15) were quantified for each larva. The number of branches were counted by tracing lines from the spinal cord ventrally, at a distance 10 µm (48 hpf) or 15 µm (72 hpf) anterior and posterior from the main axon. Branches that crossed each line were counted. This counted the number of branches but discarded small filopodia or very minor branches coming from the axon. Branches on both sides of the axon were added together and then averaged for each larva.

2.3.6 – Quantification of *chodl* -/- rescue by injection of truncated chondrolectin constructs

Truncated constructs of chondrolectin-FLAG were generated and subcloned into the pMiniTol2-HB9 plasmid. These constructs are: chondrolectin without the 3’ sequence after the predicted transmembrane domain, removing its intracellular domain (chodl w/o ID), chondrolectin without the predicted C-type Lectin domain (chodl w/o CTLD)

and chondrolectin with the serine and threonine residues converted to alanine residues in the intracellular domain (chodl w/ ST->A ID).

These truncated constructs, or the empty pMiniTol2-HB9 plasmid, or full-length pMiniTol2-HB9:Chodl-FLAG, were injected into *chodl* -/- embryos at the single-cell stage, with a volume of 1nl. Transposase mRNA was co-injected at 50 ng/µl, and the plasmid concentration was 25 ng/µl.

At 28hpf, the embryos were dechorionated, fixed, and immunohistochemistry of GFP and FLAG was performed. The embryos were imaged, and the axon length measured using ImageJ, as well as the presence or not of FLAG expression. Axons were only considered FLAG positive if the FLAG staining was visible along the full length of the axon, and if the FLAG-positive cell body matched the morphology of the CaP axon, as published in Meyer, Eisen, & Westerfield (1986). This prevented the measurement of RoP or MiP axons, which partially share the path of the CaP axon.

2.3.7 - Synapse puncta quantification

The pre- and post-synapses of zebrafish were labelled using α-SV2 and α-AChR labelling and imaged using a confocal microscope as described above. All measurement of the synaptic puncta was performed in ImageJ. For analysis, a 20 x 20 μm^2 square was drawn around the horizontal myoseptum in 28hpf embryos, with 4 axons measured and the values averaged for each embryo. To determine synaptic measurements in the axonal branches at 3dpf, a 40 x 40 μm^2 square was drawn in the dorsal region of the myotome, with 3 myotomes averaged per larva.

In each square, synaptic puncta were analysed with the following analysis pipeline, performed in ImageJ. First, the background in each image was reduced by performing background subtraction of the images, using a rolling ball subtraction with a radius of 33% of the square's length in pixels. The maximum grey value was measured after smoothing function was applied for each image, and used to calculate a 20% threshold. This had to be calculated for each image due to biological variation in the intensity of staining and thus intensity of the signal captured by the confocal. The 20% threshold was then applied to the non-smoothed image to remove the lowest 20% of grey values and generate a binary black-and-white image of the synaptic puncta.

Application of a 20% threshold was qualitatively determined to remove much of the noise in the image without removing any true synaptic staining. After application of the threshold, the Analyse Puncta function was used to count puncta number and area. The minimum area defined as a punctum for the Analyse Particle function was set as 0.5µm^2. Again, this was qualitatively determined as the minimum size to not quantify any remaining background noise and only measure true puncta.

2.3.8 - Statistical analysis

For all experiments, the person performing the analysis was blinded to the condition or group until after all measurements were concluded. Data is shown as mean ± standard error of mean (SEM), and all N numbers refer to number of embryos unless otherwise stated. All statistical tests and graphs were produced using GraphPad 7 software. All data was checked for Gaussian distribution via a D'Agostino-Pearson omnibus normality test before further statistical tests were performed. The statistical test between two groups was either a student's t-test or Mann-Whitney test, depending on whether the data set followed Gaussian distribution or not. The student's t-test also had Welch's correction applied if the variances between groups differed significantly. The statistical test between three or more groups was either a one-way ANOVA or Kruskal-Wallis test, depending on if the data set was normally distributed or not. Comparison tests between groups after a one-way ANOVA was Bonferroni's multiple comparison test and after Kruskal-Wallis was Dunn's multiple comparison test. Multiple comparison tests were always performed to compare all groups to every other group. Post-hoc power calculations were performed on statistically significant data using GPower 3.1.

2.3.9 – Software

Data was collected on Microsoft Excel before being transferred to GraphPad Prism for statistical testing and generation of graphs. All images were analysed using Fiji (ImageJ). Image macros for Zeiss Zen software and ImageJ, used to process the VAST BioImager data, are published in Early *et al.*, 2018. Figures were generated using Adobe Illustrator 6. Sequence data and plasmid maps were generated in

VectorNTI and SnapGene Viewer. The content of this thesis was written using Microsoft Word 2016 and the bibliography managed by Mendeley desktop and its associated Word plugin.

Materials

2.4 – Reagents & solvents

Name	**Company (Product no.)**
Agarose	Sigma-Aldrich (BPE1356)
Aminobenzoic acid ethylmethylester (MS-222)	Sigma-Aldrich (A5040)
Ampicillin sodium salt	Sigma-Aldrich (A9518)
Bovine serum albumin (BSA)	Sigma-Aldrich (A3912)
Dimethyl sulfoxide (DMSO)	Sigma-Aldrich (D8418)
Ethanol	VWR International (64-17-15)
6x Gel loading dye	New England Bioscience (B7025S)
Glycerol	Sigma-Aldrich (G5516)
Glycine	Sigma-Aldrich (G8898)
Hydrochloric acid (HCl)	Sigma-Aldrich (320331)
IOX1	Cayman Chemicals (11572)
Kanamycin	Fisher Scientific (BPE906-5)
Methanol	Fischer Chemicals (67-56-1)
Methylene blue	VWR International (370.0025)
Normal donkey serum	Millipore (S30)
Paraformaldehyde	Sigma-Aldrich (P6148)
Potassium chloride, KCl	Sigma-Aldrich (P9541)
Potassium dihydrogen orthophosphate (KH_2PO_4)	Scientific Laboratory Supplies (CHE2948)
Quickload 100 bp DNA ladder	New England Bioscience (N0468S)
Quickload 1 kbp DNA ladder	New England Bioscience (N0551S)
Sodium chloride (NaCl)	Sigma-Aldrich (S7653)
Sodium phosphate dibasic (Na_2HPO_4)	Sigma-Aldrich (S0876)
Sodium hydroxide (NaOH)	Sigma-Aldrich (30620)
Triton-X-100	Acros Organics (327372500)
Trizma Base	Sigma-Aldrich (93362)
Tween-20	Sigma-Aldrich (P1379)
UNC0642	Cayman Chemicals (14604)

2.5 - Solutions

Donkey Blocking Buffer	1% DMSO 1% BSA 1% Normal donkey serum (NDS) 0.7% Triton-X-100 in PBS pH7.4
4% Paraformaldehyde	16 g Paraformaldehyde 40ml 10x PBS complete using dH2O up to 400 ml
10x Phosphate-buffered saline (PBS)	160 g NaCl 28.3 g Ma2HPO4 4 g KCl 4.8g KH2PO4 Complete with dH2O to 2l
50 x TAE Buffer	484 g Tris base 114.2 ml Acetic acid 1000 ml EDTA, pH 8 Adjust pH to 7.5 using HCl make up to 2 l using dH_2O

2.6 – Antibodies

Primary Antibodies

Name	**Specific clone name**	**Dilution**	**Target antigen**	**Raised in**	**Company**	**Product #**
anti-GFP	-	1:300	GFP	Chicken	AbCam	ab13970
anti-FLAG	M2 Clone	1:100	FLAG (DYKDDDDK)	Mouse	Sigma-Aldrich	F1804
anti-SV2	-	1:200	SV2 (isoforms a,b,c)	Mouse	DSHB	SV2
anti-AChR	mAb 35	1:200	alpha-subunit of AChR	Rat	DSHB	mAb 35
Phalloidin	Alexa Fluor 568 Phalloidin	1:20	F-actin	-	Invitrogen	A12380

Secondary Antibodies

Specific description	Dilution	Target antigen	Raised in	Fluorophore	Company	Product #
Alexa Fluor ® 488 AffiniPure Donkey Anti-Chicken IgY (IgG) (H+L)	1:400	Chicken	Donkey	Alexa Fluor ® 488	Jackson Immuno research	703-545-155
Alexa Fluor® 594 AffiniPure Donkey Anti-Mouse IgG (H+L)	1:400	Mouse	Donkey	Alexa Fluor® 594	Jackson Immuno research	715-585-150
Alexa Fluor® 594 AffiniPure Donkey Anti-Mouse IgG (H+L) (Minimally cross-reactive to Rat, pre-adsorbed)	1:400	Mouse	Donkey	Alexa Fluor® 594	Jackson Immuno research	715-585-151
Alexa Fluor® 488 AffiniPure Donkey Anti-Rat IgG (H+L) (minimally cross-reactive to Mouse, pre-adsorbed)	1:400	Rat	Donkey	Alexa Fluor® 488	Jackson Immuno research	712-545-153
Alexa Fluor® 647 AffiniPure Donkey Anti-Mouse IgG (H+L)	1:400	Mouse	Donkey	Alexa Fluor® 647	Jackson Immuno research	715-605-150
Alexa Fluor® 647 AffiniPure Donkey Anti-Rat IgG (H+L) (Minimally cross-reactive to Mouse, pre-adsorbed)	1:400	Rat	Donkey	Alexa Fluor® 647	Jackson Immuno research	712-605-153

2.7 - Kits

Name	Company (Product no.)
5-alpha Competent E. coli (High Efficiency)	New England Biolabs (C287H)
Expand High-Fidelity PCR System	Roche (11732641001)
*mir*Vana miRNA Isolation Kit, without phenol	Ambion (AM1561)
mMESSAGE mMACHINE SP6 Transcription Kit	Invitrogen (AM1340)
mMESSAGE mMACHINE T3 Transcription Kit	Invitrogen (AM1348)
mMESSAGE mMACHINE T7 Transcription Kit	Invitrogen (AM1344)
QIAPrep Spin Mini Kit	Qiagen (27106)
Qiagen Plasmid Plus Midi Kit	Qiagen (12943)
QIAQuick Gel Extraction Kit	Qiagen (28706)
RNeasy Mini Kit	Qiagen (74106)
StrataClone PCR Cloning Kit, with competent cells	Agilent (240205)
TOPO TA Cloning Kit, without competent cells	Invitrogen (450641)

2.8 - Primers

	Name	Direction - Paired primer	Sequence (5' – 3')	Tm (°)
1	chodl gRNA 1	Fwd - 2	TAGGAGGATGCGCGCGACACTC	67.9
2	chodl gRNA 1	Rev - 1	AAACGAGTGTCGCGCGCATCCT	65.8
3	chodl gRNA 2	Fwd - 4	TAGGCGTTCTGGGAGGCTCTGC	67.9
4	chodl gRNA 2	Rev - 3	AAACGCAGAGCCTCCCAGAACG	65.8
5	chodl gRNA 3	Fwd - 6	TAGGTCCTGTCCCAATCTGTAC	62.1
6	chodl gRNA 3	Rev - 5	AAACGTACAGATTGGGACAGGA	60.1

7	Genotyping for gRNA 1	Fwd – 8	GACTGGAGCAAGTCTGTG	56.3
8	Genotyping for gRNA 1	Rev – 7	CTGCACGAGACCAGAAAA	53.8
9	Genotyping for gRNA 2	Fwd – 10	AAGACGTGTCGAGTCGTG	56.3
10	Genotyping for gRNA 2	Rev – 9	CTCTCGCAGAAGGTGTTC	56.3
11	Genotyping for gRNA 3	Fwd – 12	GACGGAGACTTCTGGATC	56.3
12	Genotyping for gRNA 3	Rev - 11	GAACAGCGAGACACTTCC	56.3
13	Genotyping gRNA1 (redesigned for improved efficiency)	Fwd – 8, 14, 16	GAAGAGACTTTGCCAATAAATGT	57.6
14	Genotyping gRNA1 (redesigned for improved efficiency)	Rev – 7, 13, 15	TCACAACTCTCGCGCCAC	58.4
15	Genotyping gRNA1 (redesigned for improved efficiency)	Fwd – 8, 14, 16	GTCACTCTCTCTCTCCGC	62.5
16	Genotyping gRNA1 (redesigned for improved efficiency)	Rev – 7, 13, 15	GCTGCACGAGACCAGAAAAG	60.5
19	Chodl start site (to generate edited chodl constructs)	Fwd – 20, 23, 26, 27, 28, 29	ATGCGAATTCAAACATGCGCGCGACACTCAGG	60.8
20	chodl w/o ID. + FLAG (1-266aa)	Rev - 19	GCATCTCGAGTTACTTGTCGTCATCGTCTTTGTAGTCAGGGCCAGGGAAACAGCACGTCCCTGAAG	60.5*
21	addition of SV40 to Chodl-FLAG	Fwd - 22	GATTCGAATTCAAACATGCGCG	60.1
22	addition of SV40 to Chodl-FLAG	Rev – 21	CGATGATATCAAAAAACCTCCCACACCTCCC	61.2
23	Chodl w/o CTLD (1-29aa fragment)	Rev - 19	GCATCTCGAGCACTGTCTGACCGCTCACAA	60.5
24	Chodl w/o CTLD (188-293aa fragment)	Fwd - 25	ATGCCTCGAGTATGAACCAGAAAGTCATCTGG	58.4

25	Chodl w/o CTLD (188-293aa fragment) with FLAG tag	Rev - 24	GCATTCTAGATTACTTGTCGTCATC GTCTTTGTAGTCAGGGCCAGGGAC CTCCATGCCACTGTC	58.4*
26	Chodl w/ ID (S/T->A) #1	Rev - 19	AGCTTTAGCCCGTGGTTTAGCCTTA GCCAACATCTGGAAACAGCACGTC CCTGAAG	60.5*
27	Chodl w/ ID (S/T->A) #2	Rev - 19	CGTCTTAGCGATCCAGAGAGCAGC TTGGTTGACAGCAGCTTTAGCCCGT GGTTTAGC	61.2*
28	Chodl w/ ID (S/T->A) #3	Rev - 19	GACCTCCATGCCAGCGTCTATCTTA GCCGTCTTAGCGATCCAGAGAG	60.5*
29	Chodl w/ ID (S/T->A) #4	Rev - 19	GCATCTCGAGTTACTTGTCGTCATC GTCTTTGTAGTCAGGGCCAGGGAC CTCCATGCCAGCGTC	60.8*

- Please note that the Tm listed are calculated from the portion of primer binding to the target sequence. Addition of tags or restriction sites via primer do not contribute to the binding during the first stages of the PCR and thus are not included in the Tm. The primers with added features are marked with (*) in the Tm value.

2.9 - Plasmids

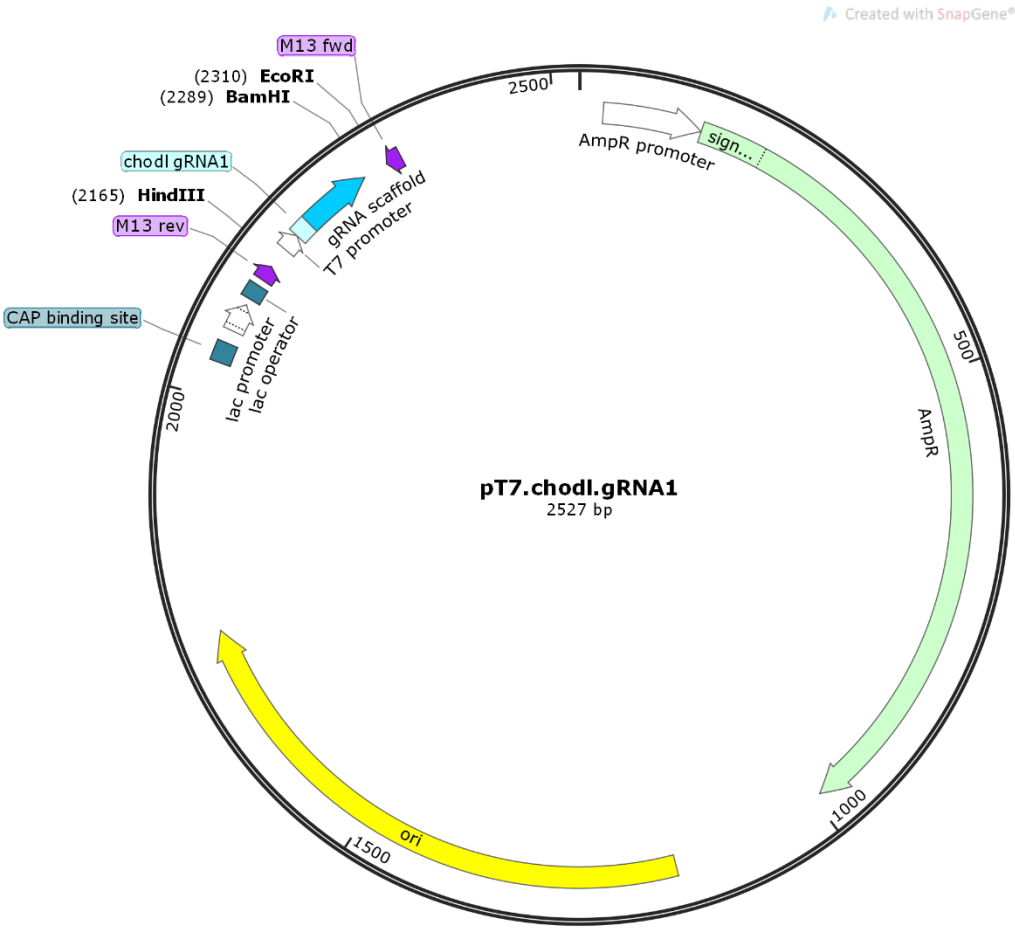

Figure 2.1: The pT7.chodl.gRNA1 map. The gRNA1 target sequence was annealed via paired oligos and subcloned into the pT7.gRNA scaffold vector (Addgene # # 46759, from Wenbiao Chen). BamHI was used to linearise the plasmid for mRNA transcription.

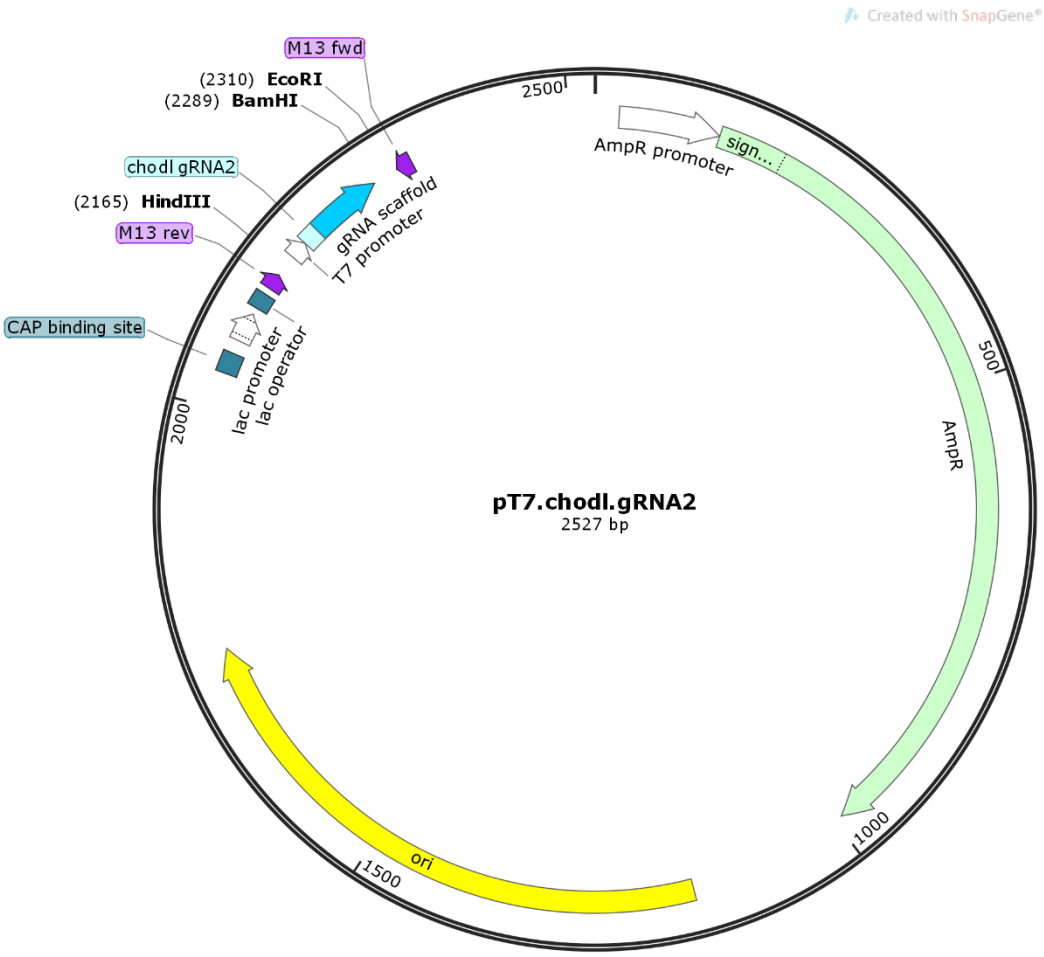

Figure 2.2 The pT7.chodl.gRNA2 map. The gRNA1 target sequence was annealed via paired oligos and subcloned into the pT7.gRNA scaffold vector (Addgene # # 46759, from Wenbiao Chen). BamHI was used to linearise the plasmid for mRNA transcription.

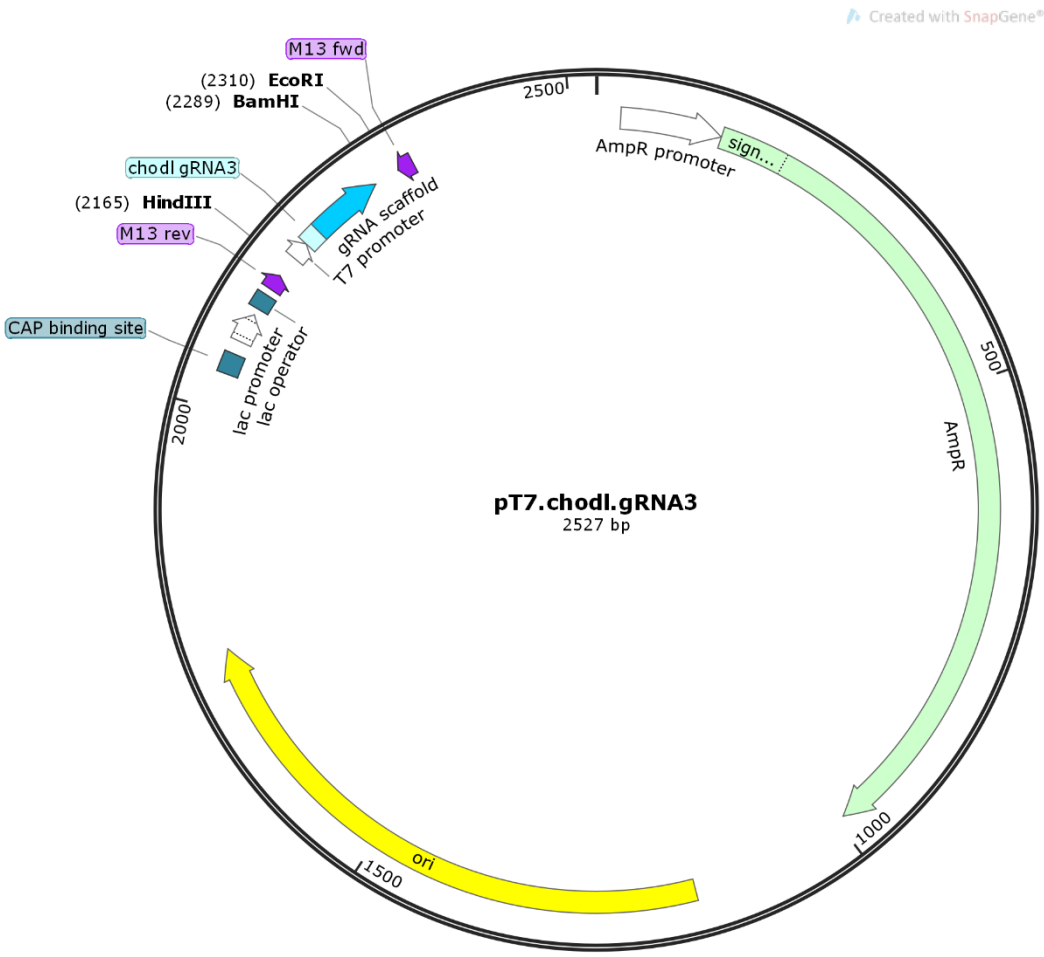

Figure 2.3: The pT7.chodl.gRNA2 map. The gRNA1 target sequence was annealed via paired oligos and subcloned into the pT7.gRNA scaffold vector (Addgene # 46759, from Wenbiao Chen). BamHI was used to linearise the plasmid for mRNA transcription.

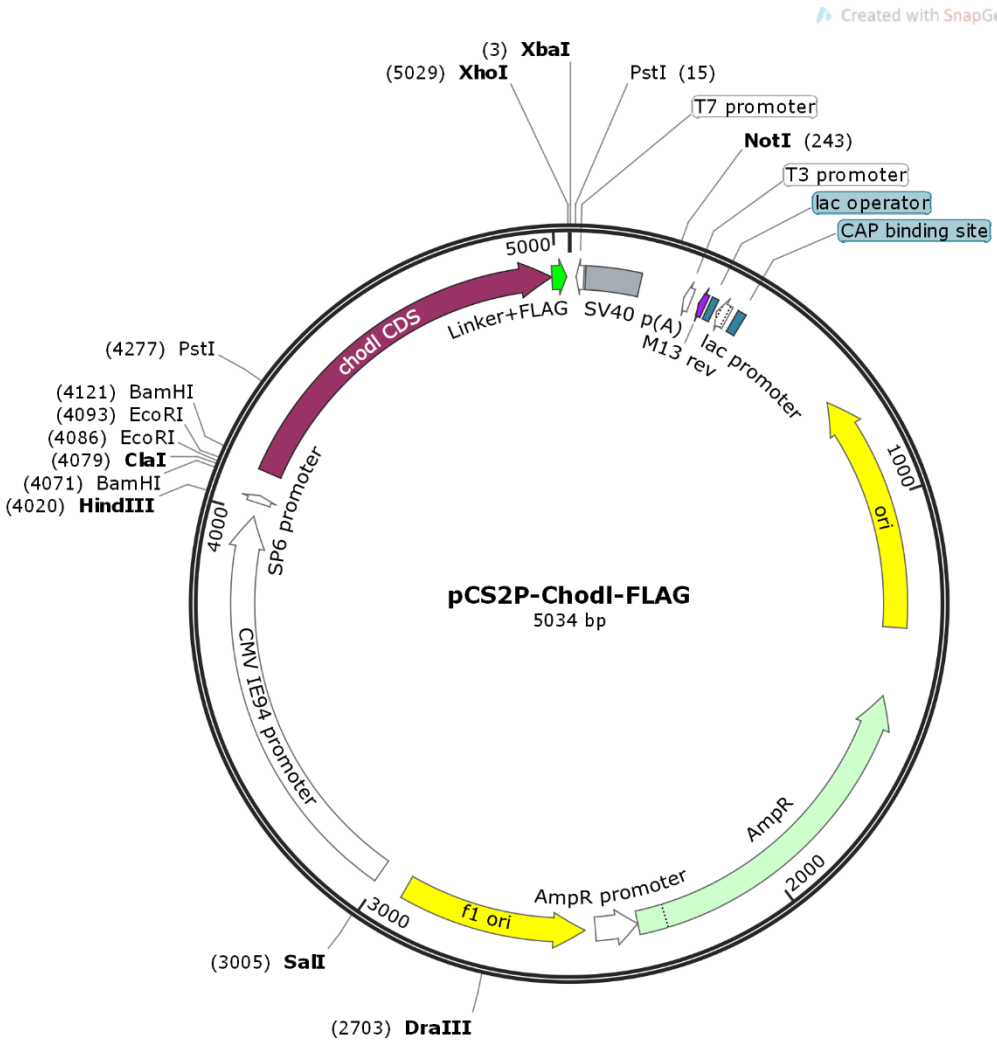

Figure 2.4: The pCS2P-Chodl-FLAG plasmid map. The chodl coding sequence without stop and with a linker and FLAG tag added was amplified and subcloned into the pCS2P+ plasmid.

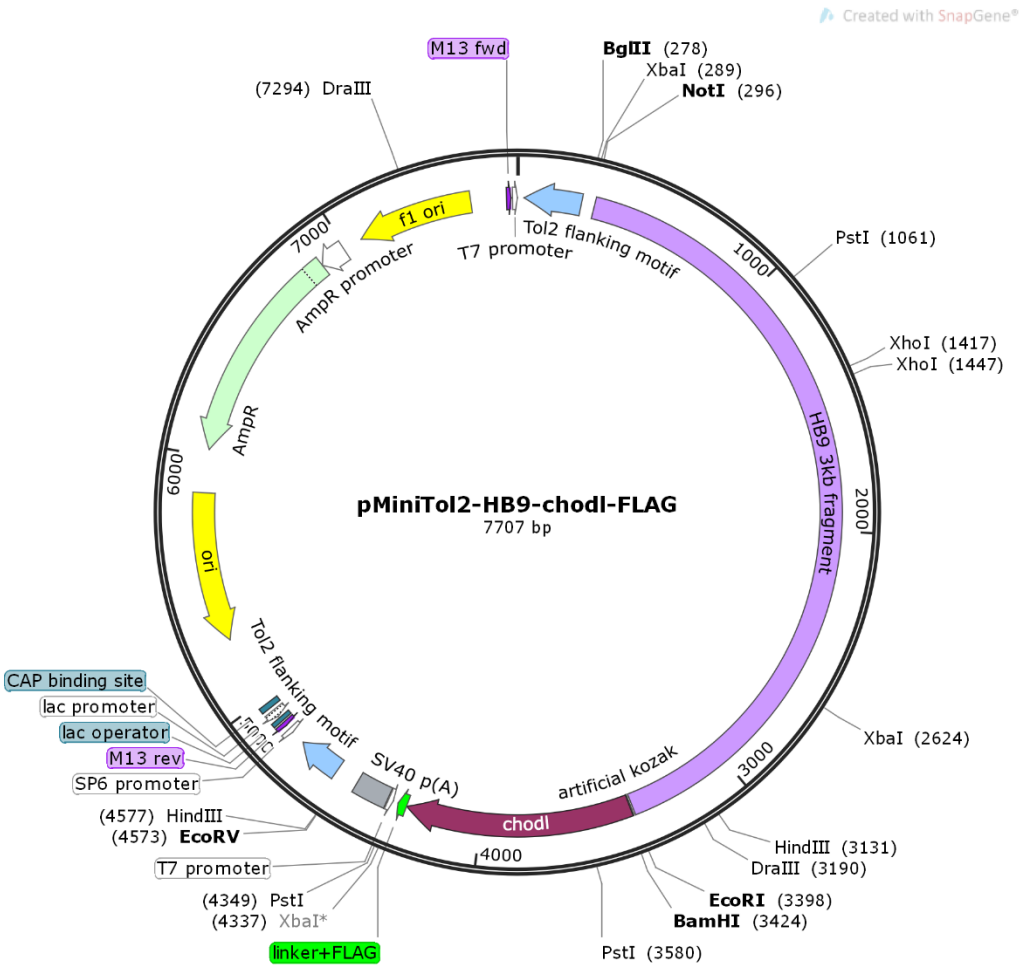

Figure 2.5: The pMiniTol2-HB9:Chodl-FLAG plasmid map. The chodl-FLAG sequence and SV40 were amplified from pCS2P-Chodl-FLAG (Figure 2.5) and subcloned into the pMiniTol2-HB9 plasmid.

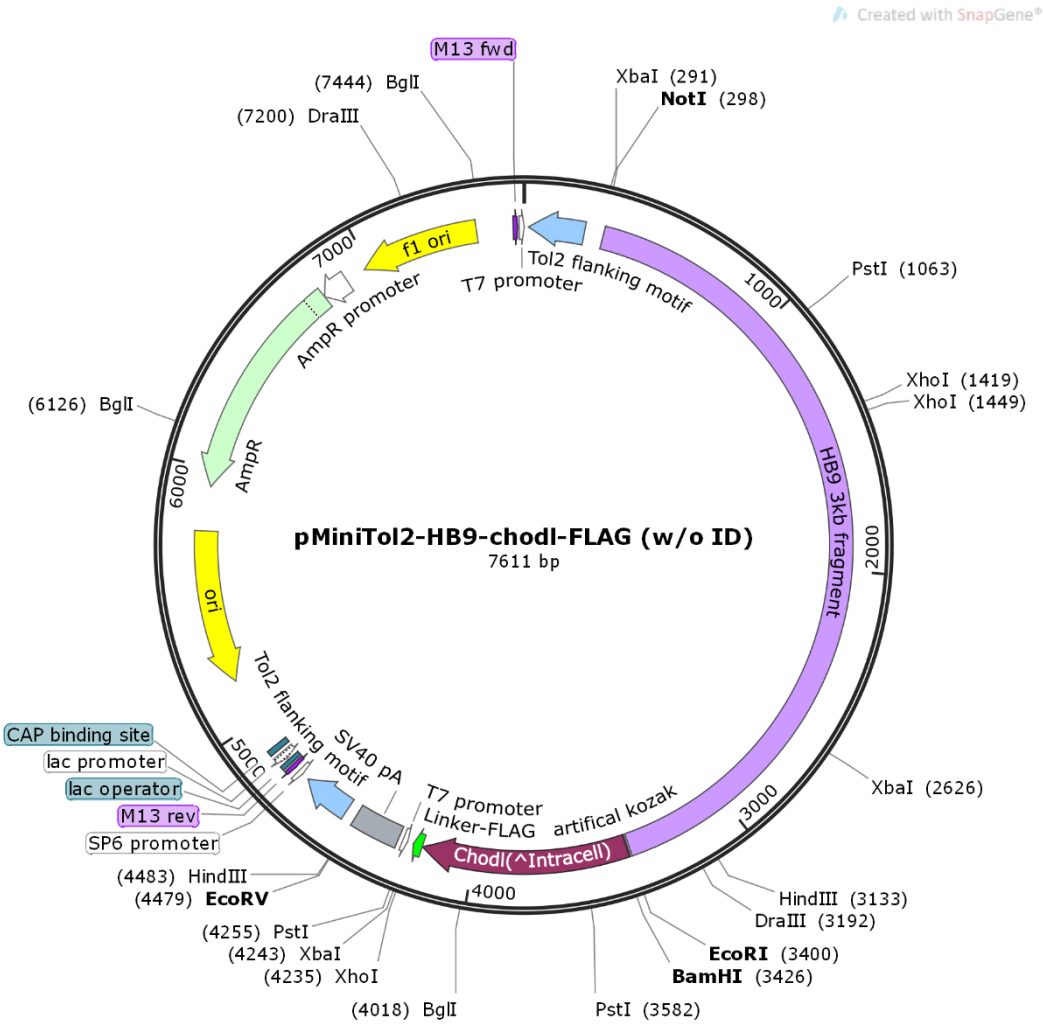

Figure 2.6: The pMiniTol2-HB9:Chodl-FLAG (w/o ID) map. The *chodl* sequence without intracellular domain and with a linker and FLAG tag were amplified and subcloned into the pMiniTol2-Hb9 plasmid.

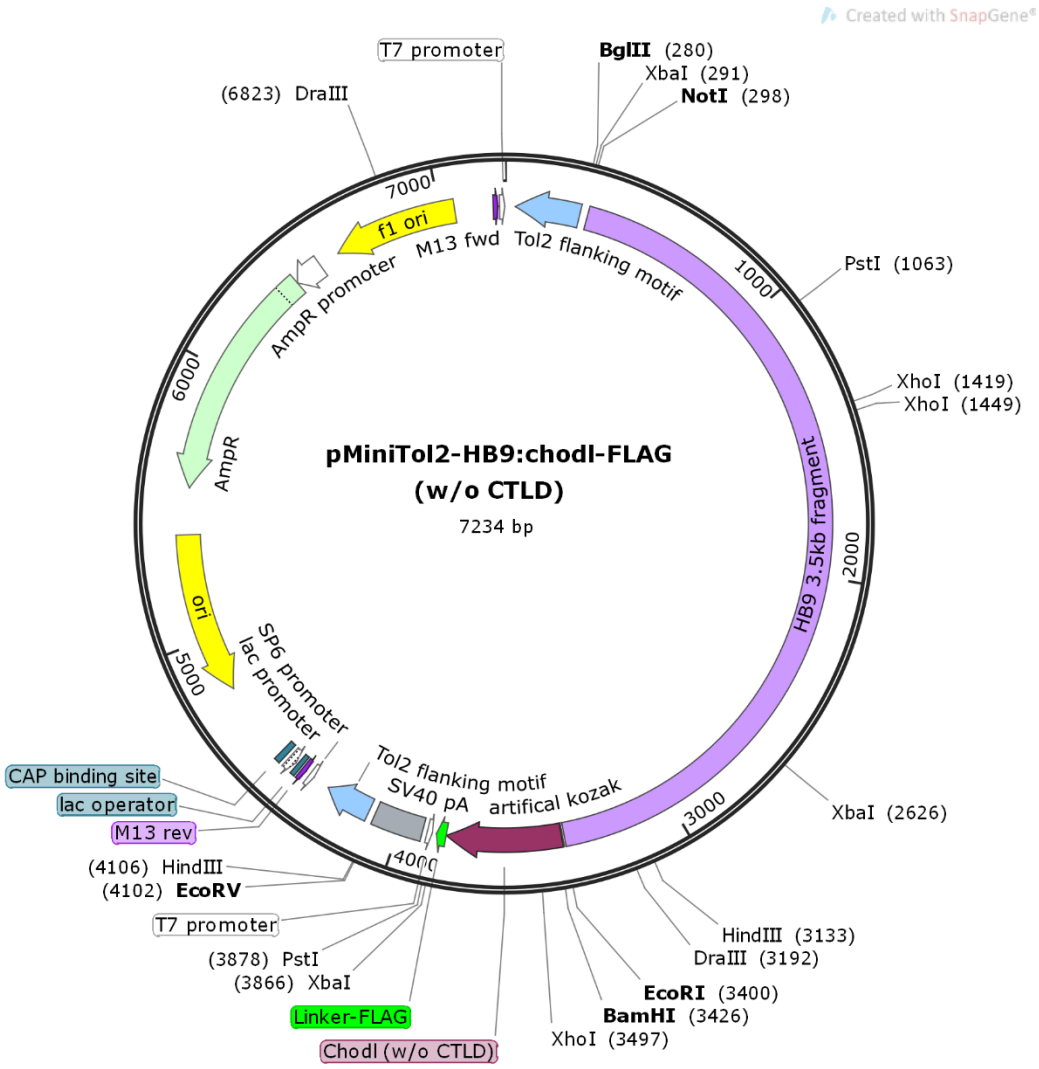

Figure 2.7: The pMiniTol2-HB9:ChodI-FLAG (w/o CTLD) map. The chondrolectin coding sequence, excluding the CTLD domain, and a linker, FLAG tag, and SV40 was amplified and subcloned into the pMiniTol2-HB9 plasmid.

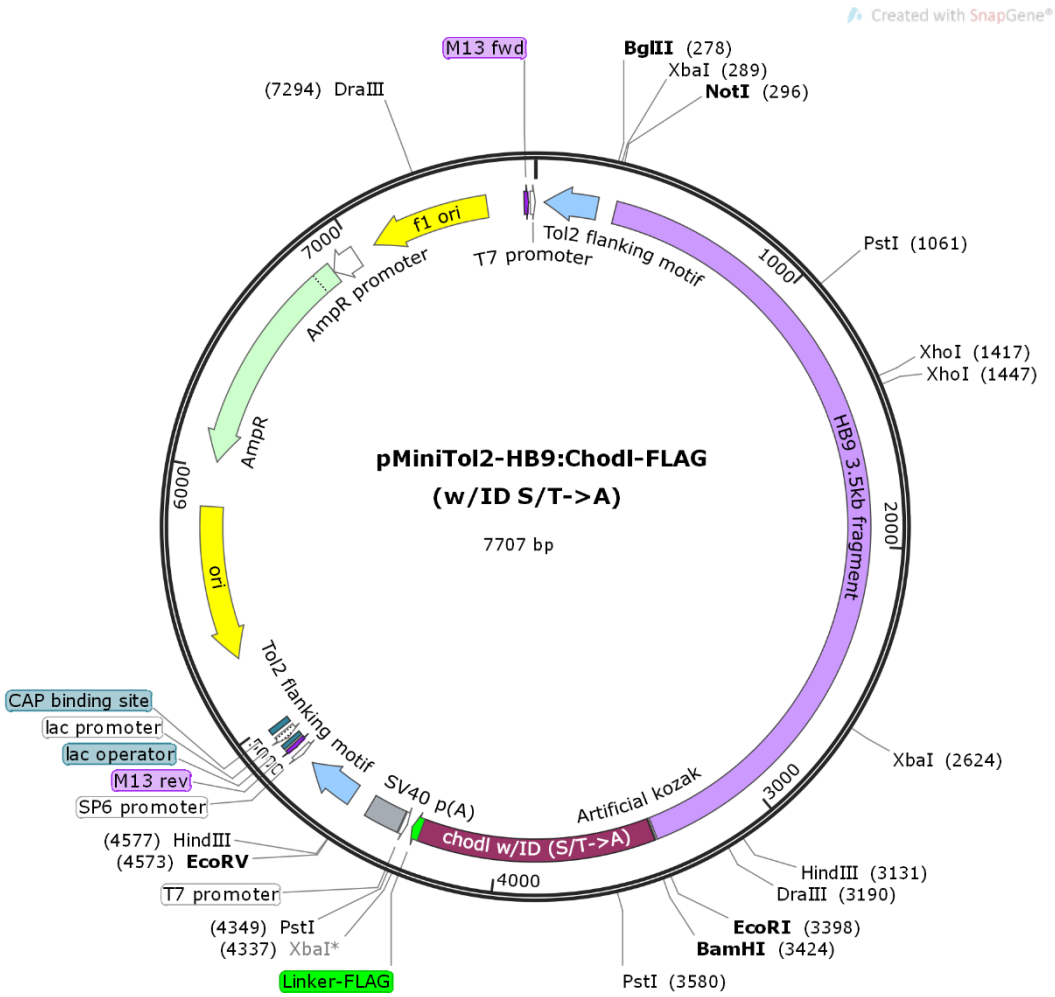

Figure 2.8: The pMiniTol2-HB9:Chodl-FLAG (w/ ID S/T->A) map. The chondrolectin cloning sequence, with the intracellular domain Ser and Thr residues mutagenised to Ala, a linker, FLAG tag, and SV40 were amplified and subcloned into the pMiniTol2-HB9 plasmid.

Chapter Three - Chondrolectin acts cell-autonomously in motor neurons and is necessary for timely axon growth

3.1 – Introduction

3.1.1 – Chondrolectin is expressed in motor neurons and is required for correct timing of motor axon outgrowth in zebrafish

As was introduced in Chapter One, chondrolectin (*chodl*) shows enriched expression in motor neurons. Chondrolectin was first isolated from the mouse tail muscle (Weng *et al.*, 2002), and shows strong expression in the brain, spinal cord, smooth muscle, and spleen (Weng, Hübner, *et al.*, 2003). In the mouse, staining for CHODL showed immunoreactivity in the fast-twitch motor neurons (Enjin *et al.*, 2010). In zebrafish, *in situ* hybridisation demonstrated detectable expression in the motor neurons and trigeminal ganglion, from ~12 hpf onwards (Zhong *et al.*, 2012) (Shown in Chapter One, Figure 1.6). Co-labelling of the chondrolectin ISH and HB9:GFP fluorescence, which labels motor neurons, demonstrates that chondrolectin expression is detectable before axons begin to extend from the spinal cord and remain detectable in the spinal during axon outgrowth, until at least 3 dpf (Zhong *et al.*, 2012, Thisse *et al.*, 2004).

Morpholino-mediated knockdown of *chodl* in zebrafish showed that the CaP axon is shorter at 24 hpf, and the CaP axon tended to stall at the horizontal myoseptum choice point. This stalling of the CaP axon persists until at least 33 hpf, and MiP axons also fail to grow. This demonstrated that chondrolectin is required for motor axon growth in zebrafish (Zhong *et al.*, 2012, discussed in Chapter One, Section 1.4.2).

Chondrolectin mRNA injection into the morphants rescued the axonal length, demonstrating the specificity of chondrolectin expression level in the axon growth. However, over-expression by chondrolectin mRNA injection into wild-type embryos also caused shorter CaP axons (Chapter One, Section 1.4.2). This suggests that the expression level of chondrolectin must be tightly controlled, as both over-expression and knockdown of chondrolectin leads to changes in the axon length compared to wild-type controls.

From the findings published in Zhong *et al*., 2012, it is clear that chondrolectin is necessary for axonal growth in zebrafish. This is supported by the findings in Enjin *et al.*, 2010, where chondrolectin is highly expressed in mouse fast-twitch α motor neurons. Primary motor neurons in zebrafish also exclusively innervate fast twitch muscle fibres (Menelaou and McLean, 2012; Babin, Goizet and Raldúa, 2014). As well as being a key gene during the development of motor axons, chondrolectin has also been linked to a form of motor neuron disease, Spinal Muscular Atrophy. Chondrolectin expression is down-regulated and mis-spliced in mouse models of SMA both before the onset of motor symptoms (Bäumer *et al.*, 2009) and into later stages of disease progression (Zhang *et al.*, 2008). Over-expression of chondrolectin also partially rescues the axonal phenotype in zebrafish with *smn* knockdown, further suggesting the link between SMA pathology and chondrolectin function (Sleigh *et al.*, 2014).

Chondrolectin is therefore a key gene for further investigation, important both due to its requirement for motor axon development and the translational aspect of its links with SMA. Given the temporal limitation of morpholino, limited to the first 3-5 days post fertilisation (Bill *et al.*, 2009), this chapter details the generation of a stable knockout of chondrolectin for characterisation.

3.1.2 - Chondrolectin is a transmembrane protein containing a C-type lectin domain

The sequence homology between the zebrafish and the human or mouse gene is 92%, indicating a high degree of conservation between zebrafish and mammals

(Zhong *et al.*, 2012). The amino acid sequence of chondrolectin predicts several protein domains, according to Uniprot (www.uniprot.org, Uniprot ID Q568T5). The protein domains include an N-terminal signal peptide, a C-type lectin domain, transmembrane domain, and short C-terminal helix (intracellular domain). A schematic representation is shown in Chapter One, Figure 1.5.

However, the mechanism by which chondrolectin performs its function is unknown. Chondrolectin does not have any close homologue, its closest related gene being layilin, with 45 % homology. Layilin has been identified as a hyaluronan receptor, but there is no detectable interaction between chondrolectin and hyaluronan (Bono *et al.*, 2001; Weng *et al.*, 2002). Although C-type lectin domains are usually ligand-binding domains, there are no published binding partners for the CTLD of chondrolectin. Chondrolectin also contains a single pass, type I transmembrane domain. Together, the transmembrane domain and C-type lectin domain suggest that chondrolectin acts as a cell-surface protein, interacting with the ECM. We hypothesise in this thesis that Collagen XIXa1 is a binding partner to chondrolectin, and this is discussed in Detail in Section 3.3.3 of this thesis. A zebrafish mutant for collagen XIXaI, stumpy, phenocopies the morphant and mutant to chondrolectin, suggesting a functional link between the proteins (Hilario, Wang and Beattie, 2010).

The intracellular domain of chondrolectin is a short helical chain of 30 aa in length, with no structural motifs. There is one published study of this domain which used an Sos recruitment screen with this domain to pull down binding proteins (Claessens, Weyn and Merregaert, 2008). The protein isolated was Rab geranylgeranyl transferase β (Rabggtb), a protein that associates with Rab GTPase, isoprenylating the Rab GTPase for its association with the plasma membrane. There is no further discussion or speculation in this paper as to why Rab geranylgeranyl transferase binds the chondrolectin domain. The authors suggest that chondrolectin could stabilise the Rabggtb during its catalytic prenylation of the Rab GTPase but assume the domain would not be prenylated itself due to lack of the usual motifs. However, the chondrolectin intracellular domain contains a high proportion of serine and threonine residues, 12/30 (40%). This means numerous amino acids of this domain can be phosphorylated, suggesting that chondrolectin could act as a signalling molecule. Supporting this hypothesis, the C-type lectin superfamily is associated with signalling proteins important for immunity or cell adhesion (Zelensky and Gready, 2005; Dambuza and Brown, 2015; Cummings and McEver, 2017). I hypothesise that

chondrolectin binds a target ligand in the ECM and a phosphorylation-dependent change occurs via the C-terminal intracellular domain. Given the largely unknown mechanism of chondrolectin, functional analysis of the protein domains was an important question posed during this thesis, and results are presented in Section 3.2.6 of this chapter.

3.1.3 - Transgenesis, expression manipulation, and genome editing in zebrafish

A key advantage of zebrafish as a model organism is its great genetic tractability. A wide range of tools are available to manipulate gene expression and perform genome editing.

Acute gene knockdown in zebrafish is performed using morpholino. Morpholino are short antisense oligos which bind to mRNA, containing a morpholine ring backbone which prevents degradation in the cell. These oligos are straightforward to design, can be commercially produced, and induce knockdown via two methods. Translation-blocking morpholinos bind the translational start site of the mRNA and cause steric blockage of the ribosome. Splice-site morpholinos bind to splicing sites, leading to intron inclusion or exon skipping during pre-mRNA processing (Eisen and Smith, 2008). Morpholino is particularly useful as the translation-blocking morpholinos can also knockdown maternally deposited mRNA present in the yolk, which may have compensatory effects in early development, while splice-site morpholinos do not, allowing comparison of these effects. However, morpholino-based approaches have some limitations in their use, particularly that the dosage of MO injected is diluted as the embryo's cells continue to divide. Thus the effect of MO knockdown usually lasts for a maximum of 3-5 days (Bill et al., 2009), preventing experiments on older larvae or adults. Morpholino also must be carefully dosed and laboriously injected into each clutch to prevent over- or under-dosage of the knockdown. Although this is more labour-intensive, it does allow titration of the knockdown effect. Some off-target effects have been reported due to potential toxicity of the morpholino and poor control of specificity, particularly activation of p53 (Robu *et al.*, 2007; Stainier *et al.*, 2017). A knockout mutant to chondrolectin is therefore a very valuable tool for further

investigation into the mechanism and function of *chodl* aside from its role in axonal growth.

Acute over-expression in zebrafish is commonly performed by injection of capped mRNA into the single-cell embryo. Much like morpholino, there is little temporal or spatial control of the expression change, as all cells can take up the mRNA or morpholino at any point after the injection. In mRNA over-expression, this can lead to exogenous translation of the protein in cell types that do not normally express it, but the amount of mRNA can be injected can be adjusted to investigate different doses of protein (Simone *et al.*, 2018).

Classical transgenesis, used to establish fluorescent reporter lines such as HB9:GFP (Flanagan-Steet *et al.*, 2005), is possible as injection of DNA can randomly integrate into the genome. However, there are limits to the size of cassette which can be integrated, the efficiency is very low, and its insertion site is random, potentially having deleterious effects. An improved method of transgenesis to insert fusion proteins or tissue reporters is the Tol2 transposon system. Utilising transposable elements, the integration sites and number of copies inserted are still stochastic, but the efficiency and size of cassette which can be inserted is improved (Kawakami *et al.*, 2004; Balciunas *et al.*, 2006). The combination of a gene's coding sequence with a tissue-specific promoter allows spatial control of the expression, which is advantageous over mRNA expression, but given the integration is mosaic, it is may be more suitable for generation of stable transgenic lines rather than the acute manipulation offered by mRNA injection.

To generate knockout mutants, recent developments have greatly improved the ability to target a gene for deletion, and its efficiency. Mutants were previously generated using forward genetic approaches, such as ENU mutagenesis, in large genetic screens such as the Tübingen screen published in Development (Mullins *et al.*, 1994; Driever *et al.*, 1996; Furutani-Seiki *et al.*, 1996; Granato *et al.*, 1996). However, reverse genetic approaches for genome editing have become more feasible in the last decade (Huang *et al.*, 2012). The CRISPR/Cas9 system represents a more streamlined method to generate indel mutants. The Cas9 nuclease is separate to the targeting gRNA, and can be introduced as either RNA or protein into the cell. The gRNA targeting each sequence is formed by the gRNA backbone and addition of the specific target site, at around 20 bp in length (Jao, Wente and Chen, 2013; Ran *et al.*,

2013). It does not therefore require generation of large recognition sequences for each target like for ZFNs and TALENs.

CRISPR/Cas9 is a modified prokaryotic immunity, where foreign DNA sequences are recognised and cleaved after insertion into the genome (Wiedenheft, Sternberg and Doudna, 2012). The Cas9 nuclease has been engineered for improved efficiency in zebrafish, including a zebrafish nuclear localisation sequence (Jao, Wente and Chen, 2013). Downsides to CRISPR are that the rate of off-target effects are thought to be higher than in TALENs (Pattanayak, Guilinger and Liu, 2014; Anderson *et al.*, 2015, 2017), but protocols of screening methods to reduce this chance have been published. Given the ease of designing and producing a gRNA oligo over the proteins for TALENs and ZFNs, I chose to use CRISPR/Cas9 to generate a chondrolectin knockout mutant.

In this chapter, I will present data on the design and generation of a chondrolectin knockout zebrafish. This chapter also characterises the *chodl* -/- zebrafish in its gross morphology and motor axon phenotype, as well as the generation of a transgenic *chodl* -/-;HB9:Chodl-FLAG line which rescues the embryonic phenotype. By limiting the Chodl expression to motor neurons with the HB9 promoter, this demonstrates a cell-autonomous function of chondrolectin. I also perform functional analysis of chondrolectin in the zebrafish, observing if chondrolectin constructs that have structural domains removed can induce acute rescue of the phenotype.

3.2 – Results

3.2.1 - Design of gRNAs for targeted chondrolectin knockout via CRISPR/Cas9

As previously described, the CRISPR/Cas9 system requires both a Cas9 protein to cut the genomic DNA, and a guidance RNA (gRNA) to bind the targeted region and direct the specific site for the Cas9 to cleave. The gRNA length is between 18-23 bp and must contain an XGG motif called the PAM (protospacer adjacent motif), but no other sequence motifs are required, making potential gRNAs easy to find in a genomic sequence, although several factors are involved in gRNA design to maximise the efficiency and specificity of the target. Fortunately, there are several online tools that

can search the genomic sequence of interest and determine potential gRNAs, and then rank them according to specificity and likelihood to generate DSBs (http://crispr.mit.edu (Hsu *et al.*, 2013), and http://zifit.partners.org/ZiFiT/Introduction.aspx (Sander *et al.*, 2010; Hwang *et al.*, 2013)).

CRISPR-mediated mutations generate frame-shifting indels which lead to premature stops and thus a truncated, non-functional protein. To find gRNAs for chondrolectin, I entered the sequence for Exon 1 and 2 into http://crispr.mit.edu to find potential gRNAs (Hsu *et al.*, 2013). This tool ranks the gRNA sequences by specificity, using the number of potential off-target matches and the number of mis-matched bases, as well as if these off-targets are located in genes or intronic regions. For ease of genotyping mutants, the potential gRNAs were then checked for restriction sites close to the PAM, as the DSBs are most likely to be generated 3-4bp upstream of the PAM (Jinek *et al.*, 2012). Destruction of a restriction site from indels generated at this position can therefore be used to screen mutants.

I aimed to find gRNA targets as close to the 5' start site of the coding sequence, to increase the likelihood that a premature stop would lead to a truncated, non-functional protein. However, it has been recently reported that exon-skipping and other splicing disruptions may be induced after CRISPR-generated indels (Sharpe and Cooper, 2017). In zebrafish, this has been shown to potentially allow mRNA transcripts to be produced which escape the usual nonsense-mediated decay process, although it is considered to occur with low frequency (Anderson *et al.*, 2017). In practice, this meant that as well as using the sequence data to predict frame-shift mutations, further controls were utilised such as morphant phenocopy and rescue of the mutant phenotype (presented later in this chapter). Three gRNAs were selected, using the online CRISPR tool to check that there were not potential off-targets either in genes or with a mismatch of fewer than 3 bases. This is because it has been shown that mismatches of 1 or 2 bases have a chance to bind off-target. However, mismatches of 3 or more bases are unlikely to bind (Ran *et al.*, 2013; Anderson *et al.*, 2015). I also cross-referenced the target sequences for restriction sites close to the PAM (Table 3.1). After generating these gRNA sequences, there is a further tool to design primers that allows insertion of the gRNA target into a plasmid containing the hairpin gRNA backbone, http://zifit.partners.org/ZiFit/Introduction.aspx (Hwang *et al.*, 2013).

gRNA	Target sequence (PAM bolded)	Number of targets with fewer than 3 mismatches (Number inside genes)	Rating	Restriction enzyme
1	GGAGGATGCGCG CGACACTC**AGG**	0 (0 inside genes)	98	BspCNI
2	GGCGTTCTGGGA GGCTCTGC**AGG**	0 (0 inside genes)	85	PstI
3	GGTCCTGTCCCA ATCTGTAC**AGG**	0 (0 inside genes)	93	BsrGI

Table 3.1: gRNAs designed to induce knockout of chondrolectin. The chosen 3 gRNAs for targeted knockout of chondrolectin, the number of potential off-targets found by the crispr.mit.edu tool, its rating, and the restriction enzyme used for genotyping.

The gRNA plasmids were generated and transcription of gRNA and Cas9 mRNA performed (see Chapter Two – Materials and Methods). Single-cell stage eggs from the HB9:GFP transgenic line were injected with each gRNA and Cas9. Several were screened for potential acute phenotypes in the g0, while the rest were raised for later breeding to generate founders. Several representative images from the injected clutches are shown below (Figure 3.1), demonstrating that all gRNAs generated efficient indels which led to a visible phenotype even in acute injection. These early mosaic phenotypes, where the CaP axon is stalled at the horizontal myoseptum, were also an indicator that the target was specific to chondrolectin, as this phenocopies the published morpholino data (Zhong *et al.*, 2012).

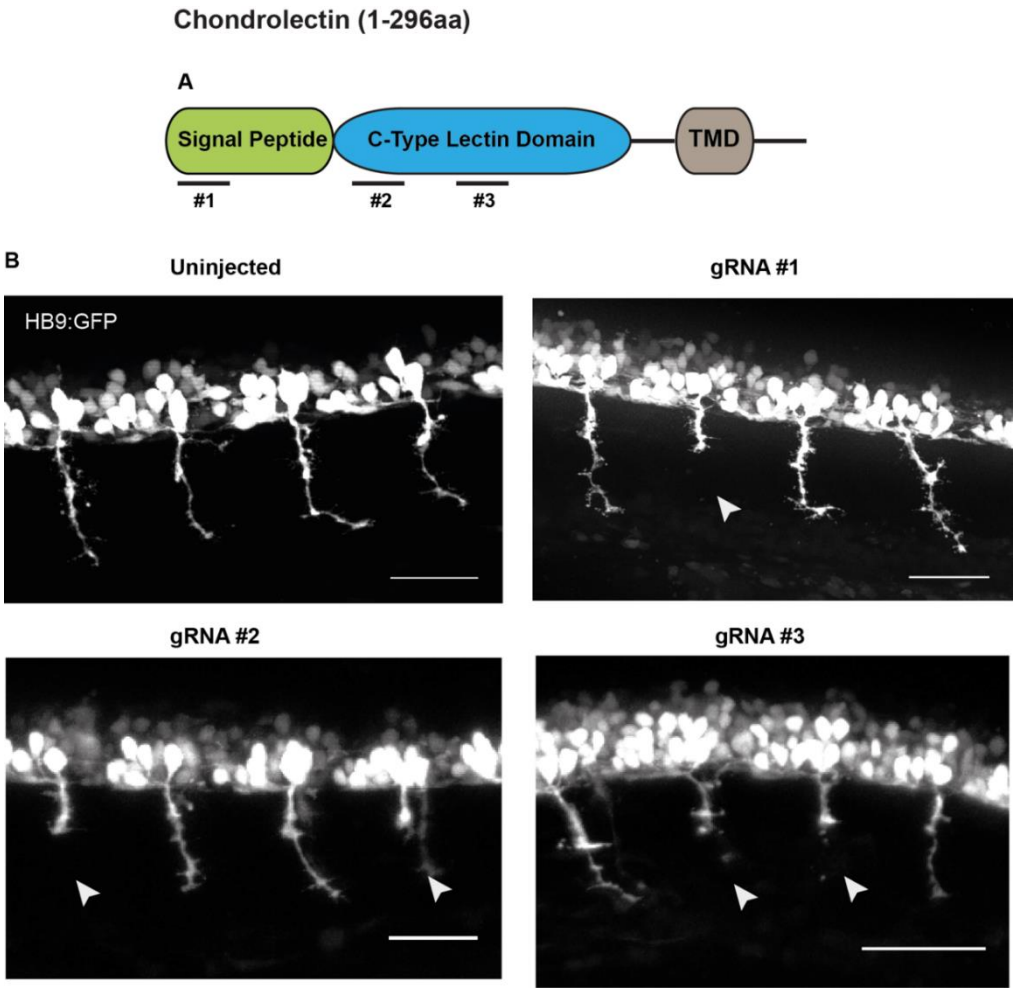

Figure 3.1: All gRNAs are able to induce an acute axon phenotype into injected clutches.

A: The domain structure of chondrolectin, and the locations of the chosen gRNAs.

B: Acute phenotypes in injected HB9:GFP embryos at 26 hpf. Uninjected embryos show all axons have grown beyond the horizontal myoseptum. For each gRNA, at least 1 axon is stalled at the HM (arrowheads). Scale bars= 50 µm

As well as assessing the acute axon phenotype in injected embryos, genotyping was performed using restriction digest analysis. PCR primers were designed to amplify a ~300 bp region flanking the gRNA target. Digestion of uninjected genomic DNA by the restriction enzymes listed in Table 3.1 above would result in bands of ~200 and ~100 bp, but loss of the restriction site due to mutations in the injected clutches means the ~300 bp amplicon would remain undigested. By pooling the DNA of several

embryos, the proportion of digested to undigested bands can be used as a qualitative measure of a gRNA's cutting efficiency.

An example gel from gRNA1 is shown below, (Figure 3.2). 5 embryos from uninjected and injected conditions were pooled at 26hpf and their genomic DNA extracted. After PCR amplification of the 300bp flanking region of gRNA1's target and half of the reaction mixture digested with BspCNI, a restriction enzyme whose recognition site aligns with the PAM and gRNA target.

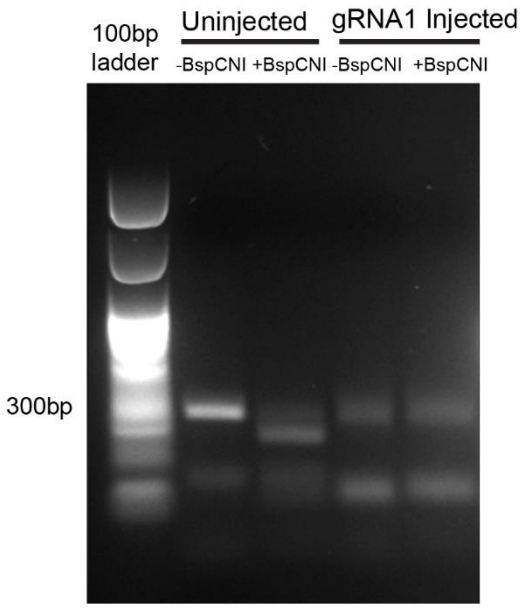

Figure 3.2: Restriction-based genotyping of CRISPR mutations.
An example gel used for genotyping potential mutation efficiency by gRNA1. A 100 bp ladder was used, with the 300 bp position marked. In the Uninjected group, the undigested band is ~300bp in length, and addition of BspCNI digests the band to two bands at ~100 and ~200 bp. In the Injected group, both the undigested and digested bands remain at 300 bp, suggesting a high efficiency of indels induced by the gRNA1 and loss of the BspCNI site.

As can be seen from the gel (Figure 3.2), in the uninjected group without BspCNI, the band remained undigested at 300bp. In the uninjected group, with addition of BspCNI, almost all of the amplicon has been digested, with bands at 100bp and 200bp. However, in the gRNA1-injected group there is almost no digestion upon addition of BspCNI. This demonstrates that the DNA of this pooled group had a high proportion

of mutation induced by the injections even at this acute phase, resulting in loss of the restriction site.

3.2.2 - Establishing the stable chondrolectin -/- line

Clutches of injected embryos were raised to adulthood, and adults injected with gRNA1 and gRNA2 were outcrossed to WIK wild-type zebrafish. Outcrossing the g0 generation is vital to reduce the chance of off-target effects, if any are present in the clutch. The g0 clutches are mosaic, with some cells containing indels and some unaffected by the Cas9. The kind of indels, and whether it will generate a frame-shift mutation, is also stochastic. Thus, the next generation (F1) will contain a mixed population, with some wild-type eggs, and some which are heterozygous for a range of indels. The efficiency of the gRNA is again important to maximise the proportion of heterozygous *chodl* +/- eggs over the wild-type population.

Because the gRNA1 was targeted at the most 5' position of the chondrolectin sequence, and had the highest rating during the gRNA design, the F1 generation from this gRNA were fin-clipped first for genotyping using restriction digest analysis, followed by sequencing. From this, three heterozygotic fish containing frame-shift mutations were detected. By total chance, one male and one female had identical 4 bp deletions, and one further female had a 5 bp deletion. The 4 bp deletion, ΔCTCA, leads to a predicted premature stop codon at amino acid position 10 from the start site, producing a protein just 9 aa in length, rather than the usual 296 aa of chondrolectin (Figure 3.3). As this stop codon occurs in the first protein domain, the signal peptide, it is highly likely that this truncated protein is non-functional, however we did not confirm nonsense-mediated decay and could not confirm loss of protein expression due to lack of antibodies to Chodl. However, we determined that our observed phenotype was specific to a loss-of-function of chondrolectin by rescuing the phenotype with re-expression of chondrolectin (discussed in Section 3.2.5).

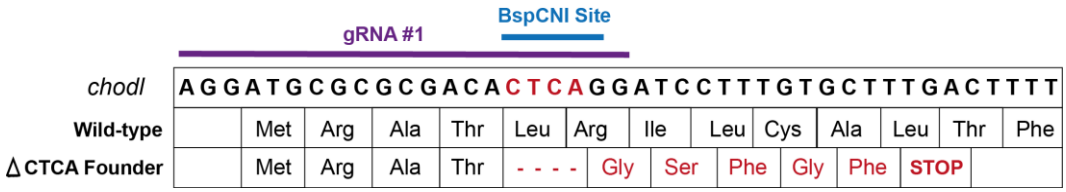

Figure 3.3: The *chodl* -/- founder contains a 4 bp deletion which causes a frame-shift mutation.
The founder of the *chodl* -/- line has the deletion ΔCTCA, which leads to a predicted premature stop codon after 9 aa. This also destroys the restriction site for BspCNI which was used for genotyping.

As we had adults with identical mutations of each sex, this F1 pair was incrossed and the offspring screened at ~26 hpf for any phenotype. As the g0 background was HB9:GFP and then outcrossed to the WIK line, the majority of the F2 clutch were GFP-positive in their motor neurons, allowing easy screening of axonal phenotypes. The GFP-positive (~75% of the population) and GFP-negative embryos (~25% of population) were separated and all the GFP-negative embryos raised for later genotyping of the *chodl* ΔCTCA mutation. However, the GFP-positive could be further separated for their shortened axonal phenotype (predicted homozygote mutants) and those with the wild-type phenotype (assumed heterozygotes or wild-types) between 26 and 30 hpf. The proportion of the GFP-positive embryos which also exhibited an axonal phenotype was around 25%, the expected Mendelian distribution for an incross of heterozygote mutants.

In the F2 GFP-positive phenotypic population, several were confirmed for mutation homozygosity by sequencing, while the rest were raised to produce the stable *chodl* -/- line. In the GFP-positive population, the visible phenotype allowed validation of homozygotes at the embryonic stages, while the GFP-negative population was genotyped by fin-clipping and restriction analysis in the adults, in order to find homozygote mutants. The axonal phenotype was also confirmed in these GFP-negative homozygous mutants using SV2 labelling, which allows the visualisation of motor axons. This led to the formation of a stable line, with a ΔCTCA mutation, on two transgenic backgrounds, either the HB9:GFP background (GFP-positive in the motor neurons), or a fully wild-type background without any transgenic reporter (GFP-negative).

3.2.3 - Motor axon phenotypes in the *chodl* -/- embryo

In the morpholino knockdown, there are two classes of stalled axons – approximately 35% of the axons remain stopped at the HM and never grow beyond it, while 55% of the axons stalled temporarily and then continued to grow, passing beyond the HM but not reaching the wild-type length by 24 hpf (Zhong *et al.*, 2012).

In the *chodl* -/- embryos, we first measured the axonal phenotype by scoring the CaP axon position at ~28 hpf, adapted from the scoring system used in Zhong *et al*, 2012. Representative images of the axonal phenotype and the scoring at 28 hpf is shown in Figure 3.4. All of the CaP axons in wild-type embryos have passed the HM choice point. In the *chodl* -/- mutants, however, only 22.66% have passed the HM, and so 77.34% of these axons are stalled at the horizontal myoseptum, which is statistically significant over the controls (Control HM= 0% ±0, n=16. *chodl* -/- HM= 77.34% ±6.062, n=16. Control HM+= 100% ±0, n=16. *chodl* -/- HM+= 22.66% ±6.062, n=16. Control vs *chodl* -/- HM, unpaired t-test with Welch's correction **** p<0.0001. Control vs *chodl* -/- HM+, unpaired t-test with Welch's correction **** p<0.0001.) The ratio of axons stalled at the HM is also more than twice the proportion stopped at the HM in the morphants observed in Zhong *et al.*, 2012. This is most likely due to the full knockout of chondrolectin compared to morpholino knockdown, where there may be residual but low expression of the protein.

As well as stalling at the HM, the axons are significantly shorter than controls at 28hpf. The *chodl* -/- axon length is 56.89% shorter than the mean control length. (Control mean= 95.73 µm ±3.212, n=13. *chodl* -/- mean= 41.27 µm ±1.763, n=10. Unpaired t-test with Welch's correction ****, p<0.0001).

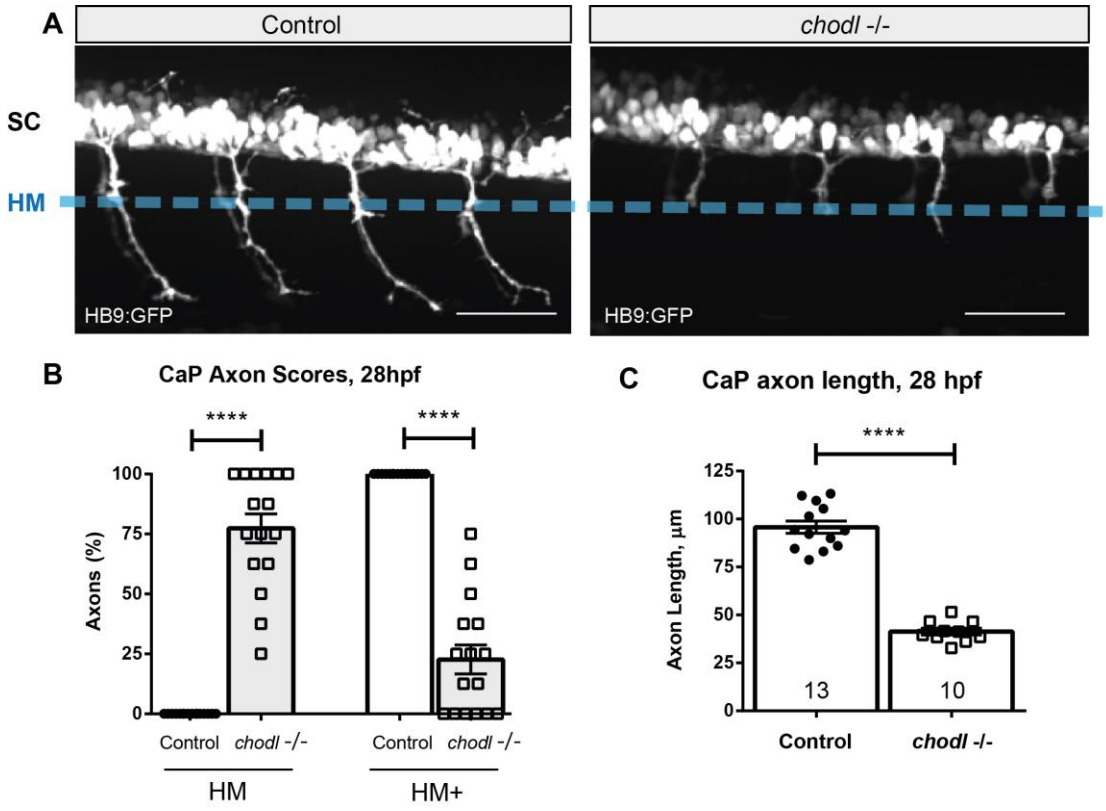

Figure 3.4: The CaP axons of *chodl* -/- embryos stall at the horizontal myoseptum.
A: Representative images show that the CaP axons in wild-type control 28 hpf embryos have extended beyond the horizontal myoseptum choice point (blue dashed line) but are stalled at this point in *chodl* -/- embryos. SC = spinal cord, HM= horizontal myoseptum. **B**: Scoring the axon position as either at the HM (HM) or beyond it (HM+) demonstrates that there is a significant difference between control and mutant axon position. (Control vs *chodl* -/- HM, unpaired t-test with Welch's correction ****. Post-hoc power= 1.00. Control vs *chodl* -/- HM+, unpaired t-test with Welch's correction ****. Post-hoc power= 1.00.) **C**: The CaP axon length is significantly shorter in *chodl* -/- embryos compared to wild-type controls. (Unpaired t-test with Welch's correction ****. **** p<0.0001 Post-hoc power=1.00.) Scale bars= 50 µm.

At 48 hpf, as well as the primary axons, the secondary axon network has also grown, using, although not requiring, the primary axons as pioneers during their pathfinding (Pike, Melancon and Eisen, 1992; Davis-Dusenbery *et al.*, 2014). The pathway taken by the CaP axon pioneers a central axon bundle for the secondary motor neurons, with further axon branching into the myotome (Babin, Goizet and Raldúa, 2014). To determine if the secondary motor neurons are also affected by the loss of chondrolectin, we measured the central axon bundle at 48hpf (shown below, (Figure 3.5 B). The axon length is significantly shorter in *chodl*-/- larva than wild-types. The axon bundle in the *chodl* -/- larva is 13.2% shorter than the controls (control mean length= 131.3 µm ±1.416, n= 20. *chodl* -/- mean length= 114 µm ± 2.023, n= 19. Unpaired t-test ****, p<0.0001). To quantify branching, I traced a line 10 µm anterior and posterior from each axon and counted the number of branches which crossed that line. There is a significant reduction in axonal branching in the chodl -/- mutant compared to the wild-type control group (Figure 3.5 C). The number of branches from the axon bundle is reduced by 46% (Control number of branches = 8.08 ±0.30, n=20. *chodl* -/- number of branches= 4.39 ±0.31, n=19. Unpaired t-test **** p<0.0001.) This suggests that as well as a growth deficit in the *chod*l -/- axons, as observed by the reduction in the main axon length, there is also a lack of branching into the muscle.

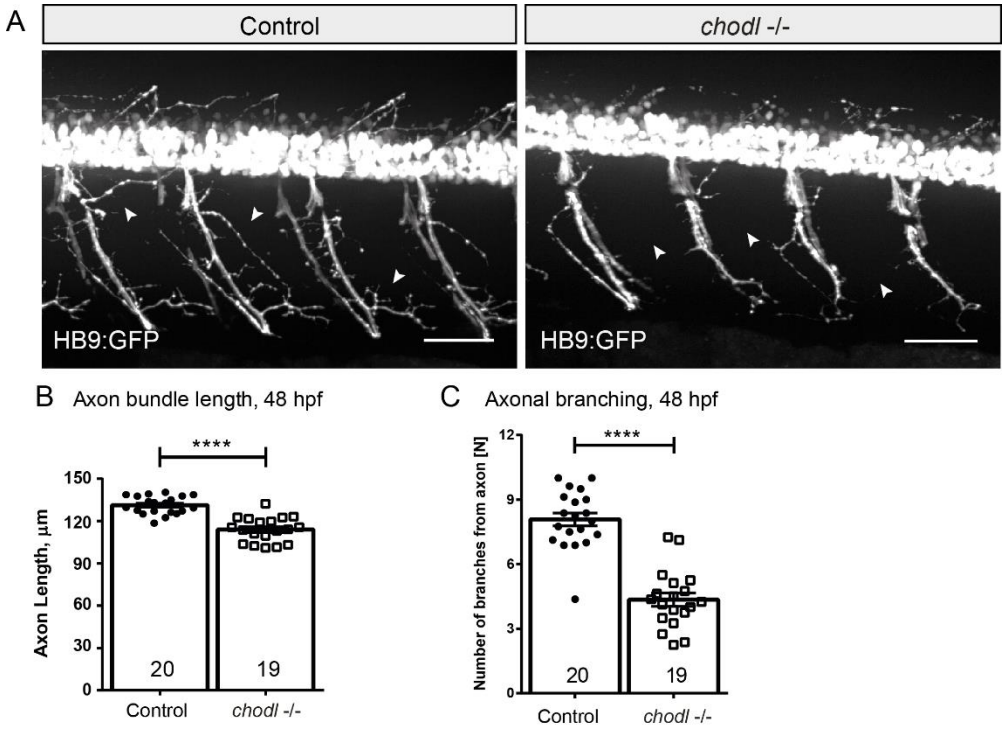

Figure 3.5: At 48pf, *chodl*-/- mutants exhibit significantly shorter axon bundles with aberrant branching compared to controls.
A: Representative images of wild-type control or *chodl* -/- larva at 48 hpf. White arrowheads show branching of the axons in the control group which are not present in the *chodl* -/- mutant. Scale bar= 50 µm. **B:** The axon bundle length is significantly shorter in the *chodl* -/- mutants compared to controls. (Unpaired t-test, **** p<0.0001. Post-hoc power= 1.00). **C**: The number of axonal branches is significantly reduced in the chodl -/- mutant compared to controls (Unpaired t-test **** p<0.0001. Post-hoc power= 1.00).

Similar measurements were performed at 72 hpf (Figure 3.6). The main axon bundle length in the *chodl*-/- larva has caught up with wild-types, and there is no significant difference in the length of these axons. (Control nerve length= 159.8 µm ±4.707, n= 10. *chodl* -/- nerve length= 160.1 µm ±3.905, n=7. Mann-Whitney test n.s., p= 0.8125). At 72 hpf, the number of branches from the main nerve bundle was analysed by tracing a line 15 µm from the ventral nerve both anterior and posterior and counting the number of branches to cross each line. It shows that there is a significant reduction in branching in the *chodl* -/- mutant compared to wild-type controls. The number of branches was reduced by 45% compared to the control value (control mean number of branches = 15.24 ±1.01, n= 10. *chodl* -/- number of branches= 8.45 ± 0.85, n= 7. Mann-Whitney test *** p= 0.0002.) This demonstrates that although the main nerve bundle catches up in length and reaches the ventral edge of the trunk, there are still deficits in the axons as they are less branched into the muscle. This is further shown in Chapter Four, where the lack of branching results in a reduction in the number of synapses in the trunk and may contribute to a behavioural deficit in the mutant larvae during turning behaviour.

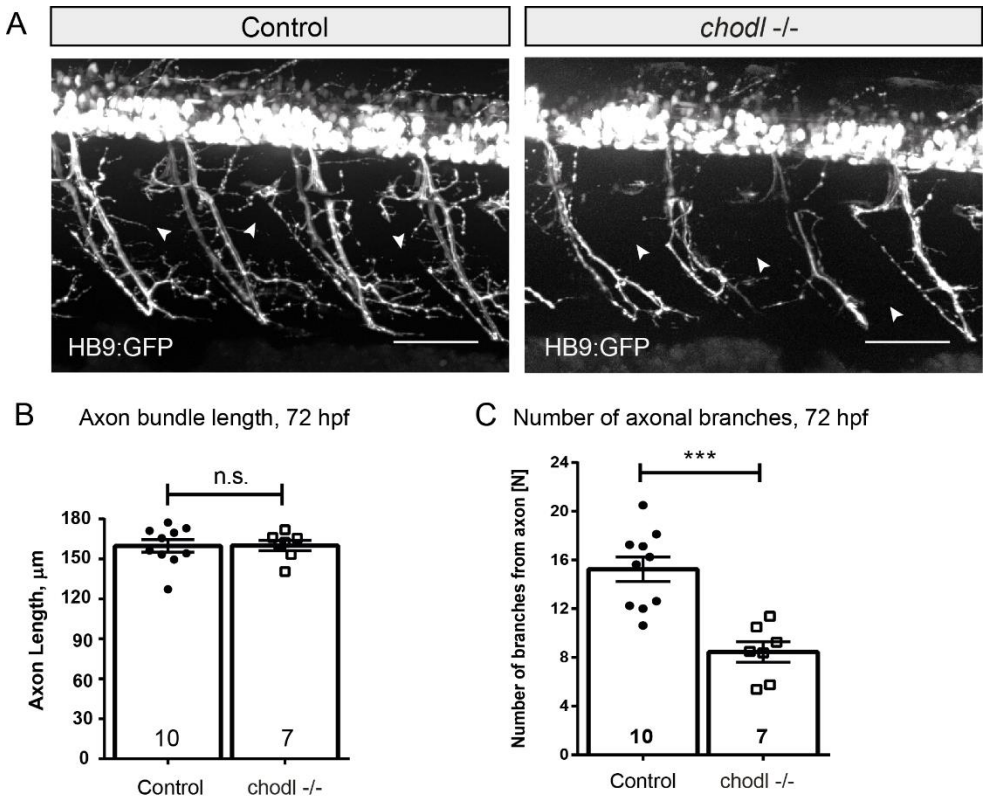

Figure 3.6: At 72 hpf, the ventral axon bundle is the same average length in *chodl* -/- larva as in control larva. However, there are qualitatively fewer branches into the myotome in the mutants than controls.
A: Representative images of the 72 hpf larvae. Axonal branching into the myotome are present in the control larvae but missing in the *chodl* -/- mutants (arrowheads). **B**: Measurements of the ventral axon bundle show no statistical differences between control and *chodl* -/- larvae. (Mann-Whitney test, n.s., p= 0.8125). Scale bars= 50 µm. **C**: There is a significant reduction in the number of branches in the chodl -/- larvae compared to the control larvae (Mann-Whitney test *** p= 0.0002, post-hoc power= 0.974).

Overall, it is clear that the *chodl* -/- zebrafish exhibit motor axon deficits from 28 hpf which continue until at least 72 hpf. The CaP primary axon is stalled at the HM and is thus shorter than in wild-types at 28 hpf. At 48 hpf, when the secondary motor axons have also grown out of the spinal cord, the *chodl* -/- larvae have reduced branching and the axons remain shorter than age-matched wild-types. At 72 hpf, the axon bundle length has caught up to those in wild-type animals, and there is a significant reduction in branching.

3.2.4 - Morphological phenotypes in the *chodl* -/- embryo

To determine if knockout of *chodl* caused other effects in the embryo beyond the axonal phenotype, we measured several aspects of the embryo morphology in comparison to wild-type controls. Firstly, the gross body morphology was analysed by measuring the body length and the eye diameter. This is a simple method to determine abnormalities in the mutant, such as developmental delay or reduced growth.

For both the body length and eye diameter measurements, there were no significant differences in either the wild-type or mutants at 30hpf. The measurements are shown below, (Figure 3.7). The body length is 0.45% shorter compared to wild-type controls. (Control average length= 2.253 mm ±0.0204, n= 14. *chodl* -/- average length= 2.243 mm ±0.0209, n=17. Unpaired t-test n.s., p= 0.7301). The eye diameter is 0.57% shorter in *chodl* -/- embryos than controls (Control average diameter = 191.7µm ±3.40, n= 15, *chodl* -/- diameter= 190.6 µm ±3.84, n=17, unpaired t-test n.s., p= 0.8295).

To determine if the muscle integrity is affected in the *chodl* -/- mutants, I performed phalloidin staining on wild-type and mutant embryos at 30hpf. Phalloidin labels the F-actin in fast muscle fibres (Pagnon-Minot *et al.*, 2008), and primary motor axons are known to innervate the fast muscle fibres (Babin, Goizet and Raldúa, 2014). Furthermore, chondrolectin has previously been found to be highly expressed in fast motor neurons in mice (equivalent to primary motor neurons in zebrafish) (Enjin *et al.*, 2010), so we expected systemic loss of chondrolectin to cause an axon phenotype without changing the muscle structure. However, mutations or knockdown in genes which change the muscle architecture may also alter axon growth or morphology, for

example the collagen 19a1 mutant, *stumpy* (Hilario *et al*, 2010). Collagen 15 knockdown with morpholino leads to wide-spread muscle defects visible by phalloidin staining, as well as branching and outgrowth aberrations in the primary motor axons (Pagnon-Minot *et al.*, 2008). Thus, to fully confirm that the axon phenotype is limited to axons, and not due to muscle defects, we performed phalloidin staining. Phalloidin is a toxin which binds actin, coupled with a fluorescent tag. I quantified any potential differences by counting the average number of myotubes, and the average thickness of each myotube. There were no differences between the wild-type controls and the chodl -/- embryos at 30 hpf (Fig 3.7, E). (Mean number of myotubes per somite in wild-type embryos = 20.94±0.81, n=6 embryos. Mean number of myotubes per somite in chodl -/- embryos = 21.56±0.54, n=6 embryos. Mann-Whitney test n.s., p= 0.331). There were also no differences in the average thickness of myotubes between the wild-type controls and chodl -/- embryos (Fig. 3.7, F). (Mean thickness of myotubes, control= 6.40 µm ±0.16, n=6 embryos. Mean thickness of myotubes, chodl -/- = 6.22 µm ±0.18, n= 6. Mann-Whitney test n.s., p= 0.589). The gross morphology of the muscle therefore seems unchanged between the two groups. However, there may be potential defects that are not detectable with the phalloidin staining. Other staining methods could be used, such as the antibody F59 which labels slow muscle fibres.

Overall, *chodl* -/- mutant embryos are morphologically indistinguishable to wild-type at the same stage. This demonstrates that the axonal phenotype is due to chondrolectin loss and not a general developmental delay in the mutants. Also, the stalled axon phenotype is due to an axon-specific change rather than deficits in the muscle architecture which affects the axon growth.

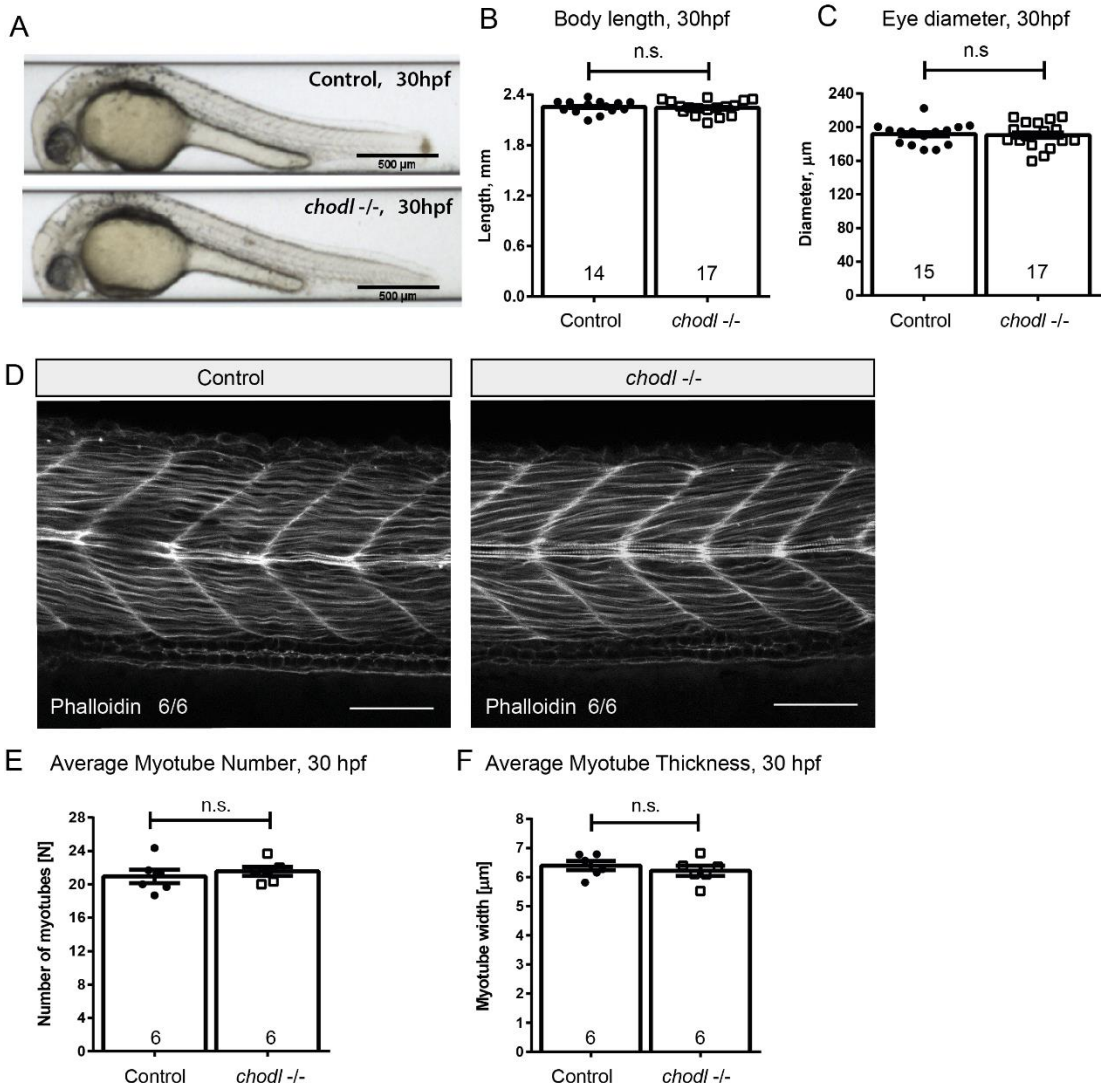

Figure 3.*7*: The chodl -/- embryos are morphologically indistinguishable from age-matched controls.
A: Representative bright-field images of wild-type control and chodl -/- embryos at 30 hpf. **B**: Body length measurements show no differences between wild-types and chodl -/- embryos at 30 hpf. (n.s., 0.7301, unpaired t-test.) **C**: The eye diameter is not significantly different between mutants and controls (Unpaired t-test n.s., 0.8295). **D**: Phalloidin staining shows no visible differences in muscle architecture between wild-type and chodl -/- embryos at 30hpf. **E**: The average number of myotubes per somite does not differ between wild-type controls and *chodl* -/- embryos at 30 hpf. (Mann-Whitney test, n.s.). **F**: The average thickness of the myotubes does not differ between the wild-type control and chodl -/- embryos at 30 hpf (Mann-Whitney test, n.s.) Scale bar A= 500 µm, D= 65 µm.

Although not quantified with a survival curve, *chodl* -/- zebrafish survived to adulthood and were able to successfully breed, with fertility success similar to wild-types. No additional husbandry measures were necessary to maintain these fish, although homozygous stocks were sorted and raised separately from non-phenotypic siblings in case of out-competition during juvenile phases. Lifespan of the mutant was not measured, as adult homozygous stocks survived until at least 18 months old when they were culled by Schedule 1 methods due to their age.

3.2.5 - Rescuing the *chodl* -/- mutant by re-expressing chondrolectin in motor neurons demonstrates that *chodl* is cell-autonomous

3.2.5.1 – The stable transgenic line *chodl* -/-;HB9:Chodl-FLAG fish shows no differences in axon length to wild-types at 28 hpf

A key control for specificity of a mutant phenotype is rescue by re-expression of the gene. In Zhong *et al.*, 2012, mRNA injection of chondrolectin rescued the axonal phenotype in the morpholino-mediated knockdown. However, global expression of *chodl* from this injected mRNA also had an effect in the wild-type zebrafish due to excess chondrolectin, resulting in shorter axons. Using mRNA allows variable dosages to determine dose-response curves, but also allows global uptake of the

mRNA and thus translation of the protein in all cells. This may lead to ectopic expression of the protein in tissue where it is not usually present. For example, in zebrafish, *in situ hybridisation* data demonstrates that *chodl* is limited to motor neurons. In mice, chondrolectin is highly expressed in fast motor neurons (Enjin *et al.*, 2010), and Southern blotting also found expression in the muscle and spleen (Weng, Van Bockstaele, *et al.*, 2003). Therefore, expression of chondrolectin only in motor neurons would be a useful tool to determine if its function is cell-autonomous and sufficient to rescue the mutant.

As well as acute rescue of the phenotype, a stable line expressing tagged chondrolectin has several advantages for other applications. Due to the lack of antibodies for chondrolectin, it is not possible to perform pulldowns or binding assays of the native protein using immunoprecipitation. However, a zebrafish line expressing chondrolectin tagged with an artificial epitope such as FLAG would allow purification of the protein from zebrafish through antibodies against this tag.

To produce a construct for generating this transgenic line, we utilised the Tol2 transposon system (Balciunas *et al.*, 2006). As has been described both in Chapter One and in the Introduction of this chapter (Section 3.13), this system allows insertion of a cassette randomly into the zebrafish genome, leading to mosaic integration in the injected embryos. This cloning methodology and primers are detailed in the Materials & Methods section. To limit expression of the cassette to motor neurons, Dr Ana-Maria Oprişoreanu amplified a 3kb section of the HB9 promoter and subcloned it into the pMiniTol2 vector. This promoter sequence has been previously published as a MN-specific promoter for transgenesis in zebrafish (Flanagan-Steet *et al.*, 2005).

I amplified the coding sequence of chondrolectin from the previously designed RNA expression vector, pCMV-*chodl*-myc (Zhong *et al.*, 2012). To enhance the likelihood of the construct successfully being expressed after integration, I added an artificial Kozak sequence optimised for zebrafish (Grzegorski *et al.*, 2014).

The pMiniTol2-HB9:*chodl*-FLAG plasmid was co-injected into *chodl* -/- embryos with transposase mRNA, and at 24 hpf, the embryos were selected for mosaic rescue of their CaP axons. Approximately 20% of the injected embryos displayed at least 3 rescued axons and were raised separately as the g0 generation of the line. The exact proportion of axons rescued and the axon length at this acute stage was not recorded, but this plasmid was used as a positive control in a later section (Section 3.2.6).

Upon reaching sexual maturity, we attempted to incross the selected g0 zebrafish together to generate the *chodl*-/-;HB9:*chodl*-FLAG line. However, we never achieved breeding success with incrossing this group (around 5 attempts). Instead, we backcrossed the g0 zebrafish into the *chodl* -/- population, maintaining homozygosity of the *chodl* knockout but allowing germline transmission of the HB9:*chodl*-FLAG through one parent. From these clutches, we selected embryos at 24 hpf in which their entire CaP axon population was rescued to raise as our stable F1 population, selecting those with the longest axons. FLAG expression was confirmed in several rescued embryos, and was limited to HB9:GFP+ motor neurons. FLAG staining was visible in both the soma and axons of these cells. From this F1 generation, we incrossed and then measured axon lengths to compare with wild-type (Control), *chodl* -/-, and *chodl*-/-;HB9:*chodl*-FLAG embryos at 28hpf (Figure 3.8).

The FLAG immunoreactivity is only present in the *chodl*-/-;HB9:*chodl*-FLAG line (Figure 3.8 A) and is limited to the motor neurons, both the cell bodies and axons. There is no signal in either the control or *chodl* -/- embryos, as expected, demonstrating the specificity of the staining and the success of the plasmid to have no leakiness in other cell types except MNs. After FLAG immunohistochemistry and measurement of the axon lengths, FLAG-negative embryos in the *chodl*-/-;HB9:*chodl*-FLAG group were excluded and only those embryos expressing the HB9:*chodl*-FLAG signal were included in the statistical analysis. The axon length between the control and *chodl* -/- mutants is significantly different, with the *chodl* -/- axons shorter than the controls. This is a similar difference in length as was observed in Section 3.2.3. The axon length of the *chodl* -/- group is also significantly shorter than the *chodl*-/-;HB9:*chodl*-FLAG group, less. This is because the axons in the *chodl*-/-;HB9:*chodl*-FLAG group are fully rescued to control lengths, only shorter and not significantly different. (Control average length=78.88 µm ±2.71 , n=13. *chodl* -/- average length= 32.69 µm ±0.50, n=13. *chodl*-/-;HB9:*chodl*-FLAG average length= 75.76 µm ±2.39, n= 15. Kruskal-Wallis ****, with Dunn's mutliple comparison test. Control vs *chodl* -/- ****, *chodl* -/- vs *chodl*-/-;HB9:*chodl*-FLAG ****, control vs *chodl*-/-;HB9:*chodl*-FLAG n.s., p=0.999. **** p<0.0001.) The complete rescue of the axon length in the stable *chodl*-/-;HB9:*chodl*-FLAG line shows that motor neuron-specific expression of chondrolectin is able to rescue the global knockout. This demonstrates the cell-autonomous function of chondrolectin in zebrafish.

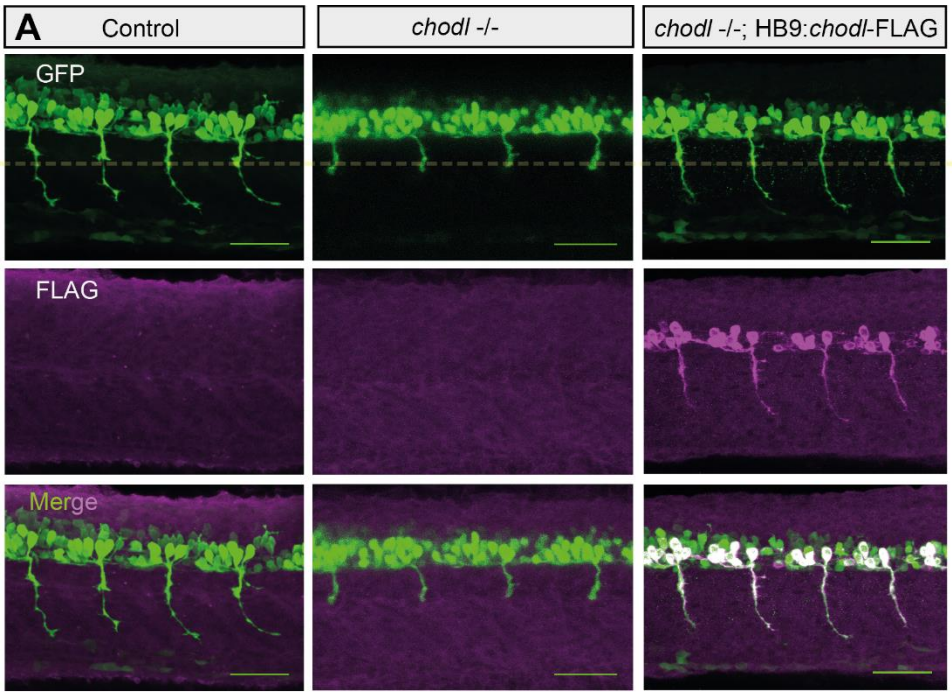
A
Control
chodl -/-
chodl -/-; HB9:chodl-FLAG
GFP
FLAG
Merge

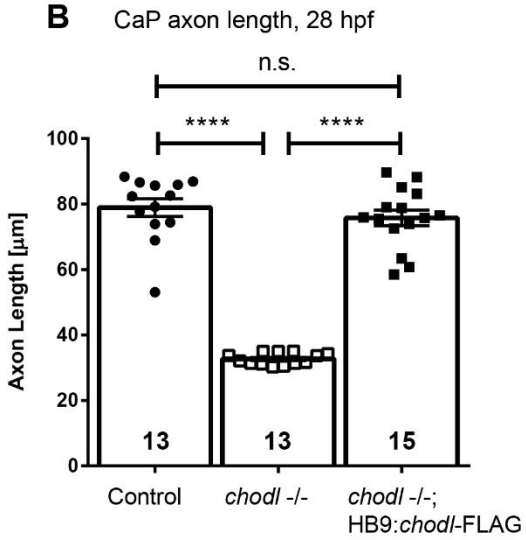
B
CaP axon length, 28 hpf
n.s.
****
****
Axon Length [µm]
100
80
60
40
20
0
13
13
15
Control
chodl -/-
chodl -/-;
HB9:chodl-FLAG

Figure 3.8: Axon length and FLAG immunoreactivity shows that the *chodl*-/-;HB9:*chodl*-FLAG line expresses the FLAG tag only in MNs and fully rescues the axonal length phenotype seen in *chodl* -/- mutants.
A: Representative images of control, *chodl* -/-, and c*hodl*-/-;HB9:*chodl*-FLAGembryos are shown. The FLAG immunoreactivity is limited to the rescue line and is not expressed by the control or mutants. The HM is marked (yellow dashed line), showing that the control and rescue axons have grown beyond this point while the *chodl* -/- axons are stalled.
B: Axon length measurements show that there is no statistical difference between the control and *chodl*-/-;HB9:*chodl*-FLAGaxons, but there are significant differences in axon length between *chodl* -/- and both control and *chodl*-/-;HB9:*chodl*-FLAG embryos. (Kruskal-Wallis ****, Dunn's multiple comparison test. Control vs *chodl*-/-;HB9:*chodl*-FLAG n.s, p= 0.999, Control vs *chodl* -/- ****, *chodl* -/- vs chodl-/-;HB9:chodl-FLAG ****. **** = p<0.0001. Post-hoc power= 1.00) Scale bar= 50 µm.

3.2.5.2 – Over-expression of chondrolectin in wild-type motor neurons leads to shorter motor axons at 28 hpf

As has been extensively discussed in this chapter, knockdown and knockout of chondrolectin leads to stalled CaP axons at the horizontal myoseptum at 28 hpf. Interestingly, over-expression of chondrolectin using mRNA also leads to shortened axons (Zhong *et al.*, 2012). This suggests that the dosage of chondrolectin needs to be tightly controlled for healthy motor axons. However, mRNA injection is not tissue-specific. This means that other tissues, such as muscle fibres or glia, may aberrantly express Chodl and influence the motor axon growth. For example, cell-surface molecules are known to have variable interactions either *cis* in the same cell membrane, or *trans* when associated in different cells (Held and Mariuzza, 2011). Our hypothesis is that chondrolectin acts as a cell-surface protein on the motor axon interacting with the ECM (discussed further in Section 3.3.3) so it may interact in both *cis* and *trans* orientation with itself and other proteins. Mis-localised expression in other tissue may lead to *trans* interactions that do not occur under normal conditions.

However, we can utilise the Tol2:HB9:*chodl*-FLAG plasmid previously used to generate the stable *chodl* -/-;HB9:*chodl*-FLAG line, in order to investigate cell-specific effects of over-expression. The FLAG expression demonstrates which neurons are expressing the Chodl-FLAG cassette, and it is limited to motor neurons (Figure 3.8). This allows us to cause mosaic over-expression in acute injections and then compare the axonal lengths of the FLAG-positive axons, the internal control of FLAG-negative axons in the same embryo, and a further negative control of embryos injected with the Tol2:HB9 vector only. If over-expression leads to changes in the motor axons, the FLAG-positive axons of the injected group will be significantly shorter than the other axonal lengths. If the mRNA caused an artefact by exogenous expression of the chondrolectin in other cell types, we would expect no changes in the axon lengths between FLAG-positive or FLAG-negative axons, or with the control vector group.

After injection, embryos were randomly selected at 28hpf and immunohistochemistry performed against GFP and FLAG. Due to the mosaicism and low efficiency of the construct integration, the number of FLAG-positive axons per injected embryo ranged from 0-3 out of 10 axons scored, with around 50% of embryos expressing FLAG in at least 1 axon. For the purposes of analysis, an axon was only accepted as FLAG-positive if the cell body and initial axon had a morphology as has been described for the CaP neuron, (Myers, Eisen and Westerfield, 1986) and if FLAG staining was present along the full length of the axon. This is because, as previously discussed, the RoP and MiP axons also follow the same path as the CaP axon up to the HM, the point where the *chodl* -/- axons stall. Therefore, false positive axons could be counted if the FLAG positive axons had FLAG-positive RoP or MiP cell bodies and the CaP cell body did not express FLAG. The data from this experiment is presented below, Figure 3.9.

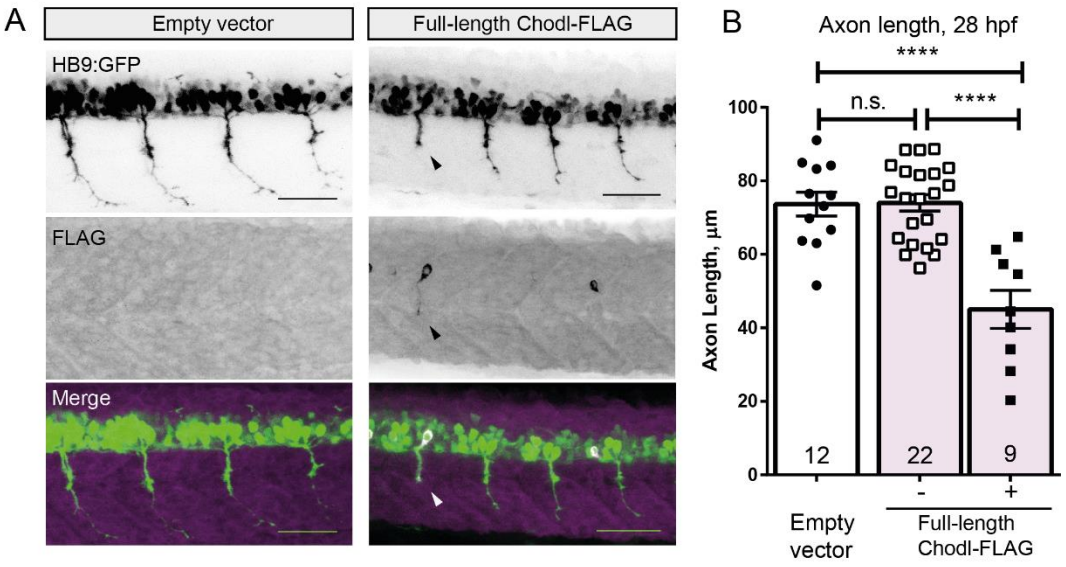

Figure 3.9: Over-expression of *chodl* in wild-type zebrafish leads to truncated CaP axons.
A: Representative images of 28 hpf zebrafish embryos injected with either the Tol2:HB9 (Empty vector) or Tol2:HB9:Chodl-FLAG (Full-length Chodl-FLAG) plasmid. Chodl-FLAG expression causes truncation of the axon with FLAG immunoreactivity (arrowhead). Scale bar= 50 µm **B**: The axon length is unchanged between axons injected with the Empty vector or FLAG-negative axons, but the FLAG-positive axons are significantly shorter than the other two groups (One-way ANOVA **** with Bonferroni's multiple comparison test, Empty vector vs Full-length Chodl-FLAG FLAG-negative, n.s. Empty vector vs Full-length Chodl-FLAG FLAG-positive ****, Full-length Chodl-FLAG FLAG-negative vs FLAG-positive ****. n.s. $p>0.999$, **** $p<0.0001$. Post-hoc power= 0.993.)

Comparing the axon length of the embryos injected with the Empty vector to the FLAG-negative axons injected with the Chodl-FLAG plasmid, there is very little difference and it is not statistically significant. The FLAG-negative axons are 0.49% longer on average than the Empty vector group. The FLAG-positive axons, which are expressing Chodl-FLAG, are significantly shorter than both their internal control, the FLAG-negative axons, and the axons in embryos injected with Empty vector. The

FLAG-positive axons are 39.2% shorter than the FLAG-negative axons, and 38.9% shorter than the average axon length in the Empty vector group. (Empty vector average length= 73.67 µm ±3.27, n= 12. Full-length Chodl-FLAG FLAG-negative axon length= 74.03 µm ±2.23, n= 22. Full length Chodl-FLAG FLAG-positive length= 45.04 µm ±5.18, n=9. One-way ANOVA **** with Bonferroni's multiple comparisons test, Empty vector vs Full-length Chodl-FLAG FLAG-negative, n.s., p>0.999. Empty vector vs Full-length Chodl-FLAG FLAG-positive **** p<0.0001. Full-length Chodl-FLAG FLAG-negative vs FLAG-positive **** p<0.0001.)

These findings confirm that the motor axon phenotype observed during mRNA over-expression of chondrolectin previously reported are in fact specific to chondrolectin over-expression in the motor neurons. It is not an artefact from chondrolectin expression in non-endogenous cell types. This demonstrates that the dosage of chondrolectin in motor neurons must be tightly controlled to maintain the correct axon length. The mechanism by which over-expression of chondrolectin leads to reduced axon length is not immediately clear. It may be due to *cis*-acting interactions between chondrolectin monomers on the axon surface, which prevents its normal function. Or, surplus chondrolectin may bind its ligands excessively and be unable to induce axon growth beyond the HM. The mechanism of chondrolectin and its potential ligands are discussed in the Discussion & Conclusions Section 3.3.3.

3.2.6 - Functional analysis of the chondrolectin protein by acute rescue using mutagenised over-expression constructs

3.2.6.1 – Both the intracellular domain and C-type lectin domain of chondrolectin are required for its function in zebrafish

We have now determined that the dosage of chondrolectin protein in the motor neuron must be tightly controlled for its correct function. At 28 hpf, knockdown or knockout stalls the CaP axon at the HM choice point, and over-expression also leads to shortened axons. This function is cell-autonomous, as over-expression limited to the

motor neurons can cause the axonal phenotype, and motor neuron-specific expression of Chodl rescues the knockout. However, the mechanism by which the protein functions under normal circumstances is still elusive. There are few published papers on the biochemistry, ligands, or mechanism of chondrolectin in any model system. A lack of commercially available antibodies specific to chondrolectin across zebrafish, mouse, and human also limit the ability of researchers to investigate chondrolectin in immunohistochemistry or binding assays. However, the excellent transgenic manipulation methods available in zebrafish allow for functional analysis of chondrolectin through other means.

As previously introduced, the chondrolectin protein is a transmembrane protein containing a C-type lectin domain at its N-terminus and a short (30aa) sequence at its C-terminus. To determine if any domains of chondrolectin are disposable for the correct function of the protein, I utilised the Tol2-HB9:*chodl*-FLAG plasmid used to generate the stable rescue line (Section 3.2.5). I further generated several related constructs which removed structural domains from chondrolectin. When injected into *chodl* -/- eggs, these constructs were used to investigate if they were also able to acutely rescue the axon phenotype. Figure 3.10 below illustrates the experimental set-up, including the potential outcomes from the experimental constructs.

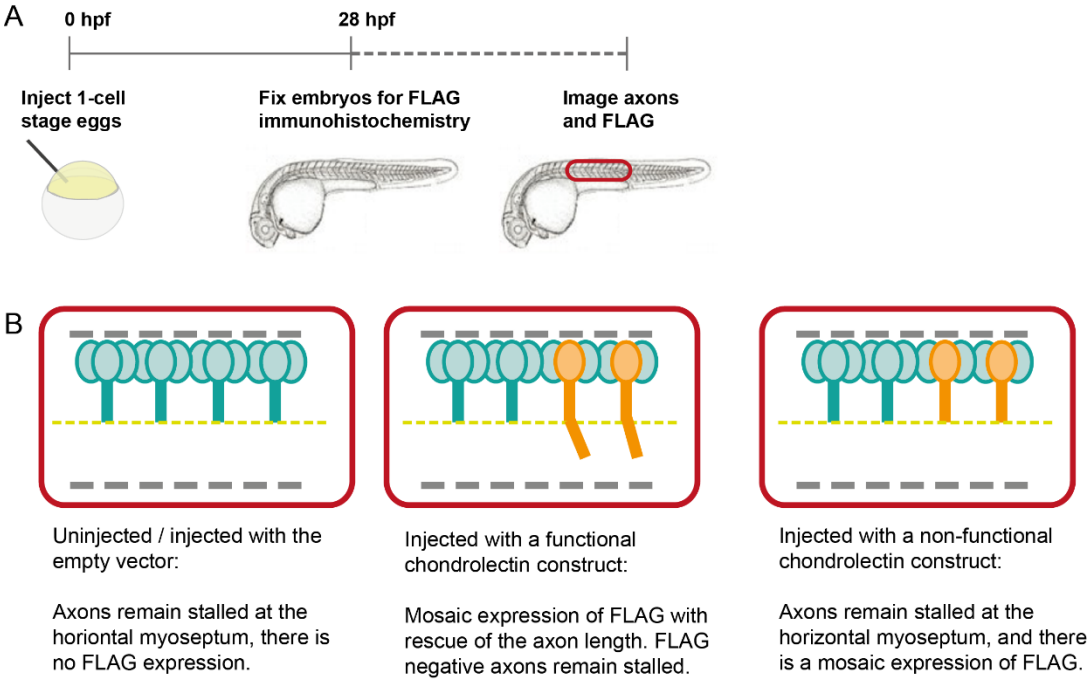

Figure 3.10: Experimental setup for acute rescue experiments in the *chodl* -/- phenotype.
A: An experimental timeline showing injection of chondrolectin constructs, followed by immunohistochemistry and imaging. The red box on the zebrafish trunk shows the region of image analysis. **B**: Examples of the phenotypic outcomes depending on the type of injected plasmid, whether there will be mosaic rescue and if this correlates to FLAG immunoreactivity. Yellow dashed line = horizontal myoseptum.

I did not generate constructs removing the transmembrane domain or signal peptide, with the logical assumption that the transmembrane domain and signal peptide are required for the correct protein function. Removal of the signal peptide would result in an inability of the chondrolectin protein to be trafficked to the membrane, and it would potentially form toxic aggregates in the cytoplasm. Removal of the transmembrane domain would also have likely resulted in toxic aggregation of the protein in the cytoplasm of the motor neurons or even export of the protein out of the neuron if the signal peptide trafficked the protein into vesicles. This aggregation would be visible in the FLAG immunohistochemistry. If the FLAG labelling was limited to the cell body or entered the nucleus, it would suggest that the protein was aggregating or misfolding. The constructs are shown below (Figure 3.11).

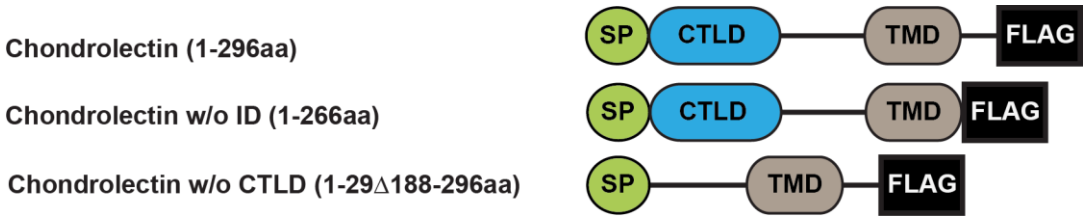

Figure 3.11: Schematic of the chondrolectin constructs.
Three constructs were generated, with the full-length chondrolectin, with the intracellular domain removed, or the C-type lectin domain removed. SP= signal peptide, CTLD= C-type lectin domain, TMD= transmembrane domain.

For an internal positive control, the plasmid containing the full-length chondrolectin was used, as this had demonstrated mosaic rescue of the *chodl* -/- phenotype during generation of the stable *chodl* -/-;HB9:*chodl*-FLAG line (Full-length Chodl-FLAG). The internal negative control was the plasmid backbone containing the HB9 promoter, as it should not exhibit toxic or rescue effects on the embryos (Empty vector).

After generating constructs with the intracellular domain and C-type lectin domain removed, the constructs were injected in a similar set-up to that used to over-express *chodl*-FLAG in the wild-types, presented in Section 3.2.5.2. The data is shown below, Figure 3.12.

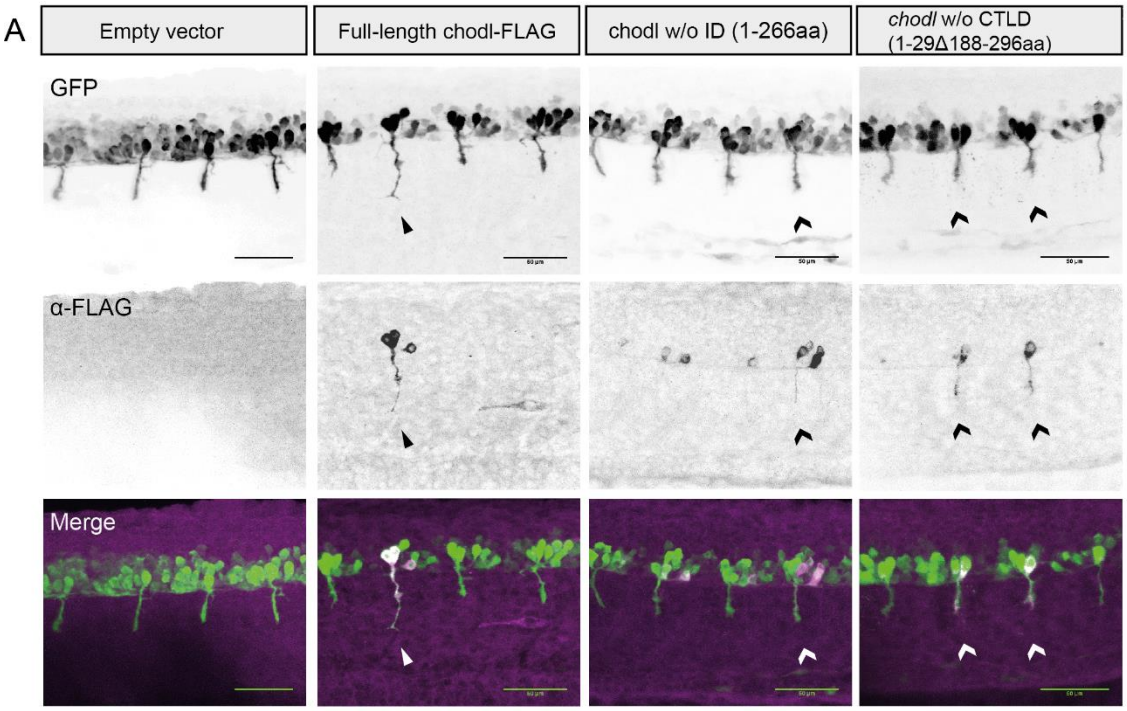

B Rescue of *chodl* **-/-** axons by injecting domain-deleted constructs

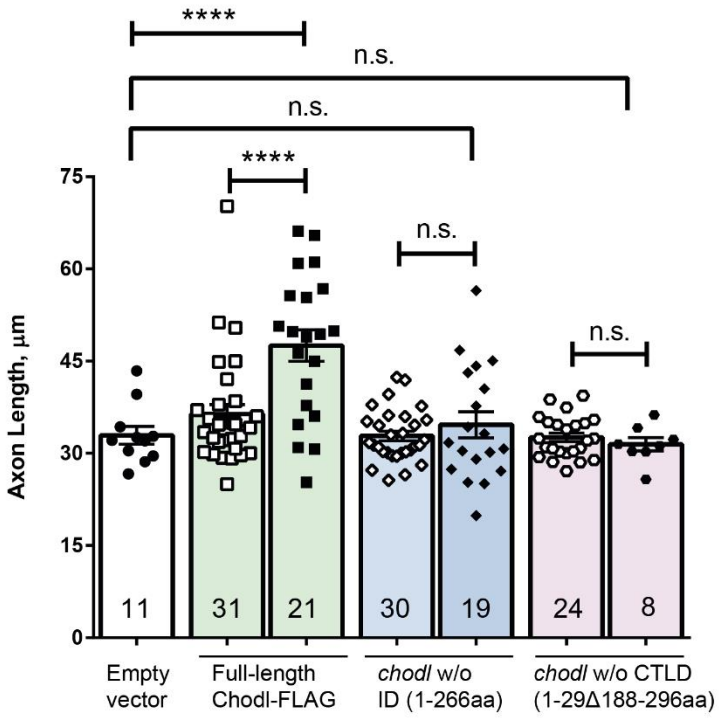

Figure 3.12: Both the C-type lectin and intracellular domains of chondrolectin are necessary for its function and to rescue the *chodl* -/- phenotype.
A: Representative lateral trunk view images of injected embryos at 28hpf, with separate GFP and FLAG staining, and the merged channel. The FLAG-positive axons are longer in the full-length Chodl-FLAG group but remain stalled at the HM in the groups missing the CTLD or intracellular domains. Solid arrowheads = rescued axons with FLAG immunoreactivity. Chevrons = FLAG positive axons that are still stalled at the HM. Scale bar= 50 µm. **B**: Graph of the average CaP axon length. For each construct, white points = FLAG-negative axons, black points = FLAG-positive axons. The Full-length Chodl-FLAG construct rescues the *chodl* -/- axons. The FLAG-positive axons are significantly longer than the FLAG-negative and the Empty vector axon lengths. However, both the *chodl* w/o ID or *chodl* w/o CTLD FLAG-positive axons are not significantly longer than their FLAG-negative counterparts or the Empty vector group. (One-way ANOVA ****, with Bonferroni's multiple comparison test. Empty vector vs Full-length Chodl-FLAG FLAG-negative n.s., Empty vector vs Full-length Chodl-FLAG FLAG-positive ****. Empty vector vs *chodl* w/o ID FLAG-negative n.s., Empty vector vs *chodl* w/o ID FLAG-positive n.s. Empty vector vs *chodl* w/o CTLD FLAG-negative n.s., Empty vector vs *chodl* wo/ CTLD FLAG FLAG-positive n.s. Full-length Chodl-FLAG FLAG-negative vs Full-length Chodl-FLAG FLAG-positive ****. *chodl* w/o CTLD FLAG-negative vs *chodl* w/o CTLD FLAG-positive n.s. *chodl* w/o ID FLAG-negative vs *chodl* w/o ID FLAG-positive n.s. n.s. p>0.999, **** p<0.0001.)

In Figure 3.12, the axon length of embryos injected with the empty vector is consistent with the axon length of *chodl* -/- embryos at the same age seen in other experiments (32.92µm), indicating that the injections do not induce any axon length changes. For all injected constructs, the FLAG-negative axons are also the same length as the empty vector control group, showing that these constructs also do not induce axon length changes in axons, and that the FLAG immunohistochemistry is specific. The Full-length Chodl-FLAG FLAG-negative value is 10.4% longer than the Empty vector. The FLAG-negative axons from the *chodl* w/o ID are 0.34% shorter than the Empty vector average length, and the *chodl* w/o CTLD is 0.95% shorter than the Empty vector length. (Empty vector average length= 32.92 µm ±1.46, n=11. Full-length Chodl-FLAG FLAG-negative mean length= 36.36 µm ±1.57, n=31. *chodl* w/o ID FLAG-negative mean length= 32.81 µm ±0.774, n= 30. *chodl* w/o CTLD FLAG-negative mean length= 32.61 µm ±0.687, n=24. One-way ANOVA with Bonferroni's multiple comparison test, Empty vector vs Full-length Chodl-FLAG FLAG-negative n.s., Empty vector vs chodl w/o ID FLAG-negative n.s., Empty vector vs chodl w/o CTLD FLAG-negative n.s., n.s. p>0.999.)

As expected, the positive control (Full-length Chodl-FLAG) was able to rescue the axon length, with the FLAG-positive axons 30.7% longer than the FLAG-negative axons. This confirms that the construct is able to mosaically rescue the axonal phenotype in a way that is specific to the expression of the FLAG-tagged protein. (Full-length Chodl-FLAG FLAG-negative mean length= 36.36 µm ±1.57, n= 31. Full-length Chodl-FLAG FLAG-positive average length= 47.53 µm ± 2.57, n= 21. One-way ANOVA with Bonferroni's multiple comparison test, **** p<0.0001).

Comparing the FLAG-positive axons to FLAG-negative axons for both the *chodl* w/o ID construct and the *chodl* w/o CTLD construct demonstrates that there is no rescue, as there is no significant difference between the values. For the *chodl* w/o ID construct, the FLAG-positive axons are only 5.55% longer than the FLAG-negative axons. For the *chodl* w/o CTLD construct, the FLAG-positive axons were 3.53% shorter than the FLAG-negative axons. (*chodl* w/o ID FLAG-negative mean length= 32.81 µm ±0.774, n= 30. *chodl* w/o ID FLAG-positive mean length= 34.63 µm ±2.12, n= 19. *chodl* w/o CTLD FLAG-negative mean length= 32.61 µm ±0.687, n=24. *chodl* w/o CTLD FLAG-positive mean length= 31.46 µm ±1.08, n= 8. One-way ANOVA with Bonferroni's multiple comparison test. *chodl* w/o ID FLAG-negative v FLAG-positive n.s., *chodl* w/o CTLD FLAG-negative vs FLAG-positive n.s. n.s. p>0.999)

The constructs are correctly translated, and the protein trafficked into the axons, as the FLAG immunoreactivity spans the length of the motor axons and was excluded from the nucleus of the cell (visible in Figure 3.12 A). Therefore, the protein is present, but without each domain it is non-functional. Overall, this data indicates that chondrolectin is likely acting as a signalling molecule, with the C-type lectin interacting with a binding partner in the ECM and the intracellular domain transducing a signal within the axon during its outgrowth. A colleague in the group also used modified versions of the constructs from this section in HEK cells, performing binding assays to determine potential ligands of chondrolectin for the C-type lectin domain. The data gained from that work is detailed in the Discussion & Conclusion section of this chapter. Given the lack of structural motif in the intracellular domain, and its relatively short length, I further investigated the biochemical properties of this domain, detailed in the next section.

3.2.6.2 – Phosphorylation of the intracellular domain is necessary for its function in zebrafish

The intracellular domain is a short 30aa chain and does not contain any structural motifs indicated by the amino acid sequence. However, it does contain 12 serine and threonine residues, and thus a high proportion of its sequence are charged residues that are classical phosphorylation targets. Due to the wealth of published material where signalling molecules transduce their signal via intracellular phosphorylation (Plattner and Bibb, 2012; Day, Sosale and Lazzara, 2016), I decided to further explore the potential phosphorylation of chondrolectin. Using a similar experimental set-up as used when removing domains, I instead mutagenised the intracellular domain to convert the serine and threonine residues to alanine. This has been previously used to remove phosphorylation targets, as alanine is a simple uncharged amino acid which cannot be phosphorylated (Dephoure *et al.*, 2013).

The full methodology to mutagenise this domain is detailed in the Materials & Methods section, but briefly, multiple overhang PCR primers were designed which bound sequentially to the intracellular domain but whose sequence replaced any Ser (AGT, AGC, TCX) or Thr (ACX) codons with Ala (GCT or GCG). Please note that one Thr was left intact due to a typing error during primer design. The same constructs for the positive and negative controls were used as previously described. Representative images and the axon length measurements are below (Figure 3.13).

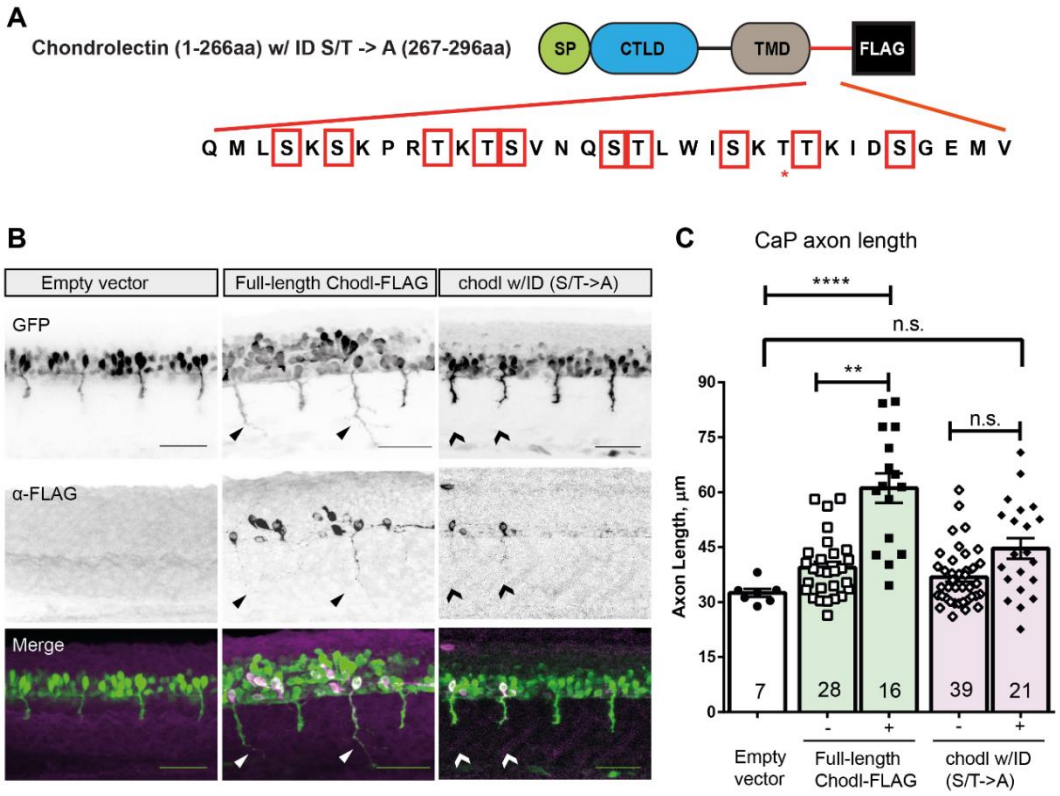

Figure 3.13: Removal of the intracellular domain's phosphorylation sites abolishes its ability to rescue axon length in *chodl* -/- embryos.
A: Schematic of chondrolectin, with the intracellular domain amino acids shown. The serine and threonine residues altered to alanine are marked with red boxes. The Thr residue left intact is marked with an asterisk. **B:** Representative images of embryos injected with the constructs empty vector, full-length Chodl-FLAG, and the construct *chodl* w/ ID (S/T->A). Solid arrowheads = FLAG-positive axons with length rescued. Chevrons = FLAG-positive axons without length rescue. Scale bars= 50 µm. **C:** Graph of axonal length measurements. There is a significant increase in length by Full-length Chodl-FLAG FLAG-positive axons over the Empty vector group and Full-length Chodl-FLAG FLAG-negative axon lengths. There is no significant difference between the chodl w/ID (S/T->A) FLAG-positive axons and the FLAG-negative axons in that group or the Empty vector group. (Kruskal-Wallis **** with Dunn's multiple comparison test. Empty vector vs Chodl-FLAG FLAG-positive axons ****, Full-length Chodl-FLAG FLAG-negative vs Full-length Chodl-FLAG FLAG-positive **. Empty vector vs chodl w/ID (S/T->A) FLAG-positive n.s., p= 0.0853 *chodl* w/ID (S/T->A) FLAG-negative vs *chodl* w/ID (S/T->A) FLAG-positive n.s., p= 0.1989. ** p= 0.001, **** p<0.0001. Post-hoc power= 0.997)

As was also observed in the previous dataset, the Empty vector axons remain at a similar length to previously measured *chodl* -/- axons. The positive control, the Full-length Chodl-FLAG construct, again shows rescue of the axon length in the FLAG-positive axon population. These FLAG-positive axons are 87.8% longer than the Empty vector average length and 55.0% longer than the FLAG-negative population, and in both comparisons, this is statistically significant. However, the construct that cannot be phosphorylated, *chodl* w/ID (S/T->A), does not have a significantly increased axon length in its FLAG-positive axons. (Empty vector mean length= 32.55 µm ±1.11, n=7. Full-length Chodl-FLAG FLAG-negative average axon length= 39.43 µm ±1.60, n=28, Full-length Chodl-FLAG FLAG-positive average length= 61.13 µm ± 3.99, n=16. *chodl* w/ID (ST->A) FLAG-negative average length= 36.84 µm ±, n= 39, *chodl* w/ID (S/T->A) FLAG-positive average length= 44.64 µm ±2.78, n= 21. Kruskal-Wallis with Dunn's multiple comparison test.)

Therefore, the removal of residues that are phosphorylation targets results in a non-functional protein which cannot rescue the mutant phenotype. This suggests that phosphorylation is necessary for the function of chondrolectin *in vivo*. Overall, these acute rescue experiments support the notion that chondrolectin acts as a signalling molecule, where the C-type lectin domain interacts with ligands in the ECM, and the intracellular domain undergoes phosphorylation to induce a signal inside the axon, allowing the axon to extend past the horizontal myoseptum. Further discussion of potential mechanisms, and other methods to confirm this hypothesis are discussed in the next section, 3.3.3.

3.3 - Discussion & Conclusions

3.3.1 – Successful generation of a chondrolectin knockout which phenocopies the published morphant

We have generated a chondrolectin knockout zebrafish using the CRISPR/Cas9 system. To ensure that the knockout is specific to *chodl*, several control checks must be employed. One of the disadvantages of CRISPR/Cas9 is the chance it will produce off-target effects. Because the Cas9 is targeted to the gene of interest via the gRNA sequence, the sequence selected must be unique to the target. 3 or more mismatches

between the off-target sequence and the gRNA are considered acceptable to abolish binding (Ran *et al.*, 2013; Anderson *et al.*, 2015), and matches in intronic regions are considered to be less risky than matches in the exonic part of a gene, as indels in intronic regions will not form frame-shift mutations. While designing the gRNA, sequences that have only 0 or 1 base change to another gene, or where the sequence similarity sits inside exonic regions, should be avoided where possible. This forms part of the CRISPR design tool published in Hsu *et al.*, 2013, where potential off-targets are displayed (Shown in Table 3.1 for each gRNA).

There are two control experiments that can be performed to ensure there are no off-target mutations. The first, and most simple, is to outcross the line sufficiently, selecting for the germline transmission of the desired indel. Given the stochastic generation of mutations in mosaic, the likelihood of transmission of both the desired mutation and a deleterious off-target is low. This is the approach I took to establish the line, as zebrafish can generate large clutches that be rapidly screened (Prykhozhij *et al.*, 2017). The second method is to design genotyping primers for the region known to be a potential off-target site (Ran *et al.*, 2013). Then, in combination with genotyping for the desired gene target, the off-target sites can be checked as well. This is frequently performed when using CRISPR/Cas9 in mice. The genome editing is carried out either in embryonic stem cells, which can be cultured and thus genotyped fully before injection into blastocysts, or directly at the zygote stage in vitro before implantation into foster mothers. Due to the labour-intensive process of implantation, pre-screening is preferable to implanting more blastocysts or extra breeding (Wang *et al.*, 2013; Sakurai *et al.*, 2014; Yang, Wang and Jaenisch, 2014).

Although I did not directly sequence the *chodl* -/- zebrafish to look for off-targets, I consider the phenotype to be true and specific to loss of chondrolectin rather than an off-target. This is due to two factors: Phenocopy of the published morphant, and the complete rescue of the phenotype by re-expression of chondrolectin in the mutant zebrafish. Firstly, all 3 gRNAs designed against multiple exons were able to induce a mosaic phenotype in the motor axons (Section 3.2.2). This demonstrates that all gRNAs were of high cutting efficiency to cause the acute phenotype, and that frame-shift mutations in different domains of the protein can cause the same loss-of-function phenotype. In the stable *chodl* -/- mutant line, 75% of the CaP axons were stalled at the horizontal myoseptum at 28 hpf (Section 3.2.3). The rescue of the axonal phenotype by re-expressing chondrolectin in the *chodl* -/- mutants is another key piece

of evidence that the knockout phenotype is specific (Section 3.2.5). This demonstrates that the axonal phenotype is solely due to the loss of chondrolectin. The rescue is quantifiable both as a stable transgenic line, and in the acute injections. Use of the HB9 promoter, limiting expression to MNs only, is also a key part of the next section, discussing the cell-autonomous function of chondrolectin.

When CRISPR/Cas9 generates a frame-shift indel, the loss of function occurs as the mRNA containing a premature stop is rapidly degraded by nonsense-mediated decay (NMD). Usually, the presence of a premature stop codon during translation signals to the NMD complex to cause rapid degradation of the mRNA. This is developmentally vital to prevent truncated proteins accumulating in the cell and causing toxicity (Wittkopp *et al.*, 2009). Methods to determine if the knockout leads to nonsense-mediated decay include *in situ* hybridisation, comparing the signal intensity between wild-type and mutant samples, although this may not be sensitive enough to detect the reduction in mRNA caused by NMD. Another method to measure changes to the transcript level include qPCR of cDNA. However, one unintended consequence of indel generation is the increase in exon skipping (Anderson *et al.*, 2017; Sharpe and Cooper, 2017), caused by sequence changes which generate exon splice enhancers. In some cases, the exon skipping leads to cryptic start sites or constitutively active protein (Mou *et al.*, 2017). For chondrolectin, further data demonstrates that removal of either the CTLD or ID causes the protein to be non-functional (Section 3.2.6). This would suggest that even if exon skipping were to occur in the *chodl* mutant, and generate a truncated protein, it would still be either a loss-of-function mutant or dominant negative mutant. A dominant negative mutant, however, would not be fully rescued by re-expression of Chodl, as I observed in Section 3.2.5. For example, the collagen19a1 mutant *stumpy* is a dominant negative mutant, and so over-expression of Col19a1 by mRNA injection does not rescue the phenotype. Instead, morpholino to knockdown the collagen 19a1 must be co-injected with the mRNA, which does cause rescue of the phenotype (Hilario, Wang and Beattie, 2010).

The lack of translated protein can be easily observed if an antibody to the protein of interest is available, as Western blotting of the embryos should demonstrate a reduction in band intensity in the heterozygotes, and loss of the band in the homozygous mutants. An example of this is the generation of *smn* mutant zebrafish to model SMA (Boon *et al.*, 2009; Hao *et al.*, 2013). As there are no zebrafish-validated antibodies for chondrolectin, I could not take that approach. However, with

the tools that I have access to, it seems likely that mutant zebrafish generated in this chapter is a successful knockout mutant of chondrolectin.

3.3.2 – Chondrolectin acts cell-autonomously in motor neurons in zebrafish to affect motor axon growth

The *chodl* -/- zebrafish generated in this thesis are robustly healthy, with no observed survival deficits, and are morphologically indistinguishable from controls. As described in Section 3.2.4, the body length at 30 hpf is not different form that of controls, showing there is no associated growth problems with the loss of chondrolectin. The eye diameter is also identical, showing that morphogenesis also occurs correctly (Section 3.2.4). As well as the normal morphology, this is observed by the lack of change to phalloidin staining, which stains the F-actin present in muscle fibres. Phalloidin has been used widely to reveal changes to muscle architecture in zebrafish, including in collagen mutants and disease models such as muscular dystrophy (Pagnon-Minot *et al.*, 2008; Johnson, Farr III and Maves, 2013). After quantifying the number of myotubes and the thickness of the myotubes per somite between the wild-type and mutant, there are no significant differences between the two groups. There is no detectable change between wild-type and *chodl* -/- embryos, suggesting that the muscle is healthy and its architecture is unchanged, but further antibodies for different muscle markers could be used to fully confirm this. For example, there are antibodies validated in zebrafish for the myosin heavy chain, F59 (Wehner *et al.*, 2017), and myosin light chain, F310 (Thomas-Jinu *et al.*, 2017).

The previous *in situ* data published in zebrafish demonstrates that a chondrolectin mRNA is highly enriched in motor neurons, the trigeminal ganglion, and the hindbrain (Chapter One, Section 1.4.2, Zhong *et al.*, 2012, Thisse et al., 2004). However, initial characterisation of chondrolectin in mice found it widely expressed in muscle and spleen (Weng *et al.*, 2002; Weng, Hübner, *et al.*, 2003). Later studies demonstrated chondrolectin is enriched in the fast-twitch motor neurons (Enjin et al., 2010). The cell-autonomous action of chondrolectin, specific to motor neurons, is demonstrated in this thesis in Section 3.2.5. Use of the HB9 promoter limits the expression of the chondrolectin only in motor neurons. This is confirmed via the fused FLAG-tag and its specific immunoreactivity in motor neurons (Section 3.2.5). The cell-specific expression is able to rescue the *chodl* -/- both in acute injections as a mosaic (Section

3.2.6) and as a stable transgenic line (Section 3.2.5). The cell-autonomous action of chondrolectin is therefore demonstrated by the full rescue of a global knockout by this MN expression. As well as mosaic expression through plasmid injection, transplantation studies could be used to demonstrate the cell-autonomous role of chondrolectin, for example as demonstrated with the splicing factor SFPQ (Thomas-Jinu *et al.*, 2017). The *sfpq* -/- mutant fails to extend axons from the spinal cord, but wild-type motor neurons explanted into sfpq -/- mutants extended axons normally. Conversely, *sfpq* -/- motor neurons transplanted into wild-type embryos were unable to extend axons.

In the mRNA injections performed in Zhong *et al.*, 2012, wild-type eggs injected with the mRNA to induce over-expression of chondrolectin exhibited axonal defects themselves (see in Section 1.4.2). However, in that case it was not possible to determine if this was due to the high level of protein in the motor axons causing growth deficits, or if aberrant expression in the muscle caused unexpected interactions with the axons. Utilising the HB9:Chodl-FLAG construct again, we over-expressed chodl in the wild-type motor neurons (Section 3.2.5.2). We measured a significant reduction in the length of FLAG-positive axons compared to their FLAG-negative axons and those injected with the vector alone. This confirms that the dosage of chondrolectin in the MN is key to the growth of the axon. The phenotype when chondrolectin is over-expressed is specific to the motor neuron expression and is not an artefact from ectopic expression of the protein from a different cell type.

The mechanism behind the dosage effects of chondrolectin in motor neurons is not immediately clear. As will be discussed in depth in Section 3.3.3, we hypothesise that chondrolectin acts as a cell-surface recognition molecule. We assert that chondrolectin is trafficked to the cell membrane and its C-type lectin domain interacts with ligand targets in the ECM to induce correct axon growth, particularly at the HM. Because of this, knockdown or knockout of the protein likely leads to a reduction in the chondrolectin-ligand binding. Without a sufficient level of this interaction, the axon is prevented from extending past the HM. When the normal level is restored, by mRNA or transgenesis, the axon is rescued. The over-expression of chondrolectin in wild-type embryos may have retarded growth if the high level of protein interacts with itself in a *cis* interaction on the axon surface, which disrupts its normal function (Held and Mariuzza, 2011).

Although the HB9 promoter was used to express chondrolectin specifically in motor neurons, it is not the endogenous promoter of chondrolectin. Attempts by a colleague in the group were made to generate the *chodl* promoter region, using the UCSC Genome Browser to identify 5' UTR regions (https://genome.ucsc.edu/index.html) and BACPAC to generate large clones of the putative sequence (https://bacpacresources.org/). However, cloning success of this potential promoter was never achieved. HB9 was chosen as it is a well-characterised promoter for motor neuron expression (Arber *et al.*, 1999; Flanagan-Steet *et al.*, 2005). However, the exact level of expression compared to the chondrolectin promoter could not be determined. The HB9 promoter is known to be active from approximately 9 hpf onwards in the zebrafish (Wendik, Maier and Meyer, 2004), compared to a detectable expression of chondrolectin from 12 hpf onwards (Zhong *et al.*, 2012).

The number of copies of the HB9:Chodl-FLAG cassette integrated into the embryos for experiments in Section 3.2.5 and 3.2.6 were also not determined, and so the true level of Chodl-FLAG expressed in each embryo is unknown. Although the *chodl* -/- axons at 28 hpf were fully rescued in the stable transgenic line in Section 3.2.5, data will be presented in Chapter Four which demonstrates that the rescue is not complete when quantified at 3 dpf. Also, the FLAG-positive axons of acutely injected embryos with the Chodl-FLAG cassette are significantly longer compared to the axon length in the *chodl* -/- embryos, but they do not reach the length of wild-types. For example, in Section 3.2.6, the FLAG-positive axons expressing the Chodl-FLAG had average lengths of 47.53 µm and 61.13 µm. In comparison, the wild-type axon length in Section 3.2.5 was 82.54 µm. This can be explained by the stochastic nature of the Tol2 transposon, where some axons will have received the optimal number of copies of Chodl-FLAG to rescue the length, and others will have received too few or too many. In each case, both an excess or deficit of chondrolectin would have affected axon length.

The axonal growth phenotype of the *chodl* -/- mutant seems to be temporally limited, which is also observed in the morphant data (Zhong *et al.,* 2012). Although at 28 hpf, only 25% of axons have extended beyond the HM, a sub-population of axons which have stalled are not permanently stopped. By 31 hpf approximately 40% of axons have extended beyond the HM (discussed in more detail in Chapter 4, section 4.2.2). The published morphant data also showed a mixed population of CaP axons which were permanently arrested at the HM and those which paused for several hours

before continuing to extend. Several mechanisms for this could be possible. In response to an arrested axon, there could be upregulation of compensatory genes from either the surrounding muscle cells or the chodl deficient axon itself. This may allow some axons to extend beyond the HM. The requirement for chondrolectin in primary axon growth may also only persist for several hours. As I did not differentially stain for primary vs secondary axons (using an antibody such as Zn-5 which only labels secondary axons) and look at the primary axons after 31 hpf, it could be possible that the primary axons also do catch up eventually, albeit after the time period that I observed.

The contribution of chondrolectin to the axonal growth also seems to differ between primary motor axons and secondary motor axons. Although the primary axons stall at the HM, the secondary axons seem able to extend, as at 48 hpf and 72 hpf the bundle of secondary axons (and potentially the primary CaP axons) have extended beyond the HM. At these time points it is not possible to distinguish individual axons, and multiple secondary axons extend at the same time before branching. Although the axon length is significantly shorter at 48 hpf compared to wild-type controls (Section 3.2.3), this difference has disappeared at 72 hpf and there are no significant differences between the lengths of axon bundles. As well as extending along the ventral pathway, using the CaP axon as a pioneer, the secondary axons begin to branch into the muscle and innervate it. At both 48 and 72 hpf, the number of branches in the *chodl* -/- group are significantly reduced compared to the wild-type larvae (section 3.2.3). This supports data later in this thesis, where the lack of branching also mirrors a reduction in the number of synaptic puncta in the muscle at 3 dpf (Chapter Four). Further investigation of the axonal phenotype at even later stages (5 dpf or older) would be useful to determine if this branching deficit is delayed or permanently arrested, especially as the *chodl* -/- mutants can feed and swim normally and have no visible phenotype as juveniles or adults.

The difference in phenotype between primary and secondary axons could be expected, as the growth pattern and branching of the two groups differ significantly. Primary and secondary axons also express different genes, such as islet-1 which is enriched in secondary motor neurons but not primary motor neurons (Babin et al., 2014). Thus the requirement of chondrolectin and its mechanism between the two groups of neurons may also differ. Although the mechanism for the chondrolectin protein is discussed in detail in the next Section, there are still many unanswered

questions about the exact pathway and other interaction partners chondrolectin may have to induce these axonal phenotypes in both the primary and secondary motor neurons.

3.3.3 – Chondrolectin acts as a cell-surface molecule

From the acute rescue data presented in Section 3.2.6, the C-type lectin domain (CTLD) and intracellular domain (ID) are both indispensable for the function of Chodl in zebrafish. Removal of either of these structural domains abolishes the rescue of the *chodl* -/- phenotype, while the full-length construct is able to rescue the axons. Furthermore, we show that the ID functions via phosphorylation of its Ser/Thr residues, as mutagenesis of these residues to alanine also abolishes the axonal rescue. Given the other domains of chondrolectin include a signal peptide and a transmembrane domain, it seems feasible that chondrolectin is a cell-surface protein that binds other proteins, either in the ECM or the intracellular region of the MNs, or both.

The involvement of the C-type lectin domain of chondrolectin in motor axon guidance and growth is rare for the domain, as CTLDs are normally expressed in immune cells, recognising microbial proteins during infection (Yan, Ohno and Tsuji, 2013; Hoving, Wilson and Brown, 2014; Dambuza and Brown, 2015). However, a transmembrane C-type lectin protein, CLEC-38, has been shown to regulate axon outgrowth in *C. elegans* (Kulkarni, Li and Wadsworth, 2008). The protein suppresses axon growth, preventing over-growth past the axon target. Interestingly, this protein was also demonstrated to remodel pre-synaptic terminals on the axon, as CLEC-38 mutants have fewer pre-synaptic puncta along the axon length. This supports our findings in the zebrafish, and Chapter Four covers the relationship between chondrolectin and synaptogenesis.

The only published binding study of the chondrolectin protein identified Rab geranylgeranyl transferase β (Rabggtb) (Claessens, Weyn and Merregaert, 2008), and that the binding occurs via the intracellular domain. However, no further functional analysis was performed. Rabggtb is the catalytic component which isoprenylates Rab GTPase during its association with the plasma membrane. Rab GTPases are involved in vesicle formation and docking, so Claessens, Weyn, and Merregaert hypothesised

that chondrolectin acts as a stabilising protein for the Rabggtb. They determine that Chodl is unlikely to be a target for isoprenylation itself, due to a lack of target motif for the modification.

Another potential ligand for chondrolectin is collagen19a1 (Col19a1). The mutant *stumpy*, a dominant negative mutant of Col19a1, phenocopies the stalled CaP axons of the *chodl* -/- embryos, (Hilario, Wang and Beattie, 2010). Morpholino knockdown of Col19a1 also induces axon stalling. Expression analysis of *colXIXa1* using *in situ* hybridisation showed a dynamic expression pattern from 19 hpf until 36 hpf, the same stages as primary axonal outgrowth from the spinal cord. Particularly of interest to my thesis work is that the expression pattern at 19 hpf is in the region of the horizontal myoseptum. This would imply that Col19a1 is present in the ECM at the HM at the same time the motor axons are reaching the HM choice point. The HM is of clear importance to both the chondrolectin and collagen19a1 function, given that the axonal phenotype is focused around the HM. At later stages, the *in situ* pattern is both more dorsal and ventral, corresponding to the path of the MiP (dorsal) and CaP (ventral). This suggests that Col19a1 is influencing the axonal growth cones of these primary motor neurons (Hilario, Wang and Beattie, 2010).

A range of unpublished data from colleagues in my group demonstrates that the C-type lectin domain of Chodl binds Col19a1. The findings are summarised in Table 3.2. Firstly, genetic interaction of *chodl* and *colXIXaI* was observed, as injection of either the *chodl* or *col19a1* morpholino alone at a sub-threshold dosage does not induce the axonal phenotype. However, combining these sub-threshold doses does lead to an axonal phenotype, demonstrating their synergistic interaction.

Using HEK cells, Dr Ana-Maria Oprişoreanu performed biochemical assays on these proteins. There are no commercially available antibodies for Col19a1 and Chodl, as the mouse CHODL antibody used in Weng, Hübner, *et al.*, 2003; Enjin *et al.*, 2010 are no longer available for sale. However, HEK cell-adapted plasmids of Col19a1-HA and Chodl-FLAG were generated to use in binding assays and Western blotting, as the HA and FLAG peptide are widely used, and their antibodies are well-characterised. Initial binding assays demonstrate that the Col19a1 and Chodl can bind *in vitro*. This was performed by isolation of both proteins from transfected HEK cells, followed by binding assays and Western blotting (unpublished data, Dr Oprişoreanu).

I speculate that chondrolectin functions as a cell-surface protein, and thus refute the previous findings that chondrolectin is mostly expressed in the perinuclear region and cytoplasm (Weng, Hübner, *et al.*, 2003; Enjin *et al.*, 2010). Instead, I hypothesise that chondrolectin is trafficked and inserted into the cell membrane, in order to interact with Col19a1 in the ECM. Unfortunately, my data in zebrafish using the HB9:Chodl-FLAG plasmid alone cannot prove this. Although the FLAG staining is excluded from the nucleus (visible in Section 3.2.5), the staining is widespread in the cytoplasm and membrane. This is due to our use of the HB9 promoter and not the endogenous *chodl* promoter. As a future experiment, co-staining of a membrane marker such as HNK-1 (Nourizadeh-Lillabadi *et al.*, 2010) and the FLAG, in high-resolution, should demonstrate that the Chodl-FLAG is present in the membrane as well as the cytoplasm in the zebrafish.

Using HEK cells Dr Oprişoreanu demonstrated that Chodl is trafficked to the plasma membrane and requires the C-type lectin domain to bind Col19a1. Col19a1 supernatant was added to Chodl-FLAG transfected HEK cells. After washing, fixation, and immunolabelling, we observe that the Chodl-FLAG constructs are membranous and can retain the Col19a1 (in other words, binding the collagen) only when the CTLD is present. This supports our hypothesis that the CTLD is interacting with ECM proteins including Col19a1, and that it does this while Chodl is bound to the membrane.

The HEK cell data supports the acute rescue experiments I performed in Section 3.2.6, and further develops it. Both the CTLD and ID are required for the chondrolectin function in zebrafish, and this may be because the CTLD binds with Col19a1 during axon outgrowth. Other proteins may also bind the CTLD, but the phenocopy of *stumpy* and *chodl* -/-, as well as the binding assays, suggest that Col19a1 is a key binding partner.

Finding	**Model system**	**Methodology**	**Researcher**
Chondrolectin and collagen19a1 genetically interact	Zebrafish	Sub-threshold dosage of both chodl and col19a1 morpholino act synergistically to induce the axonal phenotype.	Dr Zhen Zhong

Chodl and Col19a1 bind each other	HEK cells	Western blotting after binding assays, using tagged proteins produced by HEK cells. Col19a1 supernatant added to Chodl-FLAG transfected HEK cells is retained due to binding between the proteins.	Dr Ana-Maria Oprişoreanu
Chodl binds Col19a1 via its C-type lectin domain	HEK cells	In binding assays followed by WB, binding between Chodl and Col19a1 is abolished if the C-type lectin domain is removed. Col19a1 supernatant is not retained on HEK cells transfected with the Chodl-FLAG (w/oCTLD) construct.	Dr Ana-Maria Oprişoreanu
The intracellular domain of Chodl does not interact with Col19a1	HEK cells	Binding assays followed by WB are unaffected if the ID is removed from the construct transfected into HEK cells. Col19a1 supernatant added to Chodl-FLAG (w/o ID) transfected HEK cells is retained due to binding between the proteins.	Dr Ana-Maria Oprişoreanu
Chodl protein localises to the plasma membrane	HEK cells	Confocal imaging of HEK cells transfected with Chodl-FLAG shows FLAG immunoreactivity in the plasma membrane	Dr Ana-Maria Oprişoreanu

Table 3.2: Summary of unpublished findings demonstrating the interaction of chondrolectin and collagen 19a1.

At this time, we do not know which proteins bind the ID to transduce the outgrowth signal, and the exact mechanism with regard to how the ID is involved, although it is almost certain that it includes Ser/Thr kinases, as phosphorylation of the ID is also required for the function in zebrafish. In this thesis, we substituted 11/12 of the serine and threonine residues for alanine, but a further development of this would be to systematically substitute each residue, and repeat the rescue experiments, to identify the minimum phosphorylation sites that are required for the protein to function. As well as generating a construct that cannot be phosphorylated (i.e., it is constitutively non-phosphorylated), a future study could investigate the effect of a constitutively phosphorylated domain. This would offer insight into the effect of activating chondrolectin outside of its normal stages of function. Rather than substituting Ser/Thr to Ala, these 'phosphomimetic' residues are instead aspartic or glutamic acid (Dephoure *et al.*, 2013).

In mice, several splice variants have been identified with differences in the ID (Sleigh *et al.*, 2014). The 3 isoforms of chondrolectin have varying length of intracellular domain, with the C-type lectin and transmembrane domains remaining identical across the variants. The zebrafish Chodl is 293aa in length, which mostly closely corresponds to the Chodl-001 isoform at 273aa. The Chodl-002 isoform is 292aa in length, and Chodl-003 is 246 aa, with only 6 aa of the intracellular domain conserved. However, Chodl-003 isoform is not detectable in the spinal cord (Sleigh *et al*., 2014), so its potential role is unknown. The comparison between orthologues of chondrolectin isoforms between species are shown in Section 1.4.1.1. Ensembl (https://www.ensembl.org/index.html) does not predict different splice variants in the zebrafish orthologue of chondrolectin, and deleting the whole intracellular domain abolishes the rescue of the axonal phenotype in *chodl* -/- zebrafish (data presented in Section 3.2.6). It would be interesting to use these splice variants to attempt to rescue the *chodl* -/- zebrafish, to determine the minimum sequence required to rescue the axonal phenotype.

Use of kinase inhibiting compounds, to look for phenocopy of *chodl* -/- axons, might identify the specific kinases involved in chondrolectin. However, kinase inhibitors often target multiple kinases, making determination of the exact mechanism challenging (Klaeger *et al.*, 2017). One method to identify intracellular binding partners would be to perform mass spectrometry on Chodl-FLAG protein isolated from the zebrafish stable transgenic line, although the amount of protein required by mass

spectrometry is large, representing several hundred embryos. The likelihood of capturing a kinase bound to the ID would also be low, as the binding to phosphorylate the residues would be transient compared to the Col19a1 binding the CTLD. However, this is a potentially useful avenue to develop in the future, to determine other proteins which may interact with chondrolectin apart from Col19a1.

In this chapter, I have generated and characterised a chondrolectin knockout zebrafish, which exhibits motor axon growth defects but has grossly normal morphology. I have also generated a transgenic line re-expressing motor-neuron specific chondrolectin in the *chodl* -/- background, demonstrating the cell-autonomous function of chondrolectin. I have presented novel functional data offering a potential mechanism for chondrolectin, namely that it binds collagen19a1 in the ECM via its C-type lectin domain, and its intracellular domain becomes phosphorylated to induce a growth signal.

Chapter Four – Investigating the novel role of chondrolectin in synapse stabilisation

4.1 – Introduction

In this chapter, I will present data showing that chondrolectin expression affects the formation and stabilisation of motor synapses. As will be discussed, as well as evidence that chondrolectin is a downstream gene of Smn dysfunction in SMA models, synapse defects are widely observed in SMA. I thus hypothesise a relationship between chondrolectin and synaptogenesis, which may contribute to the pathology in SMA.

4.1.1 – Neuromuscular junction defects have been observed in models of Spinal Muscular Atrophy

Spinal Muscular Atrophy is an inherited form of motor neuron disease which affects children. The most severe form, Type I, has an average disease onset of six months and a life expectancy of two years (Lunn and Wang, 2008). SMA affects lower motor neurons in humans, and neuromuscular junction (NMJ) defects are detected in human patients as well as many animal models (Murray, Talbot and Gillingwater, 2010; Boyd and Gillingwater, 2016). Neuromuscular junctions are the synaptic connection between the motor axon and the muscle, with chemical signalling occurring between the pre-synapse (axon) and post-synapse (muscle) to induce motor movement (Darabid, Perez-Gonzalez and Robitaille, 2014).

During SMA disease progression, the motor neuron degeneration begins at the NMJ, and thus it is important to investigate how the NMJ develops and stabilises (Goulet, Kothary and Parks, 2013). The reasons for NMJ vulnerability in SMA are hypothesised to be due to failure of mRNA transport along axonal processes, reducing the local translation in the NMJ (Fallini *et al.*, 2016). SMN protein is also localised in the NMJ

of embryonic and post-natal mice, suggesting that the protein itself may function in the NMJ which is impaired in SMA (Dombert *et al.*, 2014). For these reasons, the NMJ is considered a key target to investigate in SMA pathology (Murray, Talbot and Gillingwater, 2010; Boido and Vercelli, 2016).

There is also increasing evidence that the motor neurons and neuromuscular junctions are affected during developmental stages, so rather than purely degenerative, SMA also has a developmental component. In foetal tissue of Type I SMA patients, there is neurofilament accumulation in the neuromuscular junctions, and a failure of the pre-synapse to fully occupy the post-synaptic compartment (Martínez-Hernández *et al.*, 2013). This demonstrates that aberrant changes to the NMJ occur even before birth of the SMA patient and onset of symptoms. In Kariya *et al*., 2008, diaphragm muscle samples donated from human SMA Type I patients also show aggregation of NF and poor arborisation of the motor terminals. This demonstrates widespread structural defects in the NMJ of human SMA patients, even in muscle considered to be less vulnerable to SMN loss, as the diaphragm is usually spared in Type I SMA (Kariya *et al.*, 2008). However, it is not known in humans if this is a fully developmental failure or extremely early degeneration.

In mouse models of SMA, several key findings demonstrate that there are neuromuscular junction defects, supporting the idea that NMJs are a key target for investigation. Firstly, motor axon growth to the muscle is unaffected even in severe SMA mice (Mcgovern *et al.*, 2008), but there are widespread changes to the NMJs even at early stages (Goulet, Kothary and Parks, 2013). As mentioned previously, in both embryonic and post-natal mice, the SMN protein localises to the pre-synaptic terminal of the motor axons, and complexes with ribonucleotide proteins (RNPs), suggesting a role for SMN in the NMJ (Dombert *et al.*, 2014). In cultured mouse motor neurons, taken from embryonic SMA model mice, there is reduced Ca^{2+} channel clustering in the axon terminals, which also leads to reduced spontaneous excitability (Jablonka *et al.*, 2007). Reduction of SMN in mice appear to prevent the maturation of the NMJs, as the post-synaptic densities are not correctly remodelled into the 'pretzel' shape, remaining a solid patch but becoming progressively weaker in AChR staining intensity, which phenocopies defects observed in diaphragm muscle samples from human patients (Kariya *et al.*, 2008). This paper also indicates pre-synaptic defects, with the axon terminal remaining bulb-shaped and failing to branch into and occupy the post-synaptic density. These defective axons also showed accumulation

of neurofilament, which supports the human data described in Martínez-Hernandez *et al.,* 2013. The concept of SMN reduction preventing maturation of NMJs was also supported by impaired synaptic vesicle release observed in mouse electrophysiology data (Kong *et al.*, 2009). A later study also demonstrated a requirement of SMN for organisation of the active zone of the motor synapse, including microtubule and synaptic vesicle maturation, as well as synaptic vesicle recycling (Torres-Benito *et al.*, 2011). Reduction in SMN protein levels in the mouse model results in fewer mitochondria. This is also observed in zebrafish Smn knockdown, where increasing mitochondrial biogenesis rescues the axonal defects, and vulnerable motor neuron populations in mouse models have an altered bioenergetic profile than those populations less vulnerable to degeneration (Boyd *et al.*, 2017).

In the zebrafish, a severe SMA model exhibits pre-synaptic deficits (Boon *et al.*, 2009). There is a reduction of SV2 staining in 11 dpf larvae, but the post-synaptic labelling remains intact, leading to a decrease in co-localisation of these two labels. However, this reduction appears to be SV2-specific, as labelling with synaptotagmin shows no change between the controls and mutants. Introduction of the human SMN2 gene in these mutant zebrafish extended their lifespan by several days, and rescued the synaptic defects for these days, although the loss of SV2 staining re-emerged by the time these mutants died (Hao, Burghes and Beattie, 2011). This demonstrates that zebrafish models of the disease recapitulate certain synaptic defects associated with SMA.

4.1.2 – Synaptogenesis in zebrafish and other organisms

During motor axon growth in zebrafish, clusters of pre- and post-synaptic proteins form between the extending axon and muscle and remodel over time. In mammals, the motor axon innervates each muscle fibre with only a single NMJ. The relationship between signalling proteins derived from axons and muscles have been explored both in axonal pathfinding and synaptogenesis.

Before motor axons exit the spinal cord in zebrafish, clusters of acetylcholine receptors (AChRs) form in pre-patterns in the muscle, from approximately 16 hpf onwards (Flanagan-Steet *et al.*, 2005). These pre-patterns form along the vertical myoseptum in advance of the motor axon pathway (Panzer *et al.*, 2005). Schematics

illustrating the pre-patterning of AChRs before axon growth is shown in Chapter One, in Section 1.2.4, with diagrams of the key developmental stages..

The pre-patterning of AChRs in zebrafish is dependent on the muscle-specific kinase (MuSK). MuSK zebrafish mutant *unplugged* exhibits axonal pathfinding defects, including stalling of the CaP axon and aberrant pathfinding of the RoP axon (Zhang *et al.*, 2004). MuSK signalling induces expression of ECM molecules in axonal pathfinding choice points including the horizontal myoseptum. *Unplugged* mutants do not express Tenascin-C, an ECM molecule important for the correct axonal pathfinding (Schweitzer *et al.*, 2005). In *unplugged* zebrafish, the pre-patterns remain scattered on the muscle fibres, and do not form into a clustered pre-pattern along the middle of the myotome as is seen in wild-types (Jing *et al.*, 2009).

During motor axon growth in zebrafish, the growth cone filopodia are preferentially stabilised upon contact with AChRs on the muscle, and so axonal pathfinding tends to follow these pre-patterns (Panzer, Song and Balice-Gordon, 2006). AChRs not contacted by axons are eventually dispersed, but the clusters contacted by axons are also stabilised ((Flanagan-Steet *et al.*, 2005). These are known as *en passant* synapses, as they cluster along the length of the axons rather than form single terminal NMJs, as in mammals (Burden, 2002; Wu, Xiong and Mei, 2010). Although initially elongated in shape, the AChRs become more punctate and condensed over time. In mice, aneural pre-pattern clusters of AChRs also form, but are dispersed if not innervated by the motor axon (Darabid, Perez-Gonzalez and Robitaille, 2014). These findings demonstrate that the clustering of AChRs on the muscle does not initially require signals from the motor neuron, but at later stages require axonal contact to stabilise the post-synapse and remodel the pre-patterns into an active synapse.

The further stabilisation of the post-synapse after axonal contact requires both muscle-derived and neuron-derived signal proteins (Wu, Xiong and Mei, 2010). One neuron-derived protein necessary for further NMJ remodelling is agrin. Agrin-null mice do not develop NMJs and die at birth (Gautam *et al.*, 1996). Similar to the MuSK mutant, morpholino-induced knockdown of agrin in zebrafish causes axonal pathfinding errors. Furthermore, the AChR pre-patterns can be induced but not stabilised, and thus the AChR clusters disperse after axonal growth (Kim *et al.*, 2007). MuSK is necessary for post-synaptic differentiation in mammals, where it recruits rapsyn and AChR to the post-synaptic density after agrin signalling from the axon

(Burden, 2002). However, zebrafish *unplugged* mutants still develop synapses, although the larvae have reduced numbers of, and smaller sized, post-synaptic puncta, showing that it is dispensable in zebrafish (Zhang *et al.*, 2004). Ectopic expression of MuSK in mice promotes synapse formation, and can rescue the lack of synapses normally observed in agrin-null mice (Kim and Burden, 2008).

Further zebrafish mutants have elucidated the synaptic proteins required for correct synapse stabilisation. The rapsyn mutant *twitch once* is unable to correctly initiate an escape swim when startled, and the mutant larvae have diffuse AChR clusters which leads to reduced motility (Ono *et al.*, 2002). Rapsyn is a scaffolding protein which forms part of the post-synaptic density on the muscle fibres, and defects in rapsyn have been linked to myasthenic syndrome in humans (Ohno *et al.*, 2002). Rapsyn requires acetylcholine receptors for the protein to be transported from the Golgi apparatus to the synapse (Ono *et al.*, 2001; Park *et al.*, 2012).

In larval zebrafish, when the secondary axons have differentiated and extended motor axons, the axons begin to branch and innervate the myotome outside of the ventral axon bundle. This pathfinding does not require pre-patterning of AChR clusters, which have dispersed if not contacted by axons before 30 hpf. Several zebrafish mutants exhibit reduced numbers of synaptic puncta in larval stages, as well as reduced branching of the axons (Panzer *et al.*, 2005). This includes the Collagen19a1 mutant *stumpy*, a putative binding partner of chondrolectin.

The relationship between axonal branching and synaptogenesis is unknown in zebrafish, but evidence in *Xenopus* motor axons and the retinal ganglion cells (RGCs) in both zebrafish and *Xenopus* suggest that synaptic sites are required to maintain nascent axonal branches. In RGC axons, *in vivo* imaging of pre-synaptic proteins demonstrates that nascent dendritic arbours are unstable and retract unless pre-synaptic proteins cluster on the branch point. Branches preferentially emerge from synaptic sites on the trunk of the axon (Meyer and Smith, 2006; Ruthazer, Li and Cline, 2006). This also occurs in the motor axons of Xenopus tadpoles (Javaherian and Cline, 2005). Overall, this suggests that axonal branching is closely related to synaptogenesis and proposes that synaptogenesis facilitates the number and location of axon branches.

4.1.3 – Zebrafish behavioural assays

The rapid development of zebrafish leads to behavioural responses within 24 hpf. Behavioural assays are thus an excellent method to functionally probe defects in the synapses. At 24 hpf the embryos are still inside the chorion, and although some spontaneous twitching is observable, the embryos are unable to swim at this age (Menelaou *et al.*, 2008). After hatching, at around 3 dpf, the larvae are capable of flight responses to escape from a stimulus, but they do not perform free swimming at this stage. Free swimming and feeding behaviour begins at 5 dpf, when the swim bladder inflates, and the larvae have exhausted their supply of yolk (Granato *et al.*, 1996; Goolish and Okutake, 1999). At this stage, the larvae must be capable of hunting and escape behaviours, and with the swim bladder can control their depth as well as their horizontal movement. The larvae also undergo avoidance behaviours from predatory stimuli such as dark areas, moving images, or open spaces (Colwill and Creton, 2011).

After a touch stimulus to the tail, the zebrafish initiates a flight escape by rapidly swimming forwards for a short period, away from the stimulus. The larvae can cover around 25 mm within the first 15 seconds (Wehner *et al.*, 2017). The swimming reaction is mediated by sensory Mauthner cells and the fast-twitch muscles, which are innervated by the primary and some secondary neurons (Kohashi and Oda, 2008). Assaying this response has been widely used in a variety of contexts, including injury and repair, disease models, and developmental studies. Mechanical lesioning of the spinal cord leaves the larvae paralysed caudal to the injury site and unable to respond to the tail tap (Ohnmacht *et al.*, 2016; Wehner *et al.*, 2017). Regeneration of the spinal cord also correlates with a functional recovery to this behaviour. Mutations in synaptic proteins, such as rapsyn, often have paralysis or show reduced movement phenotypes (Panzer *et al.*, 2005; Park *et al.*, 2014).

When startled by either touch or auditory vibration near the head of the larval zebrafish, the larvae undergo a rapid coiling of the body and swim away from the stimulus (Granato *et al.*, 1996; Bhandiwad *et al.*, 2013). This movement is mediated by the Mauthner cells, which are a pair of large reticulospinal cells in the hindbrain, which cause contraction of all motor neurons on the contralateral side of the stimulated Mauthner cell. This startle response and contraction causes a

characteristic C-bend shape in the body of the larva. A schematic of this escape is shown below, Figure 4.1.

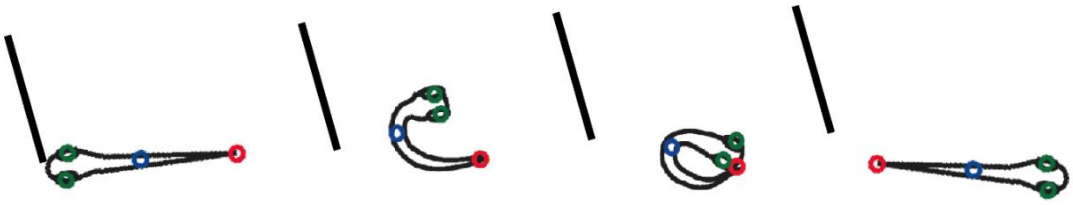

Figure 4.1: Schematic illustrating the C-bend response.
When startled by a touch stimulus or vibration, the larva performs a tight bend, with its head contacting its tail in a C-shape (third frame). The larva then swims away from the stimulus. (Adapted from Bhandiwad et al, 2013).

Changes to either the escape flight or turning response during escape have been observed in zebrafish with muscle, motor neuron, and synapse mutations. A wide-ranging behavioural screen was performed in the Tübingen ENU mutant screen, with a range of observed behaviours (Granato *et al.*, 1996). This included complete paralysis, inability to sense touch stimuli, and reduced swimming ability. A rapsyn mutant, which fails to correctly localise acetylcholine receptors (AChRs) to the muscle surface, are able to initiate an escape but have easily-fatigued muscles so cannot swim after this initial response (Ono *et al.*, 2002). In the chondrolectin mutant, with reduced axonal branching at 3 dpf (Chapter Three), we would therefore hypothesise that its behaviour either in swimming or turning at this stage would be impaired.

Zebrafish mutants with deficits in axonal pathfinding or axon growth often also exhibit synapse defects. This includes *unplugged, stumpy*, and SMA model larvae (Panzer *et al.*, 2005; Boon *et al.*, 2009; Jing *et al.*, 2009). Chondrolectin is also linked to SMA, of which NMJ dysfunction is a key pathological feature, therefore I hypothesised that synaptogenesis or synapse development would be impaired in the *chodl* -/- zebrafish compared to wild-types. In this chapter, I present data at embryonic and larval stages, showing defects in synapse labelling in the mutants which are partially rescued in the

stable rescue line. I also performed behavioural assays which demonstrated a turning defect in the *chodl* -/- larvae during an escape response.

4.2 – Results

4.2.1 - Synaptic labelling of the horizontal myoseptum at 28 hpf shows pre-synaptic defects in *chodl* -/- embryos

To determine changes to synaptic organisation in the *chodl* -/- mutants, we first compared the pre- and post-synapse at the horizontal myoseptum at 28 hpf. The horizontal myoseptum was selected as it is the location of the axonal stalling in the mutant, and morphant data demonstrated no changes in axon behaviour between the spinal cord exit and reaching the HM (e.g. the pre-HM axon) (Zhong *et al.*, 2012). Pre-synaptic defects have been observed in the SMA zebrafish models, of which chondrolectin is a downstream gene (Boon *et al.*, 2009). We therefore wanted to examine the synaptic puncta at the HM region, to determine if there are differences between the synaptic compartments in wild-type and *chodl* -/- embryos.

To label the pre-synapse, we used anti-SV2, an antibody widely used in zebrafish synaptic preparations (Flanagan-Steet *et al.*, 2005; Boon *et al.*, 2009). Synaptic vesicle protein 2 is found in all synapses and is a transmembrane transporter on the vesicle surface (Feany *et al.*, 1992). Antibodies against synaptotagmin (znp-1) were also used by colleagues to label the pre-synapse and validate the pre-synaptic phenotypes, and the data is also discussed later in this chapter. The post-synapse was labelled with an anti-AChR antibody validated in zebrafish, mAb 35 (Park *et al.*, 2014). α-bungarotoxin is frequently used to label the post-synapse, but we were unable to replicate the labelling in our hands, using protocols published in Flanagan-Steet *et al.*, 2005; Panzer, Song and Balice-Gordon, 2006; Park *et al.*, 2012.

To measure synaptic differences at the HM at 28 hpf, a 20 µm x 20 µm square region around the HM was cropped after staining and imaging. The puncta were analysed after thresholding each channel to generate binary images. Briefly, after LUT inversion to make the labelling black on white, background subtraction was applied to

each channel with a rolling ball radius at 1/3 of the image width. A 20% threshold was then applied, based on the maximum grey value measured for each image. The Analyse Particle function was then performed, with a minimum particle size of 0.5 μm^2. A detailed method on thresholding the images is described in the Materials & Methods. We first compared wild-type and *chodl* mutants, below (Figure 4.2).

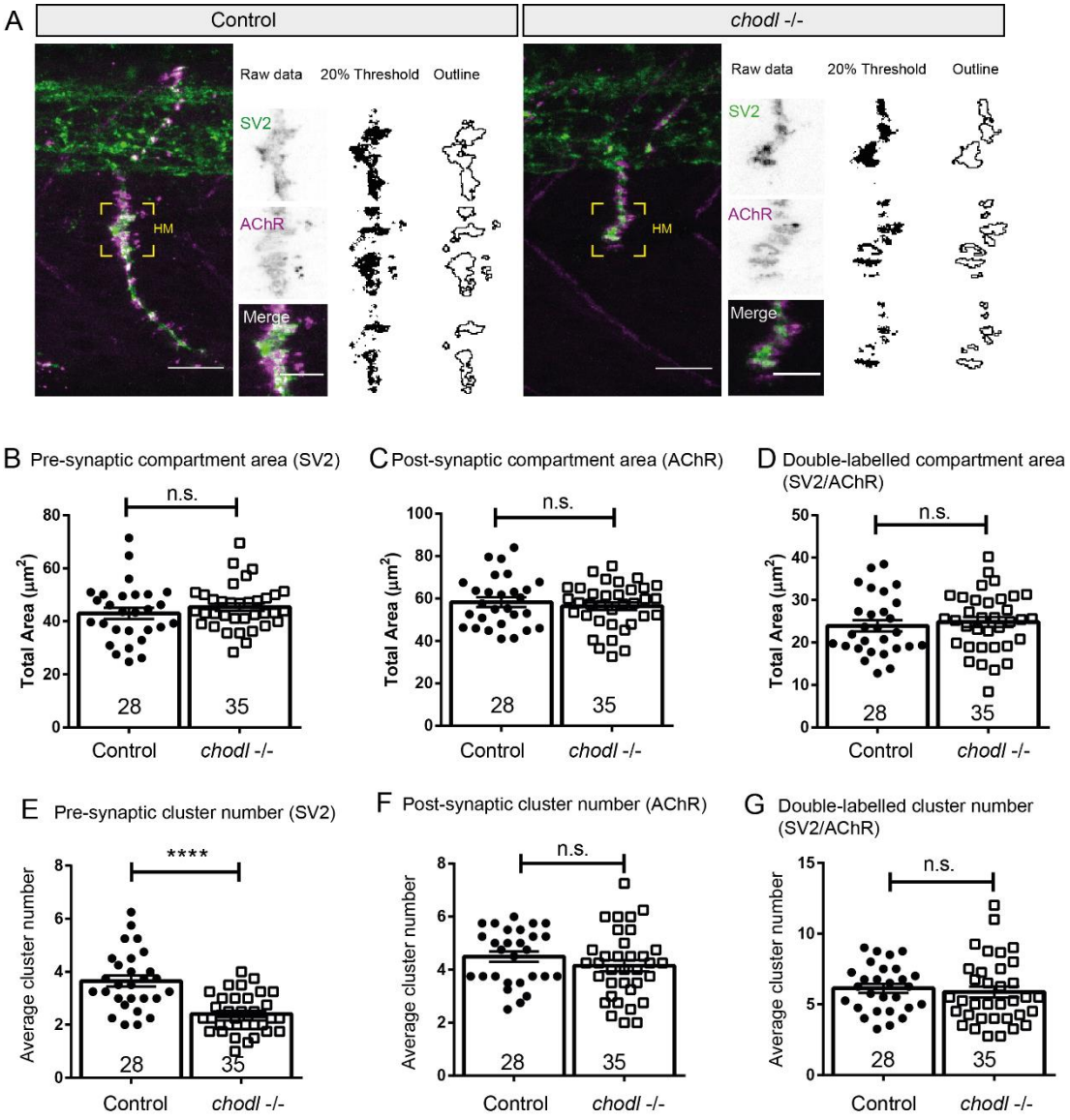

Figure 4.2: The pre-synaptic clusters are reduced in number but their total area is unchanged in *chodl* -/- 28 hpf embryos compared to controls.
A: Representative images of the lateral view of the CaP axon at 28 hpf. The HM region is shown (yellow box). The raw image, thresholded image, and cluster outline are shown. Scale bars= 20 µm and 10 µm. **B**: The total pre-synaptic compartment area is unchanged between control and *chodl* -/- embryos (Unpaired t-test n.s, p= 0.340) **C**: The total post-synaptic compartment area is unchanged between control and *chodl* -/- embryos (Unpaired t-test n.s, p= 0.502). **D**: The total double-labelled compartment area is unchanged between control and *chodl* -/- embryos (Unpaired t-test n.s., p=0.611) **E**: The average number of pre-synaptic clusters are significantly reduced in *chodl* -/- embryos compared to controls (Unpaired t-test **** p<0.0001. Post-hoc power= 0.996). **F**: The average number of post-synaptic puncta is unchanged between control and *chodl* -/- embryos (Unpaired t-test n.s. p=0.612) **G**: The average number of double-labelled clusters are unchanged between control and *chodl* -/- embryos (Unpaired t-test n.s. p= 0.257).

In the data shown in Figure 4.2, the *chodl* -/- embryos exhibit a reduction in the pre-synaptic compartment clusters at the HM, but the total area of the SV2 pre-synaptic compartment is not significantly changed.

The total area covered by SV2 labelling does not differ between chodl -/- embryos and controls (Control total area= 43.00 µm^2 ±, n= 28. *chodl* -/- total area= 45.36 µm^2 ±, n= 35. Unpaired t-test n.s., p= 0.340). However, the average number of pre-synaptic clusters are significantly reduced in the chodl -/- embryos compared to controls, with a reduction by 34% (Control cluster number= 3.652 ±0.210, n= 28. *chodl* -/- cluster number= 2.41 ±0.122, n= 35. Unpaired t-test **** p<0.0001) (B, E).

This suggests that the organisation of the SV2 protein is disrupted in the *chodl* -/- embryos, and the SV2 fails to coalesce into discernible clusters as in the wild-type. However, the overall size of the HM area is not different between groups, shown by the unchanged total area, suggesting the overall amount of SV2 is unchanged.

The post-synaptic compartment, labelled with AChR antibody, is not different between genotypes. The total post-synaptic area is unchanged between control and *chodl* -/- embryos (Control total area= 58.29 µm^2 ±2.26, n= 28. *chodl* -/- total area= 56.36 µm^2 ±1.81, n= 35. Unpaired t-test n.s., p= 0.502) The number of post-synaptic clusters are not significantly different between control and *chodl* -/- embryos (Control puncta number= 6.13 ±0.314, n= 28. *chodl* -/- cluster number= 5.869 ±0.391, n= 35. Unpaired t-test n.s. p= 0.612) (C, F). This suggests that there is an axon-mediated deficit in pre-

synaptic organisation at the HM at this developmental stage, but that this axonal loss of chondrolectin does not mediate any effect in the AChR expressed on the muscle.

With changes to the SV2 pre-synaptic label but no differences in the post-synapse, the double-labelled cluster area and number (from the overlap of SV2/AChR) is not changed between the two groups. The total double-labelled area is not significantly different between control and *chodl* -/- embryos (Control total area= 23.93 μm^2 ±1.34, n= 28. *chodl* -/- total area= 24.84 μm^2 ±1.18, n=35. Unpaired t-test n.s., p=0.611). The number of double-labelled clusters is unchanged between control and *chodl* -/- embryos (Control cluster number= 4.49 ±0.197, n= 28. *chodl* -/- cluster number= 4.15 ±0.215, n= 35. Unpaired t-test n.s. p= 0.257) (D, G).

This comparison between the wild-type controls and *chodl* -/- embryos demonstrates that loss of chondrolectin expression leads to changes in the SV2 organisation in the axon at the horizontal myoseptum. The AChR clusters, expressed on the muscle, do not change. This suggests that changes to the pre-synapse, mediated by the loss of chondrolectin, does not perturb clustering of AChR immunoreactivity on the muscle.

To determine if this pre-synaptic phenotype is rescued in the *chodl* -/-;HB9:Chodl-FLAG line, a colleague in the group utilised the same protocol and image analysis method. However, due to the transgenic background of HB9:GFP in the *chodl* -/-;HB9:*chodl*-FLAG line, the same secondary antibodies could not be used as were used in Figure 4.2. The α-AChR was originally visualised using AF488 α-rat, but this was changed to AF647 α-rat. The use of α-SV2 and AF594 α-mouse remained the same. To maintain true comparison between the groups, the HB9:GFP transgenic controls and mutants were also used, rather than the purely wild-type background used previously. A new batch of antibodies were also used. Although the SV2 antibody batches had comparable concentrations of proteins, the AChR new batch had a higher concentration of protein, which may also explain differences in labelling of the post-synapse observed by the other researcher.

The pre-synaptic data is replicated in this experiment, demonstrating its reliability across different researchers, and in the rescued chodl -/-;HB9:Chodl-FLAG line there is a full rescue of the cluster number to wild-type values, showing that the synapse defect is rescued as well as the axonal defect at 28 hpf. However, there are some differences in the post-synaptic values in that the cluster number is also reduced in the *chodl* -/- mutants compared to controls.

4.2.2 – Changes in the pre-synaptic compartment in *chodl* -/- embryos persist when the axons grow beyond the horizontal myoseptum

The *chodl* -/- phenotype at 28hpf discussed in Chapter Three shows that ~75% of the CaP axons are stalled at the horizontal myoseptum, and around ~25% have grown beyond this choice point, although the axons are still shorter than the wild-type axons at the same time point. Because of this stalling, it is possible that the enlarged pre-synapse seen in the *chodl* -/- axons are a result of the axon just being delayed, and thus a consequence of the stalled axon, rather than directly linked to the loss of chondrolectin. To further investigate this, we imaged both wild-type and *chodl* -/- embryos at 31hpf, to determine if the pre-synaptic differences persist into later time points. 31 hpf was chosen as it is before the outgrowth of the secondary axons at 33 hpf, but the proportion of mutant axons which have managed to grow beyond the HM is higher than at 28 hpf, rising to 42% (27/64 axons in 16 embryos, data not shown). The same imaging protocol was used as in Section 4.2.1 above, and the analysis was restricted to axons which had grown past the HM. The data is shown below (Figure 4.3).

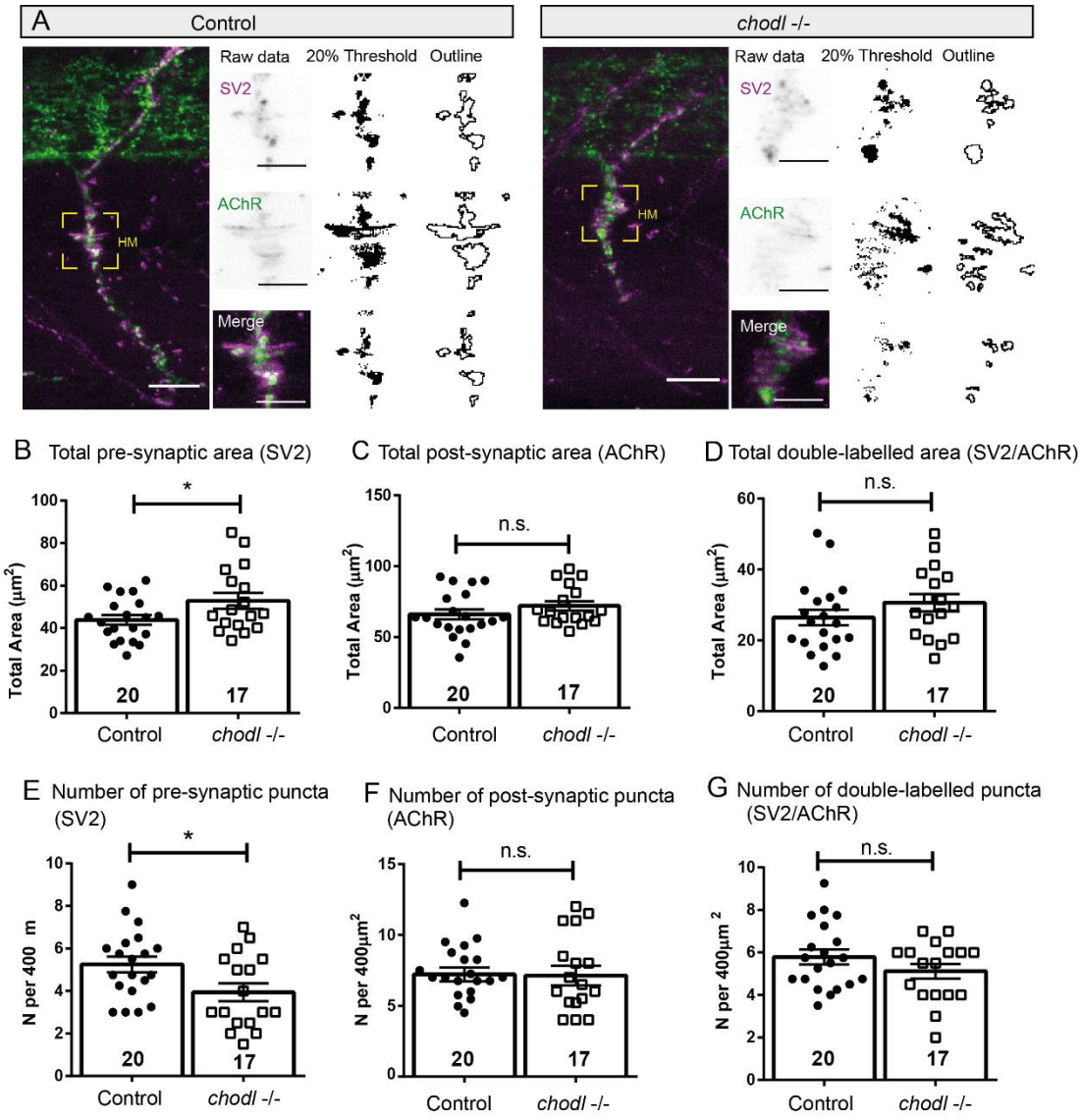
A
Control
chodl -/-
Raw data
20% Threshold
Outline
SV2
AChR
Merge
HM
B Total pre-synaptic area (SV2)
Total Area (µm²)
C Total post-synaptic area (AChR)
D Total double-labelled area (SV2/AChR)
E Number of pre-synaptic puncta (SV2)
N per 400 m
F Number of post-synaptic puncta (AChR)
N per 400µm²
G Number of double-labelled puncta (SV2/AChR)
N per 400µm ²
*
n.s.
20
17
Control
chodl -/-

Figure 4.3: Pre-synaptic defects are present at 31 hpf in axons which have passed the horizontal myoseptum.
A: Example images of wild-type control and *chodl* -/- axons which have passed the HM at 31 hpf, taken from lateral trunk views. The ROI is shown (yellow square). For both the SV2 and AChR channels, the raw, thresholded, and puncta outline are shown. Scale bars= 20 µm and 10 µm. **B**: The total pre-synaptic area labelled with SV2 is significantly larger in *chodl* -/- embryos than controls. (Unpaired t-test * p=0.040). **C**: The total post-synaptic area labelled with AChR is unchanged between *chodl* -/- and control embryos (unpaired t-test n.s., p= 0.236). **D**: The total area double-labelled with both SV2 and AChR is unchanged between control and *chodl* -/- embryos (Unpaired t-test n.s. p= 0.208). **E**: The number of pre-synaptic clusters are reduced in the *chodl* -/- embryos compared to controls (Unpaired t-test * p=0.0247). **F**: The number of post-synaptic clusters are unchanged between control and *chodl* -/- embryos. (Unpaired t-test n.s. p= 0.924). **G**: The number of double-labelled clusters are unchanged between control and *chodl* -/- embryos (Unpaired t-test n.s. p= 0.184).

The measurements of the axons shown in Figure 4.3 demonstrate that the pre-synaptic puncta are significantly larger than controls at the 31 hpf timepoint. At this timepoint, the total area labelled with SV2 is also significantly larger in the *chodl* -/- embryos, 20.4% larger compared to the control area. (Control pre-synaptic average total area= 43.9 μm^2 ±2.25, n= 20. *chodl* -/- average pre-synaptic total area= 52.86 μm^2 ±3.73, n= 17. Unpaired t-test * p=0.040). The number of pre-synaptic puncta are significantly reduced, with 25.0% fewer puncta in the *chodl* -/- embryos compared to controls. (Control pre-synaptic puncta number= 5.25 ±0.369, n= 20. *chodl* -/- pre-synaptic puncta number= 3.94 ±0.422, n= 17. Unpaired t-test * p= 0.0247) (B, D). This reduction in cluster number persists from the data at 28 hpf, where the number of pre-synaptic clusters was reduced by 34% compared to the control group.

At 31 hpf, there is no difference between the post-synaptic compartments in control or *chodl* -/- embryos. The total post-synaptic area is unchanged between *chodl* -/- and control embryos at 31 hpf (Control average area= 66.06 μm^2 ±3.53, n= 20. *chodl* -/- average pre-synaptic puncta area= 72.01 μm^2 ±3.36, n= 17. Unpaired t-test n.s p= 0.236). The number of puncta in the post-synaptic compartment is unchanged between the control and *chodl* -/- embryos at 31 hpf. (Control average puncta number= 7.21 ±0.495, n= 20. *chodl* -/- average pre-synaptic puncta number= 7.13 ±0.696, n= 17. Unpaired t-test n.s. p= 0.924) (C, F).

The double-labelled area, from the overlap of the SV2 and AChR label, is unchanged between control and *chodl* -/- embryos at 31 hpf. The total area of overlap between the SV2 and AChR label is not significantly different between the control and *chodl* -/- embryos at 31 hpf (Control average area= 26.42 μm^2 ±2.21, n= 20. *chodl* -/- average pre-synaptic puncta area= 30.63 μm^2 ±2.43, n= 17. Unpaired t-test n.s. p= 0.208). The number of double-labelled puncta is not significantly different between control and *chodl* -/- embryos at 31 hpf (Control average number= 5.79 ±0.348, n= 20. *chodl* -/- average pre-synaptic puncta number= 5.12 ±0.347, n= 17. Unpaired t-test n.s. p= 0.184) (D, G).

The 31 hpf data, limited to axons which had extended beyond the HM, demonstrates that the pre-synaptic deficits observed in the 28 hpf embryos persist even after the axons have escaped the HM. The number of pre-synaptic puncta are significantly reduced in the *chodl* -/- embryos at both 28 hpf and 31 hpf. Interestingly, the total area labelled by SV2 is not significantly different between controls and mutants at 28 hpf but is significantly larger in the *chodl* -/- 31 hpf embryos. This suggests that as the axons extend, there are continued deficits in the pre-synaptic organising into distinct clusters, which includes an increase in pre-synaptic total area at 31 hpf.

4.2.3 - At 3 dpf, *chodl* -/- larvae show reduced numbers of pre- and post-synaptic puncta, which is partially rescued in the *chodl* -/-;HB9:Chodl-FLAG larvae

After the primary motor axons have grown along the mid-segmental pathway, a secondary set of motor neurons differentiate, and the secondary motor axons exit the spinal cord at ~33 hpf. These secondary motor neurons are more numerous per somite compared to the primary neurons. The axons follow the path of the primary axons as pioneers. After growing along this midsegmental pathway, both the primary and secondary axons branch into the myotome, to fully innervate the muscle blocks (Lewis and Eisen, 2003; Menelaou and Svoboda, 2009). A schematic illustrating this is shown below (Figure 4.4).

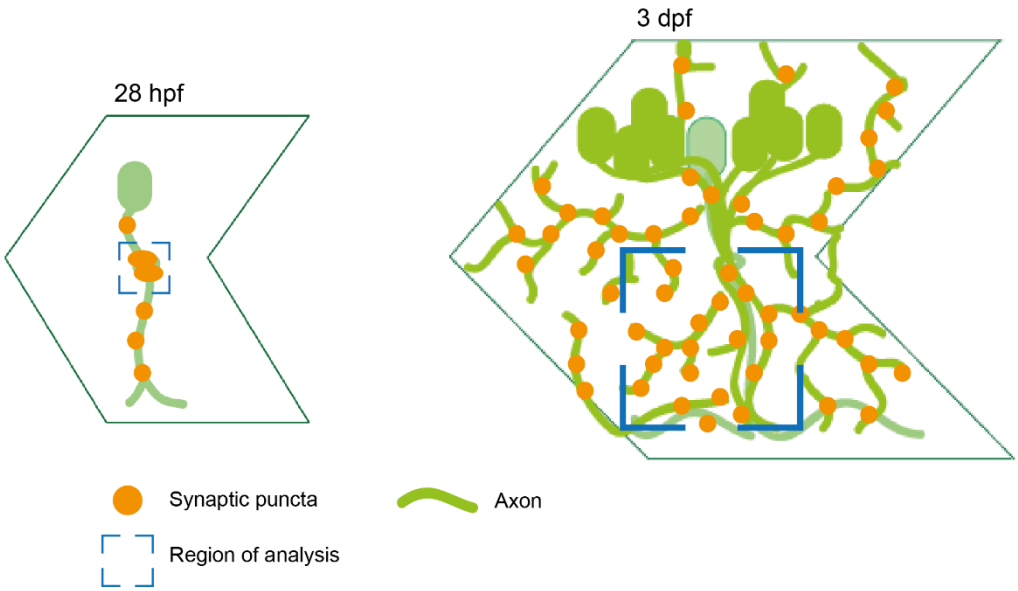

Figure 4.4: Schematic of the motor axon and synaptic puncta at 28 hpf and 3 dpf.
A single myotome in each case is shown, with the axons (green), synaptic puncta (orange) and region of interest for analysis (blue). At 28 hpf, there is a single CaP axon per somite. At 3 dpf, secondary motor neurons have differentiated, extended axons, and branched into the myotome. The number of synaptic puncta is greatly increased at 3 dpf compared to the 28 hpf time point.

To analyse the synapses in the larvae at 3 dpf, we therefore measured the number of synaptic puncta in the myotome as well as the size of the clusters. Due to the larger larval trunk compared to the embryo, a 40 µm x 40 µm square in the ventral region was selected as a region of interest. The ventral trunk was selected to avoid noise from the spinal cord in the dorsal region and limit the labelling to axonal puncta. The number of clusters and the average puncta size are shown below, comparing the wild-type controls, *chodl* -/- mutants, and the *chodl* -/-;HB9:*chodl*-FLAG rescue line (Figure 4.5).

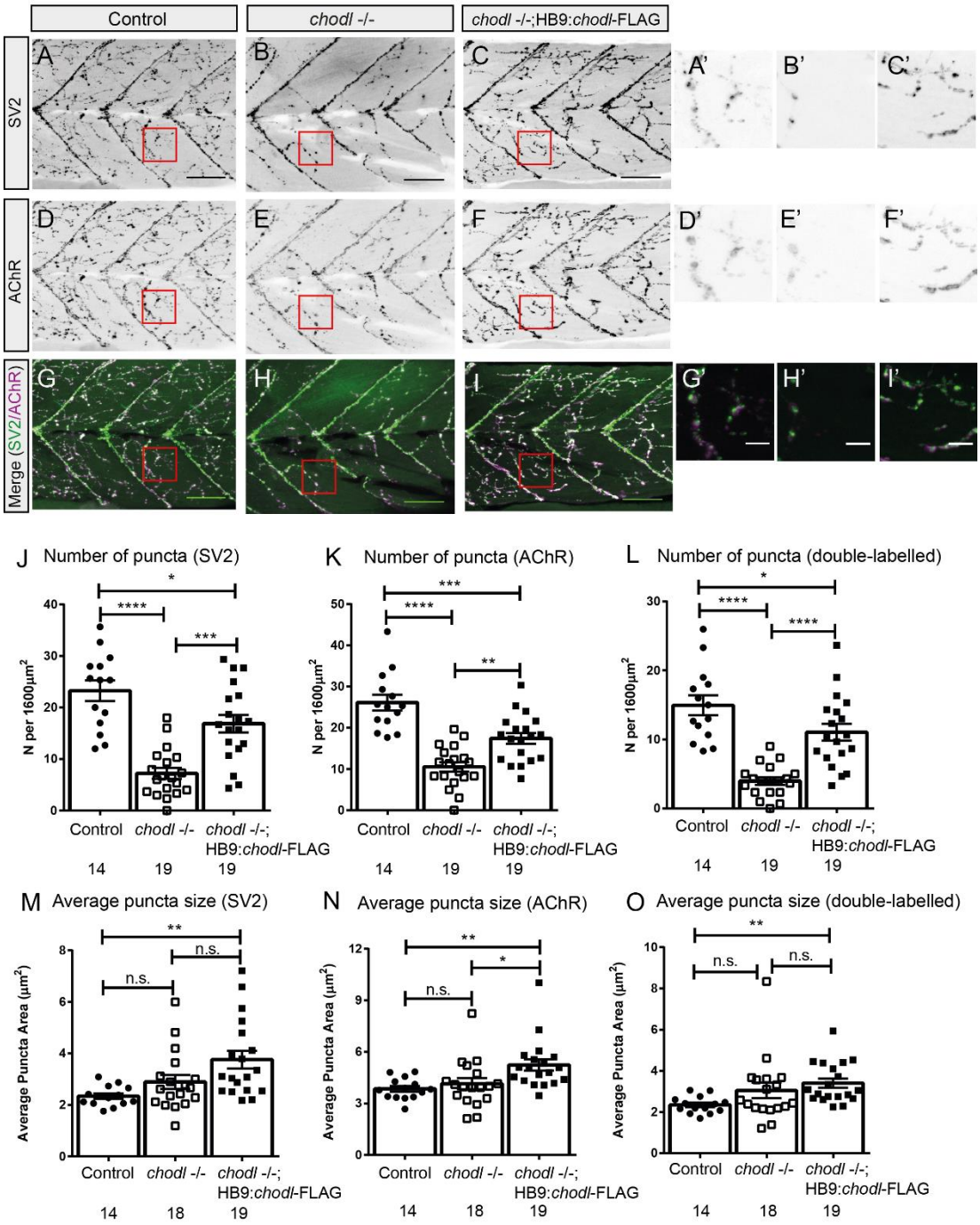
Control
chodl -/-
chodl -/-;HB9:chodl-FLAG
SV2
AChR
Merge (SV2/AChR)
A
B
C
A'
B'
C'
D
E
F
D'
E'
F'
G
H
I
G'
H'
I'
J Number of puncta (SV2)
K Number of puncta (AChR)
L Number of puncta (double-labelled)
N per 1600µm²
Control
chodl -/-
chodl -/-; HB9:chodl-FLAG
14
19
19
M Average puncta size (SV2)
N Average puncta size (AChR)
O Average puncta size (double-labelled)
Average Puncta Area (µm²)
n.s.
14
18
19

Figure 4.5: The synaptic puncta number are greatly reduced in the *chodl* -/- at 3dpf compared to controls, and this is partially rescued in the *chodl* -/-;HB9:*chodl*-FLAG line.
A-I: Representative images of the lateral trunk of 3 dpf larvae, labelled with SV2, AChR, and the merged channels. Red boxes show the ROIs selected for analysis. Scale bars = 50 µm. **A'-I'**: The higher magnification of the red ROIs. Scale bar = 10 µm. **J**: The number of pre-synaptic puncta is significantly reduced in *chodl* -/- larvae and partially rescued in the *chodl* -/-;HB9:*chodl*-FLAG group. (One-way ANOVA **** with Bonferroni's multiple comparison test, control vs *chodl* -/- **** p<0.0001, control vs *chodl* -/-;HB9:*chodl*-FLAG *p= 0.024, *chodl* -/- vs *chodl* -/-;HB9:*chodl*-FLAG *** p= 0.0001. Post-hoc power= 1.00). **K**: The number of post-synaptic puncta is significantly reduced in the *chodl* -/- larvae compared to controls, and partially rescued in the *chodl* -/-;HB9:*chodl*-FLAG group. (One-way ANOVA **** with Bonferroni's multiple comparison test. Control vs *chodl* -/- **** p<0.0001, *chodl* -/- vs *chodl* -/-;HB9:*chodl*-FLAG **p=0.0022, control vs *chodl* -/-;HB9:*chodl*-FLAG ***p= 0.0004. Post-hoc power= 1.00) **L**: The number of double-labelled puncta is significantly reduced in *chodl* -/- larvae compared to controls and partially rescued in the *chodl* -/-;HB9:*chodl*-FLAG group (One-way ANOVA **** with Bonferroni's multiple comparison test. Control vs *chodl* -/- ****p<0.0001, *chodl* -/- vs *chodl* -/-;HB9:*chodl*-FLAG ****p<0.0001, control vs *chodl* -/-;HB9:*chodl*-FLAG *p= 0.0483. Post-hoc power= 1.00). **M**: The average pre-synaptic puncta size is not significantly changed between control and *chodl* -/- larvae but is significantly larger in *chodl* -/-;HB9:*chodl*-FLAG larvae compared to controls. (Kruskal-Wallis **p=0.019 with Dunn's multiple comparison test. Control vs *chodl* -/- n.s. p= 0.371, *chodl* -/- vs *chodl* -/-;HB9:*chodl*-FLAG n.s. p= 0.111, control vs *chodl* -/-;HB9:*chodl*-FLAG **p=0.0014. Post-hoc power= 0.664). **N**: The average post-synaptic puncta size is not significantly different between control and chodl -/- larvae. The puncta size of the *chodl* -/-;HB9:*chodl*-FLAG group is significantly larger than both the control and chodl -/- larvae. (Kruskal-Wallis with Dunn's multiple comparison test. Control vs *chodl* -/- n.s. p>0.999, *chodl* -/- vs *chodl* -/-;HB9:*chodl*-FLAG *p= 0.113, control vs *chodl* -/-;HB9:*chodl*-FLAG **p= 0.0017. Post-hoc power= 0.701.) **O**: The average double-labelled puncta size for the overlap of SV2 and AChR is significantly larger in the *chodl* -/-;HB9:*chodl*-FLAG larvae compared to controls. (One-way ANOVA with Bonferroni's multiple comparison test. Control vs *chodl* -/- n.s. p= 0.270, *chodl* -/- vs *chodl* -/-;HB9:*chodl*-FLAG n.s. p= 0.184, control vs *chodl* -/-;HB9:*chodl*-FLAG **p= 0.0016. Post-hoc power= 0.23

The *chodl* -/- pre-synaptic puncta number was reduced by 70% compared to the control numbers. The *chodl* -/-;HB9:*chodl*-FLAG group has 27.52% fewer pre-synaptic puncta than the controls, and 133% more synaptic puncta than the *chodl* -/- larvae. Although the rescue is not recovered to control levels, this still demonstrates

that re-expression of chondrolectin in motor neurons is sufficient to increase the numbers of synaptic puncta compared to the knockout mutant. (SV2 puncta number control = 23.26 ±1.99, n= 14. *chodl* -/- SV2 puncta number= 7.21 ±1.07, n= 19. *chodl -/-;*HB9*:chodl*-FLAG SV2 puncta number = 16.86 ±1.72 n=19. One-way ANOVA **** with Bonferroni's multiple comparison test. Control vs *chodl* -/- ****, control vs *chodl -/-;*HB9*:chodl*-FLAG *, *chodl* -/- vs *chodl -/-;*HB9*:chodl*-FLAG***. *p= 0.024, ***p= 0.0001, **** p<0.0001) (J).

Similarly to the pre-synaptic puncta, the number of post-synaptic puncta is significantly reduced in the *chodl* -/- larvae, and partially rescued in the *chodl -/-;*HB9*:chodl*-FLAG line compared to the control values. There was a 60% reduction in post-synaptic puncta number in *chodl* -/- larvae compared to controls. The *chodl -/-;*HB9*:chodl*-FLAG values were 33.3% fewer puncta than controls, and 65.4% larger than the *chodl* -/- puncta number. (Control average post-synaptic puncta number= 26.12 ±1.90, n= 14. *chodl* -/- average post-synaptic puncta number= 10.53 ±1.15, n= 18. *chodl -/-;*HB9*:chodl*-FLAG average post-synaptic puncta number= 17.42 ±1.32, n= 19. One-way ANOVA with Bonferroni's multiple comparison test, control vs *chodl* -/- **** p<0.0001, *chodl* -/- vs *chodl -/-;*HB9*:chodl*-FLAG **p=0.0022, control vs *chodl -/-;*HB9*:chodl*-FLAG ***p= 0.0004) (K).

The number of double-labelled puncta is significantly reduced in the *chodl* -/- larvae compared to controls, with a reduction of 73.4% in the mutants compared to controls. The number of double-labelled puncta in the *chodl -/-;*HB9*:chodl*-FLAG group is 177% larger than the *chodl* -/- values, and 26.1% lower than the controls. (Control average double-labelled puncta number= 14.95 ± 1.437, n= 14. *chodl* -/- average double-labelled puncta number= 3.982 ± 0.5307, n= 19. *chodl -/-;*HB9*:chodl*-FLAG average double-labelled puncta number= 11.05 ± 1.20, n= 19. One-way ANOVA **** with Bonferroni's multiple comparison test. Control vs *chodl* -/- ****, *chodl* -/- vs *chodl -/-;*HB9*:chodl*-FLAG ****, control vs *chodl -/-;*HB9*:chodl*-FLAG *. ****p<0.0001, *p= 0.0483) (L).

Comparisons of the puncta size between controls, *chodl* -/-, and *chodl -/-;*HB9*:chodl*-FLAG larvae demonstrates that there is no significant difference between control and *chodl* -/- larvae, for any labelling, but the *chodl -/-;*HB9*:chodl*-FLAG group has significantly larger puncta.

For the pre-synaptic SV2 labelling, the *chodl* -/- puncta size is 23.5% larger than controls. The *chodl -/-;*HB9*:chodl*-FLAGpuncta size is 60.5% larger than the control

average area, which is significantly increased, and 30% larger than the *chodl* -/- area, which is not significantly different. (Control average pre-synaptic puncta size= 2.342 μm^2 ± 0.103, n= 14. *chodl* -/- average pre-synaptic puncta area= 2.893 μm^2 ±0.272, n= 18. *chodl -/-;*HB9*:chodl*-FLAG average pre-synaptic puncta size= 3.761 μm^2 ±0.344, n= 19. Kruskal-Wallis **p=0.019 with Dunn's multiple comparison test. Control vs *chodl* -/- n.s. p= 0.371, *chodl* -/- vs *chodl -/-;*HB9*:chodl*-FLAG n.s. p= 0.112, control vs *chodl -/-;*HB9*:chodl*-FLAG **p=0.0014) (M).

In the post-synaptic AChR labelling, the *chodl* -/- puncta area is 7.8% larger than the control area, which is not statistically significant. The *chodl -/-;*HB9*:chodl*-FLAG puncta area is significantly larger than the *chodl* -/- area, with an increase of 26.3%. The average *chodl -/-;*HB9*:chodl*-FLAG puncta area is statistically larger than the control area, increased by 36.1%. (Control average post-synaptic puncta area= 3.848 μm^2 ± 0.167, n= 14. *chodl* -/- average post-synaptic puncta= 4.145 μm^2 ± 0.330, n= 18. *chodl -/-;*HB9*:chodl*-FLAG average post-synaptic puncta area= 5.237 μm^2 ± 0.333, n= 19. Kruskal-Wallis ***p= 0.0009, with Dunn's multiple comparison test. Control vs *chodl* -/- n.s. p>0.999, *chodl* -/- vs *chodl -/-;*HB9*:chodl*-FLAG *p= 0.0113, control vs *chodl -/-;*HB9*:chodl*-FLAG **p= 0.0017) (N).

In the double-labelled puncta of the overlap between SV2 and AChR, there is no statistical difference in puncta area between control and *chodl* -/- larvae. The average puncta area in the *chodl -/-;*HB9*:chodl*-FLAG line is not significantly larger than the *chodl* -/- value, but 44.8% larger than the control average area, which is statistically significant. (Control average double-labelled puncta area= 2.351 μm^2 ±0.110, n= 14. *chodl* -/- average double-labelled puncta area= 3.048 μm^2 ±0.374, n= 18. *chodl -/-;*HB9*:chodl*-FLAG average double-labelled puncta area= 3.405 μm^2 ±0.225, n= 19. Kruskal-Wallis **p= 0.0023 with Dunn's multiple comparison test. Control vs *chodl* -/- n.s. p= 0.2697, *chodl* -/- vs *chodl -/-;*HB9*:chodl*-FLAG n.s. p= 0.1835, control vs *chodl -/-;*HB9*:chodl*-FLAG ** p= 0.0016) (O).

Overall, this data shows that there are deficits in motor synapses in the chondrolectin mutant at 3 dpf. Both the pre- and post-synapse are affected, with reductions to the puncta number in the *chodl* -/- larvae compared to the wild-type controls. This is partially rescued by MN-specific re-expression of chondrolectin, although the values do not return to wild-type numbers. Interestingly, there is also an enlargement of the average puncta size in the *chodl -/-;*HB9*:chodl*-FLAG group, compared to the control and *chodl* -/- larvae, although there are no differences between the control and *chodl*

-/- average puncta area. This suggests that although the number of puncta are not fully rescued, this size increase may be compensatory, as behavioural differences are fully rescued (Section 4.2.5). The potential mechanisms for these changes, and the comparisons between the data at 28 hpf, 31 hpf, and 3 dpf are discussed further in Section 4.3.

4.2.4 – Branching analysis suggests that axonal branching requires stabilisation by synapse formation

At 3 dpf in the *chodl* -/- mutants, there is an obvious lack of both axonal branches into the myotome and synaptic puncta, seen first in the HB9:GFP transgene (Chapter Three). The data shown in this chapter in Section 4.2.3 demonstrates defects in synapse formation in the *chodl* -/- larvae, with a reduction in the number of pre- and post-synaptic puncta. As these are static preparations, it is difficult to determine if the lack of axonal growth prevents synapse formation, or if the mutant has a deficit in forming stable synapses, which then leads to instability and collapse of axon branching as observed in the retinal ganglion. To determine if synapses are important for motor axonal branching in larvae, I stained and imaged wild-type HB9:GFP larvae for SV2, AChR, and GFP. I then analysed the axon branch points to determine if the branch point was also associated with the pre- and post-synaptic puncta. The data is shown below (Figure 4.6).

This analysis demonstrates that almost all branch points of motor axons are also associated with both pre- and post-synaptic puncta. Although not conclusive evidence, it does support the hypothesis that the axon branches can only emerge in the presence of synapses, as 96.8% of branch points contained the synaptic labels. This suggests that in the case of the chondrolectin mutant, the lack of axonal branching is caused by defective synaptogenesis. This further indicates a novel role for chondrolectin in stabilising synapse puncta, as well as its previously published role in axon growth.

A

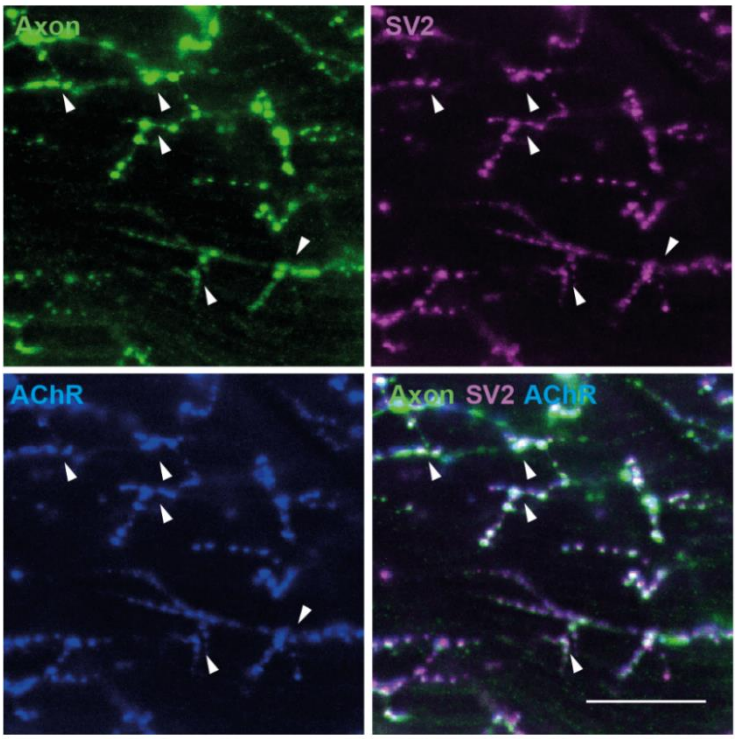

B

Branch points per myotome	12-15
Myotomes per larvae	3
Number of larvae	10
Total branch points analysed	443
n branchpoints with synaptic puncta	429
n branchpoints without synaptic puncta	14
% of branchpoints with synaptic puncta	96.8%

Figure 4.6: Axonal branch points at 3 dpf are heavily enriched with synaptic puncta.
A: Representative images of wild-type 3 dpf trunk labelled with the axon, SV2, and AChR. Single optical sections are shown. Scale bar= 25 µm. **B**: Analysis was performed on 10 larvae, 3 myotomes per larvae, and between 12-15 branch points quantified per myotome. Of 443 branch points, 429 were also associated with synaptic puncta and 14 without synapse labelling. This means 96.8% of branchpoints contained synapse puncta.

4.2.5 - Behavioural phenotypes in *chodl* -/- larvae at 3 dpf

4.2.5.1 – The distance travelled to escape a tail stimulus is unchanged between wild-type and chodl -/- larvae

Due to the widespread reduction in synaptic puncta in the *chodl* -/- larvae at 3 dpf, we sought to investigate possible differences in swim behaviour of the mutants compared to wild-type. The first behavioural assay we performed was a flight response from tail tap stimulus. As described in Wehner *et al.*, 2017, we recorded the total escape distance for 15s after touching the medial fin with a fire-pulled glass pipette. The distance travelled by the larvae was then compared between the wild-type and *chodl* -/- larvae, shown below (Figure 4.7).

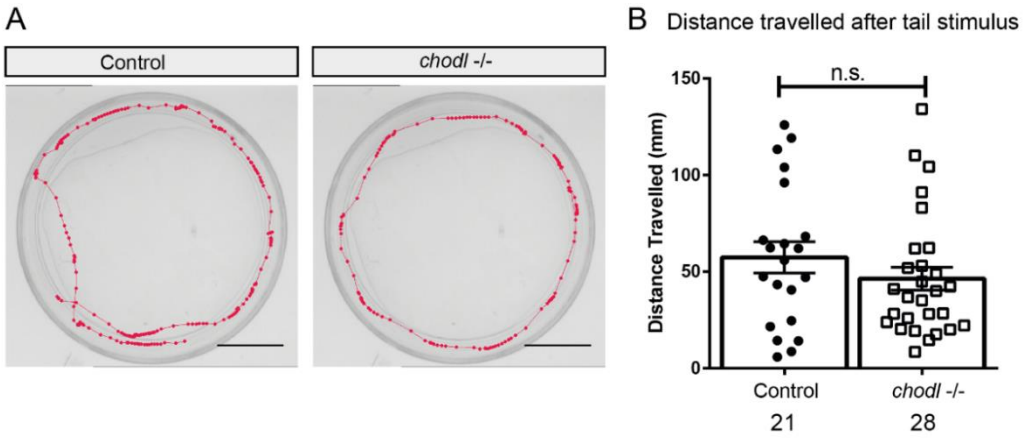

Figure 4.7: There is no difference between control and *chodl* -/- larvae in the distance travelled after a tail stimulus.
A: Example swim tracks (red) for 15s after an escape response from a tail tap, for control and *chodl* -/- 3 dpf larvae. Scale bar= 10mm. **B**: There is no significant difference between the distance travelled after a tail-tap stimulated escape. (Mann-Whitney test, n.s. p= 0.2563).

There was no significant difference in the total distance travelled between wild-type and *chodl* -/- larvae. The *chodl* -/- larvae travelled 19.2% shorter distances than controls, but this does not lead to a statistically significant difference. (Control average distance= 57.45 mm ±8.07, n= 21, *chodl* -/- distance= 46.42mm ±6.00, n=28. Mann-Whitney test n.s., p=0.256). For both groups, the variation in values is large, leading

to an SEM that is approximately 15% of the mean values. Therefore, the effect size from this data is also very small (d= 0.345). Using this effect size in an *a priori* power calculation leads to a necessary sample size of 231 for each group to gain significance. This sample size is unrealistically high and thus the non-significance between this data set means that despite the lack of synaptic puncta in the mutant larvae, there are enough functional synapses to elicit a swimming response that replicates the wild-type reaction. Reasons for this will be discussed further in the Section 4.3, the discussion and conclusions section of this chapter.

4.2.5.2 – The C-bend response is impaired in chodl -/- larvae, leading to a reduced escape angle from a head tap stimulus

Although the swimming distance between control and mutant larvae was unchanged, other assays can be used to investigate behavioural differences in larval zebrafish. The C-bend is a highly stereotyped escape behaviour seen during a startle response. The startle can originate from an auditory or vibratory stimulus, or a contact stimulus to the head of the larva (Bhandiwad *et al.*, 2013). During the C-bend, the larva makes a tight contraction of its body, bending its head to contact its tail, followed by swimming away from the dangerous stimulus. This is thus likely more sensitive to changes in the synapses and more challenging to the larvae to correctly perform.

To investigate if this contraction is impaired in the *chodl* -/- larvae, we used high-speed video recording to assay the C-bend startle response. By recording at 1000 frames/second, the initial startle turn can be analysed, which takes around 1 second (Fetcho, Higashijima and McLean, 2008). However, the high-speed recording does not produce images of sufficient resolution to measure the C-bend angle directly. Instead, we measured the angle of escape after this C-bend, when the swim is initiated. We predicted that the escape from a head touch would be to perform the C-bend, orienting the larva's head away from the danger, and then it initiates an escape swim. We hypothesised that the lack of synapse puncta in the *chodl* -/- larvae would potentially affect the ability to perform this C-bend, leading to a measurable change in this escape angle. We also included the transgenic line *chodl* -/-;HB9:*chodl*-FLAG, to determine if any behavioural phenotype is rescued. The data from this behavioural assay is shown below, Figure 4.8.

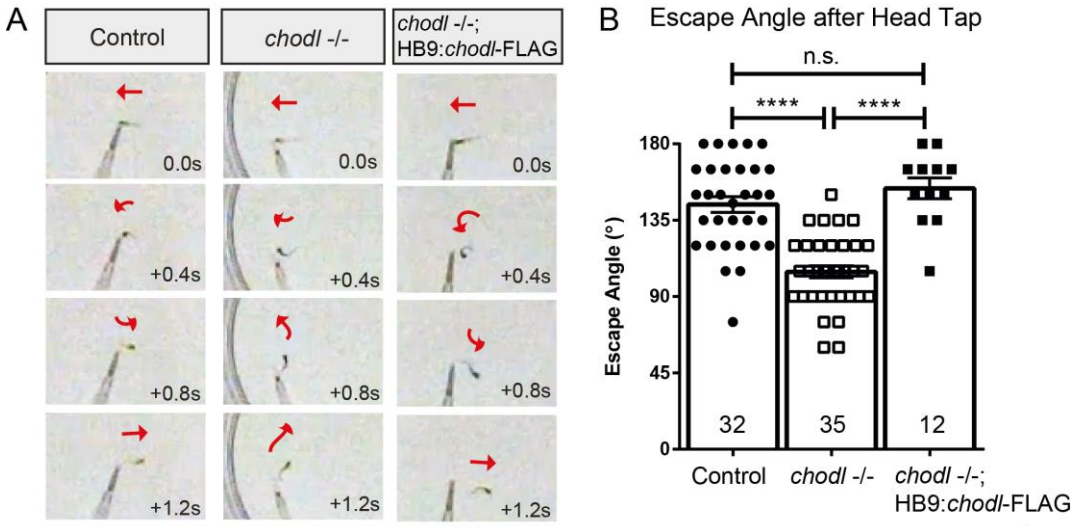

Figure 4.8: *chodl* -/- larvae exhibit a reduced turning angle after a head stimulus, which is rescued in the *chodl* -/-;HB9:*chodl*-FLAG line.
A: Montages of example turning responses. The full turn occurs within 1.2s of the touch stimulus. Red arrows show the direction and angle of the larval head. **B**: The escape angle is significantly reduced in the *chodl* -/- larvae compared to the control group. The escape angle is completely rescued in the *chodl* -/-;HB9:*chodl*-FLAG line, back to the control value. (One-way ANOVA **** with Bonferroni's multiple comparison test, control vs *chodl* -/- ****, *chodl* -/- vs *chodl* -/-;HB9:*chodl*-FLAG ****, control vs *chodl* -/-;HB9:*chodl*-FLAG n.s. **** p<0.0001, n.s. p= 0.689. Post-hoc power= 1.00)

The wild-type average escape angle is 144.2°, supporting previous data that demonstrates the larvae will turn quickly to swim away from the stimulus. The *chodl* -/- larvae make a turn with a smaller angle of escape than the control larvae, a reduction of 27.5% compared to controls. The *chodl -/-;*HB9*:chodl*-FLAGlarvae have a fully restored behaviour to control values. The *chodl -/-;*HB9*:chodl*-FLAG group angle is 47.0% larger than the *chodl* -/- angle, and only 6.7% larger than the control escape angle. (Control angle= 144.2° ±4.60, n= 32, *chodl* -/- angle= 104.6° ±3.56, n= 35, *chodl -/-;*HB9*:chodl*-FLAG angle= 153.8° ±6.16, n= 12. One-way ANOVA with Bonferroni's multiple comparison test, control vs *chodl* -/- ****, *chodl* -/- vs rescue ****, control vs rescue n.s. **** p<0.0001, n.s. p= 0.689.) This suggest that the loss of innervation in the *chodl* -/- results in a weaker C-bend contraction, and thus the reduction in escape angle. The full restoration of escape angle in the *chodl* -/-

;HB9:*chodl*-FLAG rescue larvae suggests that although the number of synapses are not fully rescued, and they are larger than in the control, they are functional and able to compensate to rescue the behaviour. The specific motor defect in this behaviour may also be caused by changes to the hindbrain organisation, which is discussed in more detail in Section 4.3.2.

4.3 – Discussion & Conclusions

4.3.1 – Chondrolectin has a novel role in synapse stabilisation

4.3.1.1 – The *chodl* -/- embryos have fewer pre-synaptic puncta around the horizontal myoseptum during embryonic stages

For measuring synaptic differences in the embryonic stages, we chose to focus on the horizontal myoseptum for several reasons. Firstly, it has been demonstrated that the axon growth rate from spinal cord exit until the HM is identical between control and *chodl* morphant embryos (Zhong *et al.*, 2012). It would therefore be unlikely that there would be any differences in examining that portion of the axon. At 28 hpf, when the *chodl* -/- axon phenotype is most visible, the axons are mostly stalled at the HM in the mutant but fully extended in the wild-type. It is not possible to quantify synapses in axons beyond the HM, as they are not present in the mutants. The HM is also enriched with ECM molecules including collagens, which were discussed as potential ligands to chondrolectin in Chapter Three. The horizontal myoseptum was thus a key location for further investigation.

The data collected at 28 hpf demonstrate that loss of chondrolectin leads to a pre-synaptic deficit, with a reduced number of defined puncta in the HM region (Section 4.2.2). Given the co-expression of chondrolectin and pre-synaptic proteins in the motor axon, it suggests a novel role for chondrolectin in synaptogenesis or synapse organisation in the motor axon. This is also supported by other staining performed by Dr Oprişoreanu (unpublished data, not shown), where synaptotagmin-positive puncta are enlarged, and the total area covered by synaptotagmin labelling is increased in

chodl -/- embryos compared to controls. Synaptotagmin is much more abundant in the pre-synapse than SV2, which may explain why its total area is increased (Wilhelm *et al.*, 2014). During synaptogenesis, it is clear that both the pre- and post-synapse clusters remodel as the axon grows, becoming more co-localised and tightly clustered (Panzer, Song and Balice-Gordon, 2006). Thus the phenotype in the *chodl* -/- embryos seem to be a failure to remodel the pre-synapse into these tighter junctions.

Explanation for this data difference may be that the new batch of AChR used by Dr Oprişoreanu was more concentrated than the batch I used, and so in using the same protocol with equal dilutions of the antibody, the staining would be stronger for her than in my data. There were also changes in the secondary antibody, where the SV2 secondary antibody remained the same, but the secondary antibody for the AChR labelling was changed due to the presence of the HB9:GFP transgene in the rescue line. This could have led to slight differences in the labelling, which cannot be discounted, and thus changes in the measurements. Dr Oprişoreanu performed similar experiments using synaptotagmin (znp-1, syt2b) as the pre-synaptic marker (unpublished, data not shown). This replicated the defects in both the pre-synapse and the post-synapse. It therefore seems that the pre-synaptic deficits in the *chodl* -/- embryos are robust, representing a failure in pre-synaptic maturation that includes multiple pre-synaptic proteins.

It is unlikely that chondrolectin directly binds pre-synaptic proteins such as SV2 or synaptotagmin, given the small intracellular domain of the chondrolectin protein, discussed in Chapter Three. SV2 and synaptotagmin are also membrane-associated proteins involved in synaptic vesicle structure and exocytosis (Feany *et al.*, 1992; O'Connor and Lee, 2002). Further binding studies or mass spectrometry to identify 'bridging' proteins which interact with both chondrolectin and the pre-synaptic proteins would need to be performed to elucidate the mechanism by which chondrolectin affects synaptic organisation.

4.3.1.2 – At 3 dpf, there is a reduction in synaptic puncta in the *chodl* -/- larvae which is partially rescued in the *chodl* -/-;HB9:Chodl-FLAG larvae

Unlike the data shown at 28 hpf, at 3 dpf both the pre-synaptic and post-synaptic puncta are affected in the *chodl* -/- larvae (Section 4.2.3). This is likely due to changes in the motor neuron network between these developmental stages. Although at 28 hpf only the primary motor axons have extended from the spinal cord, at 3 dpf the secondary motor axons have also grown across the myotome. The increased number of motor axons and their changed behaviour (branching into the trunk muscle) leads to a punctate synapse staining and widespread synaptic puncta in the musculature, compared to the focused analysis of the puncta around the HM performed in the 28 hpf data.

During synapse remodelling, the pre- and post-synaptic puncta co-localise closely together, and AChRs which are not contacted by axons are dispersed by 26 hpf (Flanagan-Steet *et al.*, 2005). However, axon growth and motor synapses are still able to form in mutants completely lacking these aneural prepatterns (Jing *et al.*, 2009). This is observed in the *chodl* -/- embryos, whose axons are temporarily stalled. At 31 hpf, approximately 42% of axons are able to grow beyond the HM despite the dispersal of these pre-patterns (Section 4.2.2).

The branching analysis presented in Section 4.2.4 demonstrates that axonal branch points are usually associated with synapses. The lack of axonal branching in *chodl* -/- larvae at 3 dpf is therefore likely due to the synaptic deficit, which prevents maintenance and stability of nascent axonal branching into the myotome. As well as a lack of axonal branches, there is a severe reduction in the number of pre-synaptic puncta at 3 dpf, and a reduction in the post-synapse as well, as the AChR puncta are not maintained without the axon present. This also causes a reduction in the double-labelled puncta, and so a reduction in active synapses. This leads to the turning deficit in the *chodl* -/- larvae observed in Section 4.2.5, discussed in more detail in Section 4.3.2.

With a reduction by 72% in the number of synapses in the *chodl* -/- mutant compared to wild-types, there is a partial rescue in the *chodl* -/-;HB9:Chodl-FLAG line (i.e. Rescue line). The *chodl* -/-;HB9*:chodl*-FLAG line has 26% fewer synapses than the wild-type larvae. The lack of full rescue in puncta values is likely to be due to differences between the chondrolectin expression due to the HB9 promoter and the

endogenous *chodl* promoter. The number of integrated HB9:*chodl*-FLAG cassettes in the transgenic line are also not known, so this may also be a consequence of the gene dosage in this line. This also may explain the increased puncta size in the *chodl -/-;*HB9*:chodl*-FLAG line compared to both the control and *chodl* -/- larvae (Section 4.2.3). I speculate that the size may also be compensatory in nature, which is why the behavioural turning phenotype is fully rescued. Electrophysiology of the larvae to determine the activity of the motor neurons (discussed later in this Section) would clarify whether the puncta size affects the activity of the synapses.

4.3.1.3 – Links between synaptic defects and Spinal Muscular Atrophy

As previously introduced, multiple SMA models demonstrate defects in the neuromuscular junction (NMJ), visible before the onset of motor symptoms. Human foetal tissue shows accumulation of neurofilament and a failure of the axon to fully occupy the post-synaptic density in Type I SMA (Martínez-Hernández *et al.*, 2013). In mouse models of SMA, the reduction in Smn protein prevents the maturation of the neuromuscular junction, with accumulation of NF and poor occupancy of the motor endplate before any motor symptoms were recorded (Kariya *et al.*, 2008; Kong *et al.*, 2009). This demonstrates that as well as being a degenerative disease of the motor neuron, synapse pathology is also a key aspect of SMA (Boyd and Gillingwater, 2016).

Importantly, a zebrafish model of SMA also exhibits deficiency in pre-synaptic SV2 staining in the larvae. The phenotype differs from the *chodl* -/- data in that there is only reduction in SV2 immunoreactivity. Synaptotagmin labelling was performed in these larvae and there was no change between the SMA model and controls. The AChR puncta labelled with α-bungarotoxin are also unaffected. Therefore, the SMA model zebrafish presented in that paper do not show a global loss of synapses as is observed in the *chodl* -/- larvae (Boon *et al.*, 2009). Synaptotagmin staining in the 28 hpf chodl -/- embryos was performed in our group (data not shown) and shows a reduction in cluster number, similar to the SV2 data shown in Section 4.2.1. The synaptotagmin area is also enlarged in the *chodl* -/- embryo, suggesting a general pre-synaptic defect which is not limited to SV2. In complete loss of chondrolectin expression, it therefore seems that synaptogenesis and synapse stabilisation is impaired. In the mutant larvae, this leads to a 73.4% reduction in the number of

double-labelled synaptic clusters in the trunk muscle. However, in the SMA model, the Smn protein level is reduced and other downstream genes (including chondrolectin) are mispliced and dysregulated. The reduction in normal chondrolectin expression may therefore also have implications for synapse stability, and this dysregulation of chondrolectin could be contributing to the synapse pathology in SMA model fish.

4.3.1.4 – Future directions for investigating the role of chondrolectin in synaptogenesis and synapse maintenance

With this novel potential role for chondrolectin in synapse stabilisation, a key future investigation would be to perform electrophysiology in the motor neurons, to see if the synaptic vesicle release is altered in *chodl* -/- larvae. In motor axons that are spared and able to form synapses, the functional abilities of these axons are unknown. Impaired synaptic vesicle release is observed in the motor neurons of SMA model mice, (Torres-Benito *et al.*, 2011), further linking the synaptic phenotype between chondrolectin loss and SMA.

Live *in vivo* imaging of synaptogenesis would also be an excellent future study. For example, acute expression of a synaptophysin-GFP plasmid in the RGCs (Meyer and Smith, 2006; Ruthazer, Li and Cline, 2006) could be applied to the motor neurons in control and *chodl* -/- embryos and larvae. This would allow confirmation of the relationship between axonal branching and synapse stabilisation, rather than relying on the static preparations in Section 4.2.4. In a similar avenue, the F-actin rich filopodia, which extend during axon growth and dendrite formation, have a reduced lifespan and lower number in SMA model zebrafish, labelled with LifeAct-GFP (Hao *et al.*, 2013). This was interpreted as a loss in the axonal stability in and thus increased likelihood to degenerate but could also be related to the loss of synaptic stability. Use of the LifeAct-GFP construct to label F-actin in the chondrolectin mutants could be used to determine if the same filopodial defects are present.

Imaging other markers of synapse proteins could also be informative. For example, SV2 is localised to synaptic vesicles, and Synaptotagmin forms the calcium-sensing portion vesicle exocytosis complex (Feany *et al.*, 1992; O'Connor and Lee, 2002). Bassoon and Piccolo are cytoskeletal proteins in the active zone of the NMJ (Gundelfinger, Reissner and Garner, 2016). Labelling of these proteins in the 28 hpf

embryos would show if the active zones of the synapses are affected as well as the general pre-synaptic density. Post-synaptic labels such as Rapsyn could also be labelled, which complex with AChRs in the muscle and tether it to the muscle surface (Lin *et al.*, 2001; Park *et al.*, 2012). However, whether the same range of synaptic antibodies would function in zebrafish immunohistochemistry as in mouse is unknown. SV2 and synaptotagmin antibodies have been well characterised in zebrafish (α-SV2 and α-znp-1), hence their use in this thesis. Rapsyn antibodies have been validated in zebrafish, and show a similar labelling pattern as the α-AChR antibody used in this chapter (Park *et al.*, 2012). Bassoon and Piccolo antibodies have not been published in zebrafish so it is unclear if these labels could be used to investigate the active zone of the motor synapses in the *chodl* -/- embryo.

4.3.2 – *chodl* -/- larvae at 3 dpf exhibit a reduction in turning angle to escape a head touch, compared to wild-type and *chodl* -/-;HB9:*chodl*-FLAG larvae

As discussed in Chapter Three, the chondrolectin mutants exhibit normal survival. From qualitative assessment of the juvenile fish and adults during development of the line, there did not seem to be any mobility issues in the mutants. They also breed normally. The ability to breed relies on close shoaling of the fish together, and failure to breed is seen in fish after ablation of their dopaminergic neurons, modelling a Parkinson's disease-like phenotype (Caldwell *et al.*, 2018). Analysis of adult swimming behaviour could be a future outlook, as there are several behavioural assays available in the adult zebrafish. For example, as well as free swimming distance, application of a water current can be used to assay the stamina of adult zebrafish to swim against resistance (Dias *et al.*, 2012). Given the synapse defects seen in the *chodl* -/- larvae, this might not affect the free swimming distance, but the reduced number of synapses could reduce the endurance of the fish to swim against a water current. The rapsyn mutant *twitch once* shows muscle fatigue in larval stages (Ono *et al.*, 2002), demonstrating that mutations to NMJ genes leads to a range of behavioural responses.

The initial behavioural test, measuring the distance travelled after a flight reaction, did not show any difference between wild-type controls and *chodl* -/- larvae. This behavioural test has been shown to demonstrate functional recovery after spinal cord

lesions in the larvae (Ohnmacht *et al.*, 2016; Wehner *et al.*, 2017), and whether manipulations of gene expression improve the recovery timeline. However, this technique does not seem sensitive enough to measure small differences in behaviour caused by the motor synapse defects. Using the HB9:GFP transgenic line, and comparing wild-type to mutant larvae, the ventral nerve bundle is intact at 3 dpf, and the somite boundaries contain synapses which are active. It is therefore possible that the motor circuit is able to compensate for this swimming distance. As also mentioned in Section 4.2.5.1, the SEM in the distances travelled are around 15% of the mean value, and the range of values covers 120 mm. This means that the distance swum during this escape is heterogeneous, even for the wild-type larvae, meaning that subtle differences between groups could be lost in the noise of the data points.

The collagen19a1 mutant, *stumpy*, also shows stalling of the primary CaP axon at 28 hpf and a reduction in synaptic clusters at 5 dpf. However, there was no detectable change to the behaviour of these mutant larvae compared to controls (Panzer, Song and Balice-Gordon, 2006; Hilario, Wang and Beattie, 2010). I speculate that the mutant, given the axonal and synaptic phenocopy of the *chodl* -/- larvae, would likely also show turning deficits if the assay I used were performed with the mutants. I hypothesise that the behavioural assays used in the published studies were not sensitive enough to detect changes to the turning, as I observed in the *chodl* -/- larvae.

Analysing the behaviour at high speed, specifically the initial turn after the head stimulus, demonstrates a reduction in turning in the *chodl* -/- larvae (section 4.2.5.2). This is fully rescued in the *chodl* -/-;HB9:*chodl*-FLAG line. This suggests that the loss of synaptic puncta in the chondrolectin mutant induces a behavioural deficit, and the behaviour can be rescued even though the synaptic puncta are only partially rescued in the *chodl* -/-;HB9:*chodl*-FLAG larvae. A good assay to measure muscle contraction would be to perform close analysis of the tail bending angles performed by the larvae, during both the C-bend and burst swimming (Budick and O'Malley, 2000; Colwill and Creton, 2011). However, the resolution of imaging equipment available to us was not sufficient to record the tail bending angle.

From the two behavioural tests, the *chodl* mutant exhibits a turning defect but swims normally in terms of distance travelled when escaping a stimulus. This suggests there is a specific response that is deficient in the *chodl* mutants. As well as the reduced numbers of motor synapses, measured at 3 dpf (Section 4.2.3), this dysfunction could be a result of an unknown hindbrain phenotype. As discussed in Section 4.1.3, the

fast escape response is mediated by motor neurons after the response is started by the Mauthner or analogous non-Mauthner cells, all of which reside in the hindbrain. mRNA expression of *chodl* visualised using *in situ* hybridisation shows expression in the hindbrain (Thisse et al., 2004, images shown in Chapter 1, Fig 1.6). I did not compare the structure of the hindbrain axons between the wild-type and mutant larvae, so cannot discount the possibility that the *chodl* -/- has a phenotype in the hindbrain. It would be possible to visualise the hindbrain neurons and their axons to confirm any changes in the mutant compared to wild-type, using an antibody such as 3A10 which labels hindbrain neurons including Mauthner cells (Brand et al., 1996).

Although the *chodl* -/- mutants are able to grow normally to adulthood, this reduction in turning ability would give an evolutionary disadvantage to the mutants in the wild. The zebrafish larvae are prey animals, which is why they perform escape behaviours after the stimulus of touch, noise, and moving dark shapes (Colwill and Creton, 2011). An inability to fully move away from the stimulus would likely result in its predation in the wild.

This chapter presents a novel role for chondrolectin in synapse stabilisation. Changes to the pre-synapse, labelled with multiple pre-synaptic proteins, show changes to the pre-synaptic clustering at 28 hpf and 31 hpf. This means that the synaptic changes are independent of the axon growth, as the *chodl* -/- axons which pass the HM still show defects. This is a clear link between SMA and *chodl*, as NMJ defects are observed in the disease model. The loss of synapses in the *chodl* -/- larvae is partially rescued in the stable *chodl -/-;*HB9*:chodl*-FLAG line, and leads to a turning behavioural defect in the mutants which is also rescued.

Chapter Five - Using the *chodl*-/- mutant zebrafish as a screening tool for molecules that enhance axon growth

5.1 – Introduction

5.1.1 – Rationale for using the *chodl* -/- phenotype for a small molecule screen

The chondrolectin mutant zebrafish are an excellent target for screening small molecules due to its link to Spinal Muscular Atrophy and its role in axonal growth. For a medium-throughput screen, there are several factors which give the *chodl* -/- embryos an advantage over using the smn morpholino. Breeding homozygote mutants is much faster and less labour-intensive than injecting morpholino. A total knockout also has advantage over a dose-dependent knockdown which must be measured and calibrated for the best phenotype.

For phenotypic scoring and determining drug-dependent rescue, axons in zebrafish after Smn knockdown have been quantified in various ways. The axonal phenotype is multidimensional, with missing, branched, or truncated axons. For example, in McWhorter *et al*., 2003, Smn knockdown is quantified by measuring the ratio of branching and ratio of truncations and presenting them separately. However, in Wishart *et al*., 2014, the phenotype is presented as a combined ratio under the umbrella of 'aberrant morphology', combining excessive branching with truncation. Sleigh *et al.,* 2014 assigns a numerical value to each axon between 0-3 depending on the severity of the phenotype, then compares the average score to the wild-type. In comparison, the *chodl* -/- phenotype is much more easily quantified, as almost all axons are stalled at the horizontal myoseptum, and at 26-30 hpf there is no other confounding morphological difference between axons except this stalling (discussed in Chapter Three). This increases the speed of scoring such axons for improved growth after treatment, as a binary judgement of stalled or not can be easily recorded.

As was introduced and discussed in Chapter One, chondrolectin is downstream of Smn dysfunction. It is mis-spliced at early timepoints in mouse SMA models, and chondrolectin over-expression rescues Smn knockdown in zebrafish (Bäumer *et al.*, 2009; Sleigh *et al.*, 2014). Therefore, although the *chodl* -/- mutants are not directly modelling SMA, the *chodl* -/- mutants can be used to find axon-stabilising compounds. The link between SMA and chondrolectin means that potential hit compounds from the *chodl* -/- screening could then be screened in Smn knockdown embryos or other models of SMA.

5.1.2 – Current strategies in drug development for SMA

For the drug screening described in this thesis, we are using a phenotypic-based approach, which is a common use for zebrafish in drug discovery (discussed in the next section). Although SMA is monogenic and thus Smn would be an excellent target, the mechanism for the disease is still unclear. Several mechanisms have been proposed, including splicing defects or improper RNA transport (Dombert *et al.*, 2014; Boyd and Gillingwater, 2016; Fallini *et al.*, 2016).

The only approved treatment for SMA is the antisense oligonucleotide (ASO) treatment nusinersen. By binding to the *SMN2* transcript, the ASO corrects the splicing error and prevents the skipping of exon 7 (Rigo *et al.*, 2012). Thus, the proportion of normal SMN protein increases due to the reduction in the defective SMNΔ7 protein. After undergoing clinical trials, (Finkel *et al.*, 2016, 2017; Swoboda *et al.*, 2016), nusinersen is now approved as the first treatment specifically for SMA. Despite the approval of nusinersen, further treatments for SMA are being developed and there is still a need for new therapies. Although nusinersen improves the symptoms in patients, it is not a complete cure and they are not completely healthy. although long-term studies are ongoing, there is no data currently for potential long-term effects of nusinersen treatment. Due to the high price of ASO production, and the likelihood that nusinersen treatment would be required every 4 months lifelong, NICE has rejected nusinersen for use by the NHS in England and Wales (NICE, 2018).

Several drugs have been repurposed for use in SMA. (Calder, Androphy and Hodgetts, 2016). As discussed in Chapter One, Section 1.3.4, SMA is caused by loss of function of SMN1, and lack of compensation by SMN2 due to its transcript degeneration, caused by exon skipping during translation. Repurposed drugs therefore were focused on increasing the expression of *SMN2*, to increase the abundance of SMN protein in cells . HDAC inhibitors such as trichostatin A or valproic acid showed increased *SMN2* transcription in patient-derived cells and mouse models (Tsai *et al.*, 2008; H. Liu *et al.*, 2014). However, these compounds are non-specific, with HDAC inhibition affecting the expression of other genes apart from *SMN2*. The neuroprotective compound riluzole, which is an approved treatment for ALS, has also been used in SMA. Riluzole has been found to prolong survival in ALS patients by approximately two to three months (Miller, Mitchell and Moore, 2012), and its exact MMOA is unknown, although it is thought to inhibit glutamate release. In a phase I trial, mean survival of the treated group was higher than in placebo, but the sample size was too small to perform statistical testing (Russman, Iannaccone and Samaha, 2003).

Several other potential treatments are undergoing clinical trials at different phases, (Shorrock, Gillingwater and Groen, 2018). These include viral vectors to deliver an enhanced *SMN1* through the blood-brain barrier to neurons, AVXS-101. It is currently entering a Phase 2 trial after success in Phase 1 (Shell *et al.*, 2018). A high-throughput screen was performed to find compounds which specifically increased the *SMN2* transcript, unlike the broad HDAC inhibitors. Roche identified a compound called RG7800 which showed pre-clinical results but failed in human trials. Structure refinement led to risdiplam (RG7916), which has been designed with improved pharmacokinetics. This compound is now entering part 2 of its first clinical trials (Ratni *et al.*, 2018).

5.1.3 – Use of zebrafish in drug screening and drug development

Zebrafish are an increasingly popular model system for modelling motor neuron diseases (MNDs). With approximately 70% gene orthology between human and zebrafish (Howe *et al.*, 2013), multiple disease models have been generated in zebrafish, including for SMA and other MNDs (reviewed in Patten *et al.*, 2014) and so

utilisation of the zebrafish for translational approaches is also increasing. MND models include C9ORF72 knockdown (Ciura *et al.*, 2013), SOD1 over-expression (Ramesh *et al.*, 2010), and SMA models (Hao, Burghes and Beattie, 2011).

Zebrafish have been traditionally used in phenotypic screens to identify biologically active compounds (MacRae and Peterson, 2015). This is because of their biological accessibility during embryonic and larval stages, and their optical transparency for imaging studies. Due to the large clutch sizes, ease of drug incubation in the aqueous medium, and physiological relevance of analysing the whole organism, zebrafish are an excellent model for medium- to high-throughput drug screening (Langheinrich, 2003; Tamplin *et al.*, 2012; Phillips and Westerfield, 2014).

Many examples of screening using zebrafish have been performed to discover new pathways or find potential therapeutics. For example, drugs which altered the gross morphology were identified as phenocopying hedgehog-null mutants. Further study into the compound target showed that it bound to other proteins than the canonical Hedgehog / Patched / Smoothened pathway (Williams *et al.*, 2015). In another screen, assays measuring increased motor response to light was used to find compounds which activate sensory neurons in the embryo (Kokel *et al.*, 2013). Cessation of a seizure response in mutant zebrafish were used to screen compounds that could treat Dravet syndrome (Baraban, Dinday and Hortopan, 2013). Ephrin4A was identified as a disease-modifying protein in ALS using a morpholino-based screen. A SOD1 overexpression model was screened for axonal rescue after injection by a library of morpholino. Knockdown of Ephrin4A rescued the axons, demonstrating that inhibition of its expression could be a therapeutic target (Van Hoecke *et al.*, 2012). A screen to identify regenerative pathways used a fin amputation model and looked for compounds which abolished regeneration. From this, glucocorticoids were identified as necessary for the regeneration, offering insight into the regenerative mechanisms (Mathew *et al.*, 2007).

In our screen, we sought to identify compounds that rescued the phenotype of the *chodl* -/- mutants, and thus compounds which improve motor axon growth. Thus, we begin with the aberrant phenotype of the mutant – stalled CaP motor axons – and from this seek compounds which improve the axon length closer to the wild-type phenotype.

5.1.4 – The VAST BioImager is an automated platform to handle, array, and image zebrafish larvae

Zebrafish are particularly amenable to drug screens due to their large clutch sizes and easy incubation directly in drug solutions in multi-well plates, all of which increase their throughput to a rate higher than that of rodent models. However, in our screen, we must be able to image and thus analyse the axonal phenotype of the *chodl* -/- embryo. The HB9:GFP transgenic line can be used to directly image the motor neurons without the need for extra staining, but the bottleneck is the imaging process. Arraying, mounting, and imaging the embryos represents the rate-limiting step in this protocol.

To increase the throughput of zebrafish screens, an automated loading and imaging platform has been designed by Union Biometrica. It is an adjusted large object flow cytometry platform, optimised for zebrafish. Known as the VAST (Vertebrate Automated Screening Tool) BioImager, it uses an automatic plate loader (the LP Sampler) and microfluidic pumps to draw anaesthetised larvae from a multi-well plate through the platform. The platform contains an imaging chamber to which a microscope can be mounted. In our centre, the imaging is performed by a custom Spinning Disk Confocal Microscope (SDCM) (Early *et al.*, 2018). This allows image acquisition much more quickly than with a standard confocal microscope (Jonkman and Brown, 2015). Inside the imaging chamber, a glass capillary holds the larvae in place and is fully rotatable, allowing complete control over imaging orientation. (Pardo-Martin *et al.*, 2010; Letamendia *et al.*, 2012). The zebrafish larva is detected as it passes through the capillary, as the imaging chamber contains a light gate which scatters light when solid objects pass through it. This triggers stoppage of the pumps and recall of the object to be rotated and imaged. Bubbles and debris can be discriminated from larva due to the differences in light scatter through the photodetection system. Recognition of the correct orientation is automated by software comparisons between the in-built CCD camera in the imaging chamber and a user-generated template of the dorsal and lateral views of the head (Chang *et al.*, 2012). Schematic representation of the VAST BioImager is shown below (Figure 5.1) (Adapted from Early *et al.*, 2018).

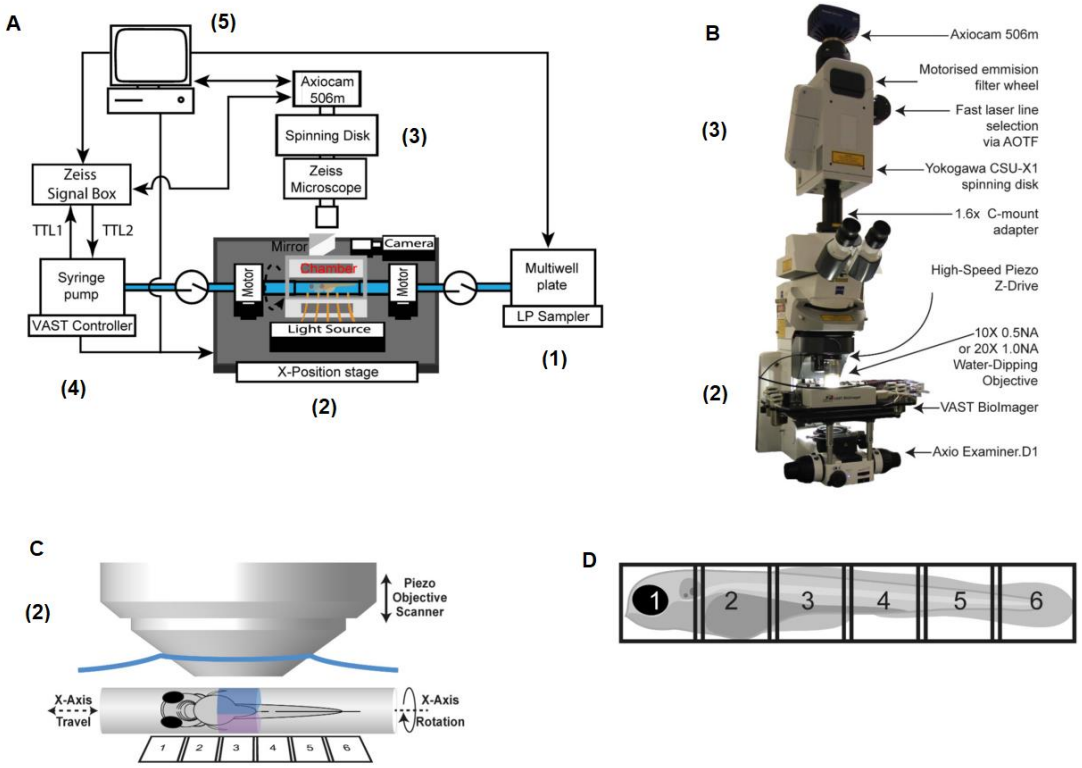
A
(5)
Axiocam 506m
Spinning Disk
(3)
Zeiss Microscope
Zeiss Signal Box
TTL1
TTL2
Syringe pump
VAST Controller
Mirror
Camera
Chamber
Motor
Motor
Light Source
X-Position stage
Multiwell plate
LP Sampler
(1)
(2)
(4)
B
(3)
(2)
Axiocam 506m
Motorised emmision filter wheel
Fast laser line selection via AOTF
Yokogawa CSU-X1 spinning disk
1.6x C-mount adapter
High-Speed Piezo Z-Drive
10X 0.5NA or 20X 1.0NA Water-Dipping Objective
VAST BioImager
Axio Examiner.D1
C
(2)
Piezo Objective Scanner
X-Axis Travel
X-Axis Rotation
1
2
3
4
5
6
D
1
2
3
4
5
6

Figure 5.1: Schematic representation of the VAST BioImager.
A: The VAST and spinning disk confocal setup. (1): The holding platform for multi-well plates and robotic sampler arm, which selects and loads larvae from each well. (2): The imaging chamber. The larvae are fed from the LP Sampler into the imaging chamber and each larva is held in the capillary during imaging. (3) The custom Spinning Disk Confocal Microscope from Zeiss allows rapid image acquisition. (4) The VAST controller and pump control the rate of movement by the larvae through the platform. (5) A computer connected to the microscope and VAST BioImager allows user control of the platforms. **B**: The custom SDCM used in our screening platform. In this image, (1) from A is out of frame. (2) The VAST imaging chamber is fixed under the imaging objective, a 10x water-dipping lens. (3) The spinning disk microscope was chosen due to its higher speed over a line-scanning confocal. The Z-stack speed is increased through use of a high-speed piezo drive. **C**: A close-up schematic of the capillary and microscope objective. (2) refers to its location in the A and B images. The capillary can be rotated, and the larvae positioned along the x-axis to be imaged. 6 tiles are shown, to image the length of the larva. **D**: A schematic of a 4 dpf larvae, marked by the number of tiles required to image the whole larva. Adapted from Early *et al*., 2018.

5.1.5 – The Epigenetic Probes Collection from the Structural Genomic Consortium is an open-access library of epigenetic compounds

When choosing a library to screen using the *chodl* -/- embryos, several factors were considered. There are many commercially available libraries, themed for their range of targets (e.g. kinase or phosphatase inhibitors, or epigenetic modifiers). The Structural Genomics Consortium is a mixed public-private, non-profit organisation which collaborates on protein structural chemistry and drug discovery. The SGC has produced and sells a 38-compound library called the Epigenetic Probes Collection. We selected this library for our initial screen due to its small number of compounds, useful for a pilot study, as well as its availability from a colleague in the University (received from Professor Neil Carragher, with thanks). Data on the targets and molecular structure for each compound are also freely available online for further investigation into hit compounds (https://www.thesgc.org/chemical-probes/epigenetics). The compounds in the library were selected by the Structural Genomics Consortium due to their known activity in cell-relevant concentrations (<1

µM), and target several methods of epigenetic modification: acetylation/deacetylation, methylation/demethylation, or histone-binding proteins (Brown and Müller, 2015; Müller *et al.*, 2018).

5.2 – Results

5.2.1 - Design of a drug screening paradigm utilising *chodl* -/- embryos

5.2.1.1 – Adaptation of the VAST BioImager protocols

According to specifications written by Union Biometrica, the company which designed and built the VAST BioImager platform (henceforth referred to as VAST), the minimum developmental stage that the platform can support is 48 hpf. This is mostly due to the physical durability of the larvae, which may be damaged by the pressure when they are passed through the apparatus. Damage or yolk tearing was not observed in any 48 hpf larvae (n=450) in the VAST's initial methods paper (Pardo-Martin *et al.*, 2010), but the yolk sac is much larger in younger embryos than 48 hpf larvae. However, it was necessary to image *chodl* -/- embryos at around 27-30 hpf as this is the stage when the axon phenotype is most striking. The method of axon analysis is discussed in the next section, but as this earlier developmental stage was necessary, we needed to adapt the VAST protocols for this screen.

Once loaded into the VAST system, the detection, alignment, and imaging of the larvae is automated using a photodetection system. As pigmented objects such as larvae, debris, or bubbles pass through and break the light beam, it signals to stop the microfluidics pump and backup the object into the viewing window. The automated program then rotates the object, attempting to match it to the template images it has for the experiment settings. It discards any object which do not match the template at a high enough threshold, and thus does not image bubbles or debris. This is more efficient in larvae older than 48 hpf, where the melanocytes have proliferated and thus the zebrafish eye and head are darkly pigmented (Kimmel *et al.*, 1995). In younger embryos, which do not have this dark pigmentation, there will be a lower chance of detection for two reasons. First, the transparent embryo may not trigger the light gate

and is thus flushed through to waste without stopping. Secondly, the automated program may also have difficulty matching the image template to the live image, as there is not a strong difference in intensity patterns that can be recognised by the computer. Shown below are example template images of wild-type zebrafish at 30 hpf and 72 dpf, used by the VAST experiment settings (72 hpf experiment settings designed by Dr Jason Early, unpublished, used with permission). In Figure 5.2, the difference in pigmentation intensities between the two developmental stages are clear. The differing head direction between stages in Figure 5.2 (i.e., the mouth of the 30 hpf embryo is oriented upwards while it is downwards in the 72 hpf larvae) is also due to the y-axis size limits of the microscope objective. To image the full trunk of the embryo, it must be oriented like this as the large yolk sac holds the trunk closer to the edge of the capillary and thus the boundary of the imaging.

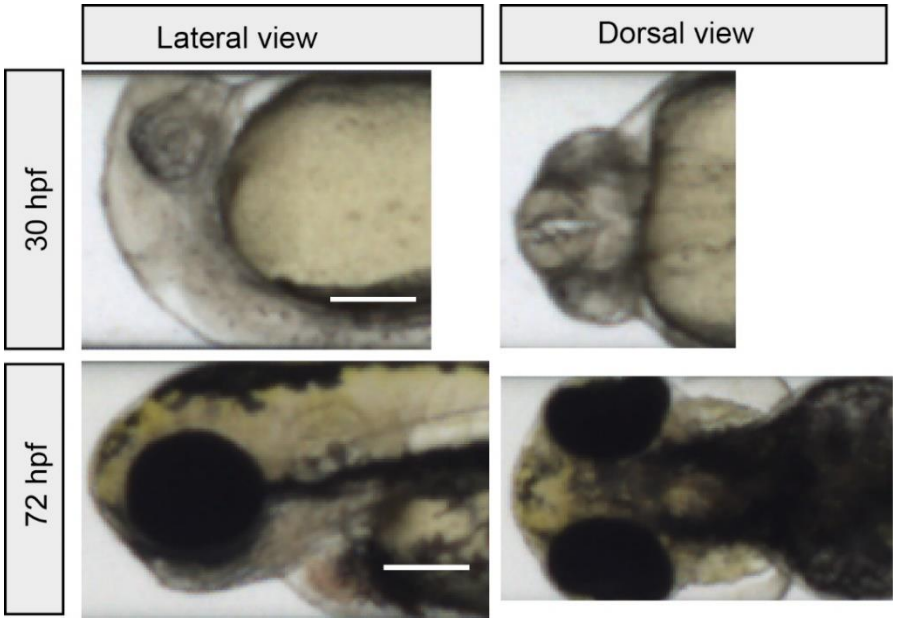

Figure 5.2: Example template images used by the VAST BioImager to orient zebrafish larvae for imaging.
Both lateral and dorsal views are used when determining the orientation. Differences in image size are due to the differing size of embryo. In each case, the program requires a coarsely sized region of interest from the head tip until approximately half of the yolk sac. Scale bar= 200 µm.

To refine the standard protocol to allow imaging of 27-30 hpf embryos, we made several adjustments to the VAST loading and detection settings. This was done by trial-and-error with wild-type embryos, and thus the exact timeline of changes has not been recorded. These changes are tabulated below, Table 5.1. Firstly, to reduce the damage caused by the hydraulic system which feeds embryos from the plate to the imaging chamber, we reduced the loading speed and thus the pump pressure (Table 5.1, Pump settings). Next, due to the larger yolk sac, the embryos loaded together from a single well could not overtake each other in the loading tube. This meant that the embryos tended to clump together and two could be loaded into the imaging capillary together. We reduced both the flushing and unloading volumes to compensate for this, so that if two were arranged closely in the loading tube the second would re-trigger the detection gate as the first was flushed post-imaging. If these changes had not been successful, we would have had to load only a single embryo per well instead of the standard 3 fish per well. This would have greatly increased the time required to screen the embryos. These changes to the pump settings did reduce the rate at which embryos could be imaged, but this was balanced by the increased rate of embryo detection (Table 5.1, Load/unload settings).

The embryo detection was extremely poor when the standard settings were applied. At first, embryos would often not be detected as objects due to the weaker pigmentation to break the light gates. We decreased the light intensity drop for object detection, to force a larger proportion of objects to be detected by the VAST (Table 5.1, Object detection settings). This meant that bubbles and debris such as damaged embryos were more likely to be detected as well, further slowing the screening rate. For the imaging, the lack of intensity differences in the template also meant that the embryo was often not rotated correctly, or it would be discarded as it was not similar enough to the template. At first, we manually corrected the embryo rotation to the lateral position before imaging. However, this completely abolished the automated aspect of the screen, and greatly increased the time it took to image each embryo. To mitigate this, we then decreased the minimum similarity to the template to be accepted for imaging. Again, this sometimes meant that embryos were imaged at an offset angle from lateral alignment, or that bubbles were accepted as embryos. However, this did allow us to automate the imaging, without need for manual correction. The specific changes to the VAST experiment settings that were made are tabulated

below, (Table 5.1).

	Standard settings (72 hpf)	Adjusted settings (30 hpf)
Pump settings		
Loading Speed	110 arbitrary units	90 arbitrary units
Load / unload settings		
Maximum volume between flushes	400 µl	300 µl
Unloading volume 2	180 µl	160 µl
Object detection settings		
Minimum intensity drop	20%	10%
Minimum similarity to template	0.35 °	0.15 °

Table 5.1: Differences in VAST experiment settings to allow automated loading and imaging of 30 hpf embryos compared to a standard protocol for 72 hpf larvae.

Despite these adjustments, there was still an attrition rate of embryos lost during this process. The loss of embryos at each stage is tabled below (Table 5.2), based on the first full screen performed using the SGC library discussed later in Section 5.2.2. Survival after drug treatment is ~95%, but during loading and imaging by VAST some embryos are still not be detected, and thus lost. Furthermore, although the reduction in template similarity increased the number of images generated, some images were crooked and not laterally aligned properly. Depending on the severity of misalignment, the axonal scoring cannot be performed. However, the throughput of the screening was still faster than manual mounting and imaging. As is clear in Table 5.2, the attrition rate is mostly caused by the VAST not detecting the embryos correctly. Despite refining settings to overcome this, the limits of our troubleshooting will be further discussed in the Discussion & Conclusions section of this chapter (5.3.1). However, this marks the first time that embryos of 26-30 hpf have been successfully imaged by the VAST system. In future screens, this attrition rate has been reduced due to minor adjustments to the loading algorithm, both from our own adjustments and updates to the software from Union Biometrica.

Stage of screening	Number of embryos that were retained after this step	Proportion of success (%)
Start of treatment	264 (starting value)	N/A (100%)
Treatment survival	251	95.1%
Loading and imaging by the VAST BioImager	166	62.9%
Scoring-quality images (i.e. without misalignment)	143	54.2%

Table 5.2: Tabulated results of screening attrition rate. At each stage, there is loss of embryos from the treatment, the loading of the VAST BioImager, and any issues with the imaging quality.

5.2.1.2 – Design of a scoring system utilising the *chodl* -/- phenotype

The main benefit of a drug screen using the *chodl* -/- embryo is that the phenotype is highly stereotyped and predictable. The aim of using the mutant over *smn* morpholino is speed in both generating embryos to treat with the compounds (injection of MO compared to breeding homozygote mutants) and speed in scoring potential hits. As discussed in Chapter Three, the *chodl* -/- mutants are homozygous viable and breed normally as adults. This allowed maintenance of two homozygous tanks that were incrossed to generate *chodl* -/- clutches for drug treatment, which were alternated to allow twice-weekly breeding and thus two screening days a week. These adults contained the HB9:GFP transgenic background, and the tanks were selected and confirmed to give 100% GFP+ offspring. As will be described later, the compounds were applied before MN generation, so the presence of GFP could not be used to pre-sort each clutch.

Similarly to previous analyses, we scored 8 axons per embryo from somite 7 caudally, the part of the trunk that contains the yolk extension. As the VAST BioImager and its associated macros processes maximal intensity projections (MIP) that are easily loaded and analysed, we analysed only the visible axons on one side of the spinal cord rather than both. An example of an image generated by the VAST BioImager is shown below (Figure 5.3) with the axons to be scored marked by a red box.

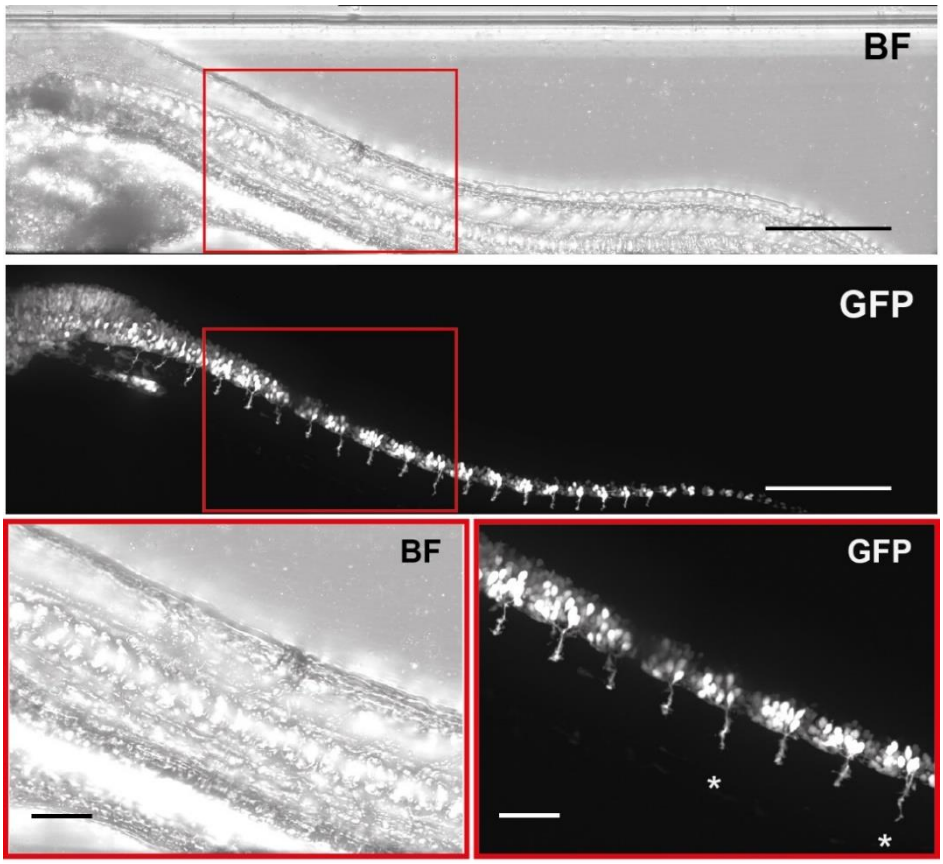

Figure 5.3: An example image generated by the VAST Bioimager.
A 30 hpf HB9:GFP *chodl* -/- embryo is shown, with both the brightfield (BF) and GFP channels. The axons scored during the drug screen are indicated in the red box, with a higher magnification shown below.
8 axons are shown, located at somites 7-15 which grow along the yolk extension. Asterisked axons are considered to have passed the HM, at the expected 25% rate, while the rest are stalled at the HM. Scale bars = 400 µm (upper images) and 50 µm (red boxes).

As was noted in Chapter Three, between 27 hpf and 30 hpf, the CaP axon is stalled at the horizontal myoseptum, and approximately 25% of the axons have crossed this

threshold, although the axons are still shorter than their wild-type counterparts. This is shown above in Figure 5.3, as the asterisked axons demonstrate the expected 25% of axons that pass the horizontal myoseptum. At the same age in wild-type embryos, 100% of the axons have crossed the HM (Chapter Three). Therefore, we chose to use the proportion of axons crossing the HM as our readout for compounds which improved axon growth. To threshold what could be considered a hit, we chose 60% of axons crossing the HM as a successful treatment. This correlated to an improvement by a factor of 2.5 and correlated to an average number of axons crossing the HM as an average 5 out of 8 per embryo scored. Because the number of axons escaping the HM increases to around 3 or 4 out of 8 by 31hpf, and the secondary axons begin to extend at 33 hpf, we limited our imaging window from 27 hpf to 31 hpf. This reduced the number of samples that could be screened each day, as our imaging was limited to this 4-hour period. However, we found that the speed of loading and imaging the embryos allowed us to screen a maximum of 48 wells containing 3 embryos, a theoretical maximum of 144 embryos per screening afternoon.

The chosen starting concentration was 10 µM. Since the stock solution of 10mM was dissolved in 100% DMSO, the final concentration of compounds contained 0.1% DMSO. The library we used showed biological activity in cell culture at 1 µM (Brown and Müller, 2015). Previous zebrafish screens have used concentrations between 2 µM and 1 mM (Baraban, Dinday and Hortopan, 2013; Early *et al.*, 2018), so we chose a starting concentration of 10 µM. To prevent developmental delays or potentially adverse effects from the compounds, the embryos were added to the drug medium after gastrulation, between 6-8 hpf. The embryos were incubated in the drug medium until 24 hpf. The treatments were performed in 24-well plates containing 1ml of medium and 6 embryos per well. This gave the embryos enough space to develop correctly without wasting drug solution. Although most small molecules can penetrate the chorion, we dechorionated all embryos before treatment to ensure direct contact between the embryo and drug-containing medium. The chorion would also risk slowing down the imaging, as any debris present in the loading wells would potentially be detected by the VAST's light gates before being classified as debris and flushed from the system.

Each screening day, the embryos were moved from the 24 well plate to 96 well plates containing fresh E3 medium at ~24hpf. To maintain developmental consistency across the imaging time course, the wells were mixed to ensure distribution of DMSO-

treated controls at both the beginning, middle, and end of the plate. This allowed internal comparison of the controls to ensure the 25% axon escape was maintained throughout the imaging. We treated 6 embryos per condition, but a maximum of 3 embryos can be loaded in each well of the 96 well plate, so each treatment well was repeated too and distributed across the plate in a similar way to the controls.

After imaging, automated imaging processing was performed (Early *et al.*, 2018). These macros generated Maximal Intensity Projections from the Z-stacks and re-tiled the images into a single file. The VAST also produces an Excel file containing the image numbers and the well location, allowing unblinding after scoring. After processing the images in this way, I scored the axons as described above. An experimental timeline of the screening protocol is shown below (Figure 5.4). The first screen completed using this protocol used a 38-compound open access library, the Epigenetic Probes Collection, from SGC. Results from this screen are shown in the next section.

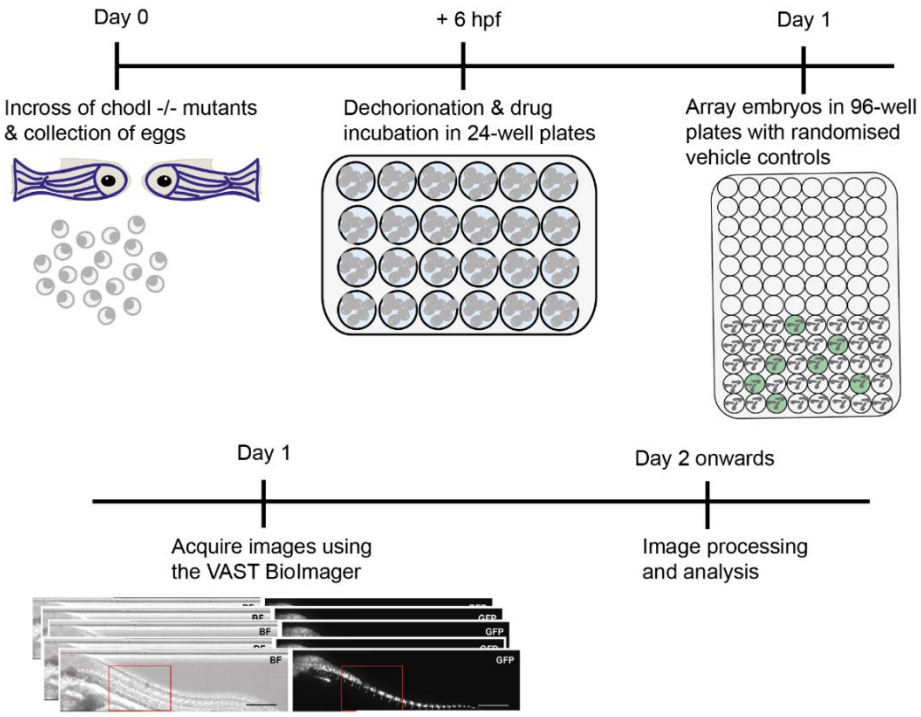

Figure 5.4: Timeline of the experimental protocol used in the drug screen. After breeding homozygous *chodl* -/- mutants, the eggs were dechorionated at 6 hpf and incubated in compound solution. On the imaging day, embryos are moved to a 96-well plate and the location of vehicle-treated controls randomised. After image acquisition by the VAST BioImager, processing and analysis can be performed.

5.2.2 – Results of a screen using the SGC Epigenetic Probes Collection

As previously mentioned, the library chosen for an initial screen using the *chodl* -/- embryos was the 38-compound SGC Epigenetic Probes Collection (Brown and Müller, 2015). The initial screen, using 6 embryos per condition, were imaged and scored. The data is presented below (Figure 5.5). Although 6 embryos were treated with each compound, there were two DMSO wells, and the library itself contained two wells of KDOAM25 and IOX2, to acts as internal controls. Thus there were 7 embryos for each of those treatments. Of the compounds that passed the 60% threshold, only IOX1 reached significance in comparison to the DMSO-treated controls. The IOX1 group increased by 247% compared to control values and was statistically significant (DMSO-treated average HM+ axons= 22.5% ±7.29, n=5. IOX1-treated average HM+ axons= 78.13% ±3.13, n= 4. One-way ANOVA **p= 0.0085 with Bonferroni's multiple comparison test, DMSO vs IOX1 **p= 0.0081).

No other compounds reached statistical significance with the number of axons crossing the HM compared to DMSO treatment. This is partially due to attrition of the embryos during the experiment. As presented previously (Table 5.2), there are losses of embryos during the treatment and imaging due to non-recognition of the embryos by the VAST. Compounds which caused the average axon score to cross the 60% threshold were re-screened to determine if the results were replicable. This re-screening was performed even if statistical significance compared to vehicle-treated controls was not reached.

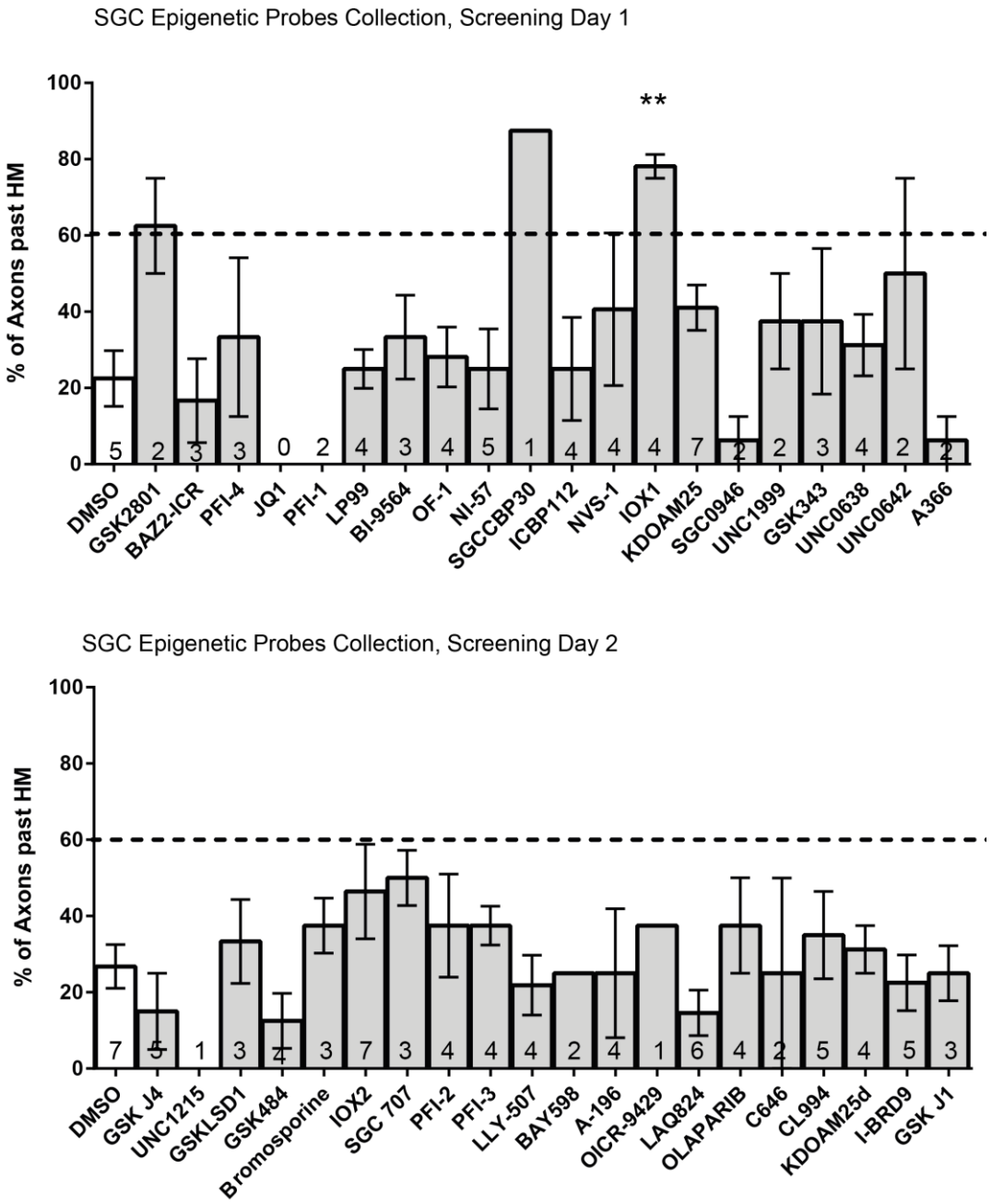

Figure 5.5: Screening of the SGC Epigenetic Probes in the *chodl* -/- embryos. Numbers on each bar refer to the number of embryos analysed for each treatment. The graphs show 2 screening days, with the % of axons that cross the HM. DMSO-treated controls (white bar) show the expected 25% of axons crossing the HM. The 60% threshold is marked with a black dashed line. From the initial screen, GSK2801, SGC CBP30, and IOX1 passed this screening threshold. IOX1 is significantly increased compared to DMSO controls (One-way ANOVA **p= 0.0085 with Bonferroni's multiple comparison test. DMSO vs IOX1 **p= 0.0081).

Several compounds reduced axon outgrowth compared to controls. One compound, JQ1 (a bromodomain inhibitor, Filippakopoulos *et al.*, 2010) caused widespread developmental delays, and an example of the embryos are shown (Figure 5.6). The embryos, although chronologically 30 hpf, grossly resemble 14 hpf embryos, demonstrating a large developmental delay. Furthermore, there is evidence of necrotic tissue in the head and tail (arrowheads, Figure 5.6). We chose not to rescreen JQ1 at a lower concentration to determine if it still resulted in toxicity, as a colleague in an adjacent group had previously screened this compound at 1 µM and still observed developmental delays and toxicity (Unpublished data by Dr Katy Cole).

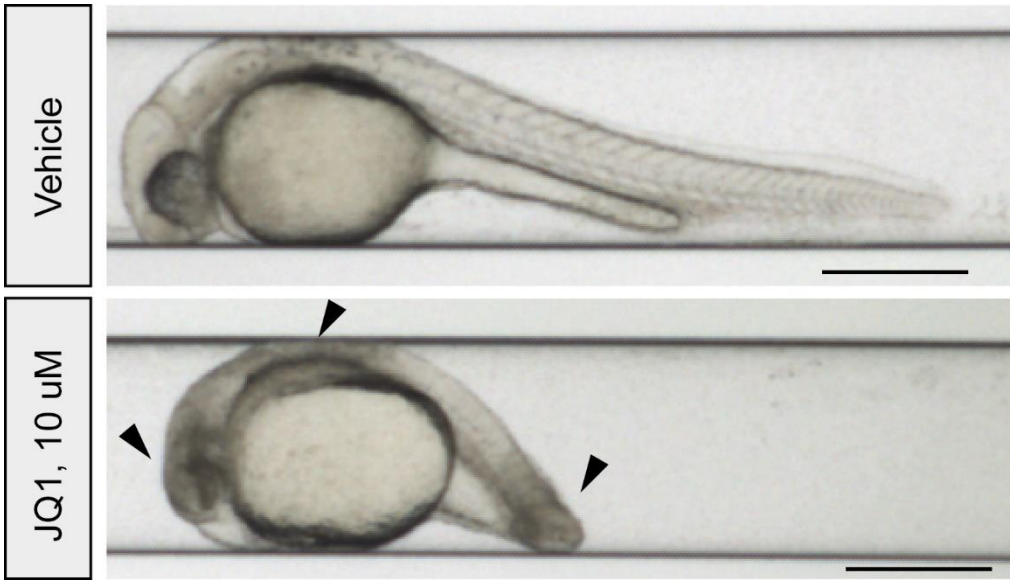

Figure 5.6: Treatment with JQ1 10 µM causes widespread developmental delays and toxicity.
Lateral views of 30 hpf embryos are shown in the VAST borosilicate tube, rostral to the left, dorsal pointed up. The vehicle-treated embryo has not been delayed by the addition of DMSO and is at the correct stage of development for a 30 hpf embryo. However, treatment of JQ1 causes widespread toxicity and severe developmental delay, visible in the shortened body and small head compared to the control. Arrowheads point to necrotic tissue. Scale bars = 400 µm.

5.2.3 – Re-screen of potential hits from the Epigenetic Probes Collection

From the initial screening, several compounds were re-screened to determine reproducibility of the rescue. We chose those that passed the 60% threshold and IOX2, which is structurally related to IOX1. The first compound which passed the 60% threshold was GSK2801, an inhibitor of BAZ2A and BAZ2B bromodomains (Chen *et al.*, 2016). The second compound was SGC-CBP30, an inhibitor of CBP/p300 bromodomains (Hay *et al.*, 2014). One compound which missed the 60% threshold, UNC0642, had one embryo with 75% of axons passing the HM and one embryo with the expected 25% of axons passing the HM, leading to a very large variance, so we chose to rescreen this compound as well. Because IOX1 had statistically significant rescue and low variance, we screened this compound in a concentration series directly, as is described in section 5.2.4. Maintaining the same concentrations and conditions, the rescreened compounds did not reach the 60% threshold, except for UNC0642 which had a significantly higher proportion of rescued axons. The rescreening data is shown below (Figure 5.7).

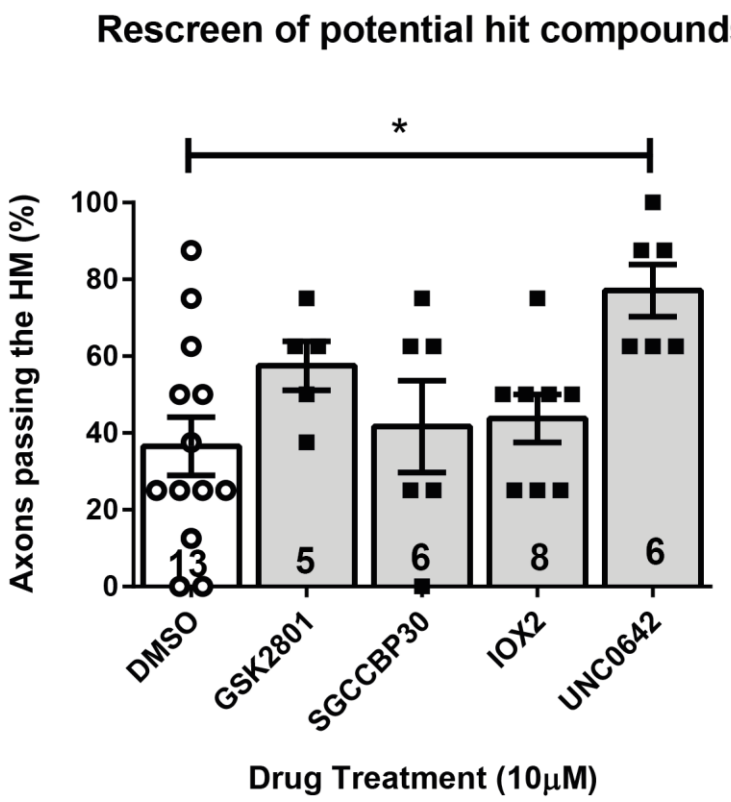

Figure 5.7: Rescreening potential hits from the SGC Epigenetic Probes Collection. This repeated the treatment of compounds from Figure 5.5 which reached or just fell short of the 60% threshold. (Kruskal-Wallis *p= 0.0246 with Dunn's multiple comparison test. DMSO vs SGC-CBP30 n.s., DMSO vs GSK2801 n.s., DMSO vs IOX2 n.s., DMSO vs UNC0642 *p= 0.0180. n.s. p>0.999)

As can be seen from the DMSO-treated embryos, in this experiment, the proportion of vehicle control axons which crossed the HM was higher than expected. The mean is higher than the expected 25% at 36%, and there are several embryos with scores higher than 50%. This was due to an error with the incubator, which had increased from 28°c to approximately 29°c. This increase in temperature was enough to accelerate the development of the embryos, leading to an increased proportion of axons passing the HM. The GSK2801 treatment group was not significantly increased, although the value increased by 57% compared to the DMSO value. GSK2801 treatment failed to reach the 60% threshold with a mean value of 57.5%. After re-screening, the SGC-CBP30 and IOX2 treatment groups were also not significantly different compared to the DMSO-treated controls. (DMSO mean HM+

axons= 36.54% ±7.55, n= 13, GSK2801 mean HM+ axons= 57.5% ±6.37, n= 5, SGC-CBP30 mean HM+ axons= 41.67% ±11.93, n= 6, IOX2 mean HM+ axons= 43.75% ±6.25, n= 8, UNC0642 mean HM+ axons= 77.08% ±6.783, n= 6. Kruskal-Wallis *p= 0.0246 with Dunn's multiple comparison test. DMSO vs SGC-CBP30 n.s., DMSO vs GSK2801 n.s., DMSO vs IOX2 n.s., DMSO vs UNC0642 *p= 0.0180. n.s. p>0.999).

Considering the higher baseline of the control group and the failure of these compounds to cross the 60% threshold after re-screening, I chose not to pursue these compounds further. Treatment with UNC0642 significantly increases the proportion of axons crossing the HM, although with the DMSO-treated group higher than expected, the value is 2.1 times larger than the control group rather than the 2.5x ratio that the 60% threshold was designed for. However, this result led us to further investigate UNC0642 as a hit and is further discussed in section 5.2.5.

5.2.4 – Further analysis of IOX1 as an axon growth enhancing compound

As it reached significance in the first screening and surpassed the 60% threshold, with a mean value of 78.13%, we took IOX1 forward as our first hit in rescuing the *chodl* -/- phenotype. Some example images from this first screening round (from Figure 5.5), comparing IOX1 to DMSO treatment, are shown below (Figure 5.8).

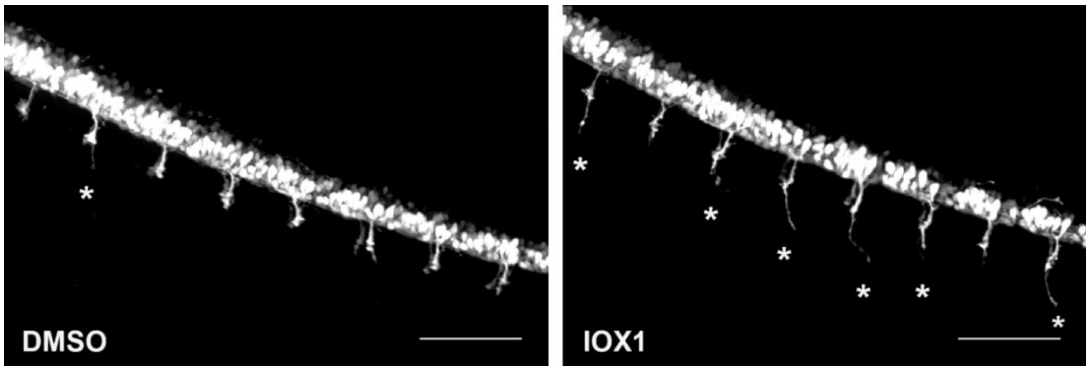

Figure 5.8: Representative example images of DMSO and IOX1 treatment from the screening presented in Section 5.2.3. Lateral views of the trunk with 28 hpf HB9:GFP;*chodl* -/- embryos are shown, after treatment with either 0.1% DMSO or 10 µM IOX1. Asterisked axons pass the horizontal myoseptum, compared to unmarked axons which are stalled at the HM. Scale bars = 100 µm

To determine the best concentration of IOX1 treatment to gain the best axon rescue, I performed a concentration series. As well as scoring the number of axons which passed the HM, I measured the lengths of the CaP axon. The scoring of axon position was fast and simple, suitable for assessing a large number of compounds in a library but gives binary data of either crossing or stalled axons. Measuring the axon length gives more information about the extent of rescue. In DMSO-treated conditions, such as in Figure 5.8 above, the axon has crossed the HM, but is still shorter than would be observed in wild-type axons. The results of the IOX1 treatment concentration series is shown below (Figure 5.9).

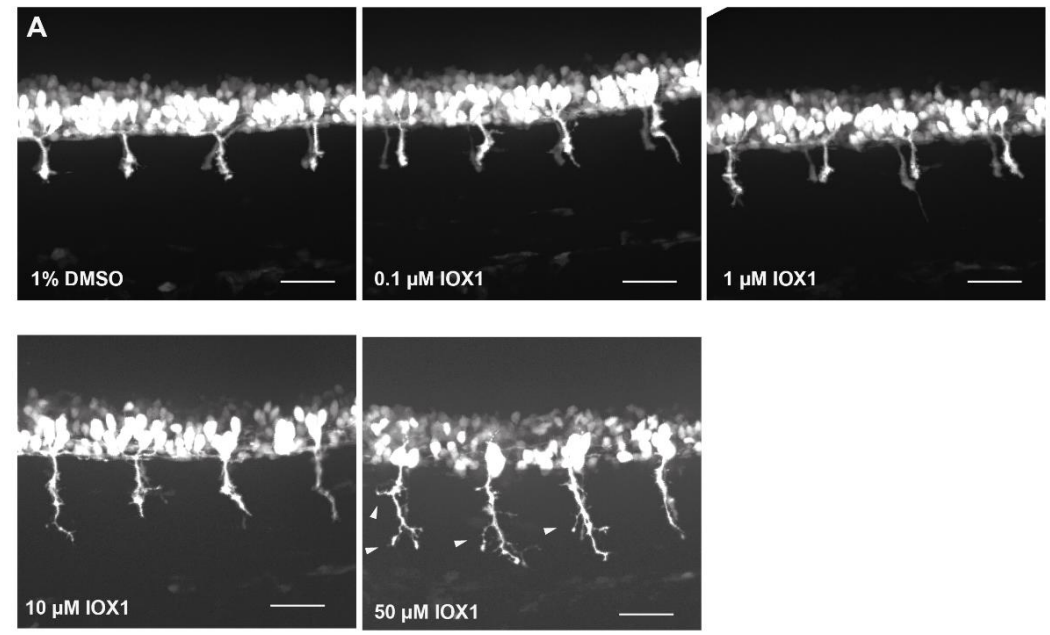
A
1% DMSO
0.1 µM IOX1
1 µM IOX1
10 µM IOX1
50 µM IOX1

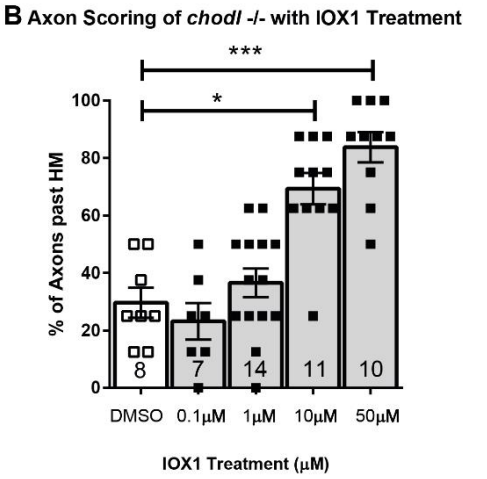
B Axon Scoring of chodl -/- with IOX1 Treatment
***
*
% of Axons past HM
100
80
60
40
20
0
8
7
14
11
10
DMSO
0.1µM
1µM
10µM
50µM
IOX1 Treatment (µM)

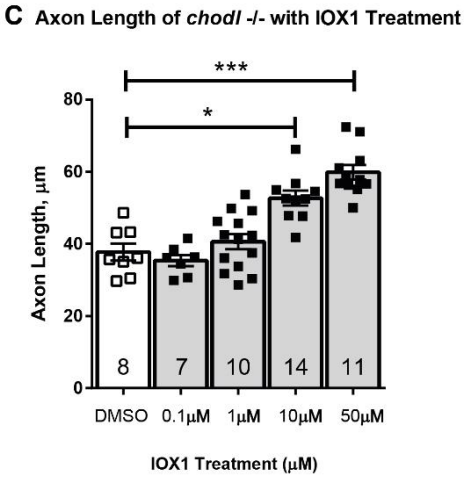
C Axon Length of chodl -/- with IOX1 Treatment
***
*
Axon Length, µm
80
60
40
20
0
8
7
10
14
11
DMSO
0.1µM
1µM
10µM
50µM
IOX1 Treatment (µM)

Figure 5.9: Treatment by different IOX1 concentrations leads to a dose-dependent rescue of the *chodl* -/- axonal phenotype.
A: Representative images of the lateral view of *chodl* -/- embryos at ~28 hpf are shown. Aberrant axonal branching is shown with white arrowheads. **B**: The proportion of axons passing the HM with treatment by DMSO or IOX1. 10 µM and 50 µM IOX1 doses lead to a significant increase in the proportion of axons crossing the HM. (Kruskal-Wallis ****, p<0.0001 with Dunn's multiple comparison test. DMSO vs 0.1 µM IOX1 n.s., p>0.999. DMSO vs 1 µM IOX1 n.s., p p>0.999, DMSO vs 10µM IOX1 **, p=0.0074. DMSO vs 50µM IOX1 ***, p=0.0003) Post-hoc power= 1.00 **C**: Axon length for each treatment group. The 10 µM and 50 µM IOX1 treatment significantly increases the axon length compared to DMSO-treated controls (Kruskal-Wallis **** p<0.0001, with Dunn's multiple comparison test. DMSO vs 0.1 µm n.s. p>0.999, DMSO vs 1 µm n.s. p>0.999, DMSO vs 10 µm IOX1 * p= 0.0444, DMSO vs 50 µm IOX1 *** p= 0.0002). Post-hoc power= 0.999. Scale bars = 50 µm.

The axon scoring in Figure 5.9 B shows a concentration-dependent increase in the proportion of axons crossing the HM with treatment by IOX1. Treatment by 0.1 µM or 1 µM did not significantly increase the proportion of axons crossing the HM compared to DMSO-treated *chodl* -/- controls. 10 µM IOX1 treatment increased the proportion of axons crossing the HM by 133% compared to controls, and 50 µM IOX1 treatment increased the percentage of axons crossing the HM by 182% compared to controls. (DMSO mean HM+ axons = 29.69% ±5.25, n=8. 0.1µM IOX1 mean HM+ axons = 23.21% ±6.36, n=7. 1µM IOX1 mean HM+ axons = 36.61% ±4.98, n= 14. 10µM IOX1 mean HM+ axons = 69.32% ±5.43, n= 11. 50µM IOX1 mean HM+ axons = 83.75% ±5.29, n= 10. Kruskal-Wallis ****, p<0.0001 with Dunn's multiple comparison test. DMSO vs 0.1 µM IOX1 n.s., p>0.999. DMSO vs 1 µM IOX1 n.s., p p>0.999. DMSO vs 10µM IOX1 **, p=0.0074. DMSO vs 50µM IOX1 ***, p=0.0003)

The increasing drug concentration also correlates to an increasing axon length, with a statistically significant difference in axon length at both 10 µM and 50 µM of IOX1 treatment. The 10 µM IOX1 treatment increases the mean axon length by 35% compared to DMSO-treated embryos. For the 50 µm IOX1 group, the CaP axon length was increased by 55% over the control values. For all other treatments, the axon length is not significantly different from the DMSO-treated group. (1% DMSO mean= 37.74 µm ±2.35, n= 8. 0.1 µM IOX1 mean= 35.37 µm ±1.56, n= 7. 1 µM IOX1 mean= 40.63 µm ±2.10, n= 14. 10 µM IOX1 mean= 52.68 µm ±2.05, n= 11. 50 µM IOX1

mean= 59.63 µm ±2.03, n= 10. Kruskal-Wallis **** p<0.0001, with Dunn's multiple comparison test. DMSO vs 0.1 µm n.s. p>0.999, DMSO vs 1 µm n.s. p>0.999, DMSO vs 10 µm IOX1 * p= 0.0444, DMSO vs 50 µm IOX1 *** p= 0.0002).

Although the length improves at the higher treatment doses, qualitative assessment of the axons treated with 50 µM IOX1 shows excessive branching compared to the 10 µM IOX1 group or wild-type axons (asterisked axons). This suggests that although the length continues to improve with increased IOX1 dose, this does not necessarily mean that the axons are comparative with wild-type axons. Treatment until 100 µM was performed, however all embryos died after treatment at 100 µM and so could not be imaged. The toxicity came from the IOX1 itself and not the DMSO solvent, as the DMSO-treated group survived exposure to the same amount of DMSO (1%).

5.2.5 – Further analysis of the hit compound UNC0642

After re-screening and seeing repeatable rescue of the *chodl* -/- phenotype by UNC0642 treatment (example images shown below, Figure 5.10), we also performed a concentration series using this compound.

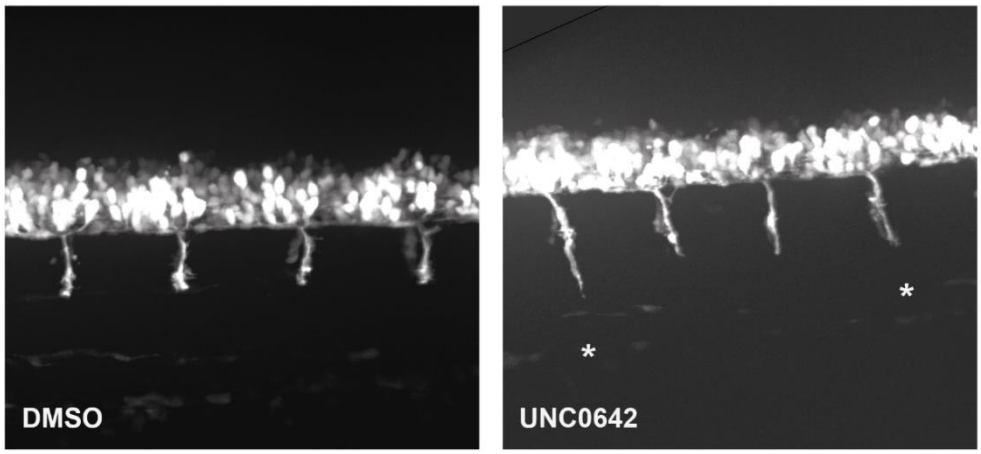

Figure 5.10: Representative images of lateral views of trunks of DMSO and UNC0642 treatment in *chodl* -/- embryos at the level of somite 7-11, from the re-screening round in Section 5.2.2. Asterisks indicate axons that pass the horizontal myoseptum.

We performed a concentration series, and this time included a 5 µM UNC0642 treatment group (Figure 5.11). Our rationale was that upon re-screening the compounds using the compound library, the compound had been freeze-thawed several times, which might have reduced its effective concentration. The concentration series was performed using a fresh batch of UNC0642, so we also included the 5 µM concentration in case it represented the optimal concentration of compound.

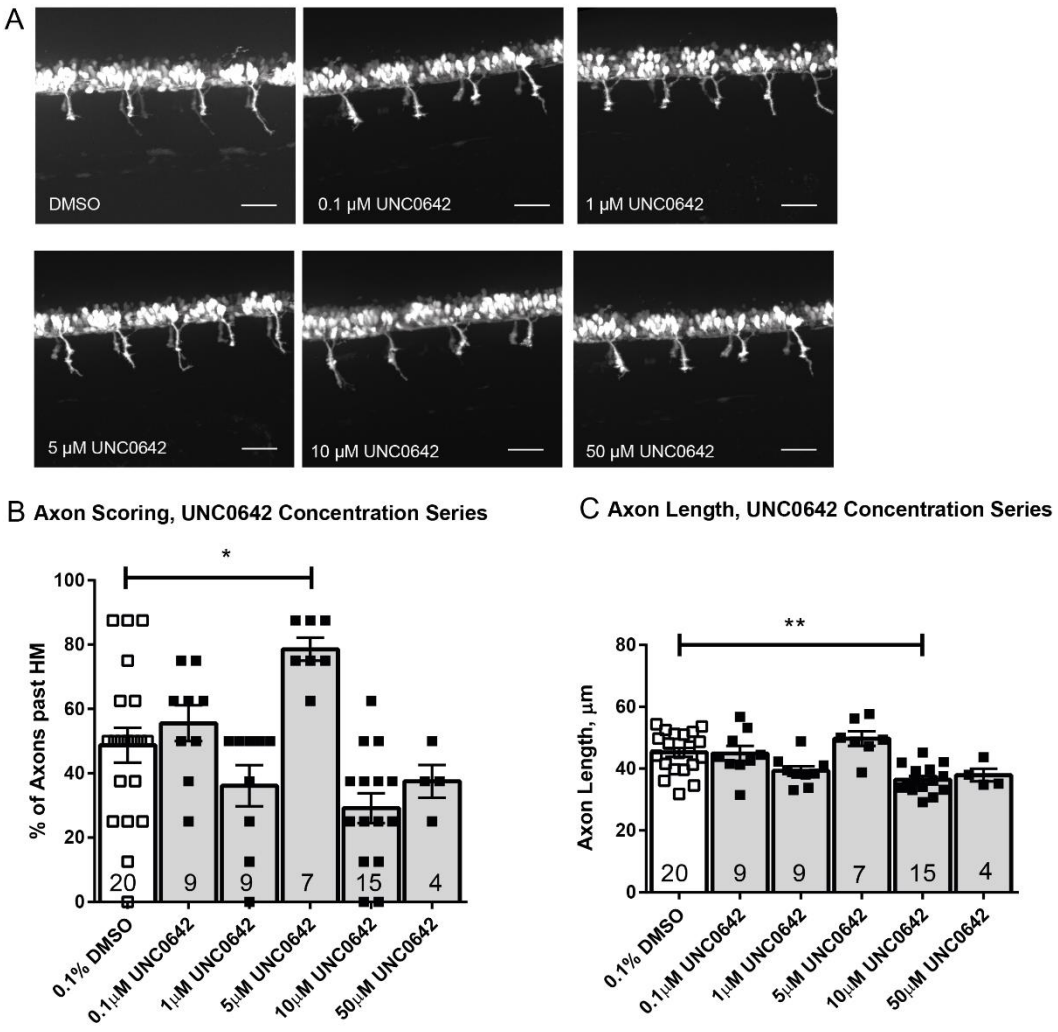

Figure 5.11: The concentration series of UNC0642 in *chodl* -/- embryos shows an increase in axons passing the HM at 5 µM UNC0642 compared to DMSO-treated *chodl* -/-, but the average axon length is unchanged. **A**: Representative images of *chodl* -/- embryos at ~28 hpf treated with either DMSO or different concentrations of UNC0642. **B**: Scoring the proportion of axons crossing the HM shows that there is a significant increase with 5 µM UNC0642 treatment compared to DMSO-treated controls. (Kruskal-Wallis **** p<0.0001, with Dunn's multiple comparison test. DMSO vs 5 µM UNC0642 *, p=0.0297.) Post-hoc power= 0.994. **C**: The average axon length is unchanged between DMSO and UNC0642 treatment, except for 10 µM UNC0642 which is significantly shorter than the DMSO group. (Kruskal-Wallis **** p<0.0001, with Dunn's multiple comparison test. DMSO vs 10µM UNC0642 ** p=0.0011.) Post-hoc power= 0.973. Scale bars= 50µm

The data in Figure 5.11 suggests that the optimal treatment concentration is 5 µM, in terms of scoring the axon position, as it is the only group significantly different to the DMSO control group. The percentage of axons crossing the HM increases by 61%. (DMSO mean= 48.75% ±5.34, n=20. 0.1 µM UNC0642 mean= 55.56% ±5.56, n= 9. 1 µM UNC0642 mean= 36.11% ±6.40, n=9. 5 µM UNC0642 mean= 78.57% ±3.57, n=7. 10 µM UNC0642 mean= 29.17% ±4.67, n=15. 50 µM UNC0642 mean= 37.5% ±5.10, n= 4. Kruskal-Wallis **** p<0.0001, with Dunn's multiple comparison test. DMSO vs 5 µM UNC0642 *, p=0.0297).

However, from analysis of the axon length measurements, there is no significant increase in the axon length from any treatment. The 10 µM treatment is significantly shorter than the DMSO controls, with a reduction in length by 19.6%. (DMSO mean= 45.31µm ±1.48, n=20. 0.1 µM UNC0642 mean= 44.93µm ±2.46, n= 9. 1 µM UNC0642 mean= 39.27 µm ±1.56, n=9. 5 µM UNC0642 mean= 49.73 µm ±2.53, n=7. 10 µM UNC0642 mean= 36.43 µm ±1.17, n=15. 50 µM UNC0642 mean= 37.92 µm ±2.05, n= 4. Kruskal-Wallis **** p<0.0001, with Dunn's multiple comparison test. DMSO vs 10µM UNC0642 ** p=0.0011).

The interpretation of this data is that although the ratio of axons passing the HM may increase, the axon length is not statistically increased. The interpretation of this data is that the axon only grows a short distance beyond the HM, so is counted as HM+ for scoring but the axon is not significantly longer. This contrasts with the IOX1 treatment, where there is correlation between the axon crossing score and the axon

length measurements. This suggests a potential pitfall in our screening method to find growth-enhancing compounds, and this will be further discussed in the Discussion & Conclusions section of this chapter.

The variability of results seen with UNC0642 might have several explanations. Firstly, the lack of statistical improvement with UNC0642 in Figure 5.11 may be due to an incubator issue, where the temperature was increased from 28° to 29. This may have accelerated the development of the embryos by a few hours, enough to affect the axonal growth. This is likely as the DMSO vehicle control has a mean score of 48.75% of axons passing the HM, compared to the 25% normally observed in other parts of this thesis and the original screening in Figure 5.5. As well as heightening the control baseline for comparison to the UNC0642 treatment groups, there is no way to know if this developmental acceleration may also have affected the mechanism of the drug itself, reducing its efficiency.

Re-examining the data from the re-screen of compounds (Figure 5.7), its statistical post-hoc power was only 0.58, below the recommended 0.8. This suggests that this re-screen was under-powered, and so the statistically significant finding of the UNC0642 rescuing the phenotype may not be true. This original statistical significance from the re-screen may be an artefact from an underpowered experiment that needed more samples. This might also be why repeated treatments in the concentration series (Figure 5.11) were not statistically significant. The concentration series is sufficiently powered for both the axon scoring and the axon lengths, at 0.994 and 0.973 respectively, and so statistically is more trustworthy as a finding.

5.2.6 – Delaying treatment by both IOX1 and UNC0642 until after motoneuron differentiation abolishes axonal rescue in *chodl* -/- embryos

The drug treatment window in the previous section was from 6 hpf until approximately 25 hpf, when the embryos were anaesthetised and transferred into fresh E3 medium

in the 96-well plate. The treatment starting at 6 hpf has previously been used in drug treatments, including compounds to ameliorate effects of Smn knockdown (Wishart *et al.*, 2014). This precedes the differentiation of motor neurons, which begins at approximately 9 hpf, and axonal growth, which begins at approximately 16 hpf (Myers, Eisen and Westerfield, 1986). To determine if the drug hits can rescue the axonal phenotype after motor neuron differentiation, I treated *chodl* -/- embryos at 16 hpf with IOX1 and UNC0642, as well as a DMSO vehicle control (Figure 5.12).

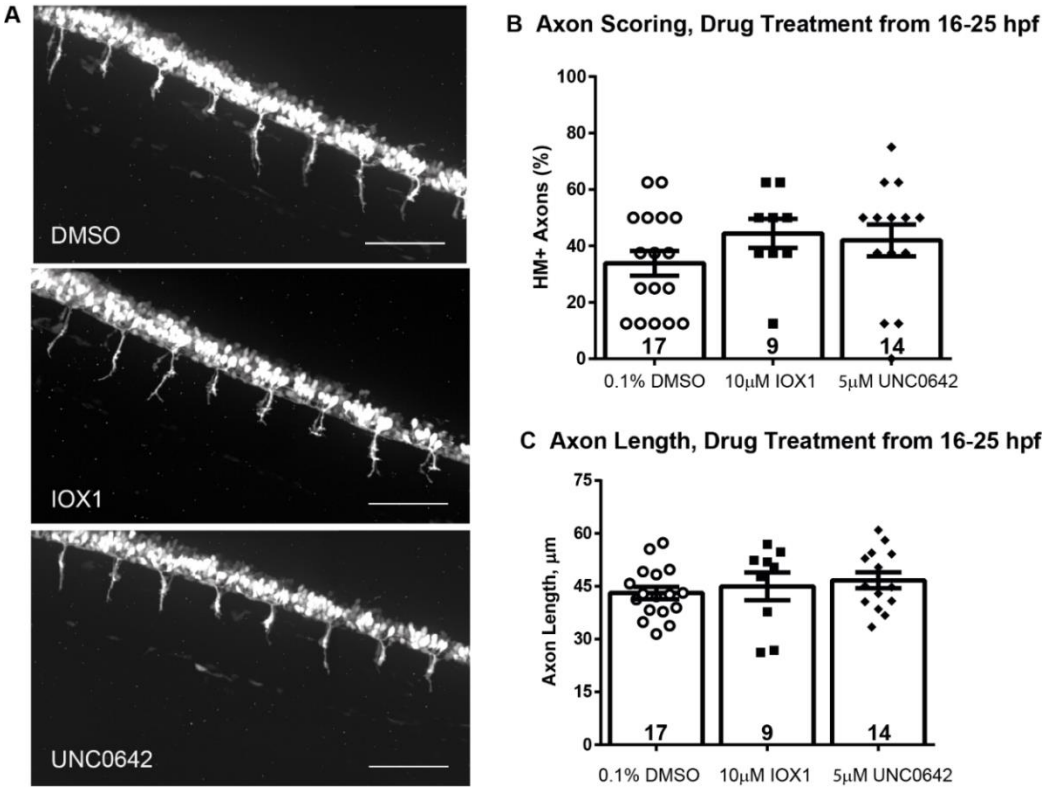

Figure 5.12: Drug treatment from 16 hpf by IOX1 and UNC0642 abolished the rescue of the *chodl* -/- phenotype seen when treatment began at 6 hpf.
A: Example images of DMSO, IOX1, and UNC0642 treated *chodl* -/- embryos at ~29hpf are shown. **B**: There is no significant difference in scores between any treatment groups for the proportion of axons passing the HM. (0.1% DMSO mean= 33.84% ±4.39, n= 17. 10 µM IOX1 mean= 44.44% ±5.15, n= 9. 5 µM UNC0642 mean= 41.96% ±5.65, n= 14. One-way ANOVA n.s. p=0.306, Bonferroni's multiple comparison test DMSO vs IOX1 n.s, p= 0.523. DMSO vs UNC0642 n.s. p= 0.707) **C**: There is no significant difference in axon length between any treatment groups. (0.1% DMSO mean= 43.09 µm ±1.75, n= 17. 10 µM IOX1 mean= 44.96 µm ±3.93, n= 9. 5 µM UNC0642 mean= 46.66 µm ±2.27, n= 14. One-way ANOVA n.s. p= 0.536, Bonferroni's multiple comparison test DMSO vs IOX1 n.s., p= 1. DMSO vs UNC0642 n.s., p= 0.805)

By delaying the drug treatment to a timepoint after motor neuron differentiation to the beginning of axon growth, the phenotype rescue is lost for both IOX1 and UNC0642 (Figure 5.13). The IOX1 group mean increases by 29% from the DMSO value to 44.44%, and the UNC0642 group mean increases by 23% to 41.96%. In comparison, the initial screening in Section 5.2.2 caused the proportion of IOX1-treated axons crossing the HM to increase by 247%. This suggests that the mechanism of both compounds to rescue the *chodl* -/- phenotype occurs before or during motor neuron differentiation, and not during the axon growth stage of 16 – 24 hpf. In other words, the effect of the compounds in rescuing the axonal growth is not targeting the active growth or extension stages but affects gene expression in the motor neuron previous to that, which offers insight into potential therapeutic timing.

In human SMA patients, the motor axon outgrowth is generally normal, as the axons reach the NMJ. However, as discussed in Chapter Four, there are some deficits in the NMJ occupancy even in fetal stages of SMA patients (Martinez-Hernandez *et al.,* 2013.). There is also evidence of neurofilament accumulation and blebbing of the motor axon (Kariya *et al.*, 2008). This suggests that although the growth is normal, the axons are unable to form a stable connection with the post-synaptic part of the NMJ, and this is the starting point for the axonal degeneration observed in SMA. Because the onset of potentially pathological changes are so early, this necessitates an early intervention window, potentially with pre-natal testing for SMA to identify affected foetuses *in utero*. The zebrafish data suggests that a very early therapeutic

intervention with IOX1 would be required for any beneficial effect, which may not be easily performed in humans. However, if the compounds can enhance growth of a zebrafish axon which is normally unable to extend, it may be able to stabilise a human motor axon which grows but is unstable and prone to degeneration. This is highly dependent on the mechanism by which these compounds target, which would need further investigation. The potential timeline for therapeutic treatment with compound hits from this drug screen are discussed in more detail in Section 5.3.1.2.

5.3 - Discussion & Conclusions

5.3.1 – Successes and failures of the VAST BioImager platform utilising *chodl* -/- embryos

5.3.1.1 - The VAST BioImager increases throughput rate, but there is also a high attrition of embryos during the screen

Using the VAST BioImager to automatically load and imaged compound-treated embryos increases the rate of throughput, although it does have a high learning curve both in operating the platform and troubleshooting protocols that are outside of its expected use. The largest change made for this project was the developmental stage of the zebrafish, as Union Biometrica recommends its system for use in larvae from 48 hpf onwards. As discussed in the Introduction, this is partially due to the pressure acting on the larva as it is loaded through the machine, which can tear the larger yolk sac in embryos. The detection and repositioning of the larva for imaging also depends on pigmentation to match a template image to the live image. Melanocytes proliferate during early larval stages, and pigmentation begins from around 24 hpf (Kimmel *et al.*, 1995) but the embryo is still mostly transparent before 30 hpf (compare the pigmentation in the template images in Section 5.2.1). This reduces the ability of the detection program (which uses interruption of a light beam) to 'see' younger embryos and correctly match them to a template image. As discussed in Section 5.2.1, several protocol changes had to be made to the VAST experiment settings to allow processing

of embryos, which also reduced the speed per embryo processed by the VAST. Overall, a theoretical highest rate of 144 embryos per screening afternoon (48 wells with 3 embryos per well) by the VAST is higher than manual mounting and imaging, although the attrition rate meant that this theoretical upper limit was never reached. The attrition rate described (Table 5.2) leads to a final proportion of usable images at 54% of the starting population. To mount and image 144 embryos manually would take 7 hours 12 minutes, assuming 1 minute to mount each embryo and 2 minutes to image each embryo with a confocal. 54% of this time would be 3 hours 53 minutes, which would approach the time taken by the VAST to process the embryos. Although a relatively low percentage of success, this initial attrition has been consequently improved in other screens performed by colleagues (data not shown) to around 75% or more. Software updates from Union Biometrica and other minor adjustments have been applied by others using the platform, which has improved the proportion of embryos that pass through the platform without damage.

5.3.1.2 - The timescale of treatment and imaging may have caveats for its translation into human patients

The timescale of treatment and then imaging was designed from a number of factors. Previous drug treatments in zebrafish screens were applied from 6 hpf onwards (Wishart *et al.*, 2014), and the 26-30 hpf imaging window was chosen for its phenotypic relevance to the *chodl* -/- mutant. The 6 hpf stage is after gastrulation, but before the differentiation of motor neurons. When IOX1 and UNC0642, our putative hits, were applied at a later stage (16 hpf, just before axons exit the spinal cord), but the rescue was abolished (Section 5.2.6). This suggests that both compounds rescue the *chodl* -/- phenotype by a mechanism involving gene expression during motor neuron differentiation. The mechanism of action cannot be during axon growth stages only, as the rescue is completely lost. This may indicate that the axonal outgrowth is determined by factors that also influence the differentiation on the motor neuron. For translating this finding into humans, zebrafish develop *ex utero*, and thus are easily accessible to drug solution, while humans are not. Pre-natal testing for SMA could be applied to high-risk pregnancies to identify SMA patients before birth. Then, a small molecule compound which pass the placenta would be an important therapeutic, compared with ASOs like nusinersen that must be delivered post-natally via intrathecal injection.

5.3.1.3 - The hit rate after screening the Epigenetic Probes Collection was 2.6%

After screening the 38 compounds in the Epigenetic Probes Collection library, we found two putative hits (IOX1 and UNC0642) using the axon passing scores (Section 5.2.3). However, due to the lack of axon length improvement, the UNC0642 will not be taken forward (Section 5.2.5). This leaves us with a hit rate of 1/38, 2.6%. This is similar to other library screens in the zebrafish. For example, when screening wild-type larvae to find compounds which increase oligodendrocyte number, 4/146 compounds caused a significant increase, a hit rate of 2.7% (Early *et al.*, 2018). In the morpholino-based screen against a SOD1 model of ALS, 13/303 morpholinos showed significant rescue of the axonal phenotype, a hit rate of 4.29% (Van Hoecke *et al.*, 2012).

After validating the screening protocol using the Epigenetic Probes as a pilot library, further libraries have been screened in the *chodl* -/- embryos by colleagues in the group. As of writing, approximately 650 compounds have been screened in these mutants, using the same experimental settings as described above. From these compounds, 6 compounds passed both an initial thresholding and also a rescreening round. This translates to to 6/650, or a 0.92% hit rate, similar to several previously published zebrafish compound screens. A screen for compounds which alleviate seizures found 4 hits out of 320, or 1.25% (Baraban, Dinday and Hortopan, 2013). A screen for inhibitors of fin regeneration found 17/2000 compounds, 0.85% (Mathew *et al.*, 2007)

5.3.1.4 - The use of *chodl* -/- mutants over *smn* knockdown streamlined screening of the drug library

I chose to use the chondrolectin mutants instead of morpholino-derived *smn* knockdown. Breeding a set of homozygous mutants generates several hundred eggs and is less labour intensive than injecting the same number of eggs with morpholino. The VAST BioImager would theoretically process 144 embryos in 4 hours, while I

estimate that manual mounting and imaging of 144 embryos would likely take 7 hours, if mounting and imaging took 3 minutes per embryo. Although the attrition rate in my screen was 54%, this has been improved with changes to the VAST software, to around 75% or higher, which gives an advantage over manual processing.

As discussed in the Introduction, the *chodl* -/- phenotype is more easily scored compared to the *smn* knockdown phenotype. We also only had access to morpholino knockdown of *smn*, and not the genetic zebrafish models of SMA which exist (discussed below). Injection of each egg with a morpholino dose would have greatly increased the workload and time needed to screen the compound library, hence our choice to use the *chodl* -/- mutant. However, the main flaw in this screening is that chondrolectin is linked to SMA but is not the causative gene. Rather than working directly with *smn* knockdown, we are using a mutant in a gene whose expression is dysregulated in SMA models (Bäumer *et al.*, 2009). This means that the screen results are already one stage removed from the SMA disease context. However, the purpose of this screen was not to directly find compounds to treat SMA. Instead, we hoped to triage and thus filter potentially useful axon-stabilising compounds from a larger population of compounds, to refine a small number of drug compounds to screen in SMA models.

Although I did not have access to them during my project, there are several zebrafish genetic models of SMA, mostly generated by the Beattie group, and recapitulate many of the phenotypes seen in the MO knockdown. The first genetic models of SMA in zebrafish selected three mutants from an ENU screen, of which had two premature stop codons, and one had an amino acid change, all of which resulted in loss of function (Boon et al., 2009). These homozygote mutants were able to survive until around 2 weeks of age due to maternal deposition of mRNA into the eggs from the heterozygote *smn* +/- females. There is no widespread axonal phenotype observed in the *smn* mutant embryo, unlike in the morpholino knockdown, as the maternally deposited mRNA is translated and is sufficient for early development. However, at larval stages as the amount of Smn protein decreases, there is an observable change to the pre-synaptic puncta. There is no way to separate these mutants from their maternally deposited mRNA, as the homozygotes do not survive long enough to breed.

An improved genetic model of SMA in zebrafish was later developed to overcome the maternal *smn* mRNA contribution (Hao *et al*., 2011, Hao *et al*., 2013). A human SMN2-

RFP cassette, under a heat-shock promoter, was introduced into one of the previously described *smn* premature stop mutant lines. A slight leakiness of the SMN2-RFP transgene extended the non-heat-shocked larvae lifespan by around 2 days. Periodically heat-shocking these larvae allowed their survival until adulthood, to generate of breeding adults which would not be able to deposit *smn* RNA into their offspring. These offspring then recapitulated the motor axonal phenotypes observed in the morpholino-induced knockdown (Hao et al., 2013).

Using these genetic models directly for the drug screening or to test the IOX1 compound would be highly useful, as they directly model the reduction in Smn protein and do not require individual injection such as the MO knockdown does. The SMA model zebrafish which is z*smn* -/-;hsp:hSMN2-RFP also expresses the human SMN2 gene, so can be used to model treatments which alter the Smn2 splicing, which is an SMN-dependent treatment approach which is a key clinical target (Bowerman *et al*., 2017).

5.3.2 – Discussion of the properties and target of the hit compound IOX1

IOX1, 5-Carboxy-8-hydroxyquinoline, was identified as an inhibitor of the 2-oxoglutarate-dependent (2OG) Jumonji C domain (JmjC) (Hopkinson *et al.*, 2013). The JmjC family act as histone lysine demethylases (KDMs), modifying the histone and chromatin assemblies in the nucleus to activate and silence gene expression. Methylation of histones was originally thought to be irreversible due to the large thermodynamic cost to remove a stable methyl group. The JmjC-domain proteins can demethylate histones by oxygenating the methyl group in a 2-oxoglutarate- and iron-dependent mechanism, reducing the stability of the bond. Although its specificity is highest in inhibiting JmjC-containing KDMs, IOX1 is also known to inhibit other 2OG oxygenases, meaning it has a broad spectrum of activity across multiple targets (Hopkinson *et al.*, 2013). A list of targets that IOX1 is able to inhibit, as well as their function, is found further in this section as Table 5.3. Other compounds whose targets overlap with IOX1 targets are also discussed later in this section.

The 2OG oxygenase family has been also been found to catalyse protein hydroxylation, which is implicated in multiple cancer models (Ploumakis and Coleman, 2015). The hydroxylation of proline and lysine residues by these oxygenases is required for collagen biosynthesis. Asparagine and proline hydroxylation is also required to activate many hypoxia-inducible factors (Markolovic, Wilkins and Schofield, 2015). In all cases, the 2OG-dependent proteins are ferrous proteins, and the IOX1 binds with the iron atom in crystal structures of the IOX1-protein complex. Solved crystal structures of KDM JMJD2A and IOX1 in complex demonstrate that IOX1 is able to dislodge the metal ion when it binds, interfering with the binding of the 2-oxoglutarate co-factor (King *et al.*, 2010).

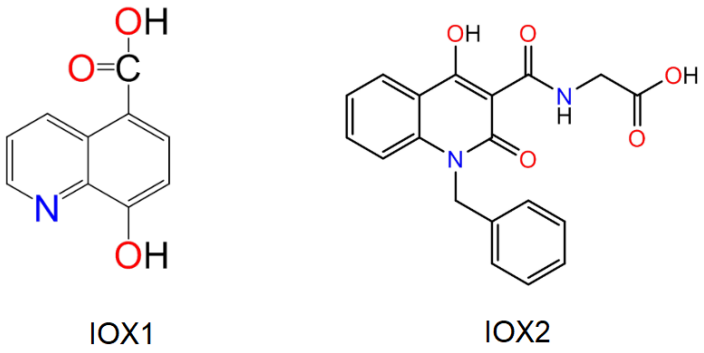

Figure 5.13: The chemical structure of IOX1 and IOX2, two structurally related compounds. Both target 2-oxoglutarate oxygensases. (Taken from https://www.thesgc.org/chemical-probes/IOX1 & https://www.thesgc.org/chemical-probes/IOX2)

Name of Compound	**Specific Target**
IOX1	pan-2-OG oxygenases
IOX2	PHD2
GSK-J1	JMJD3, UTX, JARID1B
GSK-LSD1	LSD1

Table 5.3: Lysine demethylase inhibitors (KDMs) present in the SGC Epigenetic Probes Collection and their specific enzymatic targets. (Source: https://www.thesgc.org/chemical-probes/epigenetics)

IOX1 and IOX2 share structural similarity (Figure 5.13) and have some overlapping targets, but IOX2 was unable to rescue the *chodl* -/- axon phenotype. Although both compounds target 2OG oxygenases, IOX2 binds specifically to PHD2. PHD2 (Prolyl hydroxylase 2) catalyses the degradation of hypoxia-inducible transcription factor α (HIF-α) by ubiquitination/proteosomal degradation and acts as an oxygen sensor as it requires oxygen as a cofactor. Inhibition of PHD2 therefore leads to an increased hypoxic response, and transcription of genes to mitigate low oxygen levels in the cell (Chowdhury *et al.*, 2013). Given the lack of rescue with IOX2 treatment, it seems that inhibiting PHD2, and thus reducing the degradation of HIF-α has no effect in axon growth.

The other KDM inhibitors in the SGC probe library are shown above (Table 5.3). Neither GSK-J1 or GSK-LSD1 showed rescue of the *chodl* -/- axonal phenotype. Compared to the average score of 26.79% ±5.74 (n=7) by the DMSO control group, GSK-J1 showed a very similar score of 25% ±7.22 (n=3), as did the GSK-LSD1 treatment, with a score of 33.33% ±11.02 (n=3). Because of the lack of rescue by these compounds, we can also eliminate their targets as the mechanism by which IOX1 rescues the *chodl* -/- phenotype. As well as LSD1, UTX, JARID1B, this also eliminates the JmjC-domain protein JMJD3. It is known that IOX1 inhibits JMJD3 with an IC50 of 0.14 µM and UTX with an IC50 of 1.1 µM (Hopkinson *et al.*, 2013). After eliminating these potential targets that IOX1 is able to bind, the potential mechanism by which IOX1 increases axon growth in the *chodl* -/- embryo must be one of the targets listed (Table 5.4), adapted from Hopkinson *et al.*, 2013.

2-OG oxygenase	Catalytic Function	IOX1 IC50 (μM)	Overlap with other compounds
PHD2	Prolyl-hydroxylase (HIF1a)	14.3	IOX2 - does not rescue
FIH	Aparaginyl-hydroxylase (HIF1a)	20.5	
JMJD2A	KDM	0.2	
JMJD2C	KDM	0.6	
JMJD2D	KDM	0.2	
JMJD2E	KDM	0.3	
JMJD1A	KDM	0.17	
JMJD3	KDM	0.14	GSK-J1 – does not rescue
UTX	KDM	1.1	GSK-J1 – does not rescue
FBXL11	KDM	15.4	
PHF8	KDM	15	
JARID1C	KDM	25	

Table 5.4: IOX1 is a pan-2-OG oxygenase inhibitor. Tabulated are the targets of IOX1, their catalytic function, and the IC50 of IOX1 inhibition, as well as any other compounds from the SGC library which also inhibit the same target. (Taken from Hopkinson *et al.*, 2013).

As for the mechanism by which IOX1 rescues the *chodl* -/- phenotype, the best way to determine this would be to compare the gene expression profile of IOX1-treated and DMSO-treated *chodl* -/- embryos and identify differentially-expressed genes. Confirmation of the gene expression change responsible for the axon rescue could be confirmed using either morpholino or mRNA injection to knock down or over-express these genes. In the *chodl* -/- embryo, analysis of the axons for phenotypic rescue would be sought, while in wild-type embryos we would expect to phenocopy the mutant.

5.3.3 – Outlook for future experiments

5.3.3.1 - Testing hit compounds in SMA disease models

From these results, there are several further avenues of investigation that could be pursued in future projects. Colleagues in the group are continuing the screen in *chodl* -/- embryos using other commercially-available libraries. Rescue of SMA models, such as *smn* knockdown in zebrafish, are then key to determine if the hit compounds can rescue the disease model. The axonal phenotype of the *smn* knockdown in zebrafish is more variable than the *chodl* -/- embryo, with missing truncated, and branched axons (McWhorter *et al.*, 2003; Sleigh *et al.*, 2014; Wishart *et al.*, 2014), of which there are several ways to quantify the severity of the phenotype. However, even partial rescue of one aspect could be measured and represents a potentially useful treatment. IOX1 treatment was performed in *smn* morphant zebrafish but was not able to rescue the axonal phenotype (unpublished data, Dr Oprişoreanu). This demonstrates that IOX1, although increasing axonal growth in the *chodl* -/- embryo, does not improve the axonal defects caused by *smn* knockdown.

These compounds could also be tested in human Induced Pluripotent Stem Cells (hIPSCs) to increase both the speed of throughput and the relevance to humans. hIPSCs derived from patients and their isogenic controls (i.e. the patient sample mutagenised to correct the SMN2 splicing defect) have been generated for SMA (Corti *et al.*, 2012). SMA patient-derived IPSCs show similar genetic changes as mouse models, such as UBA1 disruption in IPSCs differentiated into motor neurons (Fuller *et al.*, 2016), demonstrating similarity and thus physiological relevance. These IPSCs can be differentiated into other cell types, including neurons or glia, for analysis of expression after treatment with compounds such as IOX1.

5.3.3.2 – Testing the hit compounds for synaptic phenotype rescue as well as axonal rescue in the *chodl* -/- embryos

The hit compounds IOX1 and UNC0642 were selected due to their ability to rescue the axon length in the *chodl* -/- embryos. As has been demonstrated in Chapter Four of this thesis, as well as an axonal growth deficit there are widespread synaptic defects in the mutant at both embryonic and larval stages. I also suggest that the axonal growth deficit may be a consequence of defective synaptogenesis. In wild-type

larvae, motor axon branching is almost always associated with synaptic puncta at the branching point (data presented in Chapter Four). It would therefore be useful to analyse the synapses in *chodl* -/- mutants treated with IOX1 and determine if the axon growth rescue also correlates with a rescue of the synaptic puncta. Changes to the neuromuscular junction has also been extensively reviewed in mouse and zebrafish models of SMA (Boon *et al.*, 2009; Murray, Talbot and Gillingwater, 2010; Boido and Vercelli, 2016; Boyd and Gillingwater, 2016). This means that examination of the synapses in compound-treated mutants may again be useful, as stabilising the NMJ is increasingly becoming a target in SMA therapies.

Chapter Six – Conclusions

6.1 – Summary of novel findings in this thesis

In this thesis, I have demonstrated the cell-autonomous mechanism of chondrolectin in motor neurons, which is required for axon growth. The protein level of Chodl is tightly regulated, with both insufficiency and over-expression causing axonal growth defects. I have also established the functional domains in the protein, determining that both the C-type lectin domain and intracellular domain are required for correct protein function. To further develop this, I have demonstrated that there is a phosphorylation requirement of the intracellular domain to allow the correct function of chondrolectin. This synergises with data in our group which shows that chondrolectin binds collagen19a1 in the ECM. I also utilised the *chodl* -/- phenotype as a tool for screening small molecule libraries to find axon-stabilising compounds. I have shown that chondrolectin is not necessary for adult survival, as *chodl* -/- fish grow to adulthood. However, I have found novel roles for chondrolectin in synapse stabilisation, which leads to a change in behavioural responses in the larval zebrafish. The axonal growth defects in the *chodl* -/- zebrafish phenocopy the morphant (Zhong *et al.*, 2012), but the stable mutant allowed much deeper investigation into the mechanism of Chodl. The novel synaptic role further links chondrolectin dysfunction and SMA, as the NMJ is a focal point in SMA pathology and a therapeutic target (Murray, Talbot and Gillingwater, 2010; Boido and Vercelli, 2016).

6.2 - Chondrolectin as a cell-autonomous growth molecule in motor axons

6.2.1 – Chondrolectin is required for primary motor axon growth and secondary motor axon branching

Our CRISPR/Cas9 mutant, *chodl* -/-, shows CaP axon stalling at 28 hpf, with 75% of the axons stalled at the HM (Chapter Three Section 3.2.3). At larval stages

At 33 hpf the secondary motor axons begin to exit the spinal cord and grow along the same pathway as the primaries (Menelaou and McLean, 2012). In the *chodl* -/- embryos, 42.2% of the CaP axons escape the HM and extend beyond this choice point by 31 hpf (27/64 axons in 16 embryos, Chapter 4, Section 4.2.2). This means that at 31 hpf, 57.8% of the axons in the mutants remain stopped at the HM. We did not further investigate if these stopped primary axons ever extend beyond the HM. Differential labelling of the primary and secondary motor axons could be performed by combining the HB9:GFP transgenic line, which labels both primary and secondary neurons, with zn5 staining, which is limited to secondary motor neurons (Menelaou and Svoboda, 2009). The axons only labelled with GFP and not the GFP/zn-5 co-label would be primary axons.

As previously discussed, the secondary motor axons exit the spinal cord at ~33 hpf. Quantification of the motor axon lengths at 48 hpf showed that the *chodl* -/- axons were significantly shorter than controls (Chapter Three, Section 3.2.3). The ventral nerve bundle catches up to controls by 72 hpf (Chapter Three, Section 3.2.3). The secondary motor axons do not require the primaries to path find correctly, but are delayed in their extension when the primary motor neurons are ablated (Pike, Melancon and Eisen, 1992). Thus, although the ventral nerve bundle catches up to wild-types by 72 hpf, and extends along the mid-segmental pathway, there are aberrations to the axonal branching.

Abnormal branching was observed in both 48 hpf and 72 hpf larvae. At 48 hpf, an increased number of branches are observed, potentially due to pathfinding errors as the secondary axons extend. The aberrant branching is mostly localised to the ventral parts of the trunk, where the secondary axons growth cones would be extending. At 72 hpf, after the ventral nerve bundle has been established, there is no difference in

length but the dendritic branching into the myotome is reduced. This is observed qualitatively using the HB9:GFP transgenic line (Chapter Three, Section 3.2.3), and was confirmed by the lack of synaptic labelling in Chapter Four, Section 4.2.3. The lack of axonal branching and loss of synaptic puncta are closely related in the *chodl* -/- larvae. We hypothesised that the deficit in axonal branching is a consequence of the synaptic defect and performed branching analysis in wild-type larvae in Chapter Four, Section 4.2.4 to demonstrate that branchpoints are almost always associated with synaptic sites. This suggests that, as is demonstrated in the *Xenopus* motor axons (Javaherian and Cline, 2005), that stabilisation of axonal branches requires synaptic puncta.

6.2.2 – Chondrolectin acts cell-autonomously in motor neurons

I demonstrated in Chapter Three, Section 3.2.5 that chondrolectin acts cell-autonomously in zebrafish. By expressing Chodl-FLAG under the HB9 promoter, the expression is specific to the motor neurons, shown by FLAG immunoreactivity. Injection of the HB9:Chodl-FLAG plasmid into *chodl* -/- eggs induced mosaic rescue of the axonal phenotype, and the stable transgenic line, once established via back-crossing into the *chodl* -/- line, fully rescued the axonal length to wild-type axon lengths. The complete rescue of the global knockout by re-expression of chondrolectin demonstrates that it acts motor neuron-autonomously in zebrafish.

This consolidates previous work in the localisation of chondrolectin expression, but I have shown functional data which demonstrates the mechanism of the protein. In zebrafish*, in situ* hybridisation of chondrolectin shows detectable expression only in the trigeminal ganglion and HB9:GFP-expressing motor neurons (Zhong *et al.*, 2012). Expression of chondrolectin is detectable from ~12 hpf, after differentiation of motor neurons (Lewis and Eisen, 2003), until at least 24 hpf, when wild-type CaP axons have grown beyond the horizontal myoseptum choice point. In the mouse, expression of chondrolectin is enriched in fast motor neurons (Enjin *et al.*, 2010) as well as muscle tissue, brain, and spleen (Weng, Hübner, *et al.*, 2003).

From my data, I also suggest that the expression level of chondrolectin must be tightly controlled for correct function. Injection of the HB9:Chodl-FLAG into wild-type

embryos causes acute reduction in the axon length, correlated with the FLAG reactivity (Chapter Three, Section 3.5.2). This demonstrates that the over-expression of chondrolectin in the motor neurons leads to aberrant axon growth, and it is not an artefact due to ectopic expression of the protein. Previously published global over-expression of chondrolectin, using mRNA, caused similar phenotypes of the motor axons, but mRNA expression was not cell type-specific, and so ectopic expression of chondrolectin could have caused the axonal phenotype (Zhong *et al.*, 2012).Thus, both insufficiency and over-expression of chondrolectin in motor neuron results in defects in motor axon growth, demonstrating that Chodl protein levels are tightly controlled in motor neurons during axon outgrowth.

6.2.3 – Biochemistry of the chondrolectin protein

The acute rescue experiments using Chodl constructs with structural domains deleted (Chapter Three, Section 3.2.6) offer new insights about the mechanism of the chondrolectin protein. I first demonstrated that removal of either the C-type lectin domain or the intracellular domain of chondrolectin abolished the axonal rescue observed when the *chodl* -/- eggs were injected with full-length chondrolectin-FLAG. This supports the hypothesis that chondrolectin is a cell-surface protein, interacting with other proteins via its extracellular CTLD and intracellular domain. I further demonstrated that the intracellular domain requires phosphorylation for its function, as mutagenesis of the serine and threonine residues to alanine also abolishes the rescue of the chondrolectin mutant zebrafish. Phosphorylation of the ID is necessary for signal transduction, although the putative kinase and any intracellular binding partners are still unknown.

This data is further supported by the *in vitro* data gained by Dr Oprişoreanu in HEK cells (unpublished data in the group, shown in Chapter Three Section 3.3.3). The HEK cells localise chondrolectin to the plasma membrane, demonstrating that its endogenous signal peptide will traffic and cause insertion into the membrane. This is different from the mostly perinuclear localisation observed in the earliest studies into chondrolectin (Weng *et al.*, 2002), although punctate signalling in the membrane was also observed in this staining. In zebrafish, the HB9 promoter causes expression of the Chodl-FLAG in both cytoplasm and membrane, and the immunohistochemistry of the FLAG shows that it is excluded from the nucleus. A cell-surface-specific label such

as Zn12 (HNK-1, Nourizadeh-Lillabadi *et al.*, 2010) could be used to confirm that the Chodl-FLAG in zebrafish is trafficked to the plasma membrane. However, transfection of chondrolectin-FLAG into HEK cells does show highly enriched FLAG immunoreactivity in the HEK cell membranes.

The putative ligand Collagen19a1 was hypothesised to bind Chodl previously to this thesis, due to the phenotypic similarity between the *stumpy* collagen19a1 mutants and the chondrolectin morphants. Unpublished data by Dr Zhong discussed in Chapter Three, Section 3.3.3 also demonstrated the genetic interactions between the two genes, where sub-threshold doses of both morpholinos synergistically generate the phenotype. The chondrolectin mutant generated during this thesis phenocopies both the chondrolectin morpholino and *stumpy*, and binding between chondrolectin and collagen19a1 was confirmed in binding assays from proteins produced in HEK cells. We therefore proposed that Chodl, trafficked to the membrane, projects its C-type lectin domain onto the surface of the axon, and binds Col19a1 localised in the ECM. This is supported both by my *in vivo* rescue experiments demonstrated in the zebrafish (Chapter Three, Section 3.2.6), where deletion of the C-type lectin domain abolishes the function, and the HEK cell binding assays, where Col19a1 added as supernatant is bound only onto cells transfected with Chodl constructs containing the C-type lectin domain (Chapter Three, Section 3.3.3).

Overall, this data suggests that chondrolectin acts as a cell-signalling molecule on the motor axon surface, but there are still further avenues for investigation. There may be other proteins complexed with chondrolectin, either in the motor axon cytoplasm or in the ECM. The mechanism and kinase which phosphorylates the intracellular domain of Chodl is also unknown, as is the order of collagen binding and phosphorylation of the intracellular domain. Future experimental approaches are discussed in Section 6.5 of this chapter.

6.3 – Chondrolectin has a novel role in synapse stabilisation

Previous investigation into chondrolectin focused mostly on its role in axonal growth. In this thesis, I have proposed that chondrolectin also affects synaptic development, with enlarged pre-synaptic organisation in embryonic stages, affecting the primary

motor axons, and a reduction of synaptic puncta number at 3 dpf, affecting the secondary motor axons.

At 28 hpf, the number of pre-synapse clusters at the HM are reduced, labelled with SV2 (Chapter Four, Section 4.2.1). This analysis, repeated by a colleague using synaptotagmin labelling, also confirms this phenotype, suggesting that the pre-synapse generally is affected, and it is not limited to SV2 (data not shown, Dr Oprişoreanu). The post-synapse was unaffected in my initial images, although using different batches of α-AChR antibody and different secondary antibodies, it also showed fewer clusters (Chapter Four, Section 4.2.1, Dr Oprişoreanu). This suggests a failure of synaptic remodelling, where the pre- and post-synaptic clusters become more condensed over time (Panzer *et al.*, 2005). The pre-synaptic defects measured in the primary motor axons were independent of axon length, as 'escapees' which have extended beyond the HM at 31 hpf have persistent pre-synaptic enlargement (Chapter Four, Section 4.2.2).

The 3 dpf phenotype, after the secondary motor axons have branched to innervate the myotome, exhibited a large reduction in synaptic puncta number and no changes in puncta size in the *chodl* -/- larvae compared to wild-types (Chapter Four, Section 4.2.3). This supports the hypothesis that the axonal branches fail to establish and are retracted due to a lack of synapse sites that stabilise them. This has previously been demonstrated in Xenopus motor axons (Javaherian and Cline, 2005). By analysing 3 dpf wild-type larvae, I observed that 96.8% of the axonal branchpoints contain pre- and post-synaptic sites, suggesting a similar mechanism (Chapter Four, Section 4.2.4).

The larval phenotype of reduced puncta number is partially rescued by expression of HB9:*chodl*-FLAG, although this also leads to an enlargement of the average puncta size (Chapter Four, Section 4.2.3). However, this partial rescue is sufficient to rescue the behavioural phenotype observed in the mutants (Chapter Four, Section 4.2.5). Although the distance swum by the larvae to escape a tail touch is unchanged between the controls and mutants, there is a turning deficit in the *chodl* -/- larvae after a head tap. This means that the synapse loss affects the normal actions of the larvae, even though the mutants can successfully grow to adulthood without gross behavioural abnormalities. It also demonstrates that loss of function of chondrolectin has a direct impact on the potential survival of the zebrafish. Although the mutants

have normal survival, the reduction in turning response could weaken its ability to survive predation in the wild.

6.4 – The chondrolectin mutant as a drug screening tool

In this thesis, I have established a small-molecule screening protocol utilising the axonal phenotype in the *chodl* -/- embryo (Chapter Five, Section 5.2.1). This also represents the first use of embryos in the VAST BioImager, which recommends larvae of 48 hpf or older (Pardo-Martin *et al.*, 2010). As extensively discussed, chondrolectin is a key gene of interest due to both its requirement for motor axon growth and due to its link with Spinal Muscular Atrophy. It is down-regulated in spinal cord samples of SMA mice (Zhang *et al.*, 2008). It is also mis-spliced in pre-symptomatic time points in SMA mice, suggesting that chondrolectin dysfunction may be a contributing factor in SMA pathology (Bäumer *et al.*, 2009). In zebrafish, over-expression of chondrolectin partially rescues the axonal phenotype observed in zebrafish with knocked-down *smn* (Sleigh *et al.*, 2014).

I performed a small pilot screen using a 40-compound library, and using both scoring and axonal length measurements, I demonstrated that treatment by IOX1 rescues the motor axon growth in *chodl* -/- embryos in a dose-dependent manner (Chapter Five, 5.2.4). Although the compound does not rescue the axons knockdown of *smn* (data not shown, Dr Oprişoreanu), the screening protocol has now been established for use with more compound libraries.

6.5 – Future directions

An excellent future direction would be to perform live imaging in the zebrafish, to confirm several hypotheses that cannot be confirmed in fixed immunohistochemistry. Several different labelling approaches could be utilised to address unknown aspects

of both synapse stabilisation and axonal growth, and I will discuss some of these future directions in the following section.

Injection of constructs encoding pre-synaptic proteins such as synaptophysin-GFP (Meyer and Smith, 2006; Ruthazer, Li and Cline, 2006) and imaging both wild-type and mutant larvae would offer insight into the mechanism of axonal branching. Firstly, imaging the wild-type would confirm that motor axons preferentially branch from synaptic sites. In the *chodl* -/- larvae, live imaging would allow analysis of synaptogenesis dynamics. The data presented in Chapter Four demonstrates changes to the pre-synapse in the embryo, and defects in the pre- and post-synapses in larvae, but the static preparations do not give functional information about how the deficits occur. The dynamics of extension and retraction of the axonal branches in the mutants compared to controls are not possible to determine except through live imaging.

We further hypothesise that the filopodial stability is impaired in the motor axons of *chodl* -/- embryos. This may be dependent or independent from the synaptic stabilisation of the dendritic branches. Filopodial lifespan is reduced in SMA model zebrafish (Hao *et al.*, 2013). If filopodial defects lead to impaired axonal growth, we would thus anticipate the filopodia to be impaired in the *chodl* -/- motor axons. The filopodia can be visualised using LifeAct-GFP, a construct which labels F-actin with GFP, and was used in Hao et al., 2013 to image the filopodial dynamics.

Collagen19a1 has been demonstrated to bind the ECM-projected C-type lectin domain of chondrolectin, and we have presented evidence that the protein's intracellular domain likely acts through a mechanism involving phosphorylation. However, the precise kinase which phosphorylates the intracellular domain is unidentified, or any adaptor proteins which also interact with the intracellular domain. There may be other ECM ligands besides collagen19a1. With the establishment of the *chodl* -/-;HB9:*chodl*-FLAG stable transgenic line, the Chodl protein could be isolated using the FLAG tag, and bound ligands could be identified by mass spectrometry. Further mutagenesis of the intracellular domain to remove each Ser/Thr residue individually would also identify how many residues spared would re-establish rescue of the phenotype, if any. Also, use of phosphomimetic residues (Dephoure *et al.*, 2013) could be used to generate constiutively-active forms of chondrolectin, to determine the effects in both wild-type and *chodl* -/- mutant embryos.

Finally, the drug screening protocol I designed with the *chodl* -/- embryos can be applied in the future to screen more libraries. Colleagues in the group are continuing this work, as well as applying the hit compounds into zebrafish injected with *smn* morpholino. For compounds which rescue the *chodl* -/- phenotype, independent of the effect in zebrafish with *smn* knockdown, further investigation into the pathways which leads to axonal rescue can be performed. By comparing the expression profiles of compound-treated and vehicle-treated *chodl* -/- embryos, the genes differentially expressed in the compound-treated embryos can be used to elucidate chondrolectin's potential signalling pathways. With the axonal rescue from hit compound application, it would also be worthwhile to stain for synaptic proteins and determine if the synaptic phenotype in the *chodl* -/- embryo is also rescued. If true, this would also support the hypothesis that the axonal growth phenotype is caused by a failure in synaptic organisation.

In summary, this thesis demonstrates novel roles for chondrolectin in synapse development, and its requirement for correct motor axon growth and branching. The novel role in synapse development opens up exciting further investigations, including live imaging of synapse formation. I have also performed the first functional assays on the mechanism of the protein, showing which domains are necessary for function, although the full pathway is yet to be elucidated. Overall, this thesis shows the vital role of chondrolectin for correct motor axon development in the zebrafish, which potentially has translational prospects into Spinal Muscular Atrophy in humans.

List of Figures

List of Tables

Bibliography

Akerberg, A. A., Stewart, S. and Stankunas, K. (2014) 'Spatial and temporal control of transgene expression in zebrafish', *PLoS ONE*, 9(3). doi: 10.1371/journal.pone.0092217.

Anderson, E. M. *et al.* (2015) 'Systematic analysis of CRISPR-Cas9 mismatch tolerance reveals low levels of off-target activity', *Journal of Biotechnology*, 211, pp. 56–65. doi: 10.1016/j.jbiotec.2015.06.427.

Anderson, J. L. *et al.* (2017) 'mRNA processing in mutant zebrafish lines generated by chemical and CRISPR-mediated mutagenesis produces unexpected transcripts that escape nonsense-mediated decay', *PLoS Genetics*, 13(11), pp. 1–18. doi: 10.1371/journal.pgen.1007105.

Arber, S. *et al.* (1999) 'Requirement for the Homeobox Gene Hb9 in the Consolidation of Motor Neuron Identity', *Neuron*, 23, pp. 659–674. doi: 10.1016/S0896-6273(01)80026-X.

Asakawa, K. *et al.* (2008) 'Genetic dissection of neural circuits by Tol2 transposon-mediated Gal4 gene and enhancer trapping in zebrafish', *Proceedings of the National Academy of Sciences*, 105(4), pp. 1255–1260. doi: 10.1073/pnas.0704963105.

Asakawa, K. and Kawakami, K. (2008) 'Targeted gene expression by the Gal4-UAS system in zebrafish', *Development Growth and Differentiation*, 50(6), pp. 391–399. doi: 10.1111/j.1440-169X.2008.01044.x.

Atanasov, A. G. *et al.* (2015) 'Discovery and resupply of pharmacologically active plant-derived natural products : A review', *Biotechnology Advances*, 33(8), pp. 1582–1614. doi: 10.1016/j.biotechadv.2015.08.001.Discovery.

Auer, T. O. and Del Bene, F. (2014) 'CRISPR/Cas9 and TALEN-mediated knock-in approaches in zebrafish.', *Methods*. Elsevier Inc., 69(2), pp. 142–150. doi: 10.1016/j.ymeth.2014.03.027.

Babin, P. J., Goizet, C. and Raldúa, D. (2014) 'Zebrafish models of human motor neuron diseases: Advantages and limitations', *Progress in Neurobiology*, 118, pp. 36–58. doi: 10.1016/j.pneurobio.2014.03.001.

Bader, H. L. *et al.* (2009) 'Zebrafish collagen XII is present in embryonic connective tissue sheaths (fascia) and basement membranes', *Matrix Biology*. Elsevier B.V., 28(1), pp. 32–43. doi: 10.1016/j.matbio.2008.09.580.

Balciunas, D. *et al.* (2006) 'Harnessing a high cargo-capacity transposon for genetic applications in vertebrates', *PLoS Genetics*, 2(11), pp. 1715–1724. doi: 10.1371/journal.pgen.0020169.

Baraban, S. C., Dinday, M. T. and Hortopan, G. A. (2013) 'Drug screening in Scn1a zebrafish mutant identifies clemizole as a potential Dravet syndrome treatment', *Nature Communications*. Nature Publishing Group, 4, pp. 1–10. doi: 10.1038/ncomms3410.

Bäumer, D. *et al.* (2009) 'Alternative splicing events are a late feature of pathology in a mouse model of spinal muscular atrophy', *PLoS Genetics*, 5(12). doi: 10.1371/journal.pgen.1000773.

Beis, D. and Stainier, D. Y. R. (2006) 'In vivo cell biology: Following the zebrafish trend', *Trends in Cell Biology*, 16(2), pp. 105–112. doi: 10.1016/j.tcb.2005.12.001.

Bertini, E. *et al.* (2017) 'Safety and efficacy of olesoxime in patients with type 2 or non-ambulatory type 3 spinal muscular atrophy: a randomised, double-blind, placebo-controlled phase 2 trial', *The Lancet Neurology*, 16(7), pp. 513–522. doi: 10.1016/S1474-4422(17)30085-6.

Bhandiwad, A. A. *et al.* (2013) 'Auditory sensitivity of larval zebrafish (Danio rerio) measured using a behavioral prepulse inhibition assay', *Journal of Experimental Biology*, 216(18), pp. 3504–3513. doi: 10.1242/jeb.087635.

Bill, B. R. *et al.* (2009) 'A Primer for Morpholino Use in Zebrafish', *Zebrafish*, 6(1), pp. 69–77. doi: 10.1089/zeb.2008.0555.

Brand, M., Heisenberg, C.P., Warga, R.M., Pelegri, F., Karlstrom, R.O., Beuchle, D., Picker, A., Jiang, Y.J., Furutani-Seiki, M., van Eeden, F.J., Granato, M., Haffter, P., Hammerschmidt, M., Kane, D.A., Kelsh, R.N., Mullins, M.C., Odenthal, J., and Nüsslein-Volhard, C. (1996) Mutations affecting development of the midline and general body shape during zebrafish embryogenesis. *Development (Cambridge, England)*. 123:129-142.Boido, M. and Vercelli, A. (2016) 'Neuromuscular Junctions as Key Contributors and Therapeutic Targets in Spinal Muscular Atrophy', *Frontiers in Neuroanatomy*, 10(February), pp. 1–10. doi: 10.3389/fnana.2016.00006.

Bono, P. *et al.* (2001) 'Layilin, a Novel Integral Membrane Protein, Is a Hyaluronan Receptor', *Molecular Biology of the Cell*, 12(4), pp. 891–900. doi: 10.1091/mbc.12.4.891.

Boon, K. L. *et al.* (2009) 'Zebrafish survival motor neuron mutants exhibit presynaptic neuromuscular junction defects', *Human Molecular Genetics*, 18(19), pp. 3615–3625. doi: 10.1093/hmg/ddp310.

Bowerman, M., Becker, C. G., Yáñez-Muñoz, R. J., Ning, K., Wood, M., Gillingwater, T. H., Talbot, K., UK SMA Research Consortium (2017). Therapeutic strategies for spinal muscular atrophy: SMN and beyond. *Disease models & mechanisms*, *10*(8), 943-954.

Boyd, P. J. *et al.* (2017) 'Bioenergetic status modulates motor neuron vulnerability and pathogenesis in a zebrafish model of spinal muscular atrophy.', *PLoS Genetics*, 13(4).

Boyd, P. J. and Gillingwater, T. H. (2016) *Axonal and Neuromuscular Junction Pathology in Spinal Muscular Atrophy*, *Spinal Muscular Atrophy: Disease Mechanisms and Therapy*. Elsevier Inc. doi: 10.1016/B978-0-12-803685-3.00008-2.

Brown, P. J. and Müller, S. (2015) 'Open access chemical probes for epigenetic targets', *Future Medicinal Chemistry*, 7(14), pp. 1901–1917.

Budick, S. a and O'Malley, D. M. (2000) 'Locomotor repertoire of the larval zebrafish: swimming, turning and prey capture.', *The Journal of experimental biology*, 203(Pt 17), pp. 2565–79. doi: 10.1242/jeb.01529.

Burden, S. J. (2002) 'Building the vertebrate neuromuscular synapse', *Journal of Neurobiology*, 53(4), pp. 501–511. doi: 10.1002/neu.10137.

Burghes, A. H. M. and Beattie, C. E. (2009) 'Spinal muscular atrophy: Why do low levels of survival motor neuron protein make motor neurons sick?', *Nature Reviews Neuroscience*. Nature Publishing Group, 10(8), pp. 597–609. doi: 10.1038/nrn2670.

Calder, A. N., Androphy, E. J. and Hodgetts, K. J. (2016) 'Small Molecules in Development for the Treatment of Spinal Muscular Atrophy', *Journal of Medicinal Chemistry*, 59(22), pp. 10067–10083. doi: 10.1021/acs.jmedchem.6b00670.

Caldwell, L. J. *et al.* (2018) 'Regeneration of dopaminergic neurons in adult zebrafish depends on immune system activation and differs for distinct populations.', *bioRxiv pre-print*. doi: http://dx.doi.org/10.1101/367151.

Cantu, J. A., Flowers, G. P. and Topczewski, J. (2013) 'Notum Homolog Plays a Novel Role in Primary Motor Innervation', *Journal of Neuroscience*, 33(5), pp. 2177–2187. doi: 10.1523/JNEUROSCI.3694-12.2013.

Cartegni, L. *et al.* (2006) 'Determinants of exon 7 splicing in the spinal muscular atrophy genes, SMN1 and SMN2.', *American Journal of Human Genetics*, 78(1), pp. 63–77. doi:

10.1086/498853.

Chang, T. Y. *et al.* (2012) 'Fully automated cellular-resolution vertebrate screening platform with parallel animal processing', *Lab on a Chip*, 12(4), pp. 711–716. doi: 10.1039/c1lc20849g.

Chaytow, H. *et al.* (2018) 'The role of survival motor neuron protein (SMN) in protein homeostasis', *Cellular and Molecular Life Sciences*. Springer International Publishing. doi: 10.1007/s00018-018-2849-1.

Chen, P. *et al.* (2016) 'Discovery and Characterization of GSK2801, a Selective Chemical Probe for the Bromodomains BAZ2A and BAZ2B', *Journal of Medicinal Chemistry*, 59(4), pp. 1410–1424. doi: 10.1021/acs.jmedchem.5b00209.

Chowdhury, R. *et al.* (2013) 'Selective small molecule probes for the hypoxia inducible factor (HIF) Prolyl Hydroxylases', *ACS Chemical Biology*, 8(7), pp. 1488–1496. doi: 10.1021/cb400088q.

Ciura, S. *et al.* (2013) 'Loss of function of C9orf72 causes motor deficits in a zebrafish model of amyotrophic lateral sclerosis', *Annals of Neurology*, 74(2), pp. 180–187. doi: 10.1002/ana.23946.

Claessens, A. , Vijver, K. , Bockstaele, D. R., Wauters, J. , Berneman, Z. N., Marck, E. and Merregaert, J. (2007), Expression and localization of $CHODL_{\Delta E}$/$CHODL_{f\Delta E}$, the soluble isoform of chondrolectin. Cell Biology International, 31: 1323-1330. doi:10.1016/j.cellbi.2007.05.014

Claessens, A., Weyn, C. and Merregaert, J. (2008) 'The cytoplasmic domain of chondrolectin interacts with the β-subunit of rab geranylgeranyl transferase', *Cellular and Molecular Biology Letters*, 13(2), pp. 250–259. doi: 10.2478/s11658-007-0052-8.

Colwill, R. M. and Creton, R. (2011) 'Imaging escape and avoidance behavior in zebrafish larvae', *Rev. Neurosci*, 22(1), pp. 63–73. doi: 10.1515/RNS.2011.008.

Corti, S. *et al.* (2012) 'Genetic Correction of Human Induced Pluripotent Stem Cells from Patients with Spinal Muscular Atrophy', *Science Translational Medicine*, 4(165), pp. 1–32. doi: 10.1126/scitranslmed.3004108.Genetic.

Cummings, R. D. and McEver, R. P. (2017) 'C-type Lectins', in Varki, A. et al. (eds) *Essentials of Glycobiology*. 3rd editio. Cold Spring Harbor Laboratory Press. doi: 10.1101/glycobiology.3e.034.

Dambuza, I. M. and Brown, G. D. (2015) 'C-type lectins in immunity: Recent developments', *Current Opinion in Immunology*. Elsevier Ltd, 32, pp. 21–27. doi: 10.1016/j.coi.2014.12.002.

Darabid, H., Perez-Gonzalez, A. P. and Robitaille, R. (2014) 'Neuromuscular synaptogenesis: coordinating partners with multiple functions', *Nature Reviews Neuroscience*. Nature Publishing Group, 15(11), pp. 703–718. doi: 10.1038/nrn3821.

Davis-Dusenbery, B. N. *et al.* (2014) 'How to make spinal motor neurons', *Development*, 141(3), pp. 491–501. doi: 10.1242/dev.097410.

Day, E. K., Sosale, N. G. and Lazzara, M. J. (2016) 'Cell signaling regulation by protein phosphorylation: A multivariate, heterogeneous, and context-dependent process', *Current Opinion in Biotechnology*. Elsevier Ltd, 40, pp. 185–192. doi: 10.1016/j.copbio.2016.06.005.

Dephoure, N. *et al.* (2013) 'Mapping and analysis of phosphorylation sites: a quick guide for cell biologists', *Molecular Biology of the Cell*, 24(5), pp. 535–542. doi: 10.1091/mbc.E12-09-0677.

Dias, T. B. *et al.* (2012) 'Notch Signaling Controls Generation of Motor Neurons in the Lesioned Spinal Cord of Adult Zebrafish', *Journal of Neuroscience*, 32(9), pp. 3245–3252. doi: 10.1523/JNEUROSCI.6398-11.2012.

Dombert, B. *et al.* (2014) 'Presynaptic localization of SMN and hnRNP R in axon terminals of

embryonic and postnatal mouse motoneurons', *PLoS ONE*, 9(10). doi: 10.1371/journal.pone.0110846.

Dornseifer, P., Takke, C. and Campos-Ortega, J. A. (1997) 'Overexpression of a zebrafish homologue of the Drosophila neurogenic gene Delta perturbs differentiation of primary neurons and somite development', *Mechanisms of Development*, 63(2), pp. 159–171. doi: 10.1016/S0925-4773(97)00037-3.

Driever, W. *et al.* (1996) 'A genetic screen for mutations affecting embryogenesis in zebrafish.', *Development (Cambridge, England)*, 123(1), pp. 37–46. doi: 9007227.

Early, J. J. *et al.* (2018) 'An automated high-resolution in vivo screen in zebrafish to identify chemical regulators of myelination', *eLife*, 7, p. e35136. doi: 10.7554/eLife.35136.

Eisen, J. S. and Smith, J. C. (2008) 'Controlling morpholino experiments: don't stop making antisense', *Development*, 135(10), pp. 1735–1743. doi: 10.1242/dev.001115.

Enjin, A. *et al.* (2010) 'Identification of novel spinal cholinergic genetic subtypes disclose chodl and Pitx2 as markers for fast motor neurons and partition cells', *Journal of Comparative Neurology*, 518(12), pp. 2284–2304. doi: 10.1002/cne.22332.

Fallini, C. *et al.* (2016) 'Deficiency of the Survival of Motor Neuron Protein Impairs mRNA Localization and Local Translation in the Growth Cone of Motor Neurons', *Journal of Neuroscience*, 36(13), pp. 3811–3820. doi: 10.1523/JNEUROSCI.2396-15.2016.

Feany, M. B. *et al.* (1992) 'The synaptic vesicle protein SV2 is a novel type of transmembrane transporter', *Cell*, 70(5), pp. 861–867. doi: 10.1016/0092-8674(92)90319-8.

Fetcho, J. R., Higashijima, S.-I. and McLean, D. L. (2008) 'Zebrafish and motor control over the last decade', *Brain Research Reviews*, 57(1), pp. 86–93. doi: 10.1002/ar.20849.3D.

Filippakopoulos, P. *et al.* (2010) 'Selective inhibition of BET bromodomains', *Nature*. Nature Publishing Group, 468(7327), pp. 1067–1073. doi: 10.1038/nature09504.

Finkel, R. S. *et al.* (2016) 'Treatment of infantile-onset spinal muscular atrophy with nusinersen: a phase 2, open-label, dose-escalation study', *The Lancet*. Elsevier Ltd, 388(10063), pp. 3017–3026. doi: 10.1016/S0140-6736(16)31408-8.

Finkel, R. S. *et al.* (2017) 'Nusinersen versus Sham Control in Infantile-Onset Spinal Muscular Atrophy', *New England Journal of Medicine*, 377(18), pp. 1723–1732. doi: 10.1056/NEJMoa1702752.

Fisher, S. *et al.* (2006) 'Evaluating the biological relevance of putative enhancers using Tol2 transposon-mediated transgenesis in zebrafish', *Nature Protocols*, 1(3), pp. 1297–1305. doi: 10.1038/nprot.2006.230.

Flanagan-Steet, H. *et al.* (2005) 'Neuromuscular synapses can form in vivo by incorporation of initially aneural postsynaptic specializations', *Development*, 132(20), pp. 4471–4481. doi: 10.1242/dev.02044.

Fuller, H. R. *et al.* (2016) 'Spinal Muscular Atrophy Patient iPSC-Derived Motor Neurons Have Reduced Expression of Proteins Important in Neuronal Development', *Frontiers in Cellular Neuroscience*, 9(January), pp. 1–15. doi: 10.3389/fncel.2015.00506.

Furutani-Seiki, M. *et al.* (1996) 'Neural degeneration mutants in the zebrafish, Danio rerio', *Development*, 123(JANUARY), pp. 229–239. doi: 10.1016/0736-5748(96)80313-3.

Gautam, M. *et al.* (1996) 'Defective neuromuscular synaptogenesis in agrin-deficient mutant mice', *Cell*, 85(4), pp. 525–535. doi: 10.1016/S0092-8674(00)81253-2.

Gogliotti, R. G. *et al.* (2013) 'The dcpS inhibitor RG3039 improves survival, function and motor unit pathologies in two SMA mouse models', *Human Molecular Genetics*, 22(20), pp. 4084–4101. doi: 10.1093/hmg/ddt258.

Goldsmith, J. R. and Jobin, C. (2012) 'Think small: Zebrafish as a model system of human pathology', *Journal of Biomedicine and Biotechnology*, 2012. doi: 10.1155/2012/817341.

Gonzales, A. P. W. and Joanna Yeh, J. R. (2014) 'Cas9-based genome editing in Zebrafish', in Elsevier Inc. (ed.) *Methods in Enzymology*. 1st edn. Elsevier Inc., pp. 377–413. doi: 10.1016/B978-0-12-801185-0.00018-0.

Goolish, E. M. and Okutake, K. (1999) 'Lack of gas bladder inflation by the larvae of zebrafish in the absence of an air-water interface', *Journal of Fish Biology*, 55(5), pp. 1054–1063. doi: 10.1006/jfbi.1999.1110.

Goulet, B. B., Kothary, R. and Parks, R. J. (2013) 'At the "Junction" of Spinal Muscular Atrophy Pathogenesis: The Role of Neuromuscular Junction Dysfunction in SMA Disease Progression', *Current Molecular Medicine*, 13(7), pp. 1160–1174. doi: 10.2174/15665240113139990044.

Granato, M. *et al.* (1996) 'Genes controlling and mediating locomotion behavior of the zebrafish embryo and larva.', *Development (Cambridge, England)*, 123(1), pp. 399–413. Available at: http://www.ncbi.nlm.nih.gov/pubmed/9007258.

Grunwald, D. J. *et al.* (1988) 'A neural degeneration mutation that spares primary neurons in the zebrafish', *Developmental Biology*, 126(1), pp. 115–128. doi: 10.1016/0012-1606(88)90245-X.

Grzegorski, S. J. *et al.* (2014) 'Natural variability of Kozak sequences correlates with function in a zebrafish model', *PLoS ONE*, 9(9). doi: 10.1371/journal.pone.0108475.

Gundelfinger, E. D., Reissner, C. and Garner, C. C. (2016) 'Role of Bassoon and Piccolo in Assembly and Molecular Organization of the Active Zone', *Frontiers in Synaptic Neuroscience*, 7(January). doi: 10.3389/fnsyn.2015.00019.

Hao, L. T. *et al.* (2013) 'Temporal requirement for SMN in motoneuron development', *Human Molecular Genetics*, 22(13), pp. 2612–2625. doi: 10.1093/hmg/ddt110.

Hao, L. T., Burghes, A. H. M. and Beattie, C. E. (2011) 'Generation and Characterization of a genetic zebrafish model of SMA carrying the human SMN2 gene', *Molecular Neurodegeneration*. BioMed Central Ltd, 6(1), p. 24. doi: 10.1186/1750-1326-6-24.

Harding, B. N. *et al.* (2015) 'Spectrum of Neuropathophysiology in Spinal Muscular Atrophy Type I', *Journal of Neuropathology and Experimental Neurology*, 74(1), pp. 1–10.

Hay, D. A. *et al.* (2014) 'Discovery and optimization of small-molecule ligands for the CBP/p300 bromodomains', *Journal of the American Chemical Society*, 136(26), pp. 9308–9319. doi: 10.1021/ja412434f.

Held, W. and Mariuzza, R. A. (2011) 'Cis-trans interactions of cell surface receptors: Biological roles and structural basis', *Cellular and Molecular Life Sciences*, 68(21), pp. 3469–3478. doi: 10.1007/s00018-011-0798-z.

Hilario, J. D., Wang, C. and Beattie, C. E. (2010) 'Collagen XIXa1 is crucial for motor axon navigation at intermediate targets.', *Development (Cambridge, England)*, 137(24), pp. 4261–9. doi: 10.1242/dev.051730.

Van Hoecke, A. *et al.* (2012) 'EPHA4 is a disease modifier of amyotrophic lateral sclerosis in animal models and in humans', *Nature Medicine*, 18(9), pp. 1418–22. doi: 10.1038/nm.2901.

Hopkinson, R. J. *et al.* (2013) '5-Carboxy-8-hydroxyquinoline is a broad spectrum 2-oxoglutarate oxygenase inhibitor which causes iron translocation', *Chemical Science*, 4(8), pp. 3110–3117. doi: 10.1039/c3sc51122g.

Hoving, J. C., Wilson, G. J. and Brown, G. D. (2014) 'Signalling C-type lectin receptors, microbial recognition and immunity', *Cellular Microbiology*, 16(2), pp. 185–194. doi: 10.1111/cmi.12249.

Howe, K. *et al.* (2013) 'The zebrafish reference genome sequence and its relationship to the human genome', *Nature*, 496(7446), pp. 498–503. doi: 10.1038/nature12111.

Hsu, P. D. *et al.* (2013) 'DNA targeting specificity of RNA-guided Cas9 nucleases', *Nature Biotechnology*, 31(9), pp. 827–832. doi: 10.1038/nbt.2647.

Huang, P. *et al.* (2011) 'Heritable gene targeting in zebrafish using customized TALENs', *Nature Biotechnology*. Nature Publishing Group, 29(8), pp. 699–700. doi: 10.1038/nbt.1939.

Huang, P. *et al.* (2012) 'Reverse Genetic Approaches in Zebrafish', *Journal of Genetics and Genomics*. Elsevier Limited and Science Press, 39(9), pp. 421–433. doi: 10.1016/j.jgg.2012.07.004.

Hwang, W. Y. *et al.* (2013) 'Efficient genome editing in zebrafish using a CRISPR-Cas system', *Nature Biotechnology*. Nature Publishing Group, 31(3), pp. 227–229. doi: 10.1038/nbt.2501.

Jablonka, S. *et al.* (2007) 'Defective Ca2+channel clustering in axon terminals disturbs excitability in motoneurons in spinal muscular atrophy', *Journal of Cell Biology*, 179(1), pp. 139–149. doi: 10.1083/jcb.200703187.

Jao, L.-E., Wente, S. R. and Chen, W. (2013) 'Efficient multiplex biallelic zebrafish genome editing using a CRISPR nuclease system', *Proceedings of the National Academy of Sciences*, 110(34), pp. 13904–13909. doi: 10.1073/pnas.1308335110.

Jarecki, J. *et al.* (2005) 'Diverse small-molecule modulators of SMN expression found by high-throughput compound screening: Early leads towards a therapeutic for spinal muscular atrophy', *Human Molecular Genetics*, 14(14), pp. 2003–2018. doi: 10.1093/hmg/ddi205.

Javaherian, A. and Cline, H. T. (2005) 'Coordinated motor neuron axon growth and neuromuscular synaptogenesis are promoted by CPG15 in vivo', *Neuron*, 45(4), pp. 505–512. doi: 10.1016/j.neuron.2004.12.051.

Jinek, M. *et al.* (2012) 'A Programmable Dual-RNA – Guided DNA Endonuclease in Adaptive Bacterial Immunity', *Science*, 337(August), pp. 816–822. doi: 10.1126/science.1225829.

Jing, L. *et al.* (2009) 'Wnt Signals Organize Synaptic Prepattern and Axon Guidance through the Zebrafish unplugged/MuSK Receptor', *Neuron*. Elsevier Ltd, 61(5), pp. 721–733. doi: 10.1016/j.neuron.2008.12.025.

Johnson, N. M., Farr III, G. H. and Maves, L. (2013) 'The HDAC Inhibitor TSA Ameliorates a Zebrafish Model of Duchenne Muscular Dystrophy', *PLOS Currents Muscular Dystrophy*, (Dmd), pp. 1–17. doi: 10.1371/currents.md.8273cf41db10e2d15dd3ab827cb4b027.Authors.

Jonkman, J. and Brown, C. M. (2015) 'Any way you slice it—A comparison of confocal microscopy techniques', *Journal of Biomolecular Techniques*, 26(2), pp. 54–65. doi: 10.7171/jbt.15-2602-003.

Kariya, S. *et al.* (2008) 'Reduced SMN protein impairs maturation of the neuromuscular junctions in mouse models of spinal muscular atrophy', *Human Molecular Genetics*, 17(16), pp. 2552–2569. doi: 10.1093/hmg/ddn156.

Kariya, S. *et al.* (2014) 'Requirement of enhanced Survival Motoneuron protein imposed during neuromuscular junction maturation', *Journal of Clinical Investigation*, 124(2), pp. 785–800. doi: 10.1172/JCI72017.

Kawakami, K. *et al.* (2004) 'A Transposon-Mediated Gene Trap Approach Identifies Developmentally Regulated Genes in Zebrafish', *Developmental Cell*, 7, pp. 133–144.

Kawakami, K. (2005) 'Transposon tools and methods in zebrafish', *Developmental Dynamics*, 234(2), pp. 244–254. doi: 10.1002/dvdy.20516.

Kim, M. J. *et al.* (2007) 'Agrin is required for posterior development and motor axon outgrowth and branching in embryonic zebrafish', *Glycobiology*, 17(2), pp. 231–247. doi:

10.1093/glycob/cwl069.

Kim, N. and Burden, S. J. (2008) 'MuSK controls where motor axons grow and form synapses', *Nature Neuroscience*, 11(1), pp. 19–27. doi: 10.1038/nn2026.

Kimmel, C. B. (1989) 'Genetics and early development of zebrafish', *Trends in Genetics*, 5(C), pp. 283–288. doi: 10.1016/0168-9525(89)90103-0.

Kimmel, C. B. *et al.* (1995) 'Stages of embryonic development of the zebrafish.', *Developmental dynamics : an official publication of the American Association of Anatomists*, 203(3), pp. 253–310. doi: 10.1002/aja.1002030302.

Kimmel, C. B., Warga, R. M. and Kane, D. A. (1994) 'Cell cycles and clonal strings during formation of the zebrafish central nervous system', *Development*, 120(2), pp. 265–276. Available at: http://www.ncbi.nlm.nih.gov/pubmed/8149908%5Cnhttp://dev.biologists.org/content/120/2/265.short.

King, O. N. F. *et al.* (2010) 'Quantitative high-throughput screening identifies 8-hydroxyquinolines as cell-active histone demethylase inhibitors', *PLoS ONE*, 5(11). doi: 10.1371/journal.pone.0015535.

Klaeger, S. *et al.* (2017) 'The target landscape of clinical kinase drugs', *Science*, 358(6367). doi: 10.1126/science.aan4368.

Koga, A. *et al.* (1996) 'Transposable element in fish', *Nature*, p. 30. doi: 10.1038/383030a0.

Kohashi, T. and Oda, Y. (2008) 'Initiation of Mauthner- or Non-Mauthner-Mediated Fast Escape Evoked by Different Modes of Sensory Input', *Journal of Neuroscience*, 28(42), pp. 10641–10653. doi: 10.1523/JNEUROSCI.1435-08.2008.

Kokel, D. *et al.* (2013) 'Photochemical activation of TRPA1 channels in neurons and animals', *Nature Chemical Biology*. Nature Publishing Group, 9(4), pp. 257–263. doi: 10.1038/nchembio.1183.

Kolb, S. J., Battle, D. J. and Dreyfuss, G. (2007) 'Molecular functions of the SMN complex.', *Journal of child neurology*, 22(8), pp. 990–994. doi: 10.1177/0883073807305666.

Kong, L. *et al.* (2009) 'Impaired Synaptic Vesicle Release and Immaturity of Neuromuscular Junctions in Spinal Muscular Atrophy Mice', *Journal of Neuroscience*, 29(3), pp. 842–851. doi: 10.1523/JNEUROSCI.4434-08.2009.

Kulkarni, G., Li, H. and Wadsworth, W. G. (2008) 'CLEC-38, A Transmembrane Protein with C-Type Lectin-Like Domains, Negatively Regulates UNC-40-Mediated Axon Outgrowth and Promotes Presynaptic Development in Caenorhabditis elegans', *Journal of Neuroscience*, 28(17), pp. 4541–4550. doi: 10.1523/JNEUROSCI.5542-07.2008.

Kwan, K. M. *et al.* (2007) 'The Tol2kit: A multisite gateway-based construction Kit for Tol2 transposon transgenesis constructs', *Developmental Dynamics*, 236(11), pp. 3088–3099. doi: 10.1002/dvdy.21343.

Laird, A. S. *et al.* (2016) 'Tissue-specific models of spinal muscular atrophy confirm a critical role of SMN in motor neurons from embryonic to adult stages', *Human Molecular Genetics*, 25(9), pp. 1728–1738. doi: 10.1093/hmg/ddw044.

Langheinrich, U. (2003) 'Zebrafish: A new model on the pharmaceutical catwalk', *BioEssays*, 25(9), pp. 904–912. doi: 10.1002/bies.10326.

Lawrence, C. (2007) 'The husbandry of zebrafish (Danio rerio): A review', *Aquaculture*, 269(1–4), pp. 1–20. doi: 10.1016/j.aquaculture.2007.04.077.

Lawson, N. D. and Wolfe, S. A. (2011) 'Forward and Reverse Genetic Approaches for the Analysis of Vertebrate Development in the Zebrafish', *Developmental Cell*. Elsevier Inc., 21(1),

pp. 48–64. doi: 10.1016/j.devcel.2011.06.007.

Lefebvre, J. L. *et al.* (2004) 'Increased neuromuscular activity causes axonal defects and muscular degeneration.', *Development*, 131(11), pp. 2605–2618. doi: 10.1242/dev.01123.

Lefebvre, S. *et al.* (1995) 'Identification and characterization of a spinal muscular atrophy-determining gene', *Cell*, 80(1), pp. 155–165. doi: 10.1016/0092-8674(95)90460-3.

Lele, Z. and Krone, P. H. (1996) 'The zebrafish as a model system in developmental, toxicological and transgenic research', *Biotechnology Advances*, 14(1), pp. 57–72. doi: 10.1016/0734-9750(96)00004-3.

Lemmens, R. *et al.* (2007) 'Overexpression of mutant superoxide dismutase 1 causes a motor axonopathy in the zebrafish.', *Human molecular genetics*, 16(19), pp. 2359–65. doi: 10.1093/hmg/ddm193.

Letamendia, A. *et al.* (2012) 'Development and validation of an automated high-throughput system for zebrafish in vivo screenings.', *PloS one*, 7(5). doi: 10.1371/journal.pone.0036690.

Lewis, K. E. and Eisen, J. S. (2003) 'From cells to circuits: Development of the zebrafish spinal cord', *Progress in Neurobiology*, 69(6), pp. 419–449. doi: 10.1016/S0301-0082(03)00052-2.

Lin, W. *et al.* (2001) 'Distinct roles of nerve and muscle in postsynaptic differentiation of the neuromuscular synapse.', *Nature*, 410(6832), pp. 1057–1064. doi: 10.1038/35074025.

Ling, K. K. Y. *et al.* (2012) 'Severe neuromuscular denervation of clinically relevant muscles in a mouse model of spinal muscular atrophy', *Human Molecular Genetics*, 21(1), pp. 185–195. doi: 10.1093/hmg/ddr453.

Liu, H. *et al.* (2014) 'The Smn-independent beneficial effects of trichostatin a on an intermediate mouse model of spinal muscular atrophy', *PLoS ONE*, 9(7), pp. 3–11. doi: 10.1371/journal.pone.0101225.

Liu, Y. *et al.* (2014) 'A highly effective TALEN-mediated approach for targeted gene disruption in Xenopus tropicalis and zebrafish', *Methods*. Elsevier Inc., 69(1), pp. 58–66. doi: 10.1016/j.ymeth.2014.02.011.

Lorent, K. *et al.* (2001) 'The zebrafish space cadet gene controls axonal pathfinding of neurons that modulate fast turning movements.', *Development (Cambridge, England)*, 128(11), pp. 2131–2142.

Lunn, M. R. and Wang, C. H. (2008) 'Spinal muscular atrophy.', *Lancet*, 371(9630), pp. 2120–2133. doi: 10.1016/S0140-6736(08)60921-6.

MacRae, C. A. and Peterson, R. T. (2015) 'Zebrafish as tools for drug discovery', *Nature Reviews Drug Discovery*. Nature Publishing Group, 14(10), pp. 721–731. doi: 10.1038/nrd4627.

Markolovic, S., Wilkins, S. E. and Schofield, C. J. (2015) 'Protein hydroxylation catalyzed by 2-oxoglutarate-dependent oxygenases', *Journal of Biological Chemistry*, 290(34), pp. 20712–20722. doi: 10.1074/jbc.R115.662627.

Martínez-Hernández, R. *et al.* (2013) 'Synaptic defects in type I spinal muscular atrophy in human development', *Journal of Pathology*, 229(1), pp. 49–61. doi: 10.1002/path.4080.

Mathew, L. K. *et al.* (2007) 'Unraveling tissue regeneration pathways using chemical genetics', *Journal of Biological Chemistry*, 282(48), pp. 35202–35210. doi: 10.1074/jbc.M706640200.

Mayer, S., Raulf, M. K. and Lepenies, B. (2017) 'C-type lectins: their network and roles in pathogen recognition and immunity', *Histochemistry and Cell Biology*. Springer Berlin Heidelberg, 147(2), pp. 223–237. doi: 10.1007/s00418-016-1523-7.

Mcgovern, V. L. *et al.* (2008) 'Embryonic motor axon development in the severe SMA mouse',

Human Molecular Genetics, 17(18), pp. 2900–2909. doi: 10.1093/hmg/ddn189.

McWhorter, M. L. *et al.* (2003) 'Knockdown of the survival motor neuron (Smn) protein in zebrafish causes defects in motor axon outgrowth and pathfinding.', *The Journal of cell biology*, 162(5), pp. 919–31. doi: 10.1083/jcb.200303168.

Menelaou, E. *et al.* (2008) 'Embryonic motor activity and implications for regulating motoneuron axonal pathfinding in zebrafish', *European Journal of Neuroscience*, 28(6), pp. 1080–1096. doi: 10.1111/j.1460-9568.2008.06418.x.

Menelaou, E. and McLean, D. L. (2012) 'A Gradient in Endogenous Rhythmicity and Oscillatory Drive Matches Recruitment Order in an Axial Motor Pool', *Journal of Neuroscience*, 32(32), pp. 10925–10939. doi: 10.1523/JNEUROSCI.1809-12.2012.

Menelaou, E. and Svoboda, K. R. (2009) 'Secondary motoneurons in juvenile and adult zebrafish: Axonal pathfinding errors caused by embryonic nicotine exposure', *Journal of Comparative Neurology*, 512(3), pp. 305–322. doi: 10.1002/cne.21903.

Meng, X. *et al.* (2008) 'Targeted gene inactivation in zebrafish using engineered zinc-finger nucleases', *Nature Biotechnology*, 26(6), pp. 695–701. doi: 10.1038/nbt1398.

Meyer, M. P. and Smith, S. J. (2006) 'Evidence from in vivo imaging that synaptogenesis guides the growth and branching of axonal arbors by two distinct mechanisms.', *The Journal of neuroscience : the official journal of the Society for Neuroscience*, 26(13), pp. 3604–14. doi: 10.1523/JNEUROSCI.0223-06.2006.

Miller, N. *et al.* (2016) 'Motor neuron mitochondrial dysfunction in spinal muscular atrophy', *Human Molecular Genetics*, 25(16), pp. 3395–3406. doi: 10.1093/hmg/ddw262.

Miller, R., Mitchell, J. and Moore, D. (2012) 'Riluzole for amyotrophic lateral sclerosis (ALS)/ motor neuron disease (MND)', *The Cochrane Database of Systematic Reviews*, (3), pp. 1–28. doi: 10.1002/14651858.CD001447.pub3.www.cochranelibrary.com.

Misgeld, T. *et al.* (2005) 'Agrin promotes synaptic differentiation by counteracting an inhibitory effect of neurotransmitter.', *Proceedings of the National Academy of Sciences of the United States of America*, 102(31), pp. 11088–11093. doi: 10.1073/pnas.0504806102.

Mou, H. *et al.* (2017) 'CRISPR/Cas9-mediated genome editing induces exon skipping by alternative splicing or exon deletion', *Genome Biology*. Genome Biology, 18(1), pp. 4–11. doi: 10.1186/s13059-017-1237-8.

Müller, S. *et al.* (2018) 'Donated chemical probes for open science', *eLife*, 7, p. e34311. doi: 10.7554/eLife.34311.

Mullins, M. C. *et al.* (1994) 'Large-scale mutagenesis in the zebrafish: in search of genes controlling development in a vertebrate', *Current Biology*, 4(3), pp. 189–202. doi: 10.1016/S0960-9822(00)00048-8.

Murray, L. M. *et al.* (2008) 'Selective vulnerability of motor neurons and dissociation of pre- and post-synaptic pathology at the neuromuscular junction in mouse models of spinal muscular atrophy', *Human Molecular Genetics*, 17(7), pp. 949–962. doi: 10.1093/hmg/ddm367.

Murray, L. M., Talbot, K. and Gillingwater, T. H. (2010) 'Review: neuromuscular synaptic vulnerability in motor neurone disease: amyotrophic lateral sclerosis and spinal muscular atrophy', *Neuropathology and Applied Neurobiology*, 36(2), pp. 133–156. doi: 10.1111/j.1365-2990.2010.01061.x.

Myers, P. Z., Eisen, J. S. and Westerfield, M. (1986) 'Development and axonal outgrowth of identified motoneurons in the zebrafish.', *The Journal of neuroscience : the official journal of the Society for Neuroscience*, 6(8), pp. 2278–89. Available at: http://www.ncbi.nlm.nih.gov/pubmed/3746410.

NICE (2018) *Appraisal consultation document Nusinersen for treating spinal muscular atrophy*, *Nice.org.uk*. Available at: https://www.nice.org.uk/guidance/GID-TA10281/documents/appraisal-consultation-document (Accessed: 21 August 2018).

Nourizadeh-Lillabadi, R. *et al.* (2010) 'Early embryonic gene expression profiling of zebrafish prion protein (PrP2) morphants', *PLoS ONE*, 5(10). doi: 10.1371/journal.pone.0013573.

O'Connor, V. and Lee, A. G. (2002) 'Synaptic vesicle fusion and synaptotagmin: 2B or not 2B?', *Nature Neuroscience*, 5(9), pp. 823–824. doi: 10.1038/nn0902-823.

Ohnmacht, J. *et al.* (2016) 'Spinal motor neurons are regenerated after mechanical lesion and genetic ablation in larval zebrafish', *Development*, 143(9), pp. 1464–1474. doi: 10.1242/dev.129155.

Ohno, K. *et al.* (2002) 'Rapsyn mutations in humans cause endplate acetylcholine-receptor deficiency and myasthenic syndrome', *Am J Hum Genet*, 70(4), pp. 875–885. doi: 10.1086/339465.

Ono, F. *et al.* (2001) 'Paralytic zebrafish lacking acetylcholine receptors fail to localize rapsyn clusters to the synapse.', *The Journal of Neuroscience*, 21(15), pp. 5439–5448. doi: 21/15/5439 [pii].

Ono, F. *et al.* (2002) 'The Zebrafish motility mutant twitch once reveals new roles for rapsyn in synaptic function.', *The Journal of neuroscience : the official journal of the Society for Neuroscience*, 22(15), pp. 6491–8. doi: 20026669.

Pagnon-Minot, A. *et al.* (2008) 'Collagen XV, a novel factor in zebrafish notochord differentiation and muscle development', *Developmental Biology*, 316(1), pp. 21–35. doi: 10.1016/j.ydbio.2007.12.033.

Panzer, J. A. *et al.* (2005) 'Neuromuscular synaptogenesis in wild-type and mutant zebrafish', *Developmental Biology*, 285(2), pp. 340–357. doi: 10.1016/j.ydbio.2005.06.027.

Panzer, J. A., Song, Y. and Balice-Gordon, R. J. (2006) 'In vivo imaging of preferential motor axon outgrowth to and synaptogenesis at prepatterned acetylcholine receptor clusters in embryonic zebrafish skeletal muscle.', *The Journal of Neuroscienceeuroscience*, 26(3), pp. 934–947. doi: 10.1523/JNEUROSCI.3656-05.2006.

Pardo-Martin, C. *et al.* (2010) 'High-throughput in vivo vertebrate screening', *Nature Methods*. Nature Publishing Group, 7(8), pp. 634–636. doi: 10.1038/nmeth.1481.

Park, J.-Y. *et al.* (2012) 'Acetylcholine receptors enable the transport of rapsyn from the Golgi complex to the plasma membrane.', *The Journal of neuroscience : the official journal of the Society for Neuroscience*, 32(21), pp. 7356–63. doi: 10.1523/JNEUROSCI.0397-12.2012.

Park, J.-Y. *et al.* (2014) 'A Single Mutation in the Acetylcholine Receptor -Subunit Causes Distinct Effects in Two Types of Neuromuscular Synapses', *Journal of Neuroscience*, 34(31), pp. 10211–10218. doi: 10.1523/JNEUROSCI.0426-14.2014.

Pattanayak, V., Guilinger, J. P. and Liu, D. R. (2014) *Determining the specificities of TALENs, cas9, and other genome-editing enzymes*. 1st edn. Elsevier Inc. doi: 10.1016/B978-0-12-801185-0.00003-9.

Patten, S. A. *et al.* (2014) 'Fishing for causes and cures of motor neuron disorders', *Disease Models & Mechanisms*, 7(7), pp. 799–809. doi: 10.1242/dmm.015719.

Pelley, J. W. (2007) 'Protein Synthesis and Degradation', *Elsevier's integrated biochemistry*. Philadelphia :, pp. 147–158. doi: 10.1016/B978-0-323-03410-4.50023-7.

Phillips, J. B. and Westerfield, M. (2014) 'Zebrafish models in translational research: tipping the scales toward advancements in human health', *Disease Models & Mechanisms*, 7(7), pp. 739–743. doi: 10.1242/dmm.015545.

Pike, S. H., Melancon, E. F. and Eisen, J. S. (1992) 'Pathfinding by zebrafish motoneurons in the absence of normal pioneer axons', *Development*, 114(4), pp. 825–831. Available at: http://dev.biologists.org/content/114/4/825%5Cnhttp://dev.biologists.org/content/114/4/825.full.pdf%5Cnhttp://www.ncbi.nlm.nih.gov/pubmed/1618146.

Place, E. S. and Smith, J. C. (2017) 'Zebrafish atoh8 mutants do not recapitulate morpholino phenotypes', *PLoS ONE*, 12(2), pp. 1–12. doi: 10.1371/journal.pone.0171143.

Plattner, F. and Bibb, J. A. (2012) 'Serine and Threonine Phosphorylation', in *Basic Neurochemistry*, pp. 467–492. doi: 10.1016/B978-0-12-374947-5.00025-0.

Ploumakis, A. and Coleman, M. L. (2015) 'OH, the Places You'll Go! Hydroxylation, Gene Expression, and Cancer', *Molecular Cell*. Elsevier Inc., 58(5), pp. 729–741. doi: 10.1016/j.molcel.2015.05.026.

Popp, M. W. and Maquat, L. E. (2016) 'Leveraging rules of nonsense-mediated mRNA decay for genome engineering and personalized medicine', *Cell*. Elsevier Inc., 165(6), pp. 1319–1332. doi: 10.1016/j.cell.2016.05.053.

Prykhozhij, S. V. *et al.* (2017) 'A rapid and effective method for screening, sequencing and reporter verification of engineered frameshift mutations in zebrafish', *Disease Models & Mechanisms*, 10(6), pp. 811–822. doi: 10.1242/dmm.026765.

Ramesh, T. *et al.* (2010) 'A genetic model of amyotrophic lateral sclerosis in zebrafish displays phenotypic hallmarks of motoneuron disease.', *Disease models & mechanisms*, 3(9–10), pp. 652–62. doi: 10.1242/dmm.005538.

Ramirez, C. L. *et al.* (2008) 'Unexpected failure rates for modular assembly of engineered zinc fingers', *Nature Methods*, 5(5), pp. 374–375. doi: 10.1038/nmeth0508-374.

Ran, F. A. *et al.* (2013) 'Genome engineering using the CRISPR-Cas9 system', *Nature Protocols*, 8(11), pp. 2281–2308. doi: 10.1038/nprot.2013.143.

Ratni, H. *et al.* (2018) 'Discovery of Risdiplam, a Selective Survival of Motor Neuron-2 (SMN2) Gene Splicing Modifier for the Treatment of Spinal Muscular Atrophy (SMA)', *Journal of Medicinal Chemistry*, 2, p. acs.jmedchem.8b00741. doi: 10.1021/acs.jmedchem.8b00741.

Rigo, F. *et al.* (2012) 'Antisense-based therapy for the treatment of spinal muscular atrophy', *Journal of Cell Biology*, 199(1), pp. 21–25. doi: 10.1083/jcb.201207087.

Rini, J. M. and Leffler, H. (2010) 'Carbohydrate recognition and signaling', in Bradshaw, R. A. and Dennis, E. A. (eds) *Handbook of Cell Signaling, 2/e*. Second Edi. Elsevier Inc., pp. 85–91. doi: 10.1016/B978-0-12-374145-5.00013-9.

Robu, M. E. *et al.* (2007) 'P53 Activation By Knockdown Technologies', *PLoS Genetics*, 3(5), pp. 787–801. doi: 10.1371/journal.pgen.0030078.

Rochette, C. F., Gilbert, N. and Simard, L. R. (2001) 'SMN gene duplication and the emergence of the SMN2 gene occurred in distinct hominids: SMN2 is unique to Homo sapiens', *Human Genetics*, 108(3), pp. 255–266. doi: 10.1007/s004390100473.

Rodgers, K. and Mcvey, M. (2016) 'Error-prone repair of DNA double-strand breaks', *Journal of Cell Physiology*, 231(1), pp. 15–24. doi: 10.1002/jcp.25053.Error-prone.

Rossi, A. *et al.* (2015) 'Genetic compensation induced by deleterious mutations but not gene knockdowns', *Nature*, 524(7564), pp. 230–233. doi: 10.1038/nature14580.

Russman, B. S., Iannaccone, S. T. and Samaha, F. J. (2003) 'A phase 1 trial of riluzole in spinal muscular atrophy', *Arch Neurol*, 60(11), pp. 1601–1603. doi: 10.1001/archneur.60.11.1601.

Ruthazer, E. S., Li, J. and Cline, H. T. (2006) 'Stabilization of Axon Branch Dynamics by Synaptic Maturation', *Journal of Neuroscience*, 26(13), pp. 3594–3603. doi:

10.1523/JNEUROSCI.0069-06.2006.

Sakurai, T. *et al.* (2014) 'A single blastocyst assay optimized for detecting CRISPR/Cas9 system-induced indel mutations in mice', *BMC Biotechnology*, 14, pp. 1–11. doi: 10.1186/1472-6750-14-69.

Sander, J. D. *et al.* (2010) 'ZiFiT (Zinc Finger Targeter): An updated zinc finger engineering tool', *Nucleic Acids Research*, 38(SUPPL. 2), pp. 462–468. doi: 10.1093/nar/gkq319.

Sander, J. D. *et al.* (2011) 'Targeted gene disruption in somatic zebrafish cells using engineered TALENs', *Nature Biotechnology*. Nature Publishing Group, 29(8), pp. 697–698. doi: 10.1038/nbt.1934.

Scheer, N. and Campos-Ortega, J. A. (1999) 'Use of the Gal4-UAS technique for targeted gene expression in the zebrafish', *Mechanisms of Development*, 80(2), pp. 153–158. doi: 10.1016/S0925-4773(98)00209-3.

Schrank, B. *et al.* (1997) 'Inactivation of the survival motor neuron gene, a candidate gene for human spinal muscular atrophy, leads to massive cell death in early mouse embryos.', *Proceedings of the National Academy of Sciences of the United States of America*, 94(18), pp. 9920–5. doi: 10.1073/pnas.94.18.9920.

Schweitzer, J. *et al.* (2005) 'Tenascin-C is involved in motor axon outgrowth in the trunk of developing zebrafish', *Developmental …*, 234(3), pp. 550–66. doi: 10.1002/dvdy.20525.

Seredick, S. D. *et al.* (2012) 'Zebrafish Mnx proteins specify one motoneuron subtype and suppress acquisition of interneuron characteristics', *Neural Development*, 7(1), pp. 1–14. doi: 10.1186/1749-8104-7-35.

Sertori, R. *et al.* (2016) 'Genome editing in zebrafish: A practical overview', *Briefings in Functional Genomics*, 15(4), pp. 322–330. doi: 10.1093/bfgp/elv051.

Sharpe, J. J. and Cooper, T. A. (2017) 'Unexpected consequences: Exon skipping caused by CRISPR-generated mutations', *Genome Biology*. Genome Biology, 18(1), pp. 1240–1243. doi: 10.1186/s13059-017-1240-0.

Shell, R. *et al.* (2018) 'AVXS-101 Phase 1 Gene Replacement Therapy Clinical Trial in SMA Type 1: Continued Independence from Nutritional and Ventilatory Support in Patients Dosed Early in Disease Progression (S29.003)', *Neurology*, 90(15 Supplement). Available at: http://n.neurology.org/content/90/15_Supplement/S29.003.abstract.

Shorrock, H. K., Gillingwater, T. H. and Groen, E. J. N. (2018) 'Overview of Current Drugs and Molecules in Development for Spinal Muscular Atrophy Therapy', *Drugs*. Springer International Publishing, 78(3), pp. 293–305. doi: 10.1007/s40265-018-0868-8.

Simone, B. W. *et al.* (2018) 'Fishing for understanding: Unlocking the zebrafish gene editor's toolbox', *Methods*, (May). doi: 10.1016/j.ymeth.2018.07.012.

Sleigh, J. N. *et al.* (2014) 'Chondrolectin affects cell survival and neuronal outgrowth in in vitro and in vivo models of spinal muscular atrophy.', *Human Molecular Genetics*, 23(4), pp. 855–69. doi: 10.1093/hmg/ddt477.

Stainier, D. Y. R. *et al.* (2017) 'Guidelines for morpholino use in zebrafish', *PLoS Genetics*, 13(10), pp. 6–10. doi: 10.1371/journal.pgen.1007000.

Streisinger, G. *et al.* (1981) 'Production of clones of homozygous diploid zebra fish (Brachydanio rerio)', *Nature*, 291(5813), pp. 293–296. doi: 10.1038/291293a0.

Swinney, D. C. and Anthony, J. (2011) 'How were new medicines discovered?', *Nature Reviews Drug Discovery*, 10(7), pp. 507–519. doi: 10.1038/nrd3480.

Swoboda, K. J. *et al.* (2016) 'Results from a phase 1 study of nusinersen (ISIS-SMN Rx) in children with spinal muscular atrophy', *Neurology*, 86(10), pp. 890–897.

Tamplin, O. J. *et al.* (2012) 'Small molecule screening in zebrafish: Swimming in potential drug therapies', *Wiley Interdisciplinary Reviews: Developmental Biology*, 1(3), pp. 459–468. doi: 10.1002/wdev.37.

Thisse, B., Thisse, C. (2004) Fast Release Clones: A High Throughput Expression Analysis. ZFIN Direct Data Submission (http://zfin.org).

Thomas-Jinu, S. *et al.* (2017) 'Non-nuclear Pool of Splicing Factor SFPQ Regulates Axonal Transcripts Required for Normal Motor Development', *Neuron*. Elsevier Inc., 94(2), p. 931. doi: 10.1016/j.neuron.2017.04.036.

Thurmond, J. *et al.* (2008) 'Synthesis and Biological Evaluation of Novel 2,4-Diaminoquinazoline Derivatives as SMN2 Promoter Activators for the Potential Treatment of Spinal Muscular Atrophy', *Journal of Medicinal Chemistry*, 51(3), pp. 449–469. doi: 10.1021/jm061475p.

Torres-Benito, L. *et al.* (2011) 'SMN requirement for synaptic vesicle, active zone and microtubule postnatal organization in motor nerve terminals', *PLoS ONE*, 6(10). doi: 10.1371/journal.pone.0026164.

Tsai, L.-K. *et al.* (2008) 'Multiple therapeutic effects of valproic acid in spinal muscular atrophy model mice', *Journal of Molecular Medicine*, 86(11), pp. 1243–1254. doi: 10.1007/s00109-008-0388-1.

Tsarouchas, T. M. *et al.* (2018) 'Dynamic control of proinflammatory cytokines Il-1β and Tnf-α by macrophages is necessary for functional spinal cord regeneration in zebrafish', *bioRxiv*, p. 332197. doi: 10.1101/332197.

Urnov, F. D. *et al.* (2010) 'Genome editing with engineered zinc finger nucleases', *Nature Reviews Genetics*. Nature Publishing Group, 11(9), pp. 636–646. doi: 10.1038/nrg2842.

Walker, C. and Streisinger, G. (1983) 'Induction of Mutations by gamma-Rays in Pregonial Germ Cells of Zebrafish Embryos.', *Genetics*, 103(1), pp. 125–36. Available at: http://www.pubmedcentral.nih.gov/articlerender.fcgi?artid=1202017&tool=pmcentrez&rendertype=abstract.

Wang, H. *et al.* (2013) 'One-step generation of mice carrying mutations in multiple genes by CRISPR/cas-mediated genome engineering', *Cell*. Elsevier Inc., 153(4), pp. 910–918. doi: 10.1016/j.cell.2013.04.025.

Wehner, D. *et al.* (2017) 'Wnt signaling controls pro-regenerative Collagen XII in functional spinal cord regeneration in zebrafish', *Nature Communications*. Springer US, 8(1), pp. 1–16. doi: 10.1038/s41467-017-00143-0.

Wendik, B., Maier, E. and Meyer, D. (2004) 'Zebrafish mnx genes in endocrine and exocrine pancreas formation', *Developmental Biology*, 268(2), pp. 372–383. doi: 10.1016/j.ydbio.2003.12.026.

Weng, L. *et al.* (2002) 'Molecular Cloning and Characterization of Human Chondrolectin, a Novel Type I Transmembrane Protein Homologous to C-Type Lectins', *Genomics*, 80(1), pp. 62–70. doi: 10.1006/geno.2002.6806.

Weng, L., Van Bockstaele, D. R., *et al.* (2003) 'A novel alternative spliced chondrolectin isoform lacking the transmembrane domain is expressed during T cell maturation.', *The Journal of biological chemistry*, 278(21), pp. 19164–70. doi: 10.1074/jbc.M300653200.

Weng, L., Hübner, R., *et al.* (2003) 'Isolation and characterization of chondrolectin (Chodl), a novel C-type lectin predominantly expressed in muscle cells', *Gene*, 308, pp. 21–29. doi: 10.1016/S0378-1119(03)00425-6.

Wertz, M. H. *et al.* (2016) 'Cell type-specific miR-431 dysregulation in a motor neuron model of Spinal Muscular Atrophy', *Human Molecular Genetics*, 25(11), pp. 2168–2181. doi:

10.1093/hmg/ddw084.

Westerfield, M. (2000) *The Zebrafish Book. A Guide for The Laboratory Use of Zebrafish (Danio rerio)*, *Eugene*.

Westerfield, M. and Eisen, J. S. (1988) 'Neuromuscular specificity: pathfinding by identified motor growth cones in a vertebrate embryo', *Trends in Neuroscience*, 11(1), pp. 11–22.

Wiedenheft, B., Sternberg, S. H. and Doudna, J. A. (2012) 'RNA-guided genetic silencing systems in bacteria and archaea', *Nature*, pp. 331–338. doi: 10.1038/nature10886.

Wilhelm, B. G. *et al.* (2014) 'Composition of isolated synaptic boutons reveals the amounts of vesicle trafficking proteins', *Science*, 344(6187), pp. 1023–1028. doi: 10.1126/science.1252884.

Williams, C. H. *et al.* (2015) 'An In vivo Chemical Genetic Screen Identifies Phosphodiesterase 4 as a Pharmacological Target for Hedgehog signaling Inhibition Charles', *Cell reports*, 11(1), pp. 43–50. doi: 10.1016/j.celrep.2015.03.001.An.

Wishart, T. M. *et al.* (2014) 'Dysregulation of ubiquitin homeostasis and β -catenin signaling promote spinal muscular atrophy', *The Journal of Clinical Investigation*, 124(4), pp. 1821–34. doi: 10.1172/JCI71318DS1.

Wittkopp, N. *et al.* (2009) 'Nonsense-Mediated mRNA Decay Effectors Are Essential for Zebrafish Embryonic Development and Survival', *Molecular and Cellular Biology*, 29(13), pp. 3517–3528. doi: 10.1128/MCB.00177-09.

Wu, H., Xiong, W. C. and Mei, L. (2010) 'To build a synapse: signaling pathways in neuromuscular junction assembly.', *Development (Cambridge, England)*, 137(7), pp. 1017–1033. doi: 10.1242/dev.038711.

Yan, H., Ohno, N. and Tsuji, N. M. (2013) 'The role of C-type lectin receptors in immune homeostasis', *International Immunopharmacology*. Elsevier B.V., 16(3), pp. 353–357. doi: 10.1016/j.intimp.2013.04.013.

Yang, H., Wang, H. and Jaenisch, R. (2014) 'Generating genetically modified mice using CRISPR/Cas-mediated genome engineering', *Nature Protocols*, 9(8), pp. 1956–1968. doi: 10.1038/nprot.2014.134.

Zelensky, A. N. and Gready, J. E. (2005) 'The C-type lectin-like domain superfamily', *FEBS Journal*, 272(24), pp. 6179–6217. doi: 10.1111/j.1742-4658.2005.05031.x.

Zhang, J. *et al.* (2004) 'Zebrafish unplugged reveals a role for muscle-specific kinase homologs in axonal pathway choice', *Nature Neuroscience*, 7(12), pp. 1303–9. doi: 10.1038/nn1350.

Zhang, Z. *et al.* (2008) 'SMN Deficiency Causes Tissue-Specific Perturbations in the Repertoire of snRNAs and Widespread Defects in Splicing', *Cell*, 133(4), pp. 585–600. doi: 10.1016/j.cell.2008.03.031.

Zhong, Z. *et al.* (2012) 'Chondrolectin mediates growth cone interactions of motor axons with an intermediate target.', *The Journal of Neuroscience*, 32(13), pp. 4426–39. doi: 10.1523/JNEUROSCI.5179-11.2012.